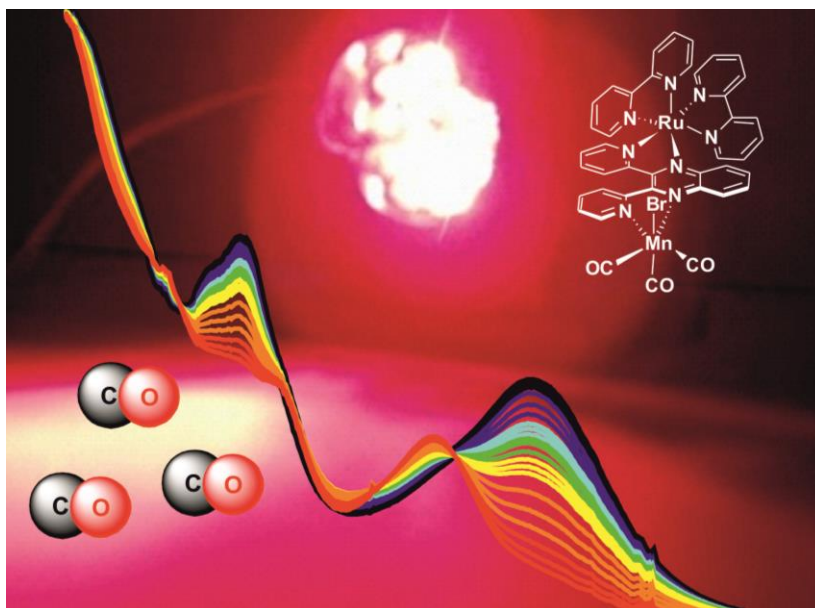


# Novel manganese- and molybdenum-based photoactivatable CO-releasing molecules: Synthesis and biological activity



Dissertation zur Erlangung des naturwissenschaftlichen Doktorgrades  
der Julius-Maximilians-Universität Würzburg

vorgelegt von

Christoph Nagel  
aus Martinsheim

Würzburg, August 2015



Eingereicht bei der Fakultät für Chemie und Pharmazie am

\_\_\_\_\_

Gutachter der schriftlichen Arbeit

1. Gutachter: \_\_\_\_\_

2. Gutachter: \_\_\_\_\_

Prüfer des öffentlichen Promotionskolloquiums

1. Prüfer: \_\_\_\_\_

2. Prüfer: \_\_\_\_\_

3. Prüfer: \_\_\_\_\_

Datum des öffentlichen Promotionskolloquiums

\_\_\_\_\_

Doktorurkunde ausgehändigt am

\_\_\_\_\_





**People who think they know everything are a  
great annoyance to those of us who do.**

*Isaac Asimov*



Diese Doktorarbeit wurde zwischen 08/2012 und 09/2015  
am Institut für Anorganische Chemie  
der Julius-Maximilians-Universität Würzburg  
unter der Anleitung von Prof. Dr. Ulrich Schatzschneider angefertigt.



## Danksagung

Mein Dank gilt an erster Stelle meinem Doktorvater Prof. Dr. Ulrich Schatzschneider für die langjährige Begleitung seit dem Master, das mir entgegen gebrachte Vertrauen, jederzeitige Förderung meiner Arbeit, die jederzeit offene Tür bei Problemen und für die Möglichkeit die interessanten und fordernden Themenkomplexe im Rahmen dieser Doktorarbeit zu bearbeiten.

Weiterhin möchte ich Prof. Dr. Todd B. Marder für die Bereitschaft danken trotz seines vollen Terminkalenders die Zweitbegutachtung meiner Arbeit zu übernehmen.

Außerdem möchte ich Prof. Dr. Robert K. Poole von der Universität Sheffield danken für die Möglichkeit im Rahmen einer COST BM 1005 STSM Zeit in seiner Arbeitsgruppe verbringen zu dürfen und somit einen tiefen Einblick in die Arbeitsmethoden der Mikrobiologie und den Umgang mit Bakterienkulturen zu erhalten. Hierbei gilt mein Dank auch Dr. Samantha McLean, Lauren Wareham, Dr. Mariana Tinajero-Trejo und Namrata Rana für die freundliche Aufnahme und die gute, noch immer andauernde Zusammenarbeit.

Weiterhin möchte ich Prof. Dr. Patrick Nürnberger und seinen Mitarbeitern Dr. Philipp Rudolf und Johannes Knorr für die gute Zusammenarbeit, anregende Diskussionen und Unterstützung meiner Arbeit durch den Zugang zu Messgeräten im PC-Praktikum danken.

Natürlich möchte ich mich auch bei all denjenigen sehr herzlich bedanken, die zum Gelingen dieser Arbeit beigetragen haben:

Dr. Thomas Kramer für die Messung und Auswertung meiner ersten Kristallstruktur. Weiterhin danke ich der gesamten Serviceabteilung des IAC für Messungen, Unterstützung und Erfüllung von vielen Sonderwünschen bei sensiblen Proben, insbesondere Dr. Rüdiger Bertermann, Marie-Luise Schäfer, Liselotte Michels und Sabine Timmroth.

Meinen ehemaligen Betreuern und Laborpartnern Dr. Hendrik Pfeiffer, Dr. Johanna Niesel, Dr. Peter Simpson und Dr. Sandesh Pai für die Unterstützung, anregende Diskussionen und vor allem die stets freundliche Atmosphäre im Labor. Mein besonderer Dank gilt auch meinen ehemaligen Praktikanten Joshua Weinmann, Anna Felghelm, Maximilian Bernard, Theresa Zang, Peter Friesen und Carolina Kiermeier die mich bei der „Massenproduktion“ von Verbindungen für Kooperationspartner in Biologie und Physikalischer Chemie tatkräftig unterstützt haben.

Der gesamten Arbeitsgruppe Schatzschneider die mich in meiner Zeit begleitet haben, meinen Dank, insbesondere Hendrik, Johanna, Pete, Sandesh, Thomas, Wanning, Christoph, Carina, Anja, Tine, Luisa, Elvan, Lucas, Ryanne, Dominic, Olivier, Paul, Flo und Flo, Benedict, Viviane, Nilab, Franziska, Caro, Nuria, Joe und Benji für das angenehme Arbeitsklima.

Auch möchte ich mich bei der „donnerstäglichen Mensagemeinschaft“ mit Nicola, Sabrina, Lisa, Michael, Fabian und Fede sowie Benji bedanken, die bei mir nicht nur immer für gute Laune sorgte, sondern auch nützliche Gedanken zu mehr oder weniger fachlichen Problemen beisteuern konnten.

Ein besonderes Dankeschön gilt meiner Familie und meinen Freunden die mich immer unterstützen und somit einen großen Beitrag am Gelingen dieser Arbeit beisteuerten.

The publication listed below is partly reproduced in this dissertation. The table itemizes to what extent the different sections of the paper have been reused at which position in this work. For the figures it is noted in the respective captions whether it is a reproduction or an adaption from the corresponding publication.

C. Nagel, S. McLean, R. Poole, H. Braunschweig, T. Kramer, U. Schatzschneider, <i>Dalton Trans.</i> <b>2014</b> , 43, 9986–9997.		
Thesis p. 59 - 65	Table 3.4, Fig. 3.31-3.32, Text mainly reproduced, modified and extended from the paper	
Contributions	C. Nagel  S. McLean, R. K. Poole T. Kramer, H. Braunschweig U. Schatzschneider	Synthesis, characterization, CO release measurements, manuscript writing Biological data collection X-ray structure analysis DFT calculations, manuscript writing

---

## Table of contents

<b>1 Introduction .....</b>	<b>1</b>
1.1 Biological activity of carbon monoxide .....	1
1.2 Antibacterial properties of carbon monoxide .....	7
1.3 CO-releasing molecules (CORMs).....	9
1.3.1 CO-release triggered by ligand exchange .....	12
1.3.2 Enzyme-triggered CO-releasing molecules .....	14
1.3.3 Photoactivatable CO-releasing molecules .....	15
1.3.4 Target specificity of CORMs.....	20
<b>2 Motivation .....</b>	<b>22</b>
<b>3 Results and Discussion.....</b>	<b>24</b>
3.1 PhotoCORMs with tetradentate ligands.....	24
3.1.1 Synthesis of tetradentate ligands .....	24
3.1.2 Synthesis and characterization of metal complexes.....	36
3.1.3 UV/Vis studies.....	53
3.1.4 Determination of log <i>P</i> values.....	57
3.1.5 NMR studies .....	58
3.1.6 IR studies and DFT calculations .....	60
3.1.7 Antibacterial properties .....	64
3.2 PhotoCORMs with hexadentate ligands .....	68
3.2.1 Synthesis of hexadentate ligands.....	68
3.2.2 Synthesis and characterization of metal complexes.....	72
3.2.3 UV/Vis studies.....	79
3.2.4 IR studies and DFT calculations .....	81
3.3 Heterobinuclear manganese/ruthenium PhotoCORMs.....	86
3.3.1 Background.....	86
3.3.2 Synthesis of the ligands.....	87

3.3.3 Synthesis of metal complexes.....	95
3.3.4 Photophysical studies of Mn(I)-Ru(II)-PhotoCORMs .....	122
3.4 Mixed CO/NO-releasing molecules .....	137
3.4.1 Synthesis of ligands and metal complexes .....	137
3.4.2 UV/Vis studies.....	145
3.4.3 Solution IR studies and DFT/TDDFT calculations.....	148
<b>4 Conclusion.....</b>	<b>155</b>
4.1 English version .....	155
4.2 Deutsche Version .....	159
<b>5 Experimental section .....</b>	<b>163</b>
5.1 General procedures and instrumentation .....	163
5.2 Synthetic procedures .....	166
5.2.1 Synthesis of the ligands.....	166
5.2.2 Synthesis of PhotoCORMs with tetradentate ligands .....	182
5.2.3 Synthesis of PhotoCORMs with hexadentate ligands .....	190
5.2.4 Synthesis of heterobinuclear manganese/ruthenium-PhotoCORMs ....	194
5.2.5 Synthesis of mixed CO/NO-releasing molecules .....	212
5.3 Myoglobin assay .....	215
5.4 Photolysis with NMR detection.....	217
5.5 Photolysis with IR detection.....	217
5.6 Determination of the <i>n</i> -octanol/water partition coefficient.....	218
5.7 Biological assays.....	219
<b>6 References.....</b>	<b>220</b>
<b>7 Appendices.....</b>	<b>226</b>
<b>Selbständigkeitserklärung.....</b>	<b>235</b>



## Abbreviations

Arg	arginine
Asp	asparagine
ATR	attenuated total reflection
bpqa	bis(2-pyridylmethyl)(2-quinolylmethyl)amine
bqpa	bis(2-quinolylmethyl)(2-pyridylmethyl)amine
bpy	2,2'-bipyridine
CBS	cystathionine- $\beta$ -synthase
cGMP	cyclic guanosine monophosphate
CSE	cystathionine- $\gamma$ -lyase
CORM	CO-releasing molecule
DAB	diaminobutane dendrimer
DMAD	dimethyl acetylene dicarboxylate
dpa	<i>N,N</i> -bis(2-pyridylmethyl)amine
dpx	2,3-di(2-pyridyl)quinoxaline
ESI	electrospray ionization
etx	ethyl(2,2':6',2''-terpyridine)-4'-carboxylate
ET-CORM	enzyme-triggered CO-releasing molecule
GTP	guanosine triphosphate
His	histidine
HO	heme oxygenase
iCORM	inactivated CO releasing molecule
IP3	inositol triphosphate
<i>iPr</i> <sub>3</sub> tacn	1,4,7-triisopropyl-1,4,7-triazacyclonane
Mb	myoglobin
NADPH	nicotinamide adenine dinucleotide phosphate
NOS	NO synthase
PBS	phosphate buffered saline
PDE	phosphodiesterase
PLC	phospholipase C
phenox	1,10-phenantroline-5,6-dione

## *Abbreviations*

---

PhotoCORM photoactivatable CO-releasing molecule

PK	protein kinase
PTA	1,3,5-triaza-7-phosphatricyclodecane
pytp	3-(pyridin-2-yl)-1,2,4-triazine[5,6- <i>f</i> ]-1,10-phenanthroline
pypt	3-(pyridin-2-yl)phenanthro[9,10- <i>e</i> ]-1,2,4-triazine
py <sub>3</sub> tacn	1,4,7-tris(2-pyridylmethyl)-1,4,7-triazacyclononane
ROS	reactive oxygen species
sCG	soluble guanylate cyclase
tacn	1,4,7-triazacyclonane
tbx	<i>N</i> -((2,2':6',2''-terpyridin)-4'-yl)2,2'-bipyridine-5-carboxamide
tmqa	tris(2-quinolylmethyl)amine
TMS	tetramethylsilane
tpa	tris(2-pyridylmethyl)amine
tpm	tris(pyrazolyl)methane
tppts	tris(sulphonatophenyl)phosphine
Trp	tryptophan

# 1 Introduction

## 1.1 Biological activity of carbon monoxide

As a colorless and odorless gas, carbon monoxide is generally known to the public only as the “silent killer”. However, together with nitric oxide and hydrogen sulfide, it belongs to an important class of small signaling molecules which are endogenously produced in higher organisms including humans by different enzymatic processes as shown in **Fig. 1.1**.

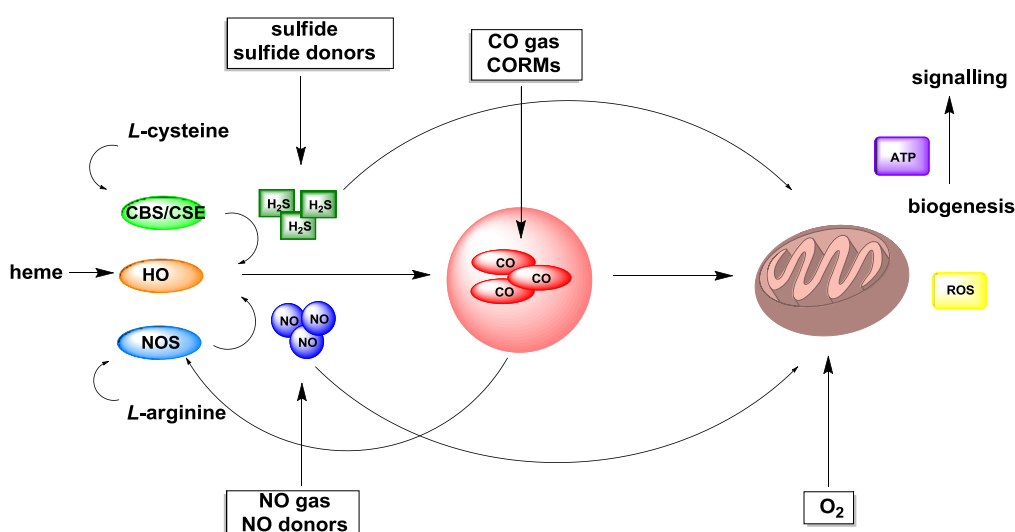
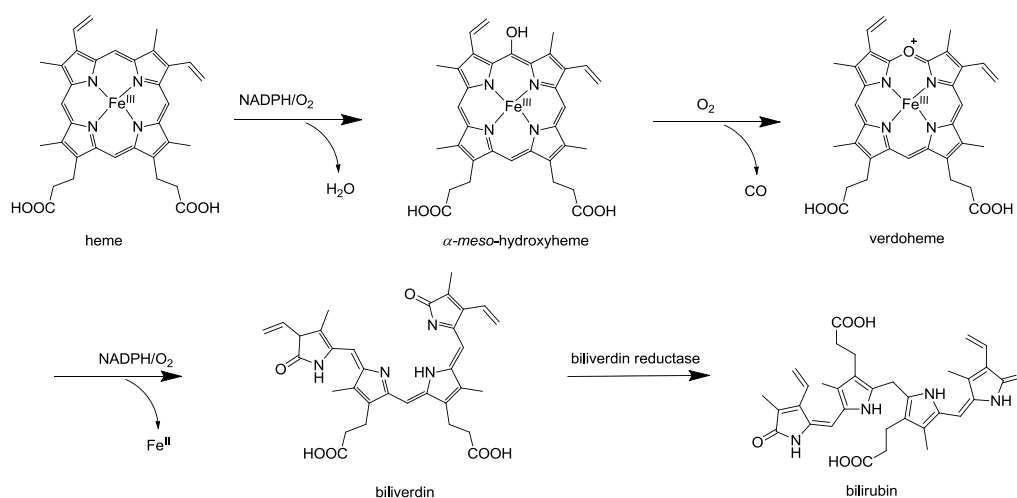


**Figure 1.1:** Sources of endogenous enzymatic generation of carbon monoxide, nitric oxide and hydrogen sulfide with their cellular targets and interaction of signaling pathways. Abbreviations: Cystathionine  $\beta$ -synthase (CBS), cystathionine  $\gamma$ -lyase (CSE), NO synthase (NOS), heme oxygenase (HO), reactive oxygen species (ROS) and CO-releasing molecules (CORMs).<sup>[1]</sup>

While the degradation of *L*-arginine by NO synthase (NOS) enzymes generates nitric oxide, hydrogen sulfide is endogenously produced by cystathionine  $\beta$ -synthase (CBS) and cystathionine  $\gamma$ -lyase (CSE) from *L*-cysteine.<sup>[2]</sup> The generation of carbon monoxide by heme oxygenase (HO) from heme is regulated by nitric oxide and hydrogen sulfide.<sup>[3]</sup> On the other hand, the carbon monoxide generated also controls the activity of NOS. All three small messenger molecules influence and regulate biogenesis in the mitochondria.<sup>[4]</sup> Heme degradation by HO is a multiple step process (**Scheme 1.1**). Initially, the porphyrin ring is regioselectively oxidized to

$\alpha$ -meso-hydroxyheme with consumption of one equivalent of NADPH and dioxygen. Further reaction with dioxygen leads to liberation of one equivalent of carbon monoxide per heme unit in addition to the formation of positively charged verdoheme. The latter undergoes one more oxidation by dioxygen with NADPH consumption under cleavage of the tetrapyrrol ring. In this step, the iron center is reduced to iron(II) and the metal released from the tetrapyrrol coordination sphere. Finally, the conjugated backbone is reduced by biliverdin reductase to bilirubin.<sup>[5]</sup>



Scheme 1.1: CO generation by heme degradation with heme oxygenase (HO).<sup>[6]</sup>

In the human body, there are two isoforms of heme oxygenase, which are encoded by the *hmx1* and *hmx2* genes. HO-1 is an inducible enzyme while the HO-2 isoform is constitutive but only found in blood vessels and testicles.<sup>[1]</sup> The function of HO-1 was characterized in detail to verify the importance of endogenously generated CO for cytoprotection and hemostatic actions.<sup>[7]</sup> Different *in vivo* studies showed a decreasing susceptibility against certain diseases of individuals with high HO-1 activity. Mice with embryonic knock-out of *hmx1* died either before birth or had a significantly reduced lifespan.<sup>[1]</sup> However, the biological activity of carbon monoxide is highly concentration dependent. High systemic doses lead to the well-known general toxicity of CO. In this case, carbon monoxide binding to heme proteins with very high affinity causes disruptions in oxygen metabolism. On the other hand, high local concentrations can be utilized in chemotherapy to eliminate

undesired cell populations from the body such as cancer cells, bacteria, and parasites. Finally, low concentrations of CO are essential for the cytoprotective and signaling properties of carbon monoxide as a small molecule messenger as shown below in Fig. 1.2.<sup>[1]</sup>

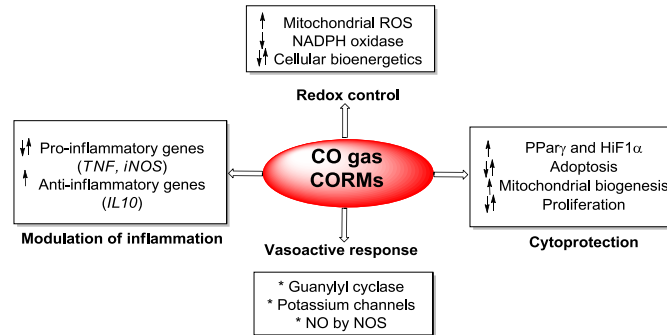


Figure 1.2: Influence of carbon monoxide on different cellular metabolic pathways.<sup>[8]</sup>

High concentrations of carbon monoxide cause an inhibition of mitochondrial respiration. In particular, the strong binding of CO to cytochrome *c* oxidase blocks an important electron acceptor in the respiratory chain. Lower concentrations of CO, on the other hand, lead to an increase in ATP production and promotion of mitochondrial biogenesis and other cytoprotective systems.<sup>[1]</sup>

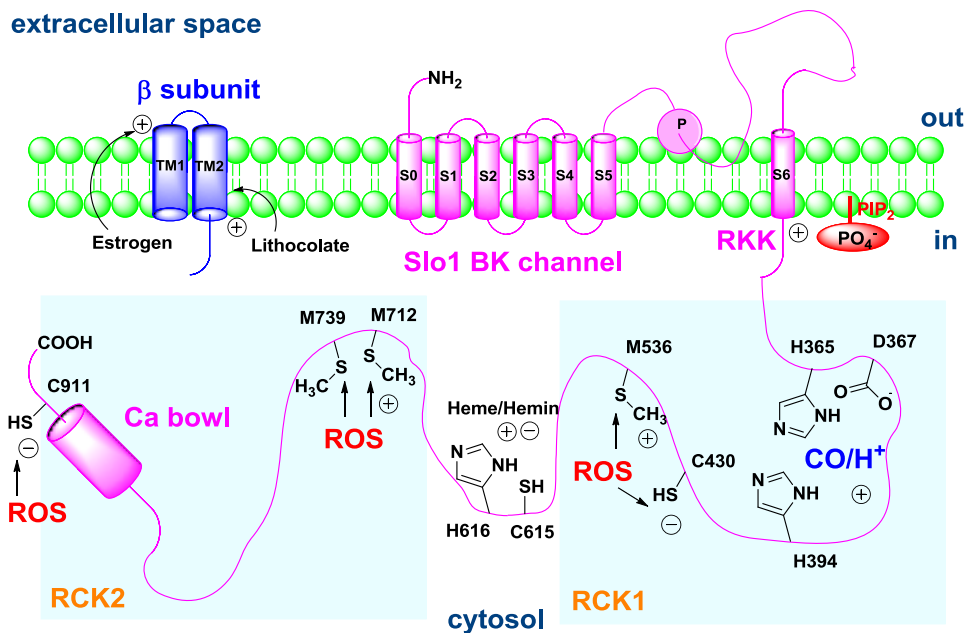


Figure 1.3: Stimulative modulators (+) and inhibitive modulators (-) of BK<sub>Ca</sub> ion channels and the key amino acid residues involved in the modulation.<sup>[9]</sup>

Other heme proteins in the cell are also influenced. Thus, carbon monoxide acts on NO synthases, NADPH oxidases, and ion channels. Heme-containing ion channels of the BK<sub>Ca</sub> type are particularly interesting as target structures for carbon monoxide (**Fig. 1.3**).<sup>[9]</sup> The heme units operate as receptors for the binding of CO. The coordination of carbon monoxide leads to a continuous stimulation of the ion channels and a promotion of their activity, which is blocked by an inhibition of HO and the resulting decrease of the carbon monoxide concentration.<sup>[10]</sup>

Interestingly, additional studies on hydrogen peroxide-oxidized BK<sub>Ca</sub> ion channels and thus inactivated heme units also show the responding to carbon monoxide application.<sup>[11]</sup> Recent investigations on the Ca<sup>2+</sup> sensors RCK1 and in the pore-forming subunit of the BK<sub>Ca</sub> (Slo1) channel showed the involvement of this moiety in the CO sensitivity.<sup>[12],[13]</sup> Mutations of the amino acids His365, His394 and Asp367 in this subunit or low pH values depress the response to applied carbon monoxide.<sup>[14]</sup> The histidine and asparagine residues influence the proton and Ca<sup>2+</sup> sensitivity of the RCK1 unit and play an important role in CO activity. The interaction of carbon monoxide with Slo1 results from electrostatic effects of the weak dipole moment of CO and the histidine-asparagine sensor pocket of the BCK1 unit.<sup>[14]</sup> The influence of carbon monoxide on intracellular dioxygen sensing was also observed.<sup>[15]</sup> Hypoxia is known to induce BK<sub>Ca</sub> ion channel inhibition while CO leads to their continuous stimulation. Thus, it was observed that low levels of dioxygen lower the activity of heme oxygenase and therefore, the endogenous generation of carbon monoxide, followed by inhibition of the BK<sub>Ca</sub> ion channels.<sup>[16]</sup> However, the regulation of BK<sub>Ca</sub> ion channels follows long signaling cascades, involving carbon monoxide, nitric oxide, nitrate, and calcium(II) ions as well as reactive oxygen species (**Fig. 1.4**).<sup>[17]</sup>

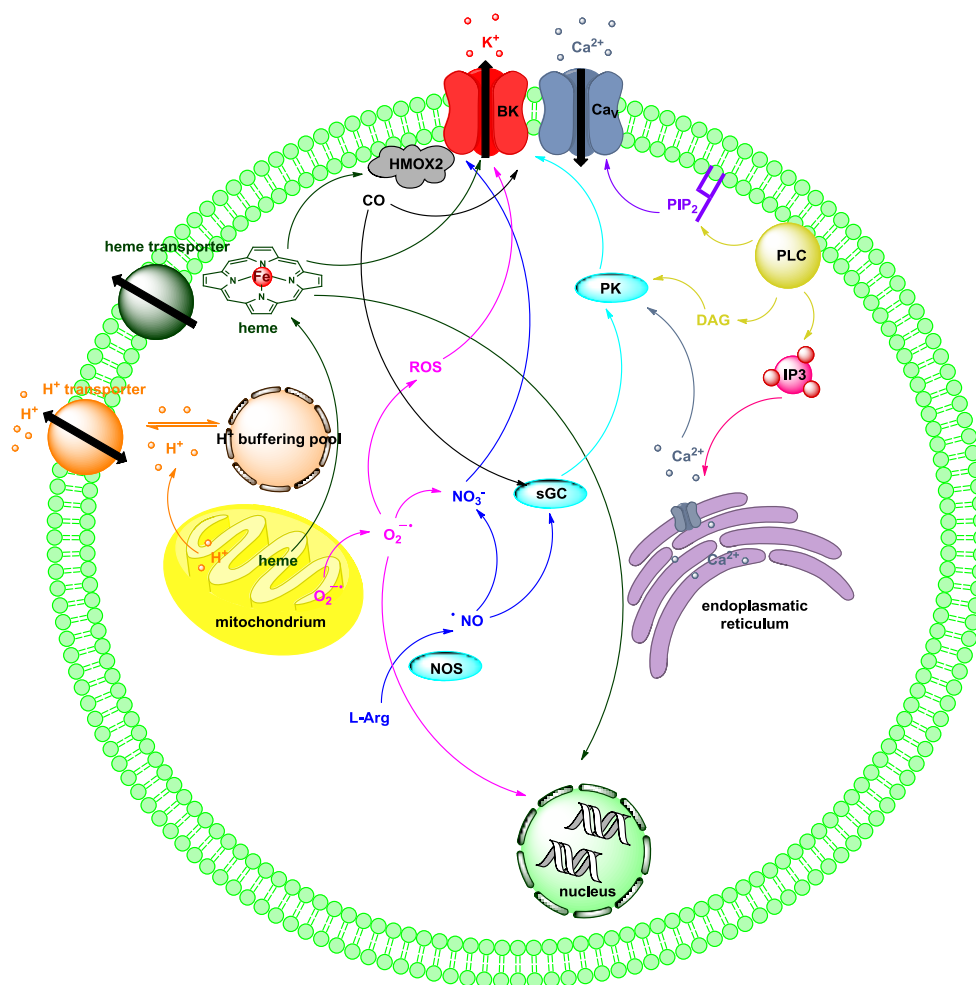


Figure 1.4: Multiple intracellular signaling cascades regulate by BK<sub>Ca</sub> ion channels.<sup>[9]</sup>

Another intracellular target of nitric oxide and carbon monoxide is soluble guanylate cyclase (sGC). This heme enzyme converts GTP to cGMP (Scheme 1.2), which activates phosphodiesterase (PDE) as well as ion channels (Fig. 1.5).<sup>[18]</sup>

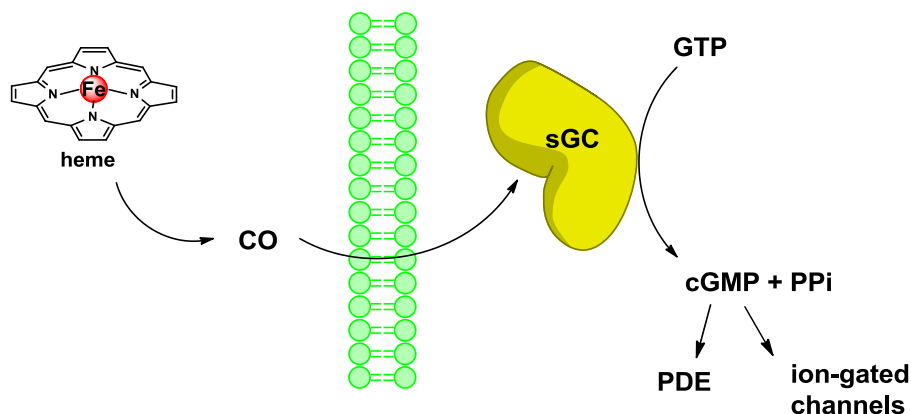
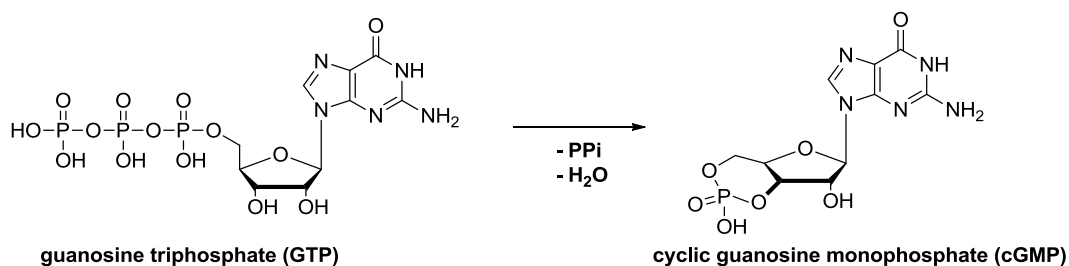


Figure 1.5: CO activated sGC producing cGMP from GTP.<sup>[18]</sup>

However, the activation of soluble guanylate cyclase (sGC) by carbon monoxide is disputed as a CO-induced increase in cGMP generation was only observed in combination with YC-1, a generally known activator of sGC, which is also promoted by carbon monoxide.<sup>[19]</sup> Without YC-1, carbon monoxide has no significant effect on sGC activity.<sup>[20]</sup> However, a naturally produced YC-1 analogue has remained elusive so far.



Scheme 1.2: Conversion of GTP to cGMP.<sup>[18]</sup>



## 1.2 Antibacterial properties of carbon monoxide

Nosocomial infections in intensive care units have become a major problem in hospitals over recent years. The majority of these infections is caused by *Pseudomonas aeruginosa* strains, which have acquired antibiotic resistance due to the usage of broad-spectrum antibiotics. Beside these serious problems, no new drugs against *Pseudomonas aeruginosa* have reached clinical application in the last 20 years.<sup>[21]</sup> Several investigations showed that carbon monoxide gas as well as CO delivered by ruthenium carbonyl complex CORM-3 bind to the bacterial cytochrome c oxidase, thus causing bactericidal effects. The use of CORMs (see next chapter for detailed introduction) has some advantages compared to the application of CO gas, which requires special equipment in connection with hospitalization. In contrast, CORMs are administered as a drug, and can be modified to change their solubility properties and minimize off-target toxicity.<sup>[22]</sup> In this context, Motterlini and Poole published very promising results on the application of CORM-3 in several *in vitro* as well as *in vivo* studies against *Pseudomonas aeruginosa*.<sup>[21]</sup> Carbon monoxide seems to be promising as it binds and interacts with iron and other metal centers of enzymes such as NADPH oxidase or ion channels.<sup>[23]</sup> Its bactericidal effects on *E. coli* strains are due to the binding to the three terminal mitochondrial cytochrome *bd-I*, cytochrome *bd-II* and cytochrome *bo oxidases*, which interferes with oxygen metabolism and leads to an increase in the production of toxic reactive oxygen species (ROS).<sup>[24]</sup> Furthermore, additional studies on *E. coli* treated with nitric oxide and carbon monoxide showed concerted biological activity.<sup>[25]</sup> The experiments showed an inhibition of the nitric oxide detoxification, which proceeds over the oxidation of NO with O<sub>2</sub> to nitrate ions, by CORM-3 delivered carbon monoxide.<sup>[26]</sup> In studies on CORM-3 and *Salmonella enterica serovar Typhimurium*, which is known as an enteropathogen causing gastroenteritis in the human body, the uptake of CORM into the bacteria cells was observed. Additional experiments with sensitive dual-beam integrating cavity absorption spectrophotometry showed the liberation of carbon monoxide, as well as the binding to heme enzymes of the respiratory

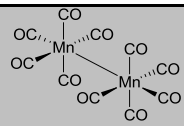
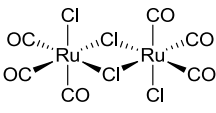
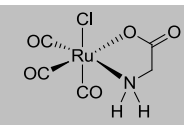
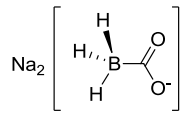
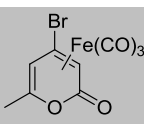
chains. The published toxic concentrations of CORM-3 on *Salmonella enterica* serovar *Typhimurium* are about 6.5 times lower than against RAW 264.7 macrophages cell lines.<sup>[27],[28],[29]</sup>

### 1.3 CO-releasing molecules (CORMs)

Since its discovery as a small signaling molecule, researchers have tried to utilize the beneficial cytoprotective properties of carbon monoxide in therapeutic applications.<sup>[1]</sup> Initial work focused on the controlled direct application of CO gas. Devices now commercially available provide exogenous carbon monoxide by inhalation and are in clinical application. However, this approach has some distinct disadvantages. First of all, special equipment is required for this mode of application, which requires hospitalization of the patient. The applied CO gas is not transported to the tissue efficiently due to the strong binding of CO to hemoglobin, which delivers it to the lungs exhalation. Also, a very strict dose control is indispensable to avoid toxicity by overdosing.<sup>[30]</sup> Thus, alternative systems were developed which are able to deliver CO in a tissue-specific manner.<sup>[1]</sup>

About 10 years ago, Motterlini first proposed the use of simple metal carbonyls such as  $[\text{Fe}(\text{CO})_5]$  and  $[\text{Mn}_2(\text{CO})_{10}]$  **1-1** (CORM-1) as *CO-releasing molecules* (CORMs) (**Tab. 1.1**).<sup>[32]</sup> However, these two compounds require light to trigger the CO release. The photolytic liberation of carbon monoxide from transition metal complexes was already observed by Strohmeier in the 1960s but not explored for biology since then.<sup>[36],[37],[38]</sup> Exposure to cold light sources resulted in a very fast liberation of CO with a half-life  $< 1$  min.<sup>[32]</sup> However, the poor water solubility and high general toxicity of these compounds precluded further investigations. Instead, ruthenium(II) compounds such as  $[\text{RuCl}_2(\text{CO})_3]_2$  **1-2** (CORM-2) and  $[\text{RuCl}(\text{glycinate})(\text{CO})_3]$  **1-3** (CORM-3) seemed more promising due to their low toxicity and better solubility in water.<sup>[1, 32]</sup> The liberation of carbon monoxide from CORM-2 and -3 is triggered by very fast ligand exchange with medium which will be discussed in detail in the next chapter. Although CORM-3 is stable in water with a half-life of 4 d, the stability significantly decreases in human plasma to only 3.6 min.<sup>[39]</sup>

**Table 1.1:** Most important CORM lead structures together with information on solubility, half-life in solution and year of publication.<sup>[31]</sup>

compound	structure	solvent	$t_{1/2}$ (PBS, pH = 7.4, 37°C)	publication year
CORM-1		DMSO ethanol	$t_{1/2} < 1$ min	2002 <sup>[32]</sup>
CORM-2		DMSO ethanol	$t_{1/2} \approx 1$ min	2002 <sup>[32]</sup>
CORM-3		water (stable at pH < 7) Human plasma	$t_{1/2} \approx 98$ h  $t_{1/2} \approx 4$ min	2004 <sup>[33]</sup>
CORM-A1		water (stable at pH > 7)	$t_{1/2} \approx 21$ min	2004 <sup>[34]</sup>
CORM-F3		DMSO ethanol	$t_{1/2} \approx 55$ min	2005 <sup>[35]</sup>

Importantly, in the case of the ruthenium compounds, liberation of carbon monoxide leads to *inactivated* CORMs (iCORM) which might have a biological activity by themselves.<sup>[40]</sup> However, CORM-3 is still the most commonly used carbon monoxide delivery system in biological studies. As an alternative, Alberto introduced  $\text{Na}_2[\text{H}_3\text{BCO}_2]$  **1-4** (CORM-A1) as a main group compound able to release CO under physiological conditions. CORM-A1 liberates one equivalent of carbon monoxide per molecule in a pH-dependent manner. While it is stable under basic conditions, it releases CO with a half-life of 21 min in a neutral or acidic environment.<sup>[34]</sup> Further investigations in the field led to the introduction of bioactive coligands for the preparation of CORMs. For example,  $[\text{Fe}(\text{CO})_3(\eta^4\text{-2-pyrone})]$  **1-5** (CORM-F3) carries a 2-pyrone ligand,<sup>[35]</sup> which is known for the inhibition of human ovarian carcinoma (A2780) and human leukemia (K562) cell lines with sub-micromolar  $\text{IC}_{50}$  values while they show no significant toxicity in healthy cell lines.<sup>[41]</sup> For better tissue specificity, amino acid ligands were also explored. For example,  $\text{Na}[\text{Mo}(\text{histidinate})(\text{CO})_3]$  **1-6** (ALF-186) interacts with lysozyme crystals resulting in polyoxomolybdate formation.<sup>[30]</sup> Furthermore, cobalamin-CORM conjugates such as  $[\text{ReBr}_2(\text{CO})_2(\text{H}_2\text{O})(\text{NC-B}_{12})]$  **1-7** ( $\text{B}_{12}$ -ReCORM-2) were

prepared by Zobi. Such systems are expected to show promising biocompatibility since these cobalamin conjugates show better stability in physiological medium than the complexes alone (**Fig. 1.6**).<sup>[42],[43],[44]</sup> Also, cobalamin Re(II)-based CORMs had no toxicity against human cardiomyocytes and efficient therapeutic effects against ischemia-reperfusion injuries. The cytoprotective effects are supposed to result from the extracellular liberation of CO as well as the antioxidative behavior of the compounds.<sup>[45]</sup> The degradation of the Re(II)-based CORMs leads to the perrhenate anion as a metabolite<sup>[44]</sup> which is known as one of the least toxic transition metal compounds.<sup>[46]</sup> Strategies to induce the release of CO range from ligand exchange reactions (CORM-2, CORM-3) over pH-dependent activation (CORM-A1) and oxidation (CORM-F3) to enzymatic pathways (ET-CORMs)<sup>[47]</sup> as well as photoactivation (CORM-1, PhotoCORMs).<sup>[31]</sup>

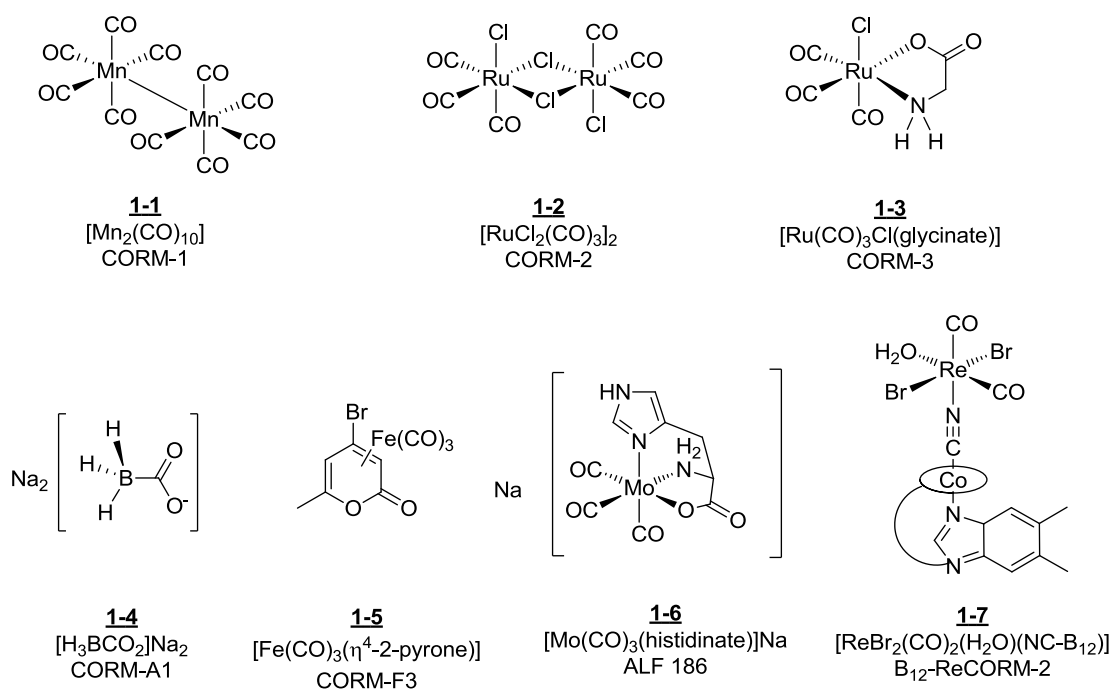
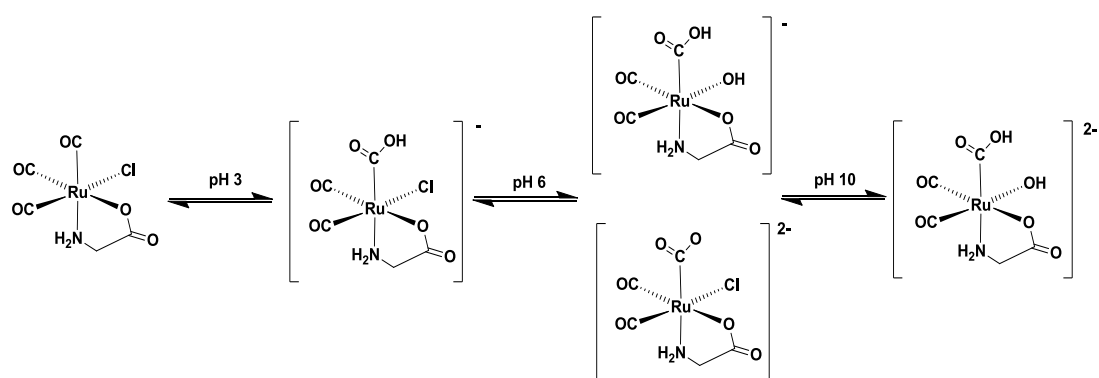


**Figure 1.6:** Selected lead structures of CO-releasing molecules (CORMs).<sup>[1]</sup>

### 1.3.1 CO-release triggered by ligand exchange

The most common mechanism for the liberation of carbon monoxide from transition metal-based *CO-releasing molecules* (CORMs) is the interaction with solvent. For example, due to its reversible reaction with dimethylsulfoxide, CORM-2 **1-2** was chosen from a series of commercially available ruthenium carbonyl compounds for further investigation of its biological activity with  $[\text{RuCl}_2(\text{dms})_4]$  used as a reference. CORM-3 **1-3** was the first water-soluble ligand-exchange triggered CO-releasing molecule studied. CORM-3 is stable under acidic conditions with a half-life of one minute in phosphate-buffered saline (PBS) at  $\text{pH} = 7.4$ , which is used as medium for CO-release studies. This is similar to CORM-2 **1-2** and the photoactivated CORM-1 **1-1**. However, the liberation of carbon monoxide from CORM-3 is strongly pH-dependent (**Scheme 1.3**).



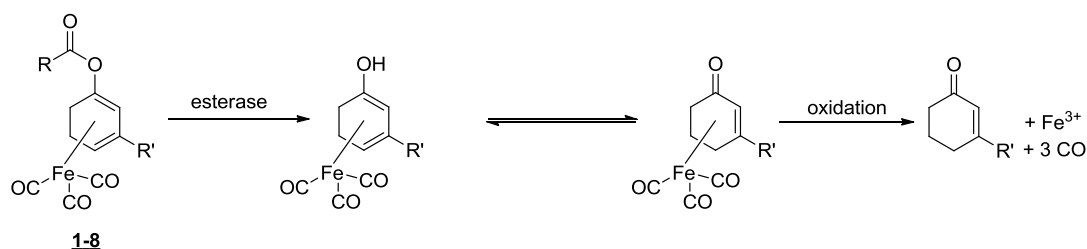
Scheme 1.3: pH-dependent speciation of CORM-3.<sup>[39]</sup>

One carbonyl ligand is already attacked by hydroxide at pH 3, resulting in  $[\text{RuCl}(\text{CO}_2\text{H})(\text{glycinate})(\text{CO})_2]^-$ . Under physiological conditions, mainly two different intermediates of CORM-3,  $[\text{RuCl}(\text{glycinate})(\text{CO})_2]^{2-}$  and  $[\text{Ru}(\text{CO}_2\text{H})(\text{glycinate})(\text{OH})(\text{CO})_2]^-$  are observed. Thus, the interpretation of the biological activity of CORM-3 is difficult, which clearly demonstrates the need for CO-releasing molecules with better controlled mechanisms for the liberation of carbon monoxide under physiological conditions.<sup>[39]</sup> When CORM-3 is treated with hydrochloric acid, the glycinate ligand is protonated at the carboxylate group, and changes to a monodentate binding mode. The generated free coordination site is then occupied by a chloride ligand. This

conversion from bidentate to monodentate glycinate was observed by several  $^{13}\text{C}$  and  $^{15}\text{N}$  NMR experiments, which also showed different pH dependent isomers.<sup>[39]</sup>

### 1.3.2 Enzyme-triggered CO-releasing molecules

In ligand-exchange triggered CORMs, the liberation of CO from the metal coordination sphere starts immediately after they are dissolved in medium. Thus, the target tissue which can be reached depends on the half-life of the compound in the circulatory system. Recent work in the field concentrates on compounds which are stable in serum to reach the desired location in the body to release CO after specific initiation mechanisms.<sup>[40]</sup> In the last decade, the group of Schmalz introduced a novel class of *enzyme-triggered CORMs* (ET-CORMs). The lead structure of these ET-CORMs is an iron(0) tricarbonyl group with a dienol coligand. The latter is functionalized with groups such as esters or phosphates, which stabilize it in the dienolate form which acts as an  $\eta^4$ -ligand to the  $\text{Fe}(\text{CO})_3$  center. The enzymatic cleavage of the relevant C-O or P-O bonds by esterases or phosphatases leads to a change in the hapticity from  $\eta^4$  to  $\eta^2$  due to the generation of the enone (**Scheme 1.4**).<sup>[48]</sup> The resulting labile 16-electron enone complex decomposes upon air oxidation to ferric iron, the enone ligand and three equivalents of carbon monoxide.<sup>[49]</sup> In addition, the dienol coligands enable promising ways of functionalization for better tissue specificity of the iron(0) tricarbonyl ET-CORMs.<sup>[50]</sup>



**Scheme 1.4:** CO-release from enzyme-triggered iron(0) tricarbonyl CO-releasing molecules.<sup>[47]</sup>



### 1.3.3 Photoactivatable CO-releasing molecules

Metal complexes in which the biological activity can be controlled by light have been in the focus of investigation for about 25 years. For example, in photoactivated chemotherapy (PACT), platinum(IV) compounds such as **1-9** are investigated which can be photochemically reduced to the active platinum(II) form which has a similar activity profile on cancer cells as cisplatin (**Fig. 1.7**).<sup>[51]</sup>

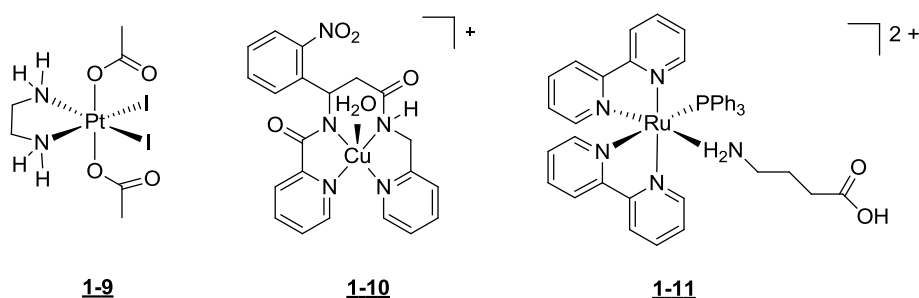


**Figure 1.7:** Three selected examples of photoactivatable metal complexes with biological activity.<sup>[51]</sup>

Another line of research focuses on the photochemical liberation of bioactive metal ions or ligands. These dark-stable transition metal complexes allow a tight temporal and local control of the biological activity.<sup>[52],[53]</sup> The Cu(II) complex **1-10** is related to purely organic “caged” compounds.<sup>[54]</sup> Photoactivation at 350 nm results in the liberation of copper(II) ions which promote the generation of reactive oxygen species (ROS) in the target tissue.<sup>[55]</sup> The ruthenium(II) compound **1-11** is an example of a glutamate delivery system which is an important neurotransmitter. The “caged” glutamate is released by one-photon absorption at 532 nm or two-photon absorption at 800 nm. Due to the Ru(bpy)<sub>2</sub> photosensitizer moiety, liberation of glutamate with visible light is possible.<sup>[56],[57]</sup> A large pool of such compounds with different photosensitizer coligands was prepared, including bipyridine ligands and large porphyrin systems.<sup>[58]</sup> For clinical applications, the excitation wavelength should be in the phototherapeutic window from 600 to 1200 nm which also draws interest to two-photon absorption. While high-energy ultraviolet or blue light can be potentially damaging to tissues and cells, it also has a low tissue-penetration depth. On the other hand, low-

energy red light is reach into skin several millimeters deep (**Fig. 1.8**).<sup>[51]</sup> The concept of photo-induced biological activity was first transferred to *CO-releasing molecules* by Ford.<sup>[59]</sup> In that context, metal carbonyl compounds are sought which show long-time stability in aqueous solution in the dark but can be used for light-triggered carbon monoxide release.

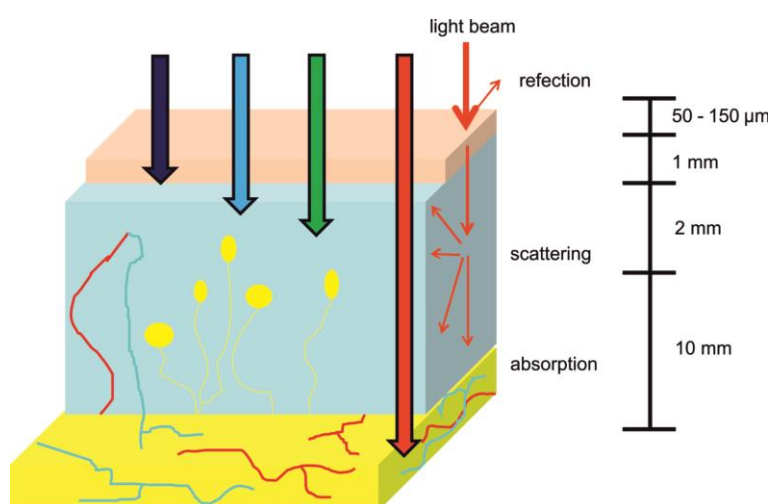
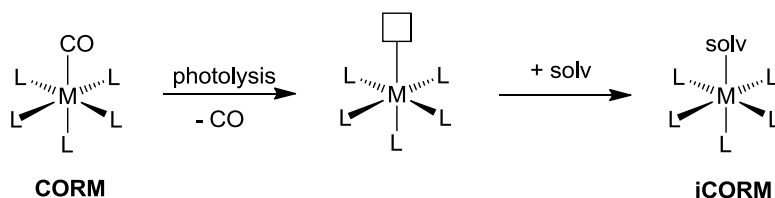


**Figure 1.8:** Inverse correlation tissue-penetration depth and illumination wavelength.<sup>[60]</sup>

Such *photoactivatable CO-releasing molecules* (PhotoCORMs) will enable an exact temporal control of the biological activity. Also, tissue specificity of the CO liberation can be achieved by focused illumination. However, the light-induced release of carbon monoxide from PhotoCORMs always results in generation of a metal-coligand fragment (iCORM) which might have a biological activity of its own (**Scheme 1.5**).



**Scheme 1.5:** General mechanism of the CO-release from PhotoCORMs and formation of iCORM.<sup>[51]</sup>

Upon illumination, a carbonyl ligand is released from the coordination sphere of the metal complex, generating a free coordination site. The liberated carbon monoxide usually leaves the coordination sphere without rebinding and is transferred to its specific target in the tissue, while the free coordination site

becomes occupied by solvent.<sup>[51]</sup> Thus, the design of the PhotoCORM is very important for an efficient liberation process. Ideally, the compound carries photoactive coligands.<sup>[61]</sup> Due to an energy transfer from the photoactive ligand to the transition metal, the strength of the  $\pi$ -backbonding to the carbonyl ligands is decreased, which facilitates release of the carbon monoxide (**Fig. 1.9**).<sup>[61]</sup>

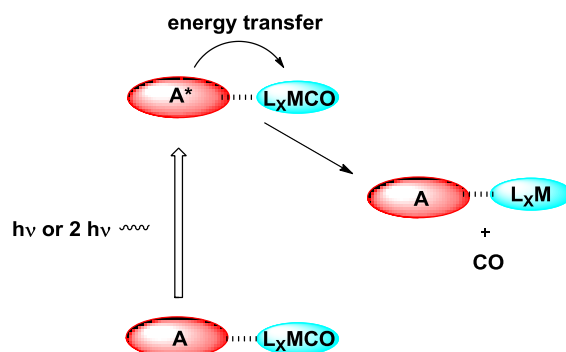


**Figure 1.9:** Mechanism of light-triggered carbon monoxide release from a sensitized PhotoCORM.<sup>[61]</sup>

In 2002, Motterlini reported the photolytic CO release from CORM candidates dimanganese decacarbonyl **1-1** and iron pentacarbonyl **1-12** (**Fig. 1.10**). Due to their poor bioavailability, high general toxicity, and lack of options for further modification, the focus however initially shifted to ligand-exchange triggered CORMs. In 2008, Schatzschneider introduced the tris(pyrazolyl)methane (tpm) manganese(I)tricarbonyl complex **1-13**, which has a broad absorption at around 365 nm and shows long term stability in aqueous buffer solution in the dark. Upon photoactivation, two equivalents of carbon monoxide are released per metal center. The accumulation in cancer cells were studied by Raman microscopy.<sup>[62]</sup> The preparation of Mo(0) tetracarbonyl complexes **1-14** led to a redshift of the excitation maxima of 500 nm.<sup>[63],[64]</sup> The group of Kurz prepared related compounds based on bis(pyrazolyl)acetate ligands such as **1-15**. Investigation with UV/VIS, IR and EPR spectroscopy verified the stepwise release of carbon monoxide. Excitation with UV light at 368 nm led to release of only one CO ligand. In the second step, the two remaining carbonyl ligands are released as the manganese(I) center is oxidized to manganese(II). Finally, an additional oxidation step and dimerization leads to

a bis( $\mu$ -oxo)Mn(III, III) moiety.<sup>[65]</sup> Manganese- and rhenium carbonyl complexes with phosphine bridged ligands **1-16** and **1-17** were reported by Kunz and co-workers. The imidazole-based ligands are centered by a phosphorus atom which binds additional heteroatoms. The release of carbon monoxide is induced by photoactivation with UV light while these compounds are stable in buffered aqueous solutions in the dark.<sup>[66]</sup>

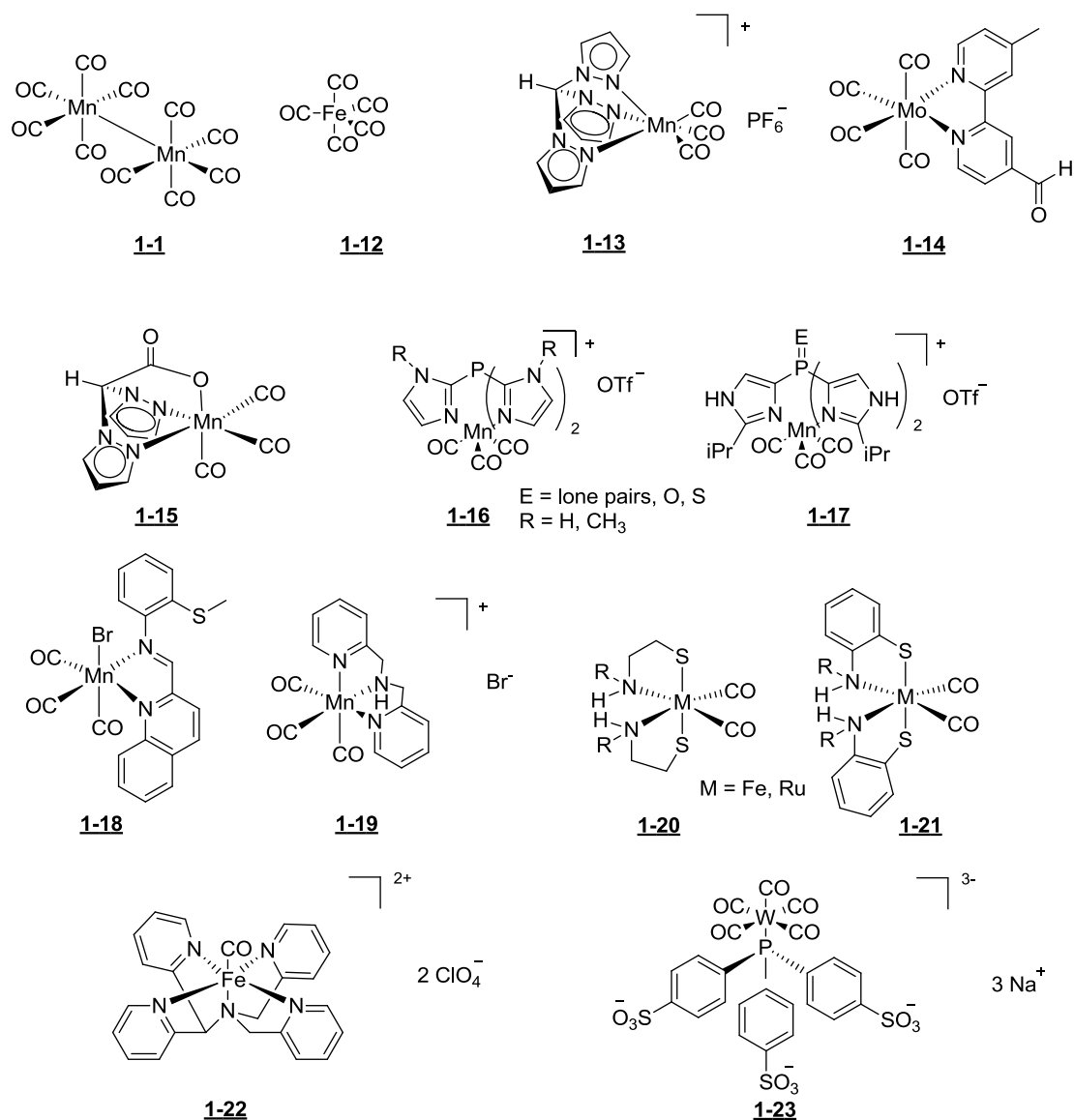


Figure 1.10: Selected examples of PhotoCORMs.<sup>[51, 61, 63-64, 67]</sup>

Manganese(I)tricarbonyl complexes **1-18** and **1-19**, with bis(2-pyridylmethyl)amine, tris(2-pyridyl)amine or (2-pyridylmethyl)(2-quinolylmethyl)amine ligand systems were published by Mascharak (Fig. 1.10).<sup>[68]</sup> The mono-cationic manganese(I) compounds are mostly isolated

as perchlorate salts.<sup>[69],[70]</sup> While they are stable in aqueous solutions, photoactivation at 350 nm leads to release of all three equivalents of carbon monoxide.<sup>[71],[72]</sup> The exchange of the pyridine groups for a quinoline moiety as well as introduction of additional heteroatoms to the ligands caused a red shift of the absorption maximum to the visible.<sup>[73]</sup> The group of Westerhausen presented iron(II)- and ruthenium(II)dicarbonyl complexes **1-20** and **1-21** with sulfur-containing amine ligands. These compounds are synthesized by deprotonating the thiol moiety of the cysteamine and addition to respective trimetal dodecacarbonyls. Studies of the photolytic CO release showed that the absorption maxima of the iron(II) compounds are in the visible range at 470 nm in contrast to the ruthenium analogs, which required UV light from a mercury lamp to induce CO release.<sup>[74]</sup> In contrast, the synthetic pathway of the N<sub>4</sub>Py-iron(II)carbonyl complexes **1-22** published by Kodanko in 2011 is quite unusual for the preparation of a PhotoCORM. The cationic complex is synthesized by bubbling a solution of the ligand and iron(II) perchlorate in organic solvents or water with carbon monoxide gas. The compounds are isolated as perchlorate salts and are stable in aqueous solutions under exclusion of light ( $t_{1/2} < 1$  d). Illumination with UV light at 365 nm causes a very fast release of the single carbon monoxide from the metal coordination sphere.<sup>[67]</sup> The tris(sulphonatophenyl)phosphine tungsten(0)pentacarbonyl **1-23** published by Ford was the first compound termed PhotoCORM for molecules with the ability of a photolytic CO release. The anionic complex is isolated as the sodium salt and shows stability in solution for several hours under exclusion of light. Due to the tris(sulphonatophenyl)phosphine ligand, the compound dissolves well in water. Upon illumination at 300 to 370 nm, one carbonyl ligand is released photolytic from the coordination sphere. In the presence of oxygen, the resulting  $[W(CO)_4(H_2O)(TPPTS)]^{3-}$  species releases two additional equivalents of carbon monoxide in a slow dark reaction.<sup>[75]</sup>

### 1.3.4 Target specificity of CORMs

Another important issue for a therapeutically application of CO delivery systems is the selective accumulation of CORM in the target tissue. Therefore, a number of metal carbonyl complexes were conjugated to delivery vectors (**Fig. 1.12**).<sup>[76]</sup>

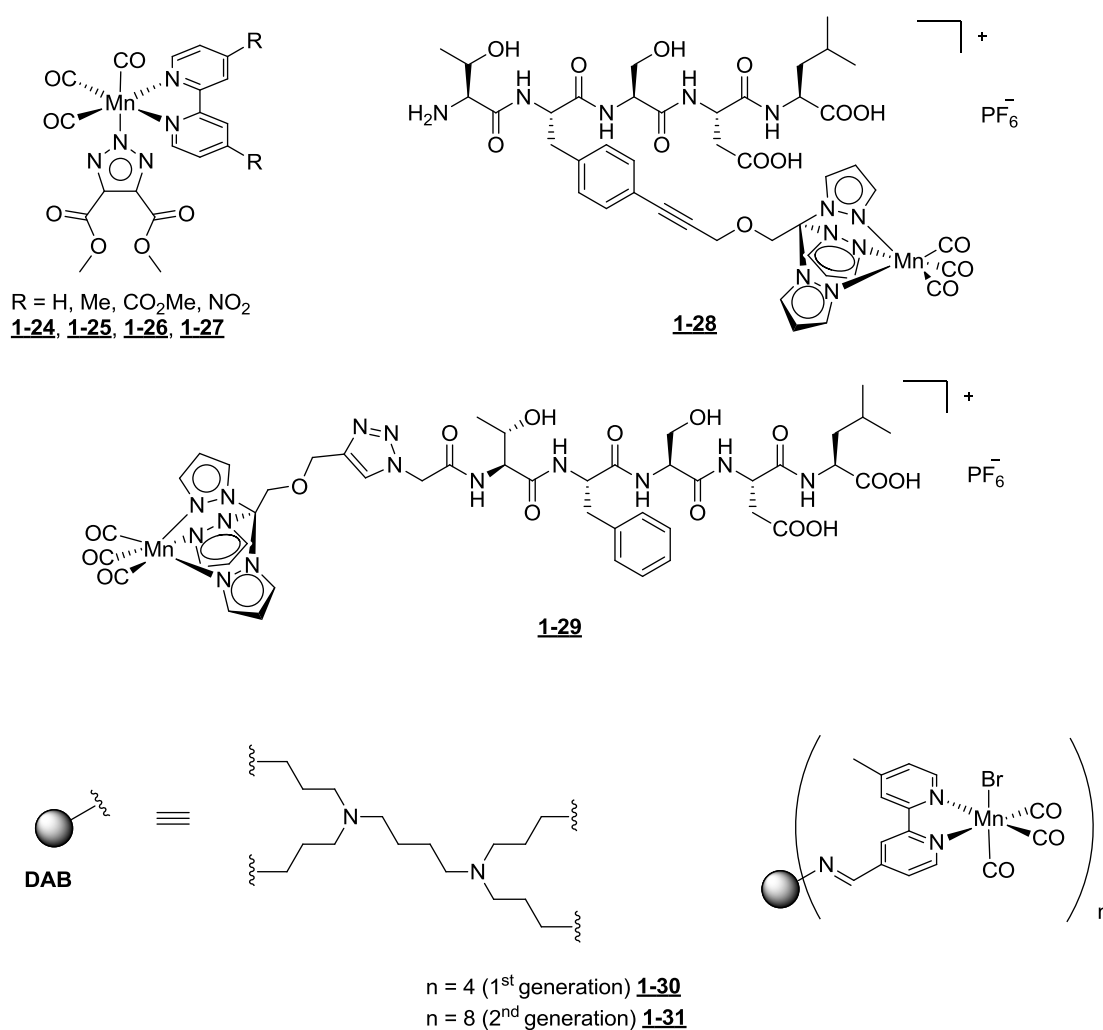


**Figure 1.12:** Functionalized Mn(I)(CO)<sub>3</sub> PhotoCORMs with triazolate ligands, peptide conjugates<sup>[77]</sup> and first and second diaminobutane (DAB) dendrimer conjugates.<sup>[78]</sup>

For the synthesis of these conjugates, several different bioorthogonal reactions such as Sonogashira coupling and copper-catalyzed or copper-free azide-alkyne „click“-reactions were used. In this kind of reaction, azides react with alkynes or nitriles to form triazols or tetrazols. Due to the toxicity of copper ions to cells, the copper-free reaction of azides with alkynes of extreme low electron density seems to be very promising. Therefore, several investigations

with dimethyl acetylene dicarboxylate (DMAD) were carried out on Mn(I)(CO)<sub>3</sub> PhotoCORMs. Also, alkynes with strongly electron withdrawing trifluoromethyl moieties are promising for this kind of reaction. Click chemistry is a mild way to functionalize PhotoCORMs with amino acids<sup>[79]</sup> or carrier-peptides, which are recognized by receptors in the target tissue.<sup>[77]</sup> Another concept is the conjugation of PhotoCORMs to silica nanoparticles. In this case, the copper-catalyzed 1,3-dipolar azide-alkyne cycloaddition (CuAAC) reaction was used.<sup>[80]</sup> Passive accumulation of nanoparticles in tumor tissue as the result of the “enhanced permeability and retention” (EPR) effect, was also studied and published.<sup>[81]</sup> Furthermore, the usage of dendrimers as delivery agents was developed, which also accumulate in tumor tissue due to the EPR effect.<sup>[82]</sup> These diaminobutane (DAB) dendrimers **1-30** and **1-31** were functionalized with Mn(I)(CO)<sub>3</sub> moieties and liberate up to 15 moles of carbon monoxide per dendrimer molecule, during illumination with a 410 nm LED cluster.<sup>[78]</sup>

## 2 Motivation

Although to the general public, carbon monoxide is usually only known as a highly toxic gas, it is now also well-established as a small signaling molecule endogenously produced in higher organisms, including humans, by the degradation of heme by heme oxygenase (HO) enzymes. Besides its cytoprotective activity in response to oxidative stress, the toxicity on cancer cells and pathogenic microorganisms can also be utilized therapeutically. In that context, metal carbonyl complexes are explored as easy-to-handle CO delivery systems. However, studies on the biological activity of such *CO-releasing molecules* (CORMs) have been hampered by the formation of a metal-coligand fragment, termed *inactivated CORM* (iCORM), in addition to the carbon monoxide liberated. The iCORMs can react with solvent and/or bio(macro)molecules to form bioactive side products and thus obliterate the effects due to the CO itself. As a novel strategy to circumvent these problems, in the present thesis, polydentate ligands with additional functional groups were developed which are to bind to the free coordination sites generated by the departing CO, and thus give rise to iCORM products of well-defined composition, which can also be independently prepared for use as controls in biological testing. This work is focused on *photoactivatable CO-releasing molecules* (PhotoCORMs). These dark-stable pro drug compounds release CO ligands only when illuminated at a specific wavelength and therefore allow precise temporal and spatial control of the biological activity. Since the tissue penetration depth of light is inversely correlated to the illumination wavelength and energy-rich light can cause tissue damage, the absorption maximum of PhotoCORMs should be in the “phototherapeutic window” between 600 and 1200 nm. Thus, a series of heterobinuclear manganese/ruthenium PhotoCORMs was to be explored to shift the excitation wavelength to the red part of the UV/Vis spectrum. Finally, nitric oxide also acts as a small messenger molecule in higher organisms, with its signaling pathways in crosstalk with those of carbon monoxide. Thus, to



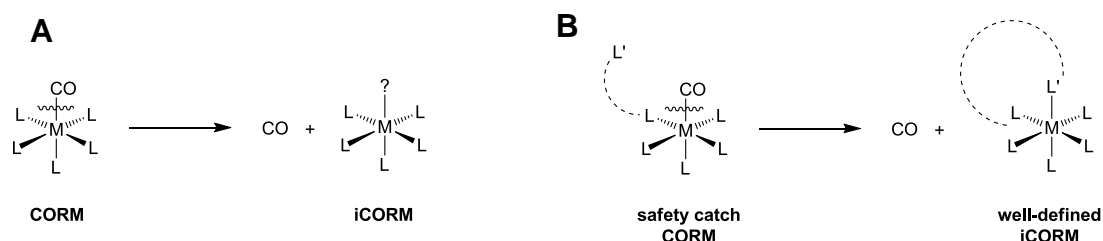
explore the potential selective dual-mode phototriggered CO- and NO-release from a single carrier molecule, a mixed-ligand molybdenum-based *CO/NO-releasing molecule* was evaluated for the first time.

## 3 Results and Discussion

### 3.1 PhotoCORMs with tetradentate ligands

#### 3.1.1 Synthesis of tetradentate ligands

In most photoactivatable CO-releasing molecules (PhotoCORMs) reported to date, side-reactions of inactivated CORM (iCORM) products can result in non-CO-mediated biological activity. Thus, polydentate ligands with additional functional groups initially uncoordinated to the metal center were prepared which can bind to the free coordination sites subsequently generated by the CO liberated, and give rise to iCORM products with well-defined composition (**Scheme 3.1**).



**Scheme 3.1:** (A) CO-release from established CORMs leading to undefined iCORMs. (B) CO-release from safety-catch CORMs resulting in well-defined „inactivated CORMs“ (iCORMs).

As a starting point for this project, the tetradentate ligands shown in **Fig. 3.1** were selected for coordination to a *fac*-Mn(CO)<sub>3</sub> moiety which had previously been established as a PhotoCORM lead structure in the group.<sup>[83]</sup>

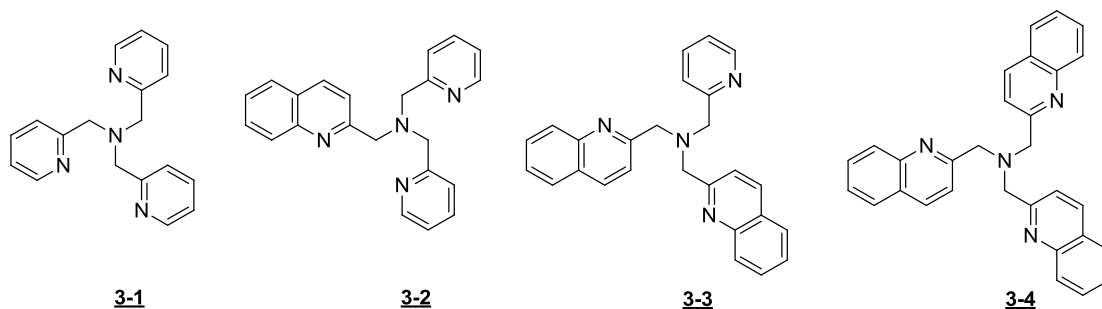
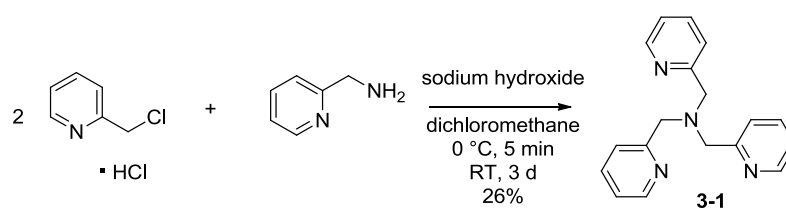


**Figure 3.1:** Tetradentate ligands tris(2-pyridylmethyl)amine (tpa) **3-1**, bis(2-pyridylmethyl)(2-quinolylmethyl)amine (bpqa) **3-2**, bis(2-quinolylmethyl)(2-pyridylmethyl)amine (bqpa) **3-3** and tris(2-quinolylmethyl)amine (tmqa) **3-4** to be used in the preparation of Mn(CO)<sub>3</sub> based PhotoCORMs.

They are expected to coordinate in a tridentate fashion to a metal-tricarbonyl group, thus leaving one donor group uncoordinated. A series of four ligands was prepared to study the influence of increasing number of quinolinyl groups on the UV/Vis spectrum and CO release properties as well as lipophilicity (**Fig. 3.1**).

## 3.1.1.1 Synthesis of tris(2-pyridylmethyl)amine (tpa)

All four ligands were synthesized by published procedures.<sup>[84]</sup> Briefly, to prepare tris(2-pyridylmethyl)amine (tpa) **3-1**, 2-pyridylmethylchloride hydrochloride was dissolved in water and neutralized by addition of sodium hydroxide. Then, 2-pyridylmethylamine in dichloromethane was added and the reaction mixture stirred for 3 d at room temperature. After separation of the organic phase and removal of the solvent, the crude product was obtained as a brown residue which was extracted with hot diethylether. The product was then obtained in moderate yield as colorless to yellowish needles by cooling to 8 °C (**Scheme 3.2**).<sup>[85]</sup>



**Scheme 3.2:** Synthesis of tris(2-pyridylmethyl)amine (tpa) **3-1**.

The <sup>1</sup>H NMR spectrum of **1** shows one singlet at 3.92 ppm with an intensity of 6H as well as two multiplets in the range of 7.11 to 7.18 and 7.56 to 7.70 ppm and a doublet at 8.53 ppm, which integrate to 3H, 6H, and 3H, respectively (**Fig. 3.2**).

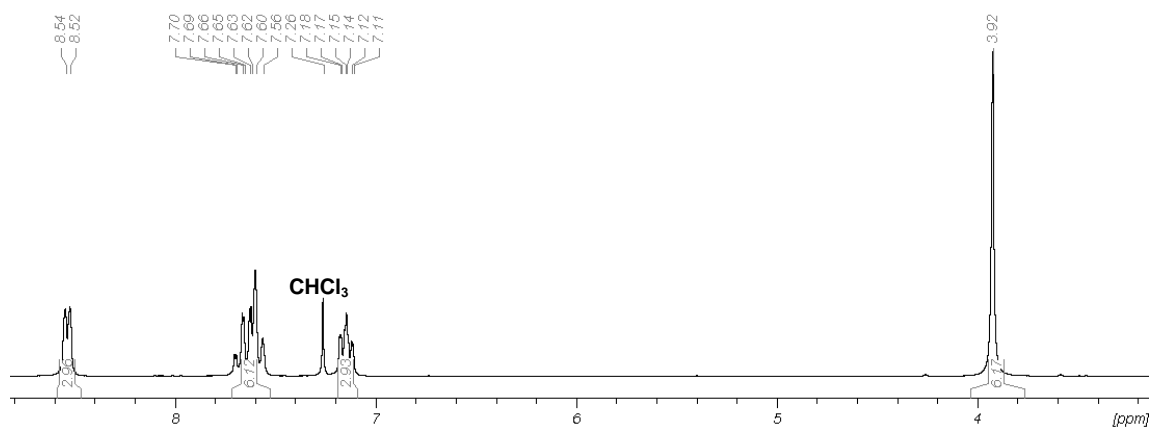


**Figure 3.2:** <sup>1</sup>H NMR spectrum (199.93 MHz, CDCl<sub>3</sub>) of **3-1**.

The singlet at 3.92 ppm is due to the six protons of the three equivalent methylene groups. The multiplet at 7.11-7.18 ppm is assigned to the protons in 5-positions of the pyridine ring with the  $^3J$ -coupling to H6 and H4 unresolved while the multiplet at 7.66 ppm result from the overlap of the doublet of the H3- and the pseudo-triplet of the H4-protons. The doublet appearing the furthest downfield at 8.53 ppm with  $^3J = 4.8$  Hz is assigned to the H6-protons of the pyridine ring due to the closeness to the nitrogen heteroatom.

The  $^{13}\text{C}\{^1\text{H}\}$  NMR shows one signal in the aliphatic region at 60.1 ppm and five signals in the aromatic region at 122.0, 122.9, 136.4, 149.1 and 159.3 ppm (**Fig. 3.3**).

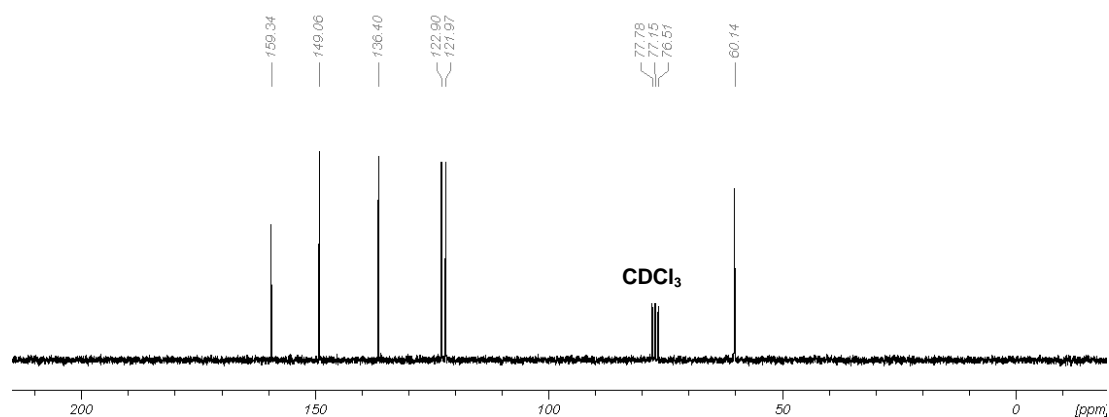
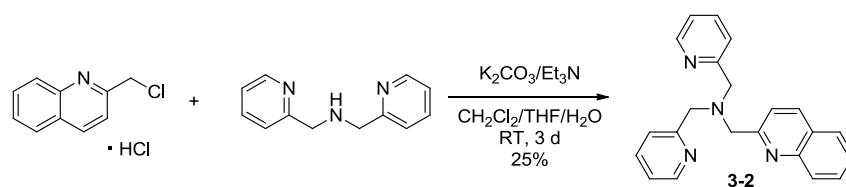


**Figure 3.3:**  $^{13}\text{C}\{^1\text{H}\}$  NMR spectra (50.27 MHz,  $\text{CDCl}_3$ ) of **3-1**.

The peak at 60.1 ppm is assigned to the three equivalent methylene carbon atoms. In the aromatic region of the spectrum, the signals at 122.0 and 122.9 ppm are due to of the C5- and C3-atoms of the pyridine ring. The signal at 136.4 ppm is assigned to the C4-atom. It is shifted more downfield due to the ring nitrogen atom in the *para*-positions. At 149.1 ppm, the signal of the C6-atoms is strongly shifted downfield because of the neighboring ring nitrogen atom, as is the signal of the quaternary C2-atoms, which appears at 159.3 ppm with significantly lower intensity. These results fit well with the data reported by Tyeklár et al.<sup>[85]</sup>

## 3.1.1.2 Synthesis of bis(2-pyridylmethyl)(2-quinolylmethyl)amine (bpqa)

Following a literature procedure, bis(2-pyridylmethyl)(2-quinolylmethyl)amine (bpqa) **3-2** was synthesized by neutralization of 2-chloromethylquinoline hydrochloride in aqueous solution with an excess of potassium carbonate.<sup>[84]</sup> The free chloride was extracted with dichloromethane and the solution was immediately used in the further reaction. Separately, bis(2-pyridylmethyl)amine was dissolved in a mixture of tetrahydrofuran and triethylamine (50 : 1 v/v). After addition of the neutralized 2-chloromethylquinoline in dichloromethane, the mixture was stirred for 3 d. After removal of the solvent mixture, the resulting brown residue was purified by column chromatography on alumina with ethyl acetate as the eluent. Product **3-2** was obtained as yellowish crystals upon standing in moderate yield (**Scheme 3.3**).



**Scheme 3.3:** Synthesis of bis(2-pyridylmethyl)(2-quinolylmethyl)amine (bpqa) **3-2**.

The <sup>1</sup>H NMR of **3-2** shows two singlets in the aliphatic region at 3.92 and 4.04 ppm with a 2:1 intensity ratio. The aromatic region of the spectrum is rather complicated. At low field, a ddd-signal appears at 7.15 ppm with an integral of 2H followed by a multiplet at 7.43-7.83 ppm with an intensity of 8H. Two additional doublets are observed at 8.04 and 8.11 ppm with an integral of 1H each. Finally, a doublet with a strong downfield shift appears at 8.53 ppm with an intensity of 2H. The two singlets at 3.92 and 4.04 ppm are assigned to the methylene groups of the two pyridine arms and the quinoline moiety, respectively based on their intensities. The ddd-signal at 7.15 ppm is due to the H5 protons of the two equivalent pyridine rings. The broad unresolved multiplet at 7.43-7.83 ppm results from the overlap of several different signals of the pyridine and quinoline moieties. The two doublets at 8.04 and 8.11 ppm are assigned to the H7- and H4-protons of the quinoline

ring while the doublet at 8.53 ppm with  $^3J = 4.7$  Hz results from the H6 atoms of the pyridine groups (**Fig. 3.4**). The  $^{13}\text{C}\{^1\text{H}\}$  NMR of **3-2** shows two peaks in the aliphatic region at 60.3 and 60.9 ppm. In the aromatic region, fourteen peaks are found at 121.0, 122.0, 123.1, 126.2, 127.4, 127.5, 129.1, 129.4, 136.4, 136.4, 147.6, 149.1, 159.3 and 160.2 ppm (**Fig. 3.5**).

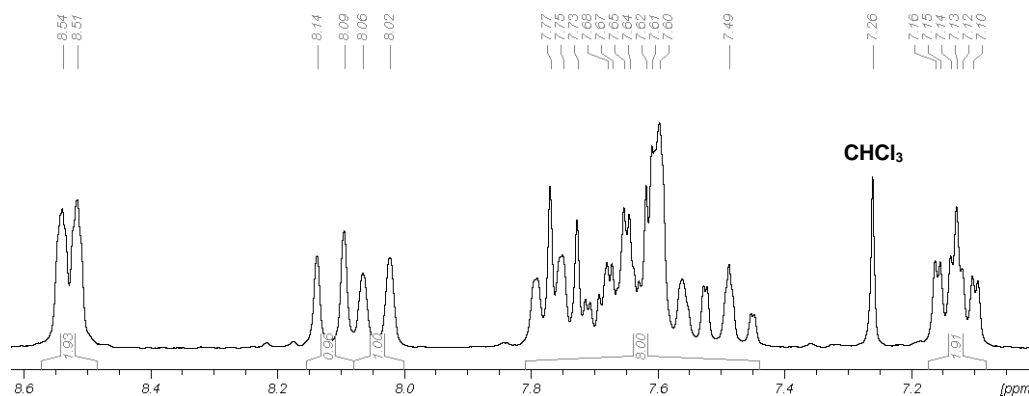


**Fig. 3.4:** Aromatic region of the  $^1\text{H}$  NMR spectrum (199.93 MHz,  $\text{CDCl}_3$ ) of **3-2**.

Thus, the  $^{13}\text{C}\{^1\text{H}\}$  NMR of **3-2** shows the expected sixteen peaks of the product as well as the peaks of small amounts of a diethyl ether impurity at 15.3 and 65.9 ppm. In the aliphatic region, the methylene signal of the two equivalent pyridylmethyl moieties is found at 60.3 ppm while the one at 60.9 ppm is due to the methylene carbon atom of the quinoline arm. The more intense signals in the aromatic region of the spectrum are due to the two identical pyridyl groups. Those at 122.0, 123.1 and 136.4 ppm are assigned to the carbon atoms in 5-, 3-, and 4-positions. The remaining two signals at 149.1 and 159.3 ppm are due to the pyridyl carbon atoms in the 6- and 2-positions, respectively. The strong downfield shift is due to the neighboring ring nitrogen atoms. The assignment of these signals is based on from comparison with the  $^{13}\text{C}$  data of the tris(2-pyridylmethyl)amine starting material as well as the DEPT135 spectrum of **3-2**.

The remaining eight peaks result from the quinoline moiety. The signals at 121.0, 126.2, 127.5, 129.1, 129.4 and 136.4 ppm represent the C8-, C7-, C10-, C9-, C3-, and C4-atoms. The remaining signals of lower intensity at 127.4, 147.6 and 160.2 ppm are due to the quaternary carbon atoms in the 5-, 6-, and 2-positions.<sup>[84]</sup>

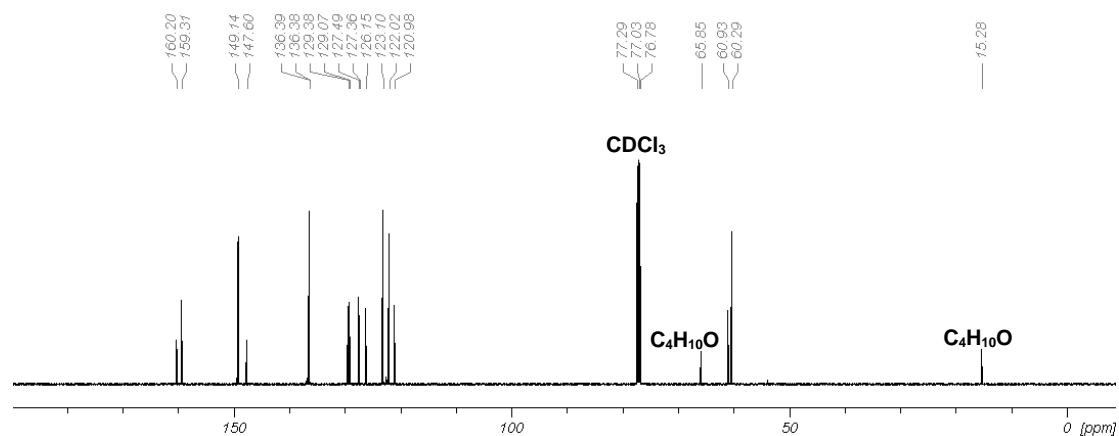
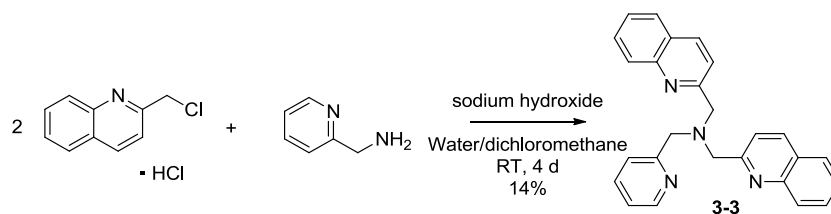


Figure 3.5:  $^{13}\text{C}\{^1\text{H}\}$  NMR spectrum (125.75 MHz,  $\text{CDCl}_3$ ) of **3-2**.



## 3.1.1.3 Synthesis of bis(2-quinolylmethyl)(2-pyridylmethyl)amine (bqpa)

Bis(2-quinolylmethyl)(2-pyridylmethyl)amine (bqpa) **3-3** was synthesized by a procedure similar to the preparation of tris(2-pyridylmethyl)amine (tpa) **3-1**. After neutralization of 2-(chloromethyl)quinoline hydrochloride with sodium hydroxide, the reaction mixture was stirred for 5 min in an ice bath. Then, a solution of 2-pyridylmethylamine in dichloromethane was added and the mixture was allowed to warm to room temperature and stirred for 4 d. The organic phase was separated and dried over magnesium sulfate. After removal of the solvent under vacuum, the brown residue was treated with diethylether, which caused the precipitation of a white solid, which was collected by filtration and dried under vacuum. The product was obtained as white powder in poor yield (**Scheme 3.4**).



**Scheme 3.4:** Synthesis of bis(2-quinolylmethyl)(2-pyridylmethyl)amine (bqpa) **3-3**.

The <sup>1</sup>H NMR spectrum of **3-3** shows two singlets in the aliphatic region at 3.92 and 4.04 ppm with integrals of 2H and 4H, respectively. In the aromatic region, two ddd-signals at 7.15 and 7.50 ppm with integrals of 1H and 2H are observed. A doublet at 7.61 ppm with an intensity of 1H and a un-resolved multiplet at 7.66-7.68 ppm with an integral of 3H are also present. Five additional doublets are observed at 7.77, 7.80, 8.08, 8.14 and 8.56 ppm with an integral ratio of 2:2:2:2:1 (**Fig. 3.6**).

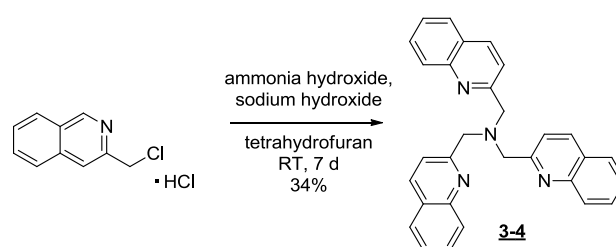
The number of signals as well as their multiplicity in the spectrum of **3-3** is similar to that of **3-2**, but the intensity of the different signal sub-groups is reversed. The ddd-signals at 7.15 and 7.50 ppm with <sup>3</sup>J = 7.4 Hz, <sup>4</sup>J = 4.9 Hz and <sup>5</sup>J = 1.3 Hz as well as <sup>3</sup>J = 8.1 Hz, <sup>4</sup>J = 6.9 Hz and <sup>5</sup>J = 1.2 Hz are due to the H5 atom of the pyridine ring and the H3 protons of the quinoline groups. The doublet at 7.61 ppm with <sup>3</sup>J = 7.9 Hz is due to the H4 atom of the pyridyl ring.



Thus, the  $^{13}\text{C}\{^1\text{H}\}$  NMR of **3-3** shows only fifteen peaks instead of the expected sixteen. In the aliphatic region, the methylene signal of the pyridyl moiety is found at 60.5 ppm while the one at 61.1 ppm is due to the methylene carbon atoms of the two equivalent quinoline arms. By comparison with the NMR data of **3-1** and **3-2**, the signals at 122.1, 123.3, and 136.4 ppm are assigned to the pyridyl carbon atoms in the 5-, 3-, and 4-positions, respectively. The remaining two signals at 149.2 and 159.2 ppm are due to the pyridyl carbon atoms in the 6- and 2-positions. The strong downfield shift is due to the neighboring ring nitrogen atom. The remaining eight peaks result from the two equivalent quinoline moieties. As already seen in the NMR data of **3-2**, the signals at 121.1, 126.2, 127.5, 129.1, and 129.4 ppm represent the C3-, C8-, C7-, C10- and C9-atoms. The remaining signals at 127.4, 147.6, and 160.1 ppm are due to the quaternary carbon atoms in the 5-, 6-, and 2-positions. By comparison with the NMR data of **3-4**, the missing signal from the 4-position of the quinoline moieties seems to overlap with the C4 peak of the pyridyl ring at 136.4 ppm.

## 3.1.1.4 Synthesis of tris(2-quinolylmethyl)amine (tmqa)

For the synthesis of tris(2-quinolylmethyl)amine (tmqa) **3-4**, 2-chloromethylquinoline hydrochloride was dissolved in tetrahydrofuran and stirred at room temperature in the presence of sodium hydroxide and ammonium hydroxide for two weeks. After stirring, a white precipitate formed which was collected by filtration. Removal of the solvent from the filtrate resulted in a brown oil which was washed with water and methanol to obtain more product as a white powder. Both fractions were combined to give **3-4** in moderate yield.<sup>[84]</sup>



Scheme 3.5: Synthesis of tris(2-quinolylmethyl)amine (tmqa) **3-4**.

The <sup>1</sup>H NMR spectrum of **3-4** shows one singlet at 4.13 ppm with an integral of 6H in the aliphatic region. In the aromatic region, a ddd-signals at 7.49 ppm and a un-resolved multiplet at 7.63-7.82 ppm in a 3:9 intensity ratio are observed, as well as two doublets at 8.06 and 8.13 ppm with integrals of 3H each (Fig. 3.8).

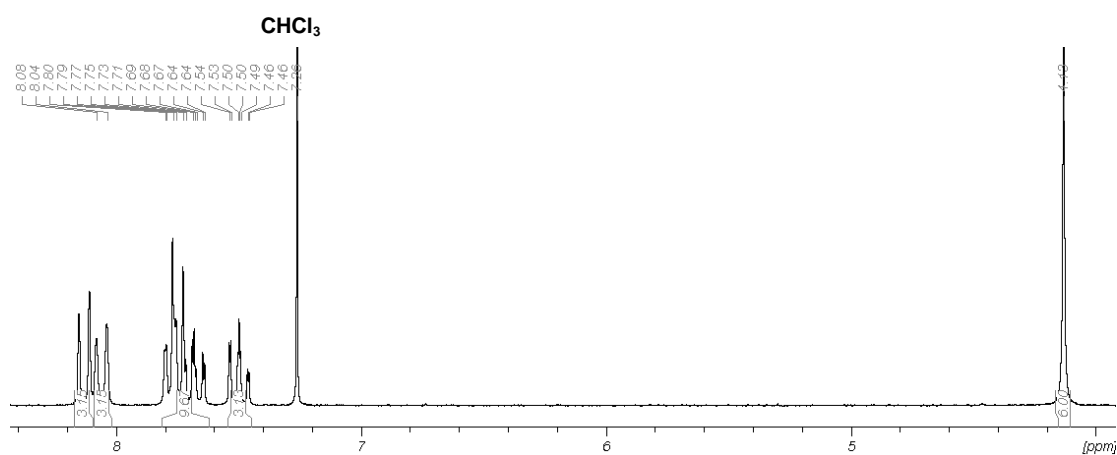


Figure 3.8: <sup>1</sup>H NMR spectrum (199.93 MHz, CDCl<sub>3</sub>) of **3-4**.

The singlet at 4.13 ppm results from the six protons of the three equivalent quinoline methylene groups. In the aromatic region, the ddd-signals at 7.49 ppm is assigned to the H3-protons of the quinoline ring. The multiplet at 7.63-7.82 ppm results from the overlap of the signals of the H8-, H9-, and H10-atoms of the quinoline moiety. The two doublets at 8.06 and 8.13 ppm with  $^3J = 4.5$  Hz belong to the protons in the 8- and 4-positions. Because of the proximity of the ring nitrogen, the H4-atoms are shifted more downfield than the H7-atoms.

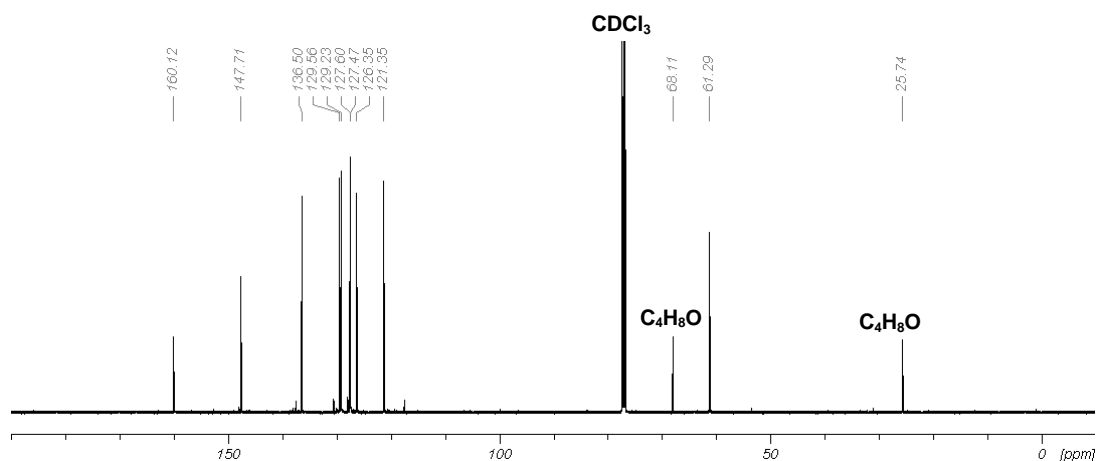


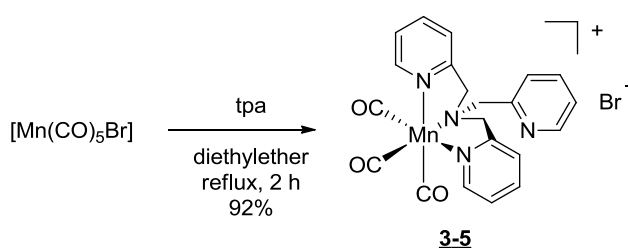
Figure 3.8:  $^{13}\text{C}\{^1\text{H}\}$  NMR spectrum (125.75 MHz,  $\text{CDCl}_3$ ) of **3-4**.

The  $^{13}\text{C}\{^1\text{H}\}$  NMR of **3-4** shows one peak in the aliphatic region at 61.3 ppm, while in the aromatic region, nine peaks are found at 121.4, 126.4, 127.5, 127.6, 129.23, 129.2, 129.6, 136.5, 147.7, and 160.1 ppm (Fig. 3.8). In addition to those expected ten signals, peaks of a tetrahydrofuran impurity are also observed at low intensity at 25.7 and 68.1 ppm. The signal at 61.3 ppm belongs to the equivalent methylene carbon atoms of the quinoline arms. The aromatic signals at 121.4, 126.4, 127.6, 129.2, 129.6 and 136.5 ppm result from the C3-, C8-, C7-, C10-, C9-, and C4-atoms while the signals at 127.5, 147.7, and 160.1 ppm are assigned to the quaternary carbon atoms in the 5-, 6- and 2-positions.

### 3.1.2 Synthesis and characterization of metal complexes

#### 3.1.2.1 Synthesis and characterization of $[\text{Mn}(\text{CO})_3(\text{tpa}-\kappa^3\text{N})]\text{Br}$

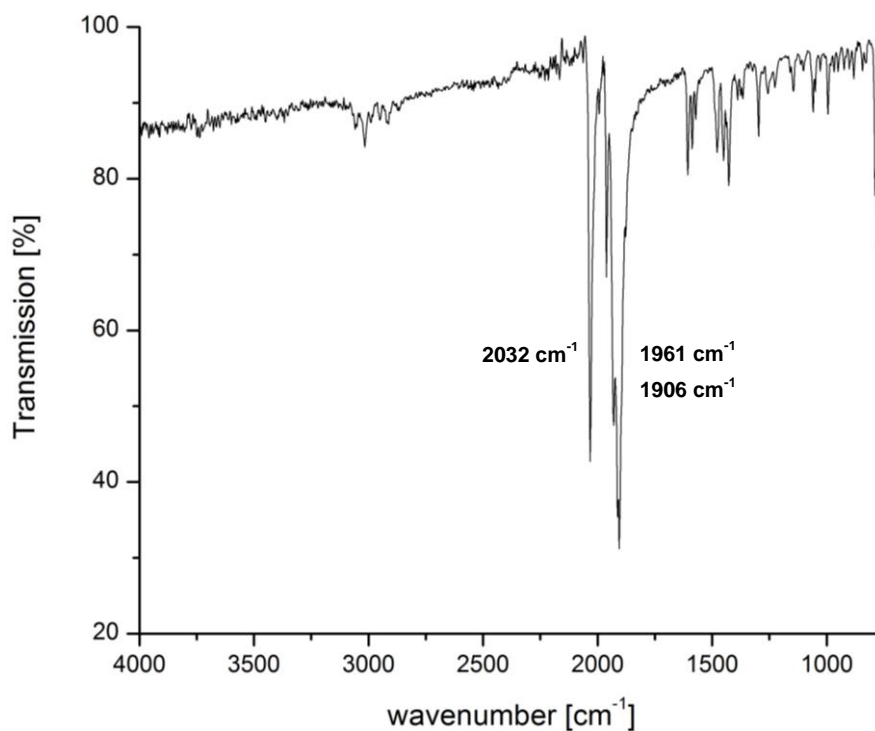
Following the procedure established in the group for the synthesis of tris(pyrazolyl)methane (tpm) manganese(I) tricarbonyl complexes,<sup>[86]</sup> tris(2-pyridylmethyl)amine (tpa) was reacted with manganese pentacarbonyl bromide in diethylether under reflux for 2 h with exclusion of light. During the reaction, the yellow product precipitated from the solution and was isolated without further purification in excellent yield (**Scheme 3.6**).



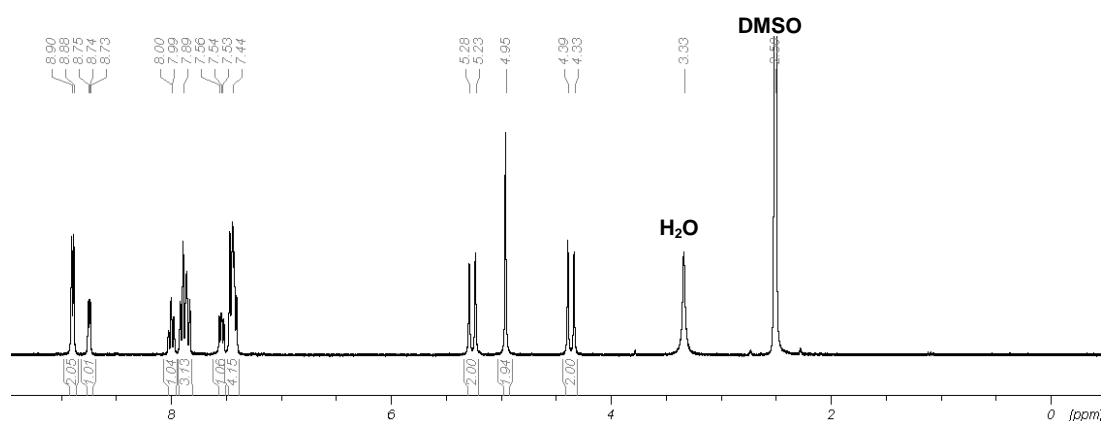
**Scheme 3.6:** Synthesis of  $[\text{Mn}(\text{CO})_3(\text{tpa})]\text{Br}$  **3-5**.

Since a large amount of  $[\text{Mn}(\text{CO})_3(\text{tpa})]\text{Br}$  **3-5** was required for biological testing (see section 3.1.7), the synthesis was scaled up without loss of yield to 3.5 g. Compound **3-5** is soluble in polar solvents such as water, dimethylsulfoxide, acetonitrile and acetone as well as less polar ones such as chloroform and dichloromethane.

The IR spectrum of **3-5** shows three very strong bands at 2032, 1961, and 1906  $\text{cm}^{-1}$ . Furthermore, some medium to weak bands are found at 1606, 1596, 1477, 1449, 1427, 1296, and 780  $\text{cm}^{-1}$  (**Fig. 3.9**). The very intense peak at 2032  $\text{cm}^{-1}$  results from the symmetric stretch while the bands at 1961 and 1906  $\text{cm}^{-1}$  are due to the two antisymmetrical stretching vibrations of the CO ligands. The characteristic band at 780  $\text{cm}^{-1}$  is from the stretching vibration of the C-N amine bond and is found for all four tetradentate ligands. The peaks between 1300 and 1600  $\text{cm}^{-1}$  result from the vibrations of aromatic C-C- and C-N bonds.

Figure 3.9: ATR-IR-spectrum of **3-5**.

The  $^1\text{H}$  NMR spectrum of **5** in  $\text{DMSO-d}_6$  (Fig. 3.10) shows in the aliphatic region two doublets at 4.36 and 5.25 ppm as well as one singlet at 4.95 ppm with integrals of 2H each. The aromatic region shows two sets of signals in a 2:1 ratio. Each set consist of a doublet with a strong downfield shift, two triplets and one additional doublet. Due to partial overlap, only the two doublets at 8.89 and 8.74 ppm with integrals of 2H and 1H, one triplet of a doublet at 8.00 ppm with an integral of 1H and three multiplets at 7.89, 7.54, and 7.44 ppm with integral 3H, 1H and 4H are resolved.

Figure 3.10:  $^1\text{H}$  NMR (300.13 MHz,  $\text{DMSO-d}_6$ ) spectrum of **3-5**.

In the aliphatic region, two doublets and one singlet are found. The singlet at 4.95 ppm results from the two equivalent methylene protons of the uncoordinated pyridylmethyl arm while the two doublets at 5.25 and 4.36 ppm show large geminal couplings of  $^2J = 16.9$  Hz each and thus are due to the inequivalent methylene protons of the two coordinated pyridyl groups, which are fixed in different environments and therefore diastereotopic. This pattern also confirms the tridentate coordination mode of the tpa ligand to the manganese tricarbonyl center and is also found in a similar manner in all other compounds of this series. The two sets of aromatic signals in the  $^1\text{H}$  NMR of **3-5** indicate the presence of two inequivalent pyridyl groups. The two doublets at 8.89 and 8.74 ppm result from the H6 atoms of the coordinated and uncoordinated pyridyl groups of the tpa ligand, respectively. Due to the neighboring pyridine nitrogen atoms, these H6-protons are strongly shifted downfield. Interestingly, the coordination to the  $\text{Mn}(\text{CO})_3$  moiety only leads to a small downfield shift of 0.15 ppm. The doublet splitting results from the  $^3J$ -coupling to the H5-protons. The triplet of a doublet (td) at 8.00 ppm results from the not fully resolved coupling of the H5-atom with the protons in 4- and 6-positions of the free arm. The multiplet at 7.89 ppm is the result of the overlap of the signal for the H5-protons of the coordinated arms as well as the H3 doublet of the uncoordinated pyridylmethyl group. The multiplet at 7.54 ppm results from the H4 of the free arm while the multiplet at 7.44 ppm is the result of the overlapping signals of the H3 triplet and the H4 doublet of the coordinated arm.

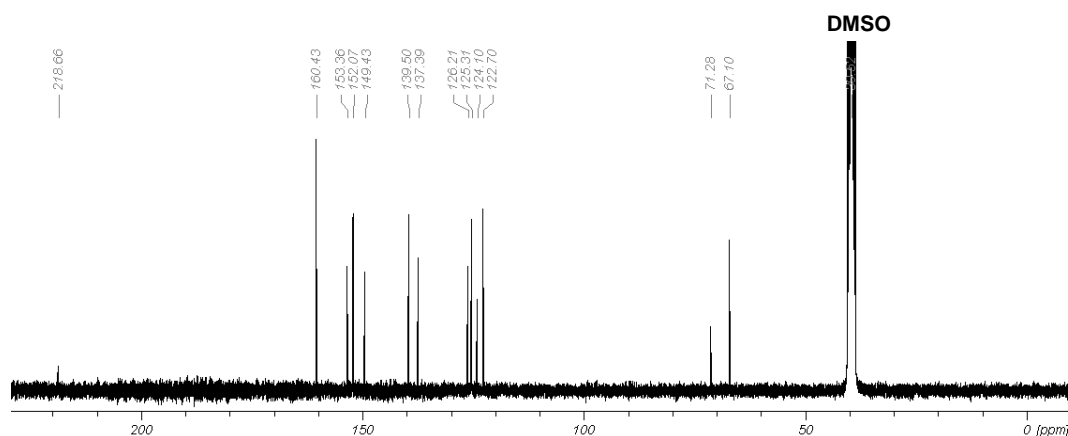


Figure 3.12:  $^{13}\text{C}\{^1\text{H}\}$  NMR (75.47 MHz,  $\text{DMSO-d}_6$ ) spectrum of **3-5**.

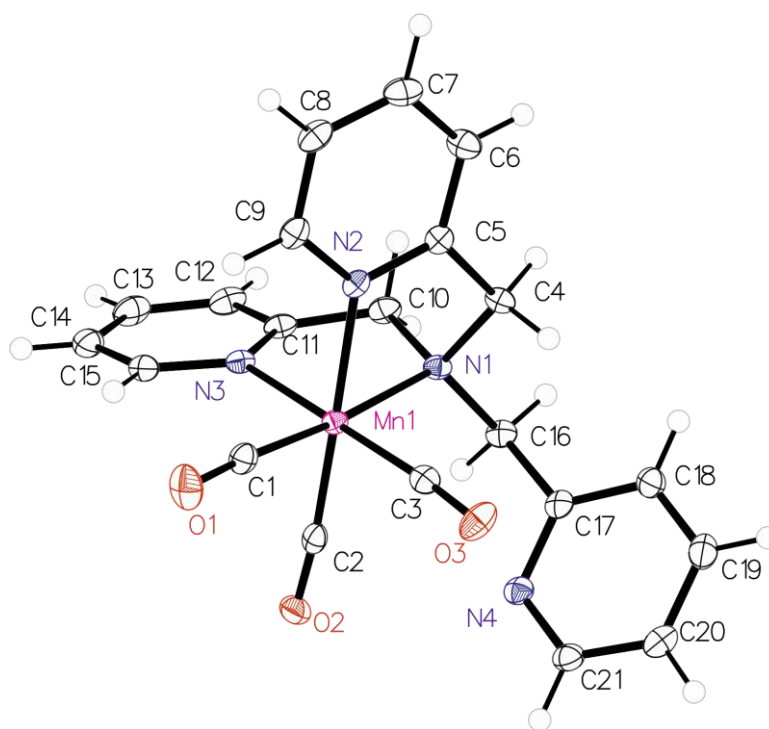


The  $^{13}\text{C}\{^1\text{H}\}$  NMR-spectrum (**Fig. 3.12**) of **3-5** also shows two distinct set of signals. Two peaks are found in the aliphatic region at 67.1 and 71.3 ppm while 10 signals appear in the aromatic region at 122.7, 124.1, 125.3, 126.2, 137.4, 139.5, 149.4, 152.1, 153.4, and 160.4 ppm. Furthermore, the spectrum shows a strongly downfield shifted signal at 218.7 ppm. The two signals in the aliphatic region at 67.1 and 71.3 ppm are due to the methylene groups of the coordinated and the uncoordinated arms of the tpa-ligand, respectively. In the aromatic region, the signals of the different C5- and C3-atoms are observed at 122.7 and 124.1 ppm as well as at 125.3 and 126.2 ppm. At a chemical shift of 137.4 and 139.5 ppm, the signals of the C4-atoms are observed, while the C6-atoms appear at 149.4 and 152.1 ppm due to their proximity to the ring nitrogen. The overlapping quaternary carbons in the 2-positions are shifted even further downfield to 160.4 ppm. At 218.7 ppm, the signal of the three equivalent carbonyl ligands is observed.

In the positive-mode ESI mass spectrum of **5**, signals at  $m/z = 345.09$ ,  $429.08$ , and  $939.07$  Da are observed. At  $m/z = 345.09$  Da, a cation corresponding to  $[\text{M}-3\text{CO}-\text{Br}]^+$  appears which has lost all three carbonyl ligands as well as the bromide upon ionization. The signal at  $m/z = 429.08$  Da results from the complex cation  $[\text{M}-\text{Br}]^+$ . At  $m/z = 939.07$  Da, a cluster cation with a composition of  $[2\text{M}-\text{Br}]^+$  is observed which also shows the typical isotope pattern of bromine-containing compounds.

Single crystals of **3-5** were obtained by slow diffusion of *n*-hexane into a dichloromethane solution of the complex. Compound **3-5** crystallizes in the  $P 2_1/n$  space group (**Fig. 3.13**). The unit cell contains the cationic  $[\text{Mn}(\text{CO})_3(\text{tpa})]^+$  moiety as well as a bromide counterion. The manganese(I) center is in an octahedral coordination sphere with a  $\text{MnN}_3\text{C}_3$  ligand environment. The bond lengths between the carbonyl ligands and the manganese(I) center are nearly equal with values of Mn1-C1 at  $1.790(3)$  Å, Mn1-C2 at  $1.814(2)$  Å, and Mn1-C3 at  $1.800(3)$  Å. The Mn-N bond lengths are  $2.110(3)$  Å for Mn1-N1,  $2.038(2)$  Å for Mn1-N2, and  $2.026(2)$  Å for Mn1-N3. The *trans*-angles between the carbonyl ligands and the nitrogen atoms of the

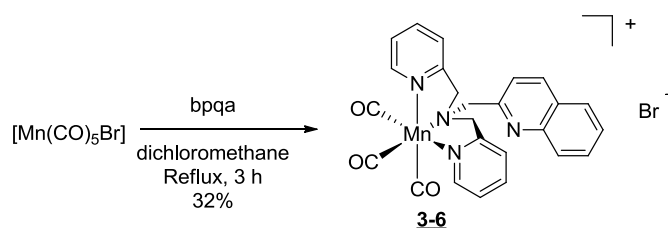
tpa ligand are C1-Mn1-N1 at  $174.57(8)^\circ$ , C2-Mn1-N2 at  $175.82(7)^\circ$  and C3-Mn1-N3 at  $177.55(9)^\circ$  and thus all close to  $180^\circ$ . The angles between the carbonyl ligands are C1-Mn1-C2 at  $87.4(1)^\circ$ , C1-Mn1-C3 at  $86.1(1)^\circ$  and C2-Mn1-C3 at  $89.67(9)^\circ$  and thus close to  $90^\circ$ . The angles between the amine nitrogen and the coordinated pyridyl nitrogen are for N1-Mn1-N3 at  $82.91(7)^\circ$  and N1-Mn1-N2 at  $79.60(6)^\circ$ . Furthermore, the presence of a uncoordinated pyridylmethyl group is clearly confirmed. The N2-Mn1-N3-angle has a value of  $87.48(7)^\circ$ . The crystallographic data are in line with the published structure of  $[\text{Mn}(\text{CO})_3(\text{dpa})]^+$  with dpa = di(2-pyridylmethyl)amine. Although this compound crystallizes in the orthorhombic space group Pnma, the bond lengths and angles are comparable. In particular, the distance between the Mn(I) center and the carbonyl ligands at Mn-C7 of  $1.794(5) \text{ \AA}$ , Mn-C8 of  $1.805(4) \text{ \AA}$  and Mn-C8(A) of  $1.805(4) \text{ \AA}$  are equal to those of the tpa-complex **3-5**. The bond lengths of the coordinated nitrogen atoms and the manganese atom are also equal with values of Mn-N1 at  $2.053(3) \text{ \AA}$ , Mn-N1(A) at  $2.053(3) \text{ \AA}$  and Mn-N2 at  $2.063(4) \text{ \AA}$ .<sup>[73]</sup>



**Figure 3.13:** Molecular structure of  $[\text{Mn}(\text{CO})_3(\text{tpa})]^+$  **3-5** with ellipsoids drawn at the 50% probability level. The bromide counterion is not shown for clarity.

3.1.2.2 Synthesis and characterization of  $[\text{Mn}(\text{bpqa}-\kappa^3\text{N})(\text{CO})_3]\text{Br}$ 

To investigate the influence of a larger  $\pi$ -ligand-system on the photophysical properties of the compounds, bis(2-pyridylmethyl)(2-quinolylmethyl)amine (bpqa) **3-2** was also employed as a ligand. Conditions similar to the synthesis of tpa-complex **3-5** were used. However, manganese pentacarbonyl bromide and bis(2-pyridylmethyl)(2-quinolylmethyl)amine were dissolved in dichloromethane due to poor solubility of the ligand in diethylether and heated to reflux for 3 h. The solvent was partly removed under vacuum and the yellow product precipitated upon addition of diethylether in moderate yield of 32%. The solubility of **3-6** is comparable to that of  $[\text{Mn}(\text{CO})_3(\text{tpa})]\text{Br}$  with exception of water, in which it is less soluble (**Scheme 3.7**).

Scheme 3.7: Synthesis of **3-6**.

The IR spectrum of **3-6** shows three very strong bands at 2027, 1921 and 1913  $\text{cm}^{-1}$ . Furthermore, some medium to weak bands are found at 1609, 1596, 1485, 1440, 1429, 1302, and 761  $\text{cm}^{-1}$  (**Fig. 3.13**). The sharp peak at 2027  $\text{cm}^{-1}$  is assigned to the symmetric and the broader signals at 1921 and 1913  $\text{cm}^{-1}$  to the antisymmetric stretching vibrations of the CO ligands. The C-N stretching vibration of the amine bond is observed at 761  $\text{cm}^{-1}$ . The peaks between 1300 and 1600  $\text{cm}^{-1}$  result from in the stretching vibrations of the aromatic C-C- and C-N bonds.

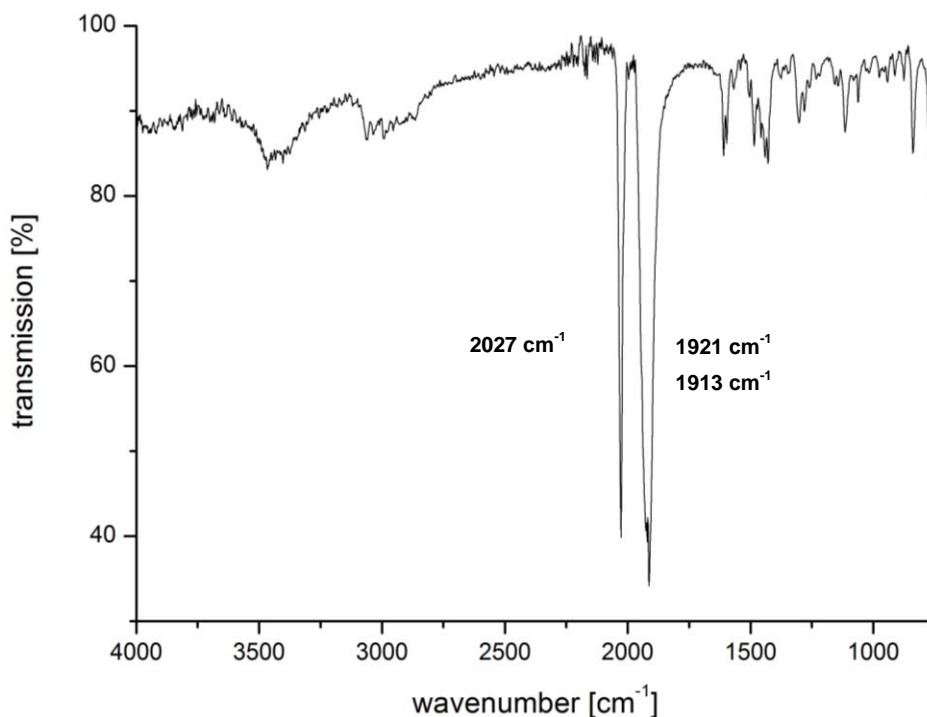


Figure 3.13: ATR-IR spectrum of **3-6**.

In the aliphatic region, the  $^1\text{H}$  NMR of  $[\text{Mn}(\text{CO})_3(\text{bpqa})]\text{Br}$  **3-6** shows a singlet at 5.22 ppm and two doublets at 4.64 and 5.31 ppm with integrals of 2H each, similar to the spectrum of  $[\text{Mn}(\text{CO})_3(\text{tpa})]\text{Br}$  **3-5**. The aromatic region of the spectrum shows a multiplet at 7.44-7.53 ppm with an integral of 4H and two triplets at 7.70 and 7.84 ppm with integrals of 1H each. Another multiplet is observed at 7.89-7.95 ppm with an integral of 3H. Further shifted downfield are four doublets, three at 8.02, 8.08 and 8.55 with integrals of 1H each and one at 8.92 ppm with an integral of 2H (Fig. 3.14).

The two doublets in the aliphatic region at 4.64 and 5.31 ppm with a large geminal splitting of  $^2J = 17.0$  Hz each are assigned to the inequivalent methylene protons of the coordinated pyridyl moieties while the singlet at 5.22 ppm results from the two methylene protons of the uncoordinated quinoline arm. Since the can latter rotate freely, the two protons are chemical equivalent and thus result in a singlet. The multiplet at 7.44 - 7.53 ppm stems from the overlap of the H5 triplet and the H3 doublet signals of the pyridyl moieties. The two triplets at 7.70 and 7.84 ppm with  $^3J = 7.9$  Hz belong to the H8- and H9-atoms of the quinoline group. The multiplet at 7.89-7.95 ppm also

results from an overlap of two signals. At this chemical shift, the H4 doublets of the pyridine rings as well as the H10 doublet of the quinoline ring are expected. The three doublets at 8.02, 8.08 and 8.55 ppm with  $^3J = 8.4, 7.9, 8.4$  Hz, respectively, are assigned to the protons in the 3-, 7-, and 4-positions of the quinoline moiety. The strongly downfield shifted doublet with  $^3J = 5.5$  Hz at 8.92 ppm belongs to the H6-atom of the two equivalent pyridine rings.

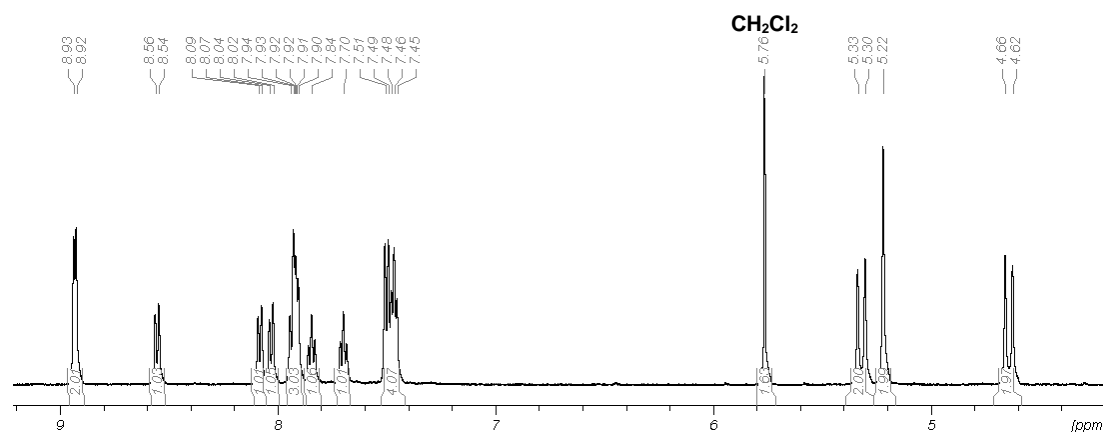


Figure 3.14:  $^1\text{H}$  NMR spectrum (500.13 MHz,  $\text{DMSO-d}_6$ ) of **3-6**.

The  $^{13}\text{C}\{^1\text{H}\}$  NMR spectrum of **3-6** shows a total of eighteen signals (Fig. 3.16). In the aliphatic region, two peaks at 67.4 and 71.3 ppm are found while the aromatic region is comprised of fourteen signals at 122.7, 122.8, 125.3, 127.2, 127.2, 127.1, 129.0, 130.0, 137.2, 139.5, 146.8, 152.1, 154.6, and 160.7 ppm. Further shifted downfield, two additional peaks at 218.5 and 218.8 ppm appear. The signal at 67.4 ppm is due to the two methylene carbon atom of the coordinated pyridyl groups while the one at 71.3 ppm is assigned to the one uncoordinated quinoline group. The aromatic signals with higher intensity are due to the carbon atoms of the two coordinated pyridine rings. At 122.7, 125.3 and 139.5 ppm, the peaks of the C5-, C3-, and C4-atoms of the three groups are observed. The weaker signals at 152.1 and 160.7 ppm result from the quaternary pyridyl ring carbons in the 6- and 2-positions. The remaining nine signals belong to the quinoline moiety. The quaternary C5-, C6-, and C2- atoms of the quinoline moiety were identified in the  $^{13}\text{C}$  DEPT135 spectrum at 127.2, 146.8 and 154.6 ppm. The signals of the CH

groups in the 3-, 8-, 7-, 10-, and 9-positions appear at 122.8, 127.2, 127.9, 129.0, and 130.0 ppm, respectively. The carbon atom in the 4-positions is shifted downfield to 137.2 ppm due to the ring nitrogen in *para*-positions. The signals at 218.5 and 218.77 ppm are assigned to the carbon atoms of the carbonyl ligands.

In the positive-mode ESI-MS of **3-6**, three signals at  $m/z = 284.02$ , 395.11 and 479.09 Da are observed. At  $m/z = 284.02$  Da, a cation is observed with a composition of  $[M-3CO-C_9H_7N+H_2O-Br]^+$  which has lost all three carbonyl ligands as well as the quinoline unit and the bromide replaced by water upon ionization. The signal at  $m/z = 395.11$  Da is due to a cation with the composition of  $[M-3CO-Br]^+$  and at  $m/z = 479.09$  Da, the molecule cation  $[M-Br]^+$  is observed.

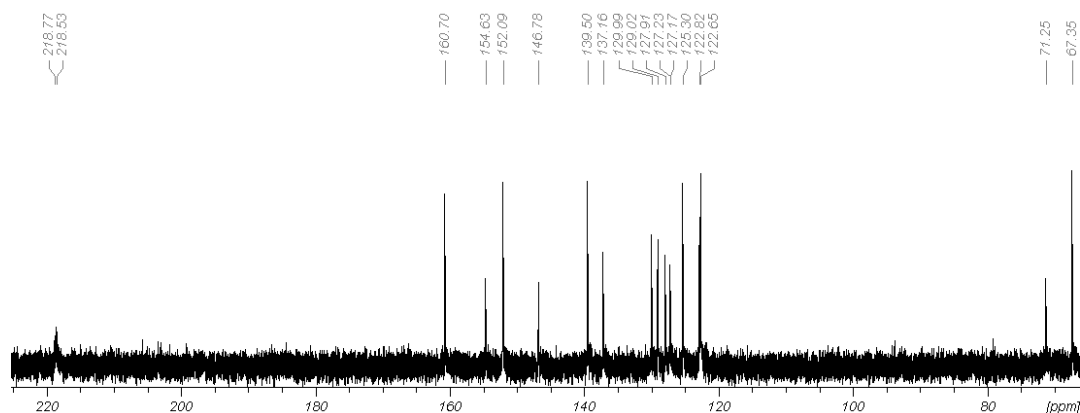
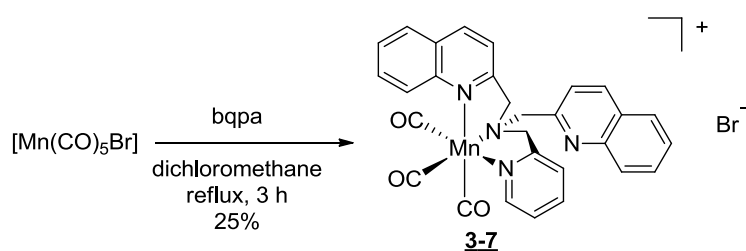


Figure 3.16:  $^{13}C\{^1H\}$  NMR spectrum (125.75 MHz, DMSO- $d_6$ ) of **3-6**.

3.1.2.3 Synthesis and characterization of  $[\text{Mn}(\text{bqpa}-\kappa^3\text{N})(\text{CO})_3]\text{Br}$ 

For the synthesis of  $[\text{Mn}(\text{bqpa})(\text{CO})_3]\text{Br}$  **3-7**, manganese pentacarbonyl bromide and bis(2-quinolylmethyl)(2-pyridylmethyl)amine (bqpa) **3-3** were dissolved in degassed dichloromethane and heated to reflux for 3 h. The resulting yellow precipitate was collected by filtration and dried under vacuum. Reaction control by  $^1\text{H}$  NMR showed the presence of several different species. These could be separated by column chromatography using silica gel as the stationary phase and methanol/dichloromethane 20:80 as the eluent. The first fraction collected contained the desired product which was obtained as a yellow powder in low yield of 25% (**Scheme 3.8**).

Scheme 3.8: Synthesis of **3-7**.

The IR spectrum of **3-7** is dominated by two very strong signals at 2026 and 1913  $\text{cm}^{-1}$  (**Fig. 3.17**). Furthermore, medium to weak signals are observed at 1601, 1504, 1431 and 761  $\text{cm}^{-1}$ . The sharp peak at 2026  $\text{cm}^{-1}$  is assigned to the symmetric and the broader signal at 1913  $\text{cm}^{-1}$  to the antisymmetric CO stretching vibration of the facial coordinated carbonyl ligands. The C-N stretching vibration of the amine bond is observed at 761  $\text{cm}^{-1}$ . The peaks at 1601, 1504 and 1431  $\text{cm}^{-1}$  results from the stretching vibrations of the aromatic C-C- and C-N bonds.

In contrast to the  $^1\text{H}$  NMR spectra of **3-5** and **3-6**, the one of  $[\text{Mn}(\text{bqpa})(\text{CO})_3]\text{Br}$  **3-7** is more complicated (**Fig. 3.18**). It shows one singlet at 5.30 ppm with an integral of 2H and four doublets at 4.35, 5.05, 5.19 and 5.64 ppm with integrals of 1H each. The aromatic region of the spectrum shows a doublet at 7.50 ppm and two triplets at 7.56 and 7.67 ppm with integrals 1H each. At 7.73-7.82 ppm, a multiplet is observed with an integral of 4H. Furthermore, a doublet with an integral of 1H and a multiplet with an

integral of 2H are found at 7.89 and 7.96-8.05 ppm, respectively. Five additional doublets with integrals of 1H each are observed at 8.06, 8.16, 8.54, 8.58, 8.65, and 9.22 ppm.

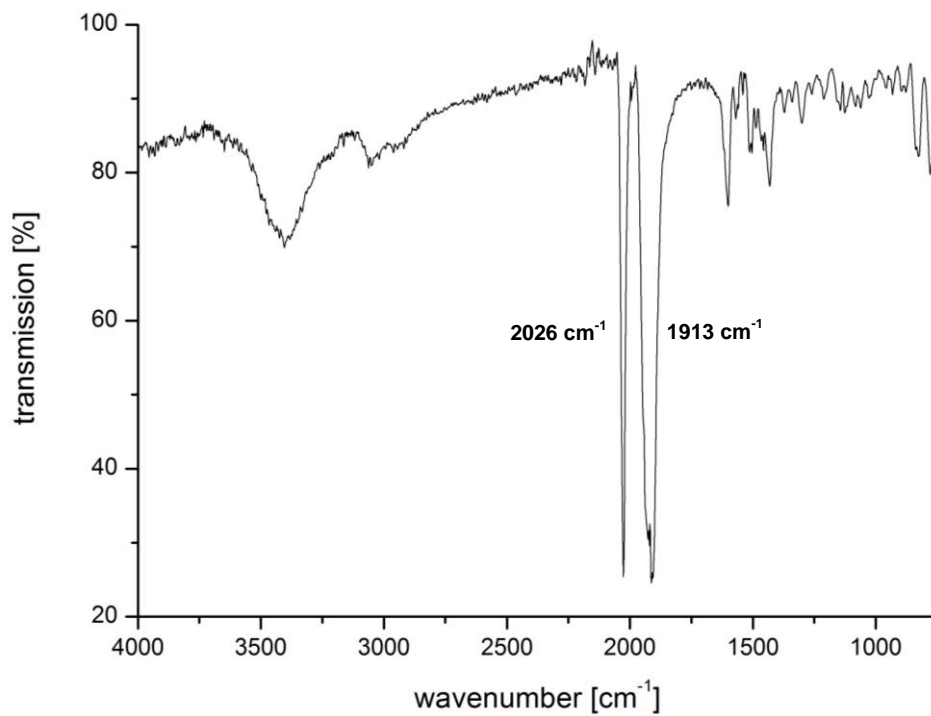


Figure 3.17: ATR-IR spectrum of **3-7**.

The singlet at 5.30 ppm is assigned to the methylene protons of a uncoordinated quinoline group. The two sets of doublets at 4.35 and 5.19 ppm as well as 5.05 and 5.64 ppm show large geminal splitting of  $^2J = 17.6$  and 17.4 Hz, respectively. This indicates the special coordination mode of bqa in this complex with one pyridyl and one quinoline arm coordinated, likely due to steric hindrance preventing the binding of the second quinoline group. Based on comparison with the other compounds in the series, the doublets at 4.35 and 5.05 ppm are assigned to the diastereotopic methylene protons of the coordinated pyridine arm while the doublets at 5.19 and 5.64 ppm are due to the methylene protons of the metal-bound quinoline group. In the aromatic region of the spectrum, the doublet at 7.50 ppm with  $^3J = 8.3$  Hz is assigned to the H3-atom of the free quinoline arm. The two triplets at 7.56 and 7.67 ppm with  $^3J = 7.4$  and 8.2 Hz are due to the protons in the 8-positions of the two non-identical quinoline units. The multiplet at 7.73–7.82 ppm results from the



overlap of the signals of the H5- and H3-atoms of the pyridine moiety as well as the H9-atom of the free and the H3-atom of the coordinated quinoline arm. The doublet at 7.89 ppm with  $^3J = 8.5$  Hz is assigned to the proton in 4-positions of the pyridine ring. The multiplet at 7.96-8.05 ppm results from the overlap of two signals, as the H9-atom of the coordinated quinoline and the proton in the 10-positions of the free quinoline unit appear in the same range of the spectrum. The doublet at 8.06 ppm belongs to the coordinated H10-atom of the quinoline group with  $^3J = 7.6$  Hz. The two doublets at 8.16 and 8.54 ppm with couplings of  $^3J = 7.0$  and 8.6 Hz are assigned to the protons in the 7-positions of the two non-identical quinoline moieties. The two doublets at 8.58 and 8.65 ppm belong to the H4-atoms of both the coordinated and uncoordinated quinoline groups with coupling constants of  $^3J = 8.7$  and 8.6 Hz, respectively. The strongly downfield shifted doublet at 9.22 ppm with  $^3J = 4.9$  Hz is assigned to the H6-atom of the pyridine moiety. The small amount of **3-7** isolated did not allow the collection of a  $^{13}\text{C}\{^1\text{H}\}$  NMR spectrum with satisfying intensity.

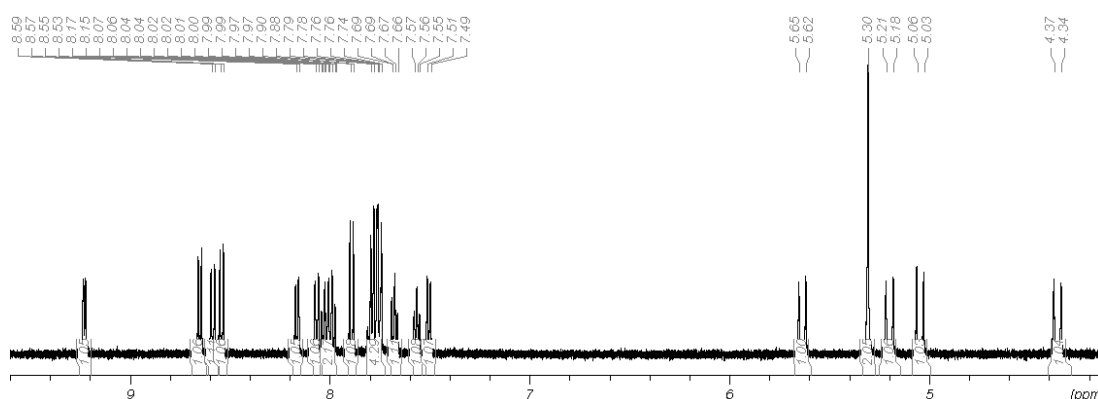
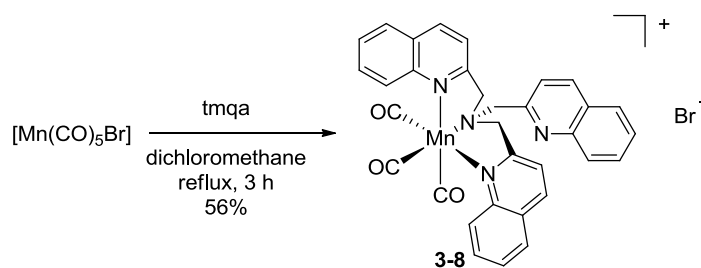


Figure 3.18:  $^1\text{H}$  NMR spectrum (500.13 MHz,  $\text{DMSO-d}_6$ ) of **3-7**.

In the positive-mode ESI-MS of **3-7**, three signals at  $m/z = 334.04$ , 445.12, and 529.11 Da are observed. At  $m/z = 334.04$  Da, a cation is observed with a composition of  $[\text{M}-3\text{CO}-\text{C}_9\text{H}_7\text{N}+\text{H}_2\text{O}-\text{Br}]^+$ . The peak at  $m/z = 445.12$  Da results from a  $[\text{M}-3\text{CO}-\text{Br}]^+$  cation which has lost all three carbonyl ligands and the bromide upon ionization. At  $m/z = 529.11$  Da, the molecule cation  $[\text{M}-\text{Br}]^+$  is found.

3.1.2.4 Synthesis and characterization of  $[\text{Mn}(\text{CO})_3(\text{tmqa-}\kappa^3\text{N})]\text{Br}$ 

To complete the series of compounds,  $[\text{Mn}(\text{CO})_3(\text{tmqa})]\text{Br}$  **3-8** was synthesized under the same conditions as **3-6** and **3-7**. The yellow product was obtained by precipitation with diethylether and was dried in vacuum without further purification in a moderate yield of 56% (**Scheme 3.9**).



**Scheme 3.9:** Synthesis of **3-8**.

The IR spectrum of **3-8** shows three very strong bands at 2026, 1935 and 1913  $\text{cm}^{-1}$ . Additionally, weak bands are found at 1600, 1514, 1432 and 780  $\text{cm}^{-1}$  (**Fig. 3.19**).

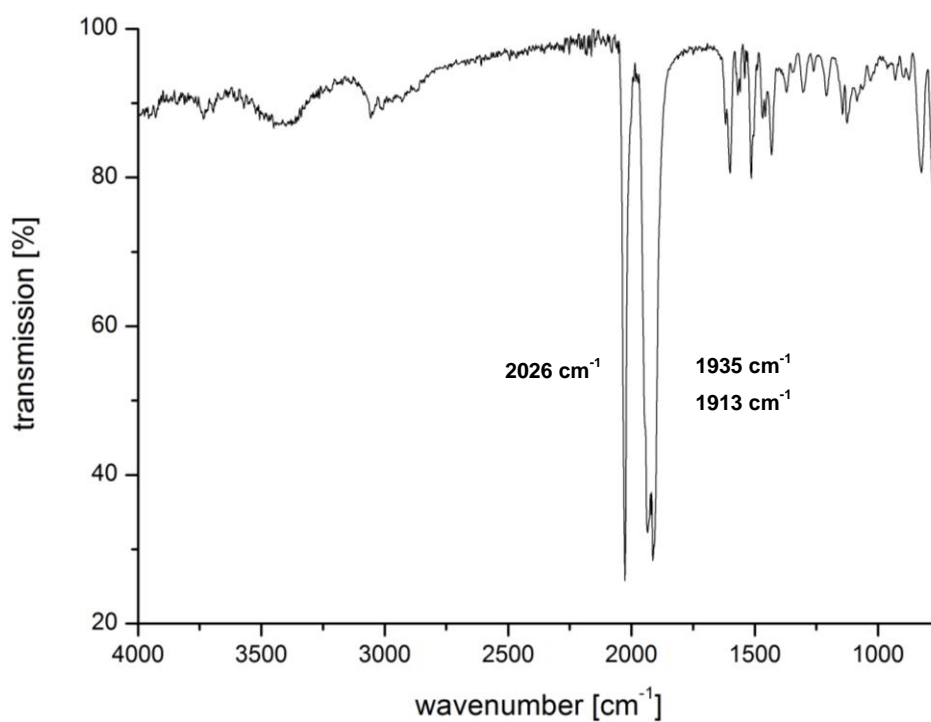


**Figure 3.19:** ATR-IR spectrum of **3-8**.

The sharp signal at  $2026\text{ cm}^{-1}$  is assigned to the symmetric and the bands at  $1935$  and  $1913\text{ cm}^{-1}$  to the antisymmetric CO stretching vibration of the facially coordinated carbonyl ligands. The peaks at  $1601$ ,  $1504$  and  $1431\text{ cm}^{-1}$  result from the stretching vibrations of the aromatic C-C- and C-N-double bonds. The C-N stretch of the tertiary amine bond is observed at  $780\text{ cm}^{-1}$ .

The  $^1\text{H}$  NMR of **3-8** shows one singlet at  $5.41\text{ ppm}$  and two doublets at  $4.95$  and  $5.60\text{ ppm}$  with integrals of  $2\text{H}$  each (**Fig. 3.20**). In the aromatic region, six doublets are found at  $7.48$ ,  $8.04$ ,  $8.18$ ,  $8.39$ ,  $8.53$  and  $8.64\text{ ppm}$  with an integral ratio of  $1:1:2:2:1:2$  as well as three multiplets at  $7.60\text{--}7.72$ ,  $7.74\text{--}7.81$ , and  $7.87\text{--}7.97\text{ ppm}$  with an integral ratio of  $4:2:3$ .

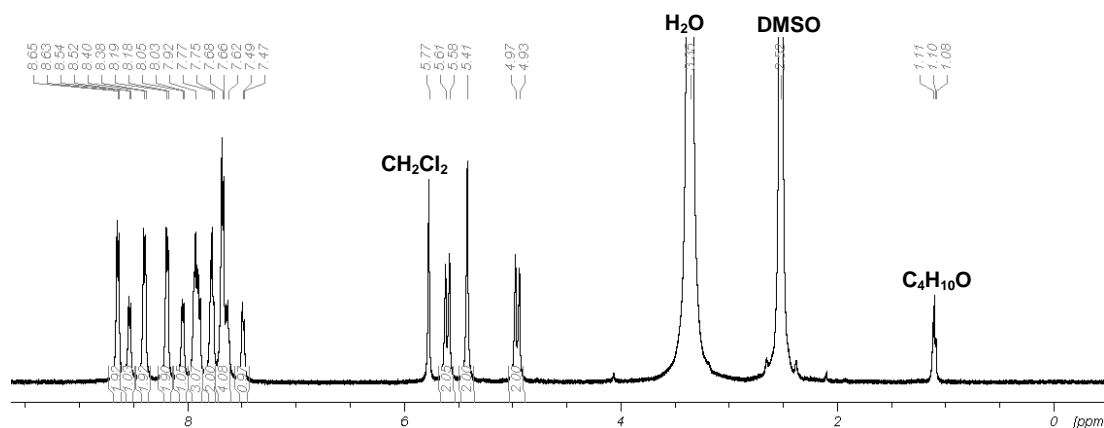


**Figure 3.20:** Aromatic region of the  $^1\text{H}$  NMR spectrum ( $500.13\text{ MHz}$ ,  $\text{DMSO-d}_6$ ) of **3-8**.

The two doublets at  $4.95$  and  $5.60\text{ ppm}$  with a large geminal splitting of  $^2J = 18.4\text{ Hz}$  are due to the diastereotopic methylene protons of the two coordinated quinoline groups while the singlet at  $5.41\text{ ppm}$  is assigned to the equivalent methylene protons of the uncoordinated quinoline group. In the aromatic region, two sets of signals in  $2:1$  ratio are observed which also demonstrates the presence of one uncoordinated quinoline moiety, similar to the signal pattern of the methylene protons. The doublet at  $7.48\text{ ppm}$  with  $^3J = 7.9\text{ Hz}$  is due to the H3-atom of the uncoordinated quinoline group. The multiplet at  $7.60\text{--}7.72\text{ ppm}$  is assigned to the protons in the 3-positions of the coordinated as well as the protons in the 9- and 8-positions of the uncoordinated quinoline group. The multiplet at  $7.74\text{--}7.81\text{ ppm}$  is assigned to the H8-atoms of the coordinated groups while the multiplet at  $7.87\text{--}7.97\text{ ppm}$

results from the protons in the 9-positions of the coordinated and the protons in the 10-positions of the free arm. The doublet at 8.04 ppm with  $^3J = 7.6$  Hz belongs to the H7-atom of the uncoordinated group. The two doublets at 8.18 and 8.39 ppm with  $^3J = 7.6$  and 8.7 Hz are assigned to the protons in the 10- and 7-positions of the coordinated quinoline moieties. The two doublets at 8.53 and 8.64 ppm with  $^3J = 8.2$  and 8.4 Hz each are due to the H4-atoms of the coordinated and uncoordinated quinoline groups. The large downfield shift results from the ring nitrogen in the para-positions.

The  $^{13}\text{C}\{^1\text{H}\}$  NMR spectrum of  $[\text{Mn}(\text{CO})_3(\text{tmqa})]\text{Br}$  **3-8** shows two signals in the aliphatic region at 68.4 and 69.3 ppm (**Fig. 3.21**) and 19 signals in the aromatic region, which appear at 119.7, 122.7, 126.0, 127.1, 127.6, and 128.0 ppm as well as 128.4, 128.5, 129.9, 130.0, 132.2, 137.2, 140.5, 146.5, 147.0, 155.2, and 165.4 ppm as well as signals with a large downfield shift at 218.4 and 219.8 ppm.

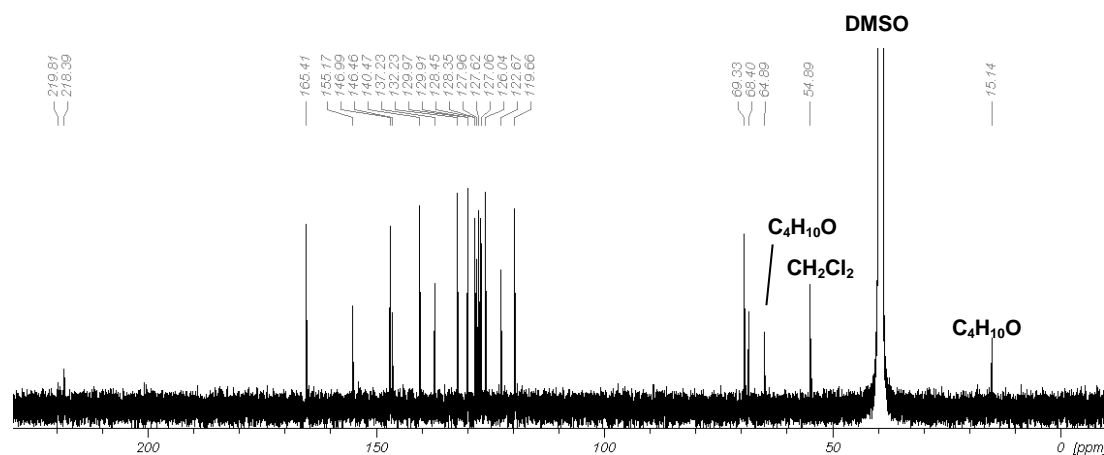


Figure 3.21:  $^{13}\text{C}\{^1\text{H}\}$  NMR spectrum (125.75 MHz,  $\text{DMSO-d}_6$ ) of **3-8**.

The two signals in the aliphatic region at 68.4 and 69.3 ppm are assigned to the methylene carbon atoms of the coordinated and uncoordinated quinolinemethyl groups, respectively. In the aromatic region of the spectrum, two sets of signals are found. The peaks with higher intensity result from the two coordinated quinoline groups and appear at 119.7, 126.0, 127.6, 128.5, 130.0, 132.2, 140.5, 147.0, and 165.4 ppm. They are assigned to the carbons in the 3-, 8-, 7-, 5-, 10-, 9-, as well as 4-, 6- and 2-positions, respectively. The remaining signals in the aromatic region at 122.7, 127.1, 128.0, 128.4, 129.9,

137.2, 146.5, and 155.2 ppm are due to the single uncoordinated quinoline group and are assigned to the C3-, C8-, and C5-, C7-, C10-, C9-, C4-, C6-, and C2-atoms. The peak at 127.1 ppm has a higher intensity than the others which is a result of the overlap of C8 and C5, which was observed also in the  $^{13}\text{C}$  DEPT 135 spectrum of **3-8**. The two signals with a large downfield shift at 218.4 and 219.8 ppm result from the three carbonyl carbon atoms of the *fac*-Mn(I)tricarbonyl group. The splitting is due to their different environments. The peak with higher intensity at 218.4 ppm is assigned to the two carbonyl ligands which are in a *trans*-positions to the coordinated quinoline nitrogen atoms while the signal with lower intensity at 219.8 ppm is due to the carbonyl ligand in *trans*-positions to the backbone amine nitrogen atom. This pattern is observed in all compounds of the series with the exception of **3-7**, which has all carbonyl ligands in a different environment and thus shows three signals.

In the positive-mode ESI-MS of **3-8**, signals at  $m/z = 384.05$ ,  $495.14$  and  $579.12$  Da are observed. At  $m/z = 384.05$  Da, a cation is found with the composition of  $[\text{M}-3\text{CO}-\text{C}_9\text{H}_7\text{N}+\text{H}_2\text{O}-\text{Br}]^+$ . This species is observed for all compound of the series with one or more quinoline moiety and indicates the lability of this group even under ESI ionization conditions. The peak at  $m/z = 495.14$  Da results from a  $[\text{M}-3\text{CO}-\text{Br}]^+$  cation which has lost all three carbonyl ligands and the bromide upon ionization. At  $m/z = 579.12$  Da the molecular ion of  $[\text{M}-\text{Br}]^+$  is found.

Single crystals of **3-8** were obtained by slow diffusion of *n*-hexane into a dichloromethane solution of the complex. Compound **3-8** crystallizes in the  $P 2_1/c$  space group (**Fig. 3.22**). The unit cell contains the cationic  $[\text{Mn}(\text{CO})_3(\text{tmqa})]^+$ -moiety as well as a bromide counterion and three solvate water molecules. The manganese(I) center is in an octahedral coordination sphere with a  $\text{MnN}_3\text{C}_3$  ligand environment. The bond lengths between the carbonyl ligands and the manganese(I) center are nearly equal with Mn1-C1 of  $1.793(2)$  Å, Mn1-C2 at  $1.817(2)$  Å and Mn1-C3 at  $1.821(2)$  Å. The Mn-N bond lengths are  $2.1007(18)$  Å for Mn1-N1,  $2.1056(18)$  Å for Mn1-N2 and  $2.0926(17)$

Å for Mn1-N3. The *trans*-angles between the carbonyl ligands and the coordinated quinoline groups of the tmqa ligand are N2-Mn1-C2 at 174.21(8)° and N3-Mn1-C3 at 176.84(8)°, thus close to 180°, while the *trans*-angle between the carbonyl and the amine nitrogen N1-Mn1-C1 is more bent at 171.60(8)°. The angles between the carbonyl ligands are C1-Mn1-C2 at 80.99(9)°, C1-Mn1-C3 at 85.93(9)° and C2-Mn1-C3 at 90.05(9)° and thus close to 90° as expected. The angles between the amine nitrogen and the coordinated quinoline nitrogen are N1-Mn1-N3 at 78.02(7)° and N1-Mn1-N2 at 82.01(7)°, while the N2-Mn1-N3-angle has a value of 87.18(7)°. The crystal structure also confirms the  $\kappa^3$ -coordination mode of the tmqa ligand with the one uncoordinated quinoline group.

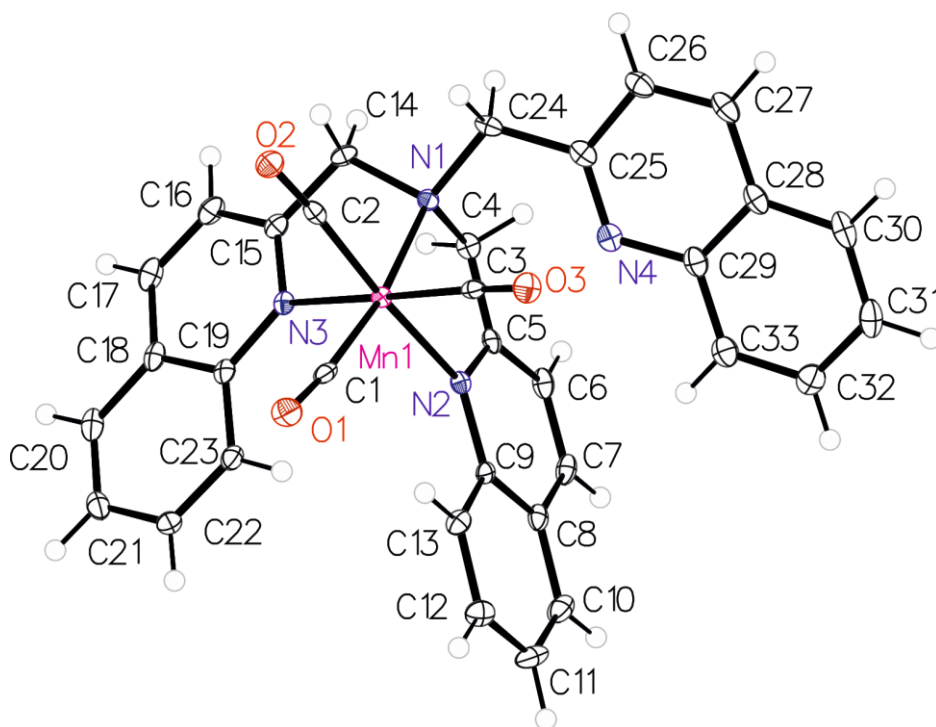


**Figure 3.22:** Molecular structure of  $[\text{Mn}(\text{CO})_3(\text{tmqa})]^+$  **3-8** with ellipsoids drawn at the 50% probability level. The bromide counterion and three water molecules in the unit cell are not shown for clarity.

### 3.1.3 UV/Vis studies

To study the light-triggered CO release from the four  $[\text{Mn}(\text{CO})_3(\text{L-}\kappa^3\text{N})]\text{Br}$  complexes **3-5** to **3-8** (Fig. 3.23), a number of UV/Vis experiments were carried out.

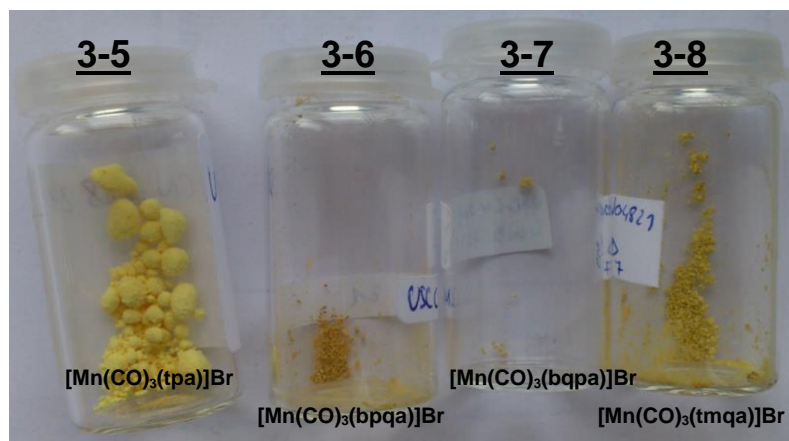


Figure 3.23: Solid samples of  $[\text{Mn}(\text{CO})_3(\text{L-}\kappa^3\text{N})]\text{Br}$  **3-5** to **3-8**.

To determine the extinction coefficient of the four complexes **3-5** to **3-8**, absorption spectra at different concentrations were recorded in dimethylsulfoxide. A concentration range between  $10^{-5}$  and  $10^{-3}$  M was chosen to keep the maximum absorption at  $A < 1$ . The UV/Vis spectra of the four compounds look quite similar. Each complex shows two overlapping intense absorption bands in the range of 300-320 nm as well as an additional broad shoulder around 360 nm.

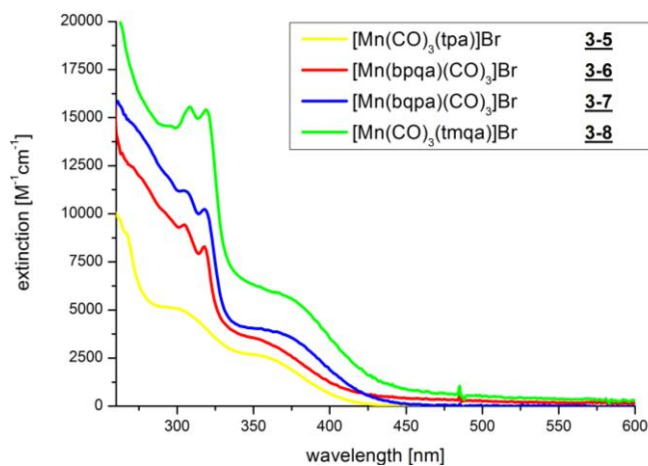
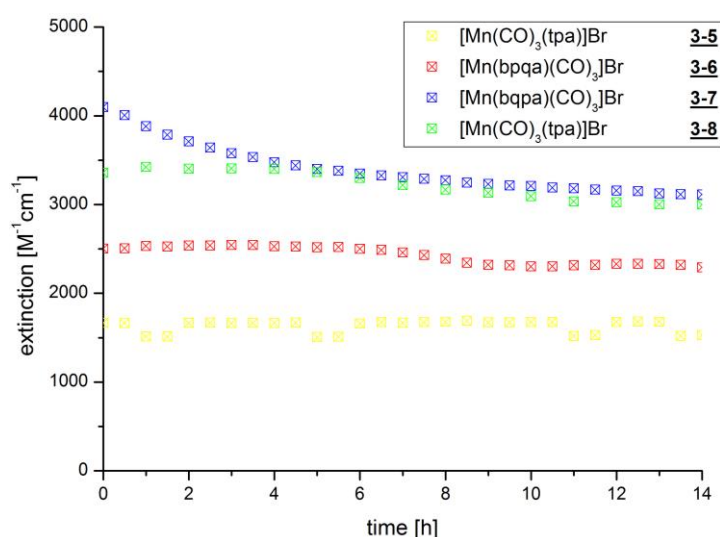


Figure 3.24: UV/Vis spectra of complexes **3-5** to **3-8** in DMSO.

For determination of the extinction coefficients, the high intensity bands at 297, 318, 318 and 320 nm were evaluated. As evident from **Table 3.1**, the extinction coefficient increases with the number of quinoline groups. However, this increase is not linear. Upon replacement of one pyridine group by a quinoline from **3-5** to **3-6**, the extinction coefficient nearly doubles from 5000 to 9600  $M^{-1}cm^{-1}$  while introduction of a second, uncoordinated quinoline group results in only a small further increase in **3-7**. However, for the tris-quinoline compound, **3-8** the extinction coefficient nearly doubles again from 10300 to 18100  $M^{-1}cm^{-1}$ .

**Table 3.1:** Coordinated (c) and uncoordinated (nc) donor groups, absorption maxima and extinction coefficients of the  $[Mn(CO)_3(L-\kappa^3N)]Br$  complexes in the series **3-5** to **3-8**.

	Pyridyl (c/nc)	Quinoly (c/nc)	$\lambda_{max}$ [nm]	$\epsilon_{\lambda_{max}}$ [ $M^{-1}cm^{-1}$ ]	$\epsilon_{365\text{ nm}}$ [ $M^{-1}cm^{-1}$ ]
<b>3-5</b>	3 (2/1)	0 (0/0)	297	5000 $\pm$ 100	2300 $\pm$ 100
<b>3-6</b>	2 (2/0)	1 (0/1)	318	9600 $\pm$ 400	4200 $\pm$ 500
<b>3-7</b>	1 (1/0)	2 (1/1)	318	10300 $\pm$ 300	4300 $\pm$ 600
<b>3-8</b>	0 (0/0)	3 (2/1)	320	18100 $\pm$ 700	7400 $\pm$ 500



**Figure 3.25:** Changes in the UV/Vis spectra at 360 nm of **3-5** to **3-8** upon incubation in PBS under exclusion of light for 0 to 14 h.

Stock solutions of **3-5** to **3-8** in dimethylsulfoxide were prepared and then diluted to a total volume of 1 mL in a quartz cuvette with phosphate-buffered saline (PBS) at a pH of 7.4 to give a concentration of 0.3 mM. The samples



were placed in the UV/Vis spectrophotometer overnight with UV/Vis spectra taken automatically every 30 min (**Fig. 3.25**). The measurements showed no significant change in the spectra. At the end of the dark incubation time, the same samples were illuminated with a 365 nm UV hand lamp and spectra were taken every minute while illumination was briefly interrupted. Illumination of the complexes **3-5** to **3-8** led to complete decomposition as indicated in the UV/Vis spectra by the decrease of all absorption bands between 300 and 1000 nm to zero.

To study the CO-release properties of **3-5** to **3-8**, the standard myoglobin assay was used. Thus, a degassed solution of myoglobin in phosphate-buffered saline (PBS) was reduced with sodium dithionite and added to a 1 mL quartz cuvette. Stock-solutions of **3-5** to **3-8** in dimethylsulfoxide were added to give a total concentration of 10  $\mu\text{M}$  of complex, 60  $\mu\text{M}$  of myoglobin, and 10 mM of dithionite in the cuvette. The solutions were placed in the UV/Vis spectrometer under exclusion of light and UV/Vis spectra were taken automatically every 30 min for 16 h. After this dark incubation, the same samples were illuminated with a 365 nm UV hand lamp and spectra recorded every 5 min until no further changes were observed. The carbon monoxide released binds to the myoglobin forming carboxymyoglobin (MbCO). Its concentration was calculated from changes in the Q-band absorption at 540 nm (**Fig. 3.26**).<sup>[87]</sup>

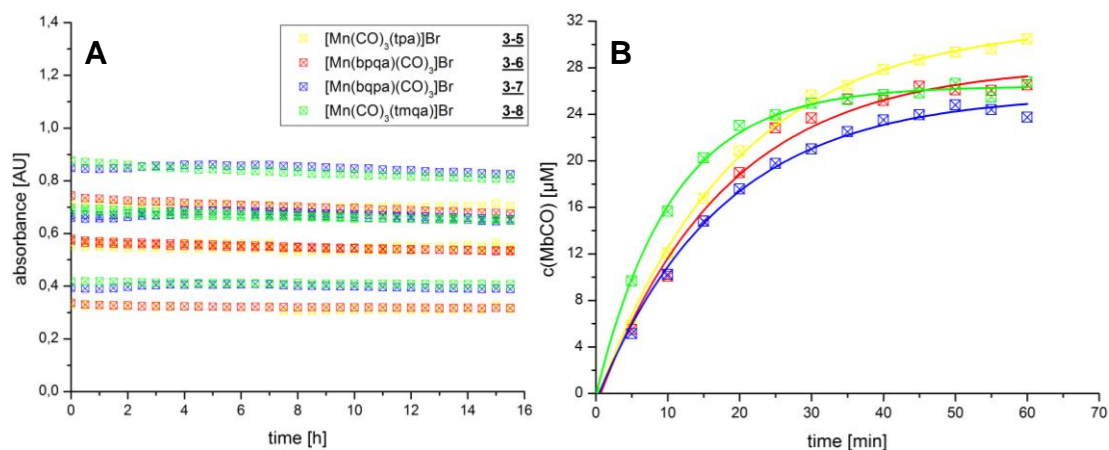


**Figure 3.26:** Dark stability trace of **3-5** to **3-8** at 510, 540, 557 and 577 nm in PBS in presence of myoglobin (60  $\mu\text{M}$ ) and sodium dithionite (10 mM) (A). Concentration of MbCO generated upon illumination of **3-5** to **3-8** at 365 nm (B) in PBS in the presence of myoglobin (60  $\mu\text{M}$ ) and sodium dithionite (10 mM).

All samples **3-5** to **3-8** did not show any spectral changes under the conditions of the myoglobin assay when kept in the dark, similar to the results in pure PBS. However, upon illumination at 365 nm, formation of MbCO was observed which levelled off after about 1 h. The final concentration of MbCO at the plateau thus reached was calculated from the absorption at the MbCO Q-band at 540 nm. For compound **3-5**,  $(26.6 \pm 4.9)$   $\mu\text{M}$  of MbCO were released. The mixed ligand complexes **3-6** and **3-7** behaved slightly different. The concentration of MbCO formed for **3-6** was  $(23.7 \pm 4.4)$   $\mu\text{M}$ . In contrast, compound **3-7** generated  $(28.1 \pm 3.0)$   $\mu\text{M}$  of MbCO. Compound **3-8** gave a value of  $(26.7 \pm 2.5)$   $\mu\text{M}$ . Thus, the influence of the exchange of pyridine against quinoline moieties on the CO-release behavior is marginal (**Tab. 3.2**).

**Table 3.2:** Coordinated (c) and uncoordinated (nc) groups, concentrations of MbCO formed and half-lives of the  $[\text{Mn}(\text{CO})_3(\text{L-}\kappa^3\text{N})]\text{Br}$  series.

	Pyridyl (c/nc)	Quinolyl (c/nc)	c(MbCO) [ $\mu\text{M}$ ] <sup>a</sup>	CO [eq.]	$t_{1/2}$ [min]
<b>3-5</b>	3 (2/1)	0 (0/0)	$26.6 \pm 4.9$	$2.7 \pm 0.5$	10.1
<b>3-6</b>	2 (2/0)	1 (0/1)	$23.7 \pm 4.4$	$2.4 \pm 0.4$	9.4
<b>3-7</b>	1 (1/0)	2 (1/1)	$28.1 \pm 3.0$	$2.8 \pm 0.3$	12.9
<b>3-8</b>	0 (0/0)	3 (2/1)	$26.7 \pm 2.5$	$2.7 \pm 0.3$	7.1

<sup>a</sup>  $c(\text{MbCO})_{\text{max}} = 30 \mu\text{M}$

The half-lives of compounds **3-5** to **3-8** were all in the range of 7-13 min. With  $t_{1/2} = 7.1$  min, compound **3-8** is the fastest releaser followed by **3-6** at 9.4 min and **3-5** at 10.1 min. Complex **3-7** has the longest half-life of 12.9 min. Compounds **3-5** to **3-6** and **3-8** all incorporate either two equivalent pyridyl moieties or two quinoline groups on the Mn(I)-center, while complex **3-7** is the only one in the series which coordinates one pyridyl and one quinoline group. Thus, the CO release rate is influenced by the number of quinoline moieties incorporated in the ligand. Generally, the more quinoline units are coordinated to the *fac*- $\text{Mn}(\text{CO})_3$  core, the faster the CO-release is.

### 3.1.4 Determination of log*P* values

In order to study the influence of the increasing number of quinoline groups on the lipophilicity of the  $[\text{Mn}(\text{CO})_3(\text{L}-\kappa^3\text{N})]\text{Br}$  complexes **3-5** to **3-8**, the partition coefficient log*P* in an *n*-octanol/water mixture was determined. This value is used in pharmacological models to predict the distribution of drug candidates between organs and tissue.<sup>[88]</sup> Compounds with positive log*P* are considered as lipophilic while those with negative values as hydrophilic.<sup>[66]</sup> Together with molecular weight, lipophilicity, and the number of hydrogen donor and acceptor groups, the log*P* value is very important for the assessment of a drug candidate<sup>[89]</sup> with the resulting “rule of five” devised by Lipinski.<sup>[88, 90]</sup> For the determination of the log*P* values, the “shake-flask” method was used. Thus, equal volumes of *n*-octanol and phosphate-buffered saline (PBS) were shaken together for 72 h for saturation of both phases. Then, 750  $\mu\text{L}$  of each phase were combined and 10  $\mu\text{L}$  of a stock solution of metal complexes **3-5** to **3-8** in dimethylsulfoxide added and shaken for 15 min. The phases were then separated by centrifugation and UV/Vis spectra of the two samples were obtained.<sup>[66]</sup> The log*P* values were then calculated. While the UV/Vis spectra recorded in *n*-octanol showed the highest extinction values for compound **3-8** followed by **3-7**, **3-6** and **3-5**, for the spectra recorded in PBS a reversed behavior was observed. Within the series, the log*P* value increases with the number of quinoline groups present. While **3-5** and **3-6** have negative values of -0.92 and -0.60 and thus are to be considered as hydrophilic, **3-7** and **3-8** show positive log*P* values 0.13 and 1.13, and are considered as lipophilic (Tab. 3.3).

**Table 3.3:** Number of coordinated (c) and uncoordinated (nc) pyridyl and quinoliny groups as well as log*P* values in the series  $[\text{Mn}(\text{CO})_3(\text{L}-\kappa^3\text{N})]\text{Br}$  complexes **3-5** to **3-8**.

<i>compound</i>	<i>Pyridyl (c/nc)</i>	<i>Quinolyl (c/nc)</i>	<i>logP</i>
<b>3-5</b>	3 (2/1)	0 (0/0)	-0.92
<b>3-6</b>	2 (2/2)	1 (0/1)	-0.60
<b>3-7</b>	1 (1/0)	2 (1/1)	0.13
<b>3-8</b>	0 (0/0)	3 (2/1)	1.13

### 3.1.5 NMR studies

To study the potential binding of the uncoordinated pyridyl group to a free coordination site generated by photolytic release of a carbonyl ligand, NMR studies were carried out. Upon coordination of the pedant pyridyl group to the  $\text{Mn}(\text{CO})_3$  center, changes in the  $^1\text{H}$  NMR spectrum should be observed due to the changes in the local environment of the pyridyl and methylene protons. Therefore, a stock solution of  $[\text{Mn}(\text{CO})_3(\text{tpa-}\kappa^3\text{N})]\text{Br}$  **3-5** in deuterated dimethylsulfoxide was prepared and degassed for 20 min by bubbling with dinitrogen under exclusion of light. Six different standard NMR tubes were then filled with the same amount of stock solution and five of them were illuminated with a 365 nm UV hand lamp for a different period of time. The sixth sample was immediately placed in the NMR spectrometer and a  $^1\text{H}$  NMR spectrum was obtained as a reference.

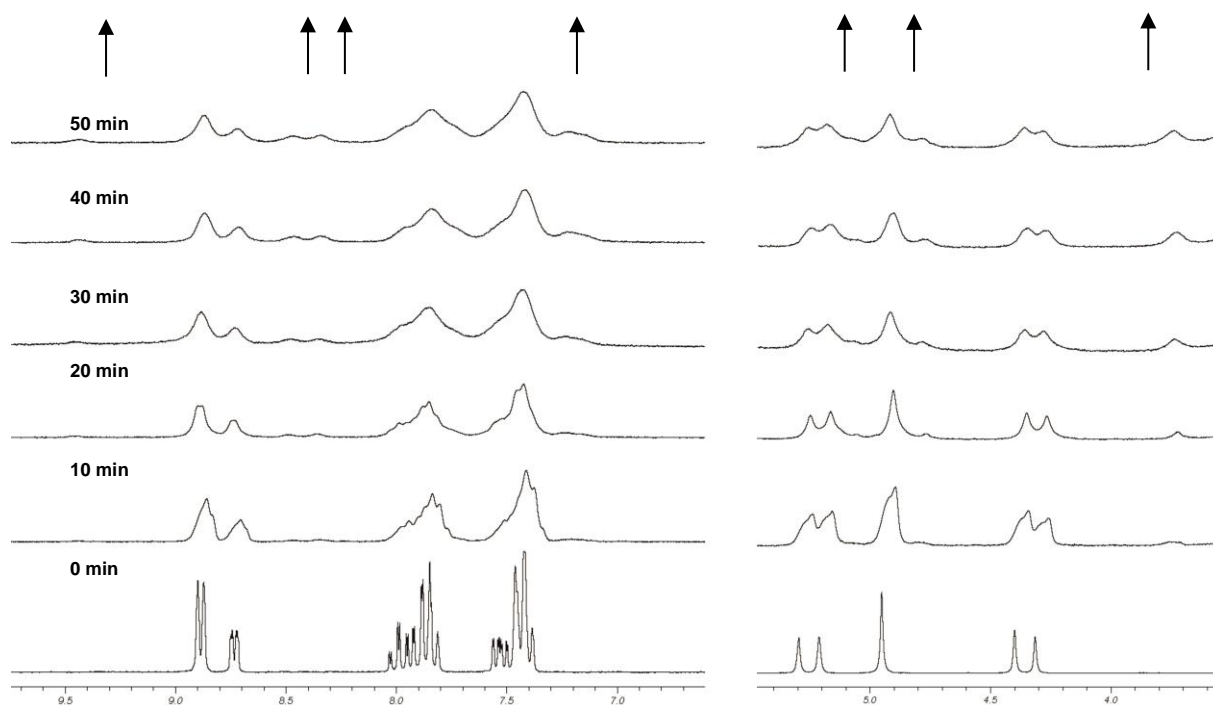


Figure 3.27:  $^1\text{H}$  NMR spectra (199.93 MHz,  $\text{DMSO-d}_6$ ) of samples of **3-5** illuminated at 365 nm for different periods of time (0-50 min). (left) Aromatic and (right) aliphatic region.

At  $t = 0$  min, the  $^1\text{H}$  NMR spectrum of the yellow solution of **3-5** showed the same pattern of peaks as already discussed in section 3.1.2.1 (Fig. 3.27). The color of the solution changed with illumination time from yellow to dark orange. After 10 min, all peaks were already significantly broadened. New

peaks had appeared at 3.80, 4.83, 5.13, 7.23, 8.44 and 9.47 ppm, with relative intensities of 1:5 each relative to the original signals. With increasing illumination time, these signals become more intense while the broadened peaks of  $[\text{Mn}(\text{CO})_3(\text{tpa-}\kappa^3\text{N})]\text{Br}$  **3-5** slowly disappear. The new peaks that show up upon illumination result from the coordination of the pendant pyridyl group while the observed signal broadening is probably due to some formation of paramagnetic manganese(II) species as oxidation products after the complete release of the CO ligands from the *fac*- $\text{Mn}(\text{CO})_3$ -moiety.

### 3.1.6 IR studies and DFT calculations

To identify the photolysis products of **3-5**, a solution IR experiment was carried out. Thus, a 8.4 mM stock solution of the metal complex **3-5** in dimethylsulfoxide was prepared and filled into an IR liquid cell with calcium fluoride windows under exclusion of light. Higher concentrations had to be used compared to the UV/Vis illumination studies for good signal intensities. The cell was illuminated with a 365 nm UV hand lamp and spectra were taken every 30 s. Later in the experiment, the time interval was increased to 60, 120, 180, 300 and finally 600 s (**Fig. 3.28**).

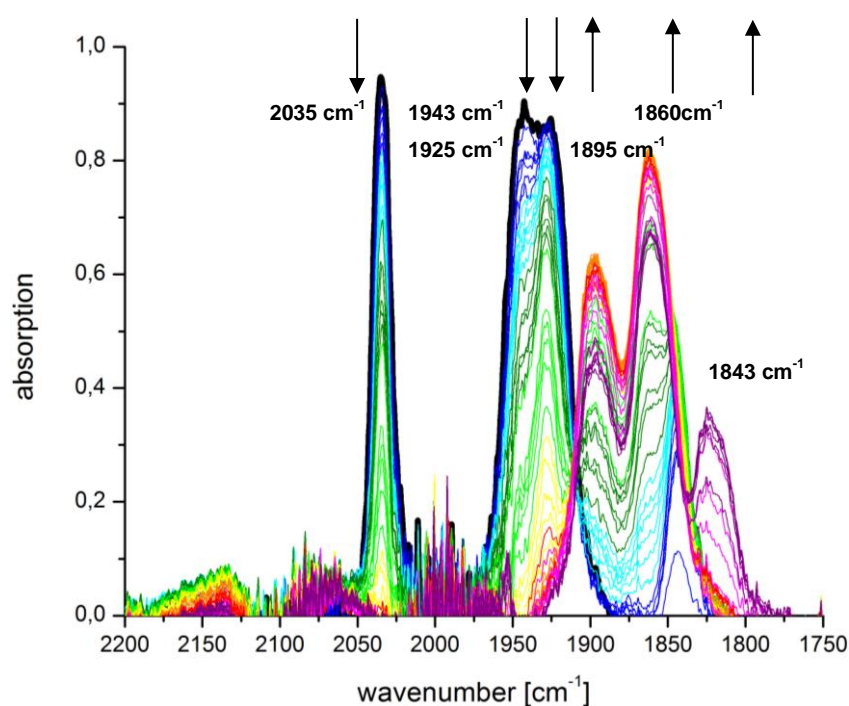


**Figure 3.28:** Changes in the IR spectra of a DMSO solution (8.4 mM) of **3-5** upon illumination at 365 nm for 0-16 min.

Upon illumination, the band of the symmetric CO stretching vibration at  $2035\text{ cm}^{-1}$  and those of the antisymmetric vibrations at  $1943\text{ cm}^{-1}$  and  $1925\text{ cm}^{-1}$  continuously decreased in intensity (**Fig. 3.29**). A new band at  $1843\text{ cm}^{-1}$  grew in almost immediately and persisted for about 150 s while disappearing again later in the experiment. With longer illumination time, two additional bands at  $1895$  and  $1860\text{ cm}^{-1}$  increased with some broadening and remained until the end of the experiment. After 600 s, a further band at  $1825\text{ cm}^{-1}$  also grows in. The weak IR signal of dissolved CO at  $2140\text{ cm}^{-1}$  could not be detected due to the limited sensitivity of the instrument.

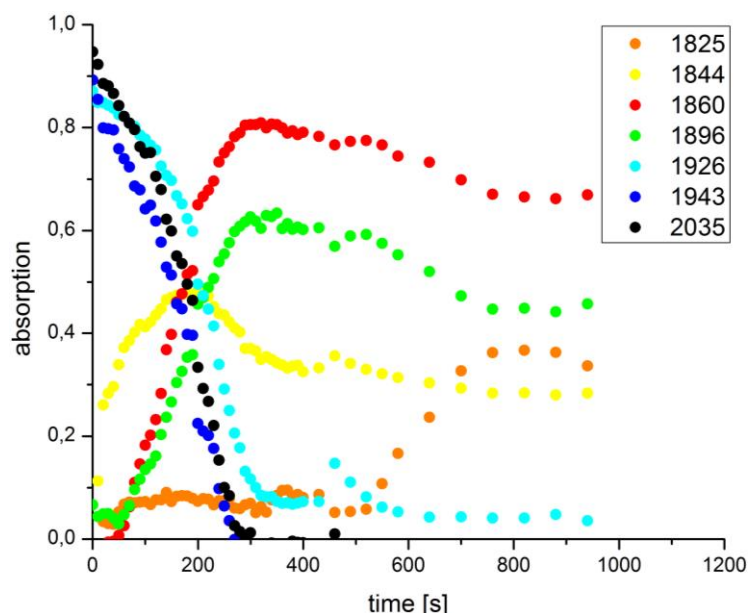
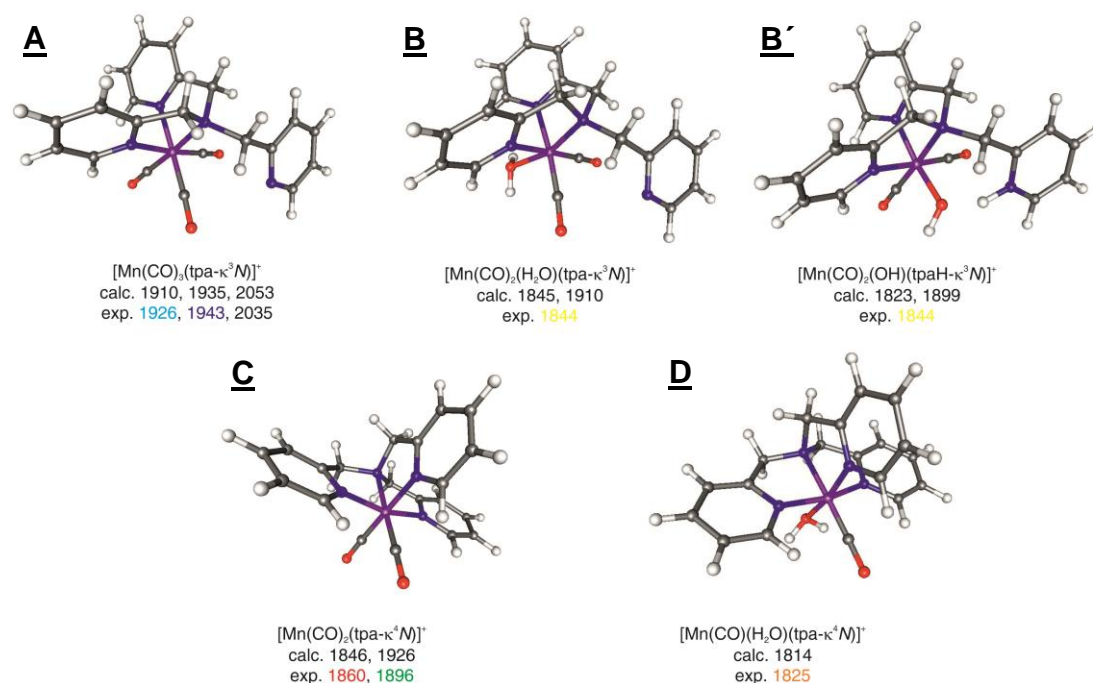


Figure 3.29: Time depend changes in the experimental IR traces of **3-5** in DMSO.<sup>[29]</sup>

To assign these signals to different species, potential iCORM intermediates were constructed from the X-ray structure coordinates of **3-5** and optimized by DFT. The calculated CO stretching vibrations were then compared to the experimental values. The DFT model chemistry was verified by comparison of the calculated and experimental CO stretching vibrations (Fig. 3.30). With the use of a proper scaling factor of 1.034, the deviation for the symmetric and antisymmetric modes was  $< 20 \text{ cm}^{-1}$  for  $[\text{Mn}(\text{CO})_3(\text{tpa-}\kappa^3\text{N})]^+$  **3-5**. Femtosecond time-resolved UV pump/ IR probe spectroscopy experiments on  $[\text{Mn}(\text{CO})_3(\text{tpm})]\text{Cl}$  by Nürnbergger *et al.* showed that small solvent molecules initially occupy the vacant coordination site resulting from the release of the CO ligands.<sup>[91]</sup> Thus initially, one carbonyl ligand was removed either *trans* to the amine or *trans* to a coordinated pyridyl moiety, replaced by a water molecule and the structure then optimized again. This lead to minimum geometry **B** with a  $\text{Mn}(\text{CO})_2(\text{H}_2\text{O})\text{N}_3$  coordination environment when the carbon monoxide ligand *trans* to the amine nitrogen is removed while the third pyridyl group stays pedant. By removal of the carbonyl ligand *trans* to one of the coordinated pyridyl groups, an alternative geometry **B'** is obtained in which the uncoordinated pyridyl nitrogen is protonated by water.



ORCA 2.8 RI-BP68 TZVP, TZVP/J, tightSCF grid4 COSMO(DMSO)

**Figure 3.30:** Structure of the cationic unit of parent compound **3-5** and potential iCORM intermediates **B-D** optimized with DFT at the BP86 level of theory with basis set TZVP and COSMO(DMSO) after subsequent removal of carbonyl ligands and replacement with solvent water or pendant pyridyl group.<sup>[29]</sup>

Comparison of the calculated antisymmetric CO stretching vibrations for the two intermediates **B** and **B'** with the experimental one of the early intermediate at  $1844\text{ cm}^{-1}$  lead to the assignment of this species to structure **B'**. This is based on the antisymmetric CO stretching vibrations usually underestimated by 10 to  $15\text{ cm}^{-1}$  upon scaling, leading to a good match with the value calculated for **B'** while the deviation of only  $1\text{ cm}^{-1}$  for **B** is considered as too close. The symmetric CO stretching vibration of the first intermediate was not observed in the IR experiment due to an overlap with remaining signals of the starting material. For structure **C**, the calculations on the fully coordinated tpa ligand bound to a *cis*- $\text{Mn}(\text{CO})_2$  moiety lead to minimum energy structure **C** with an octahedral *cis*- $\text{Mn}(\text{CO})_2\text{N}_4$  geometry. The calculated scaled CO stretching vibrations are found at  $1926$  and  $1846\text{ cm}^{-1}$ . These two signals match well with the experimental stretches found at  $1896$  and  $1860\text{ cm}^{-1}$ . By removal of a second carbonyl ligand and replacement with a water molecule, the minimum geometry **D** is obtained which has a  $\text{Mn}(\text{CO})(\text{H}_2\text{O})\text{N}_4$  coordination environment. For monocarbonyl



species **D**, the calculated stretch at 1814 cm<sup>-1</sup> also matches well with the signal of the late intermediate found at 1825 cm<sup>-1</sup> in the experiment. The photolytic release of just two carbonyl ligands from **3-5** are in line with the data obtained from the myoglobin assay with a short pre-incubation time.<sup>[29]</sup> IR and EPR spectroscopic studies on [Mn(CO)<sub>3</sub>(tpm)]<sup>+</sup> by Kurz *et al.* also showed the photolytic release of just two of the three CO ligands from the metal complex. The third carbonyl is liberated by an oxidative dark process which leads to Mn(II) and finally dimerized oxo-bridged Mn(III) species.<sup>[92]</sup> The results show that the identification of different iCORM intermediates by IR spectroscopy allows us to demonstrate the coordination of the pedant pyridyl arm (**Tab. 3.4**).

**Table 3.4:** Comparison of experimental and scaled calculated frequencies for compound **A** and potential iCORM intermediates **B-D** resulting from the photolysis of **5** at 365 nm.

structure	$\tilde{\nu}_{\text{sym}}(\text{CO})$ [cm <sup>-1</sup> ]	$\tilde{\nu}_{\text{antisym}}(\text{CO})$ [cm <sup>-1</sup> ]	$\tilde{\nu}_{\text{antisym}}(\text{CO})$ [cm <sup>-1</sup> ]
<b>A</b> exp	2035	1943	1926
<b>A</b> calc	2053	1935	1910
<b>Diff. calc-exp</b>	+18	-8	-16
<b>B</b> exp	<i>a</i>	1844	<i>b</i>
<b>B</b> calc	1919	1845	<i>b</i>
<b>Diff. calc-exp</b>	<i>a</i>	+1	<i>b</i>
<b>B'</b> exp	<i>a</i>	1844	<i>b</i>
<b>B'</b> calc	1899	1823	<i>b</i>
<b>Diff. calc-exp</b>	<i>a</i>	-21	<i>b</i>
<b>C</b> exp	1896	1860	<i>b</i>
<b>C</b> calc	1926	1846	<i>b</i>
<b>Diff. calc-exp</b>	+30	-14	<i>b</i>
<b>D</b> exp	1825	<i>c</i>	<i>c</i>
<b>D</b> calc	1814	<i>c</i>	<i>c</i>
<b>Diff. calc-exp</b>	-11	<i>c</i>	<i>c</i>

<sup>a</sup> Not observed, probably covered by remaining signals of **A**. <sup>b</sup> Dicarbonyl species, only one antisymmetric CO vibrational mode. <sup>c</sup> Monocarbonyl species, only one CO vibrational mode.

ORCA 2.8 RI-BP68 TZVP, TZVP/J, tightSCF grid4 COSMO(DMSO), scaling factor = 1.034

### 3.1.7 Antibacterial properties

The bactericidal activity of CORMs against several pathogenic microorganisms, including *St. aureus*, *E. coli*, and *P. aeruginosa* has already been studied which might also be of clinical interest in the development of novel antibiotics.<sup>[22]</sup> The successful intervention of CORMs in microbial infections was shown in previous work, where increased survival of mice infected with *P. aeruginosa* upon application of CORM.<sup>[25]</sup> Therefore, the antibacterial properties of **3-5** were tested in the group of Prof. Robert Poole at the Department of Molecular Biology and Biotechnology at the University of Sheffield. First, the cellular uptake of CORM **3-5** by *E. coli* was studied with ICP-MS. The bacteria cells were incubated with **3-5** in the dark at 50  $\mu\text{M}$  and samples were collected at different time points. After an induction period of 20 min, the intracellular manganese concentration increased from about 10 to 85  $\mu\text{M}$  at the final incubation time of 80 min (**Fig. 3.31**). This ICP-MS results clearly demonstrate the uptake of manganese by the cells against the concentration gradient.

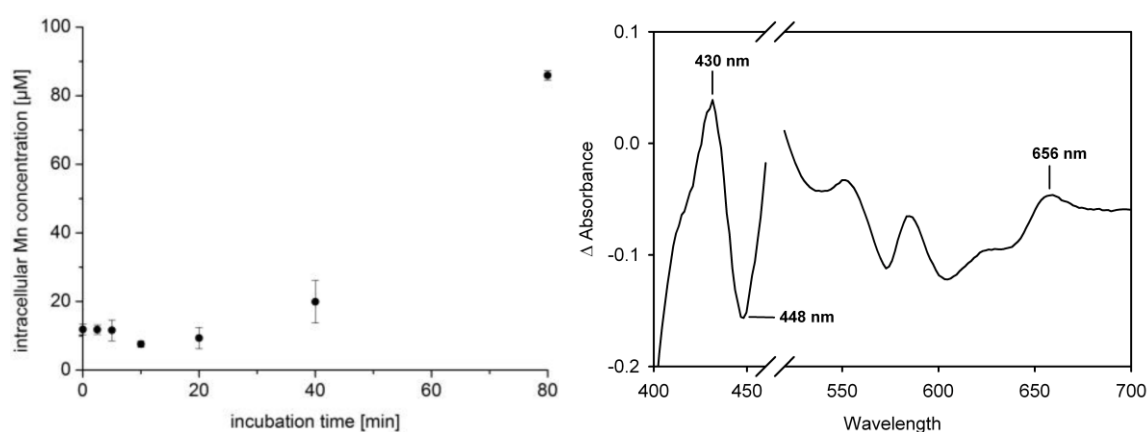


**Figure 3.31:** (left) Changes in intracellular manganese content of *E. coli* upon treatment with **3-5** with increasing incubation time. (right) Whole cell UV/Vis difference spectrum of *E. coli* after treatment with **3-5**.

To obtain more information on the potential biological target structures of CORM **3-5**, mid-exponential phase *E. coli* cultures were harvested, washed, and resuspended in phosphate-buffered saline (PBS) and reduced with sodium dithionite. The cell suspensions were then analyzed by dual wavelength spectroscopy using an Olis RSM 1000 spectrometer to examine

the bacterial terminal oxidases after incubation with **3-5** (100  $\mu\text{M}$ ) for 20 min and illumination with a 365 nm UV hand lamp. Difference spectra were taken of pure reduced cell suspensions as the base line. Photolytic CO release from **3-5** resulted in clear changes in the spectra. A new peak at 430 nm formed which is due to contributions from carbon monoxide-bound cytochromes *o* in the *bo* complex as well as cytochrome *b595 / d* in the *bd* and *bd-II* complexes. At 448 nm and between 550 and 600 nm, new troughs formed due to the disappearance of the reduced forms of cytochromes *d* and *b595*. Also, a characteristic peak at 656 nm grows in. This signal is assigned to the presence of carbon monoxide-bound cytochrome *d*. Due to the strong absorption of **3-5** and its photolysis products, the spectral region between 460 and 520 nm could not be evaluated and is not shown for clarity (**Fig. 3.31**).

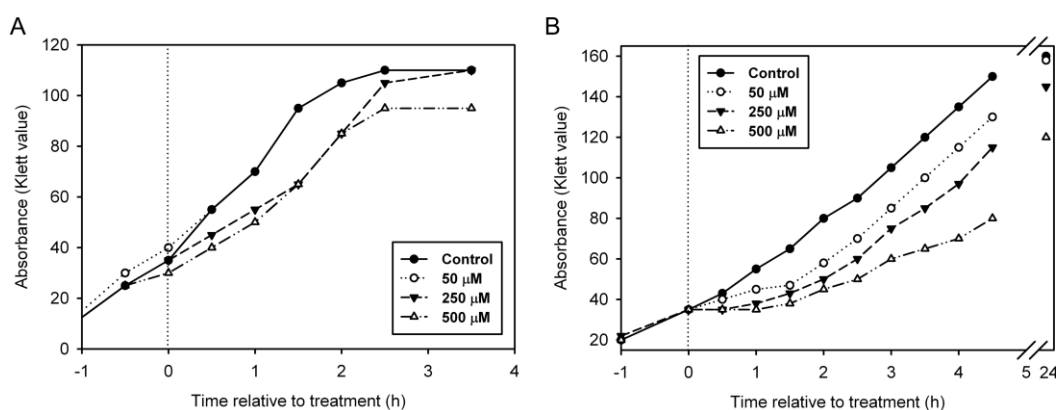


**Figure 3.32:** Growth inhibition experiments on *E. coli* grown on (A) glucose- or (B) succinate-Evans media treated with **3-5** in DMSO (0-500  $\mu\text{M}$ ) in the dark for 1 h and then illumination at 365 nm up to 24 h. Absorbance was measured by a Klett-Summerson photoelectric colorimeter fitted with a Nr. 66 red filter which keeps 85% of all the light transmitted at wavelengths between 485 and 550 nm.

To study the antibacterial activity of  $[\text{Mn}(\text{CO})_3(\text{tpa})]\text{Br}$  **3-5**, cultures of *E. coli* were grown to early-exponential phase in Evans medium with glucose as the sole carbon source. The cells were incubated with **3-5** (0-500  $\mu\text{M}$ ) at the time of inoculation and cultures were kept at 37  $^\circ\text{C}$  with shaking at 200 rpm under exclusion of light ( $t = -1$  h).

The absorbances of the cell suspensions were measured by a Klett-Summerson photoelectric colorimeter equipped with a filter which kept 85% of all the light transmitted at wavelengths between 485 and 550 nm. On this instrument, the Klett value of the cell suspensions was measured, which is converted to absorbance by the following eq. 1.

$$Klett = \frac{A}{0.002} \quad (1)$$

After reaching a cell density of ~30 Klett units, the samples were illuminated with a 365 nm UV hand lamp for 5 min and then placed back in the shaking incubator ( $t = 0$  h). During the initial 1 h of incubation (-1 to 0 h), no growth inhibition was observed, which verifies that  $[\text{Mn}(\text{CO})_3(\text{tpa})]\text{Br}$  **3-5** is not toxic to *E. coli* cells under the exclusion of light at up to 500  $\mu\text{M}$ . Illumination of the control sample not incubated with metal complex solution showed no growth inhibition which demonstrates that even 365 nm UV light is not harmful to the cells for short exposure times. After illumination, for samples incubated with solutions of **3-5** some transient reduction in growth rate was observed (Fig. 3.32 A). Taken together with the data of the whole cell spectroscopy, this demonstrates that **3-5** is not toxic to the bacteria itself, but it is the CO released after illumination which reduces the growth rate transiently due to carbon monoxide binding to the terminal oxidases. This effect saturated at 250  $\mu\text{M}$  of metal complex. However, by switching to an alternate form of energy metabolism such as mixed acid fermentation, the *E. coli* cells can bypass the CO-bound cytochromes. To block this particular pathway, cells were grown in Evans medium containing sodium succinate as the only carbon source since *E. coli* is not able to utilize this substrate for mixed acid fermentation. After changing the cell media, growth inhibition introduced by photoinduced CO released from **3-5** was permanent in a concentration-dependent manner. Furthermore, the effect was stronger than for cells grown in the presence of glucose. These results show that the bactericidal activity of photoactivated  $[\text{Mn}(\text{CO})_3(\text{tpa})]\text{Br}$  **3-5** is more pronounced when the energy metabolism of the

cell cultures is constrained. The results provide strong evidence that the inhibition of growth is caused by the carbon monoxide released and not by the metal compound **3-5** itself or its iCORM products (**Fig. 3.32 B**).

Thus, a series of  $\text{Mn}(\text{CO})_3$  complexes **3-5** to **3-8** was prepared and fully characterized. The calculation of the  $\log P$  values of the compounds showed an increase of lipophilicity by increasing number of quinoline groups. All four complexes **3-5** to **3-8** showed a similar CO-release. The coordination of the free arm was shown by UV/Vis, IR and NMR experiments as well as verified with DFT calculations on complex **3-5**. Primary data on bactericidal activity of **3-5** were carried out at the University of Sheffield in the group of Prof. Robert Poole.

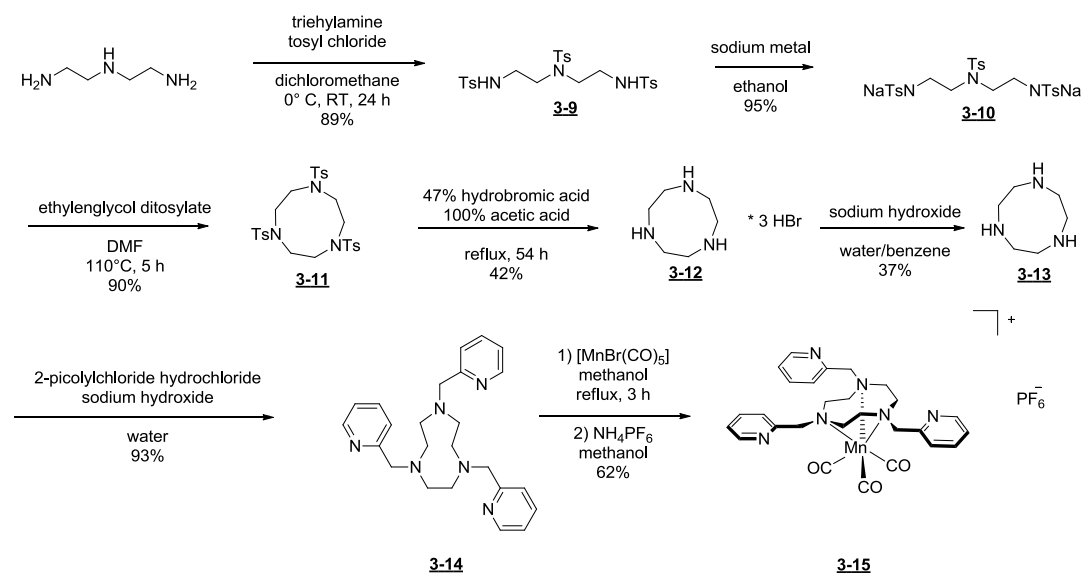
## 3.2 PhotoCORMs with hexadentate ligands

### 3.2.1 Synthesis of hexadentate ligands

While the UV/Vis, IR, and  $^1\text{H}$  NMR spectroscopy as well as DFT calculations presented in the previous chapter show that the additional uncoordinated pyridine group in tris(2-pyridylmethyl)amine (tpa) can take the place of a CO photolytically released, the system requires further optimization. As demonstrated by the myoglobin assay, complete release of all three CO ligands occurs under these conditions. Since there are no further pendant ligand groups to take the generated free coordination sites, the release of the second and third CO equivalent in first generation of the prepared PhotoCORMs still faces the problem of non-specific iCORM product formation. Thus, a ligand is required with one uncoordinated functional group per labile CO. In the case of manganese(I)-based PhotoCORMs with a stable *fac*-Mn(CO)<sub>3</sub> moiety, a hexadentate ligand would thus be needed which is initially coordinated by only three functional groups to the metal center, leaving three pendant groups for later replacement of the CO ligands as they are released. In addition, an independent synthesis of the resulting final *inactivated* CORM (iCORM) is highly desirable to serve as a negative control in biological testing.

Inspired by a publication of Wiegardt on manganese(II) complexes with hexadentate ligands, 1,4,7-tris(2-pyridylmethyl)-1,4,7-triazacyclononane (py<sub>3</sub>tacn-κ<sup>3</sup>N) **3-14** was chosen as hexadentate ligand. The coordination of **3-14** to a *fac*-Mn(CO)<sub>3</sub> unit by the three tacn nitrogen atoms would leave the three 2-pyridylmethyl moieties uncoordinated.<sup>[93]</sup> Thus, as the starting material for the synthesis of **3-14**, 1,4,7-triazacyclononane (tacn) **3-13** was prepared in a five-step procedure starting from diethylene triamine (**Scheme 3.10**).<sup>[94]</sup> In the first step, the three nitrogen atoms in diethylene triamine are protected as tosylates. Reaction of the tosylated compound **3-9** with sodium ethanolate, generated *in situ* from anhydrous ethanol and sodium metal, led to the sodium salt **3-10**. The cyclic 1,4,7-triazacyclononane-*N,N',N''*-tritosylate **3-11**

was then obtained by reaction of **3-10** with ethylene-glycol ditosylate, which is prepared by the reaction of ethylene glycol with tosylchloride in *N,N*-dimethylformamide at 130 °C. A slow addition of the ethylene-glycol ditosylate to the reaction mixture is required to obtain a good yield of the cyclic product **3-11**. This method ensures a complete cyclization and prevents the possible formation of long-chain polymerization byproducts.



**Scheme 3.10:** Synthetic pathway to a hexadentate ligand CORM with a free arm for every CO ligand.

In the next step, the tosyl groups in **3-11** were removed by heating it in a mixture of concentrated hydrobromic acid and concentrated acetic acid to reflux over 2 d. The resulting 1,4,7-triazacyclononane trihydrobromide **3-12** was neutralized with sodium hydroxide in water and extracted into benzene. Finally, distillation under reduced pressure gave the free 1,4,7-triazacyclononane **3-13** in moderate yield but excellent purity, which was stored under dinitrogen in the refrigerator to prevent decomposition. All reaction intermediates were analyzed by IR, NMR and elemental analysis, which was fully in line with the published data.<sup>[94]</sup>

For the synthesis of 1,4,7-tris(2-pyridylmethyl)-1,4,7-triazacyclononane ( $\text{py}_3\text{tacn-}\kappa^3\text{N}$ ) **3-14**, an aqueous suspension of **3-13** and 2-pyridylmethylchloride hydrochloride in 1:3 ratio was neutralized with sodium hydroxide to obtain a deep red solution. Upon standing for 1 h, a





respectively. The peaks in the aromatic region at 121.8, 123.2, 136.2 and 148.9 ppm are assigned to the pyridyl carbon atoms in the 5-, 3-, 4-, and 6-positions. The quaternary C2-atoms experience the strongest downfield shift due to the neighboring ring nitrogen and appear at 160.4 ppm.

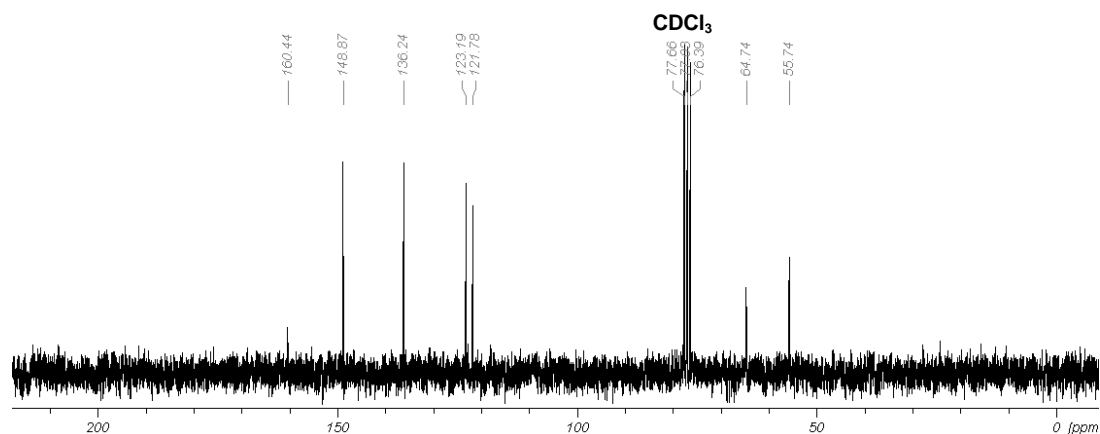
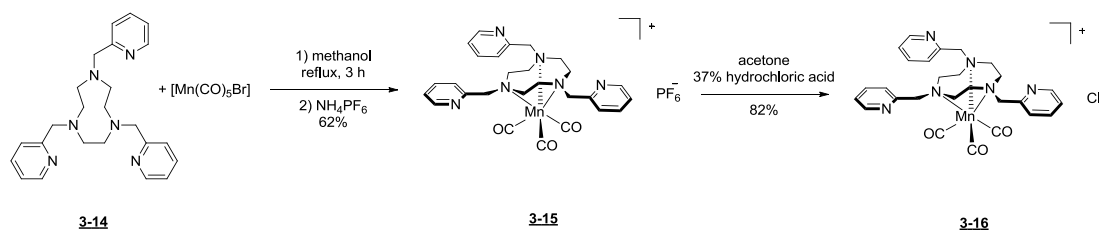


Fig. 3.34:  $^{13}\text{C}\{^1\text{H}\}$  NMR spectrum (50.27 MHz,  $\text{CDCl}_3$ ) of **3-14**.

### 3.2.2 Synthesis and characterization of metal complexes

#### 3.2.2.1 Synthesis and characterization of $[\text{Mn}(\text{CO})_3(\text{py}_3\text{tacn-}\kappa^3\text{N})]\text{Cl}$

The synthesis of  $[\text{Mn}(\text{CO})_3(\text{py}_3\text{tacn-}\kappa^3\text{N})]\text{PF}_6$  **3-16** was carried out by a procedure similar to that of the complexes of the tpa-series and the work of Wieghardt *et al.*<sup>[93]</sup> Due to its honey-like consistence, the py<sub>3</sub>tacn-ligand **3-14** was dissolved in methanol before the whole mixture was degassed by three freeze-pump-thaw cycles. Manganese pentacarbonyl bromide was added and the reaction mixture was heated to reflux for 3 h under exclusion of light. From the resulting yellow solution, **3-15** was obtained as the hexafluorophosphate salt by addition of a saturated solution of ammonium hexafluorophosphate in methanol in good yield (**Scheme 3.11**).



**Scheme 3.11:** Synthesis of **3-15** and **3-16**.

To increase the water solubility for biological testing, the hexafluorophosphate cation of **3-15** was exchanged to chloride by careful dropwise addition of concentrated hydrochloric acid to a solution of **3-15** in acetone. The resulting yellowish precipitate was applied to a Waters SepPak C-18 reversed phase column and eluted with water/acetonitrile as the eluent and dried by lyophilization.

The IR spectrum of **3-15** shows two very strong bands at 2028 and 1921  $\text{cm}^{-1}$  (**Fig. 3.35**). Furthermore, weak to medium bands at 1592, 1466, 1441 and 793  $\text{cm}^{-1}$  as well as a strong band at 831  $\text{cm}^{-1}$  are observed. The sharp signal at 2028  $\text{cm}^{-1}$  is assigned to the symmetric CO stretching vibration while the broader band at 1921  $\text{cm}^{-1}$  is due to the antisymmetric stretch of the facial manganese(I) tricarbonyl moiety. The peaks at 1592, 1466 and 1441  $\text{cm}^{-1}$  result from the stretching vibrations of the aromatic C-C- and C-N-double bonds. The C-N stretching vibration of the amine bond is observed at 780  $\text{cm}^{-1}$ . The

strong band at  $831\text{ cm}^{-1}$  is due to the P-F stretching vibration of the hexafluorophosphate counterion. After ion exchange to the chloride salt **3-16**, this signal was no longer present in the IR.

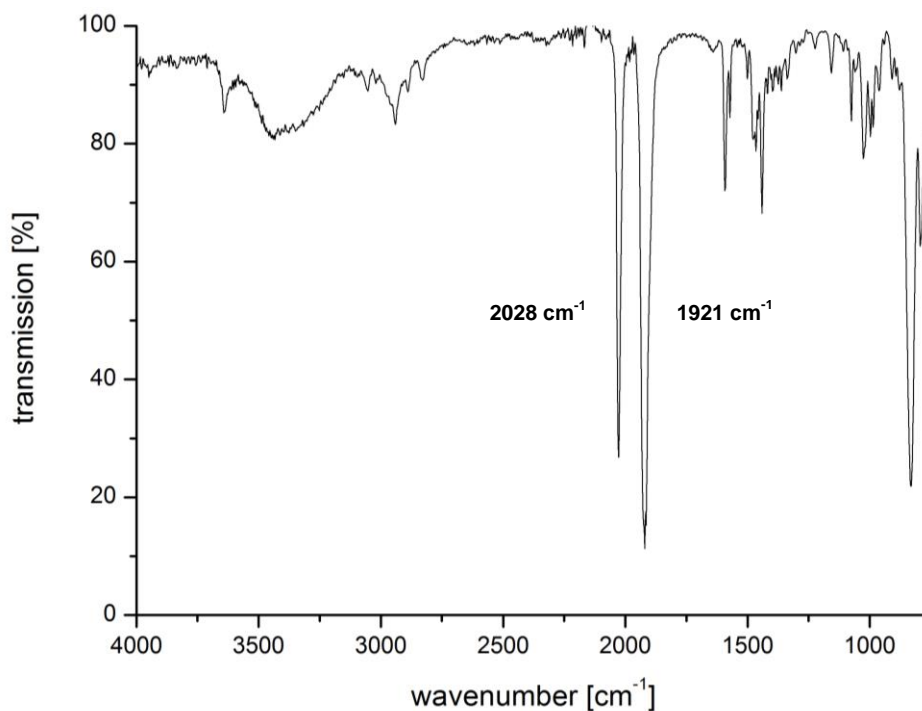


Figure 3.35: ATR-IR spectra of **3-15**.

The  $^1\text{H}$  NMR-spectrum of hexafluorophosphate salt **3-15** was recorded in chloroform while the chloride salt **3-16** is also soluble in  $\text{DMSO-d}_6$  (Fig. 3.36). However, the exchange of the counterion had no influence on the overall appearance of the spectra. Thus, only the results obtained for the chloride compound **3-16** are presented here. In the aliphatic region, two doublets at 2.77 and 3.76 ppm as well as one singlet at 4.74 ppm with integrals of 6H each are observed. The aromatic region shows a doublet with a strong downfield shift at 8.68 ppm, two triplets at 7.95 and 7.49 ppm and one additional doublet at 7.75 ppm with integrals of 3H each.

An obvious difference between the spectrum of **3-16** and those of the tpa complexes is the appearance of just one set of signals for the three pyridylmethyl groups at 4.74 ppm. The two doublets at 2.77 and 3.76 ppm with  $^2J = 7.9\text{ Hz}$  are assigned to the twelve ring protons of the triazacyclononane backbone. The two signals result from the different

environment of the methylene protons which become diastereotopic as some point towards the  $\text{Mn}(\text{CO})_3$  moiety and some away from the metal center. The triplet at 7.49 ppm with  $^3J = 4.8$  Hz is assigned to the H5 atoms of the pyridine rings. The doublet at 7.75 ppm with  $^3J = 7.7$  Hz is due to the protons in 3-positions. The triplet at 7.94 ppm with  $^3J = 7.7$  Hz is the result of the H4 atoms, while the doublet with strong downfield shift at 8.68 ppm with  $^3J = 4.8$  Hz is assigned to the hydrogen atoms in the 6-positions.

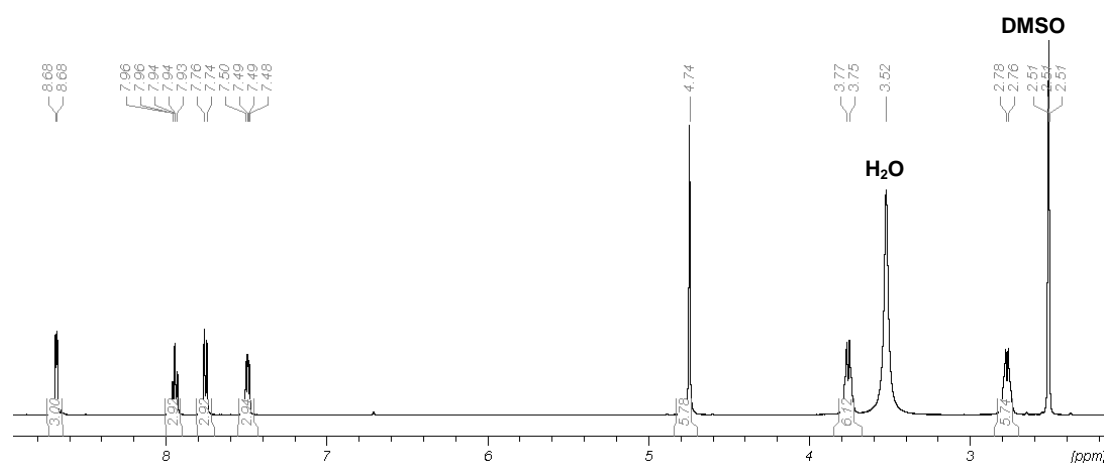


Figure 3.36:  $^1\text{H}$  NMR spectrum (500.13 MHz,  $\text{DMSO-d}_6$ ) of **3-16**.

The  $^{13}\text{C}\{^1\text{H}\}$  NMR-spectrum (Fig. 3.37) of **3-16** shows two peaks in the aliphatic region at 55.0 and 68.5 ppm and five signals in the aromatic region at 124.0, 126.8, 137.3, 149.3 and 153.1 ppm plus a strongly downfield shifted signal at 218.0 ppm.

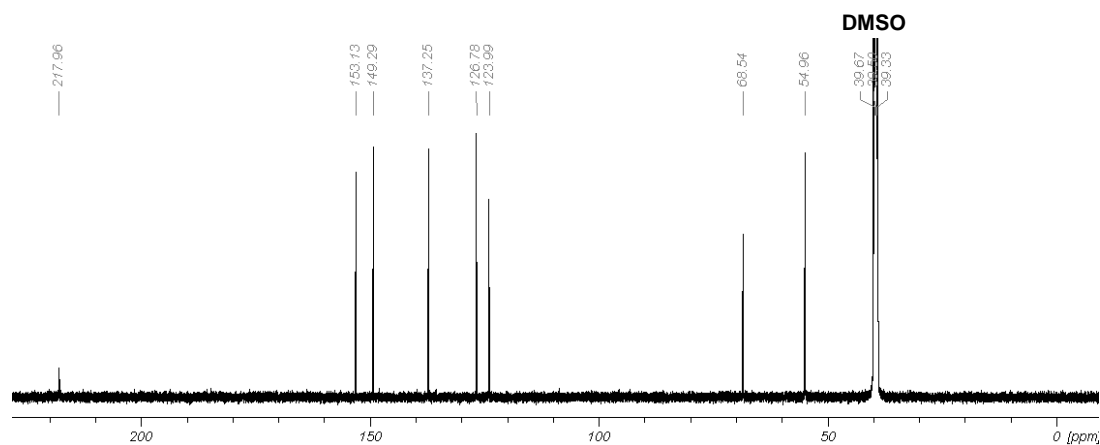


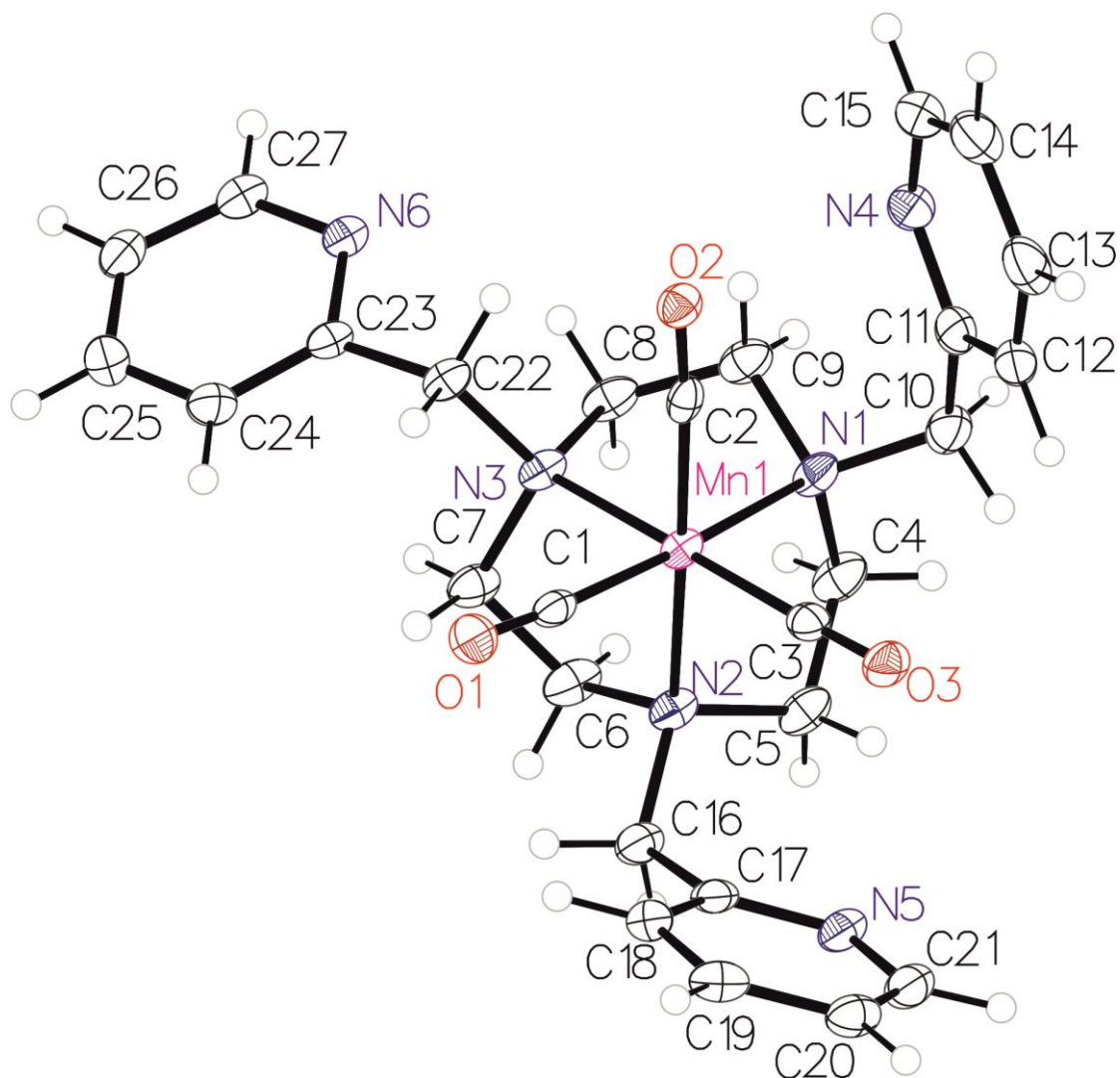
Figure 3.37:  $^{13}\text{C}\{^1\text{H}\}$  NMR spectrum (125.75 MHz,  $\text{DMSO-d}_6$ ) of **3-16**.

The two signals at 55.0 and 68.5 ppm in the aliphatic region are assigned to three methylene groups of the triazacyclononane backbone and those of the pyridyl groups, respectively. The aromatic region of the spectrum shows the signals of the pyridine rings. The signals of the C5- and C3-atoms are observed at 124.0 and 126.8 ppm while the peak at 137.3 ppm is assigned to the C4 atom with the ring nitrogen in para-positions. The two signals at 149.3 and 153.1 ppm belong to the C6- and the quaternary C2-atom with the ring nitrogen in direct neighborhood. At 218.0 ppm, the signal of the three equivalent carbonyl ligands is observed.

In the positive mode ESI-MS of **3-15**, signals at  $m/z = 365.14$ ,  $383.15$  and  $541.17$  Da are observed. The peak at  $m/z = 365.14$  Da matches with a cation with a composition of  $[M-3CO-CH_2C_5H_4N-PF_6]^+$ , which has lost all three carbonyl ligands and one of the pyridylmethyl moieties even under ESI ionization conditions. At  $m/z = 383.15$  Da, the water adduct of this cation with a composition of  $[M-3CO-CH_2C_5H_4N+H_2O-PF_6]^+$  is observed. At  $m/z = 541.17$  Da the complex cation  $[M-PF_6]^+$  is found.

Single crystals of **3-15** were obtained by slow diffusion of *n*-hexane into a dichloromethane solution of the complex. Compound **3-15** crystallizes in the P-1 space group. The unit cell contains the cationic  $[Mn(CO)_3(py_3tacn-\kappa^3N)]^+$  moiety as well as the hexafluorophosphate counter ion (**Fig. 3.38**). The manganese center is in an octahedral coordination sphere with a  $MnC_3N_3$  ligand environment and the three pyridyl groups stay uncoordinated as intended. The bond lengths between the carbonyl ligands and the manganese(I) center are nearly identical with Mn1-C1 at 1.804(2) Å, Mn1-C2 at 1.794(3) Å and Mn1-C3 at 1.819(2) Å, which is very similar to the values found for the complexes in the tpa series. The Mn-N bond lengths range from 2.107(2) Å for Mn1-N1 and 2.104(2) Å for Mn1-N2 to 2.1084(19) Å for Mn1-N3. The angles between the carbonyl ligands and the  $py_3tacn$ -backbone with C1-Mn1-N1 at 175.93(9)°, C2-Mn1-N2 at 175.32(8)° and C3-Mn1-N3 at 177.58(9)° are all close to 180°. The angles between the carbonyl ligands with C1-Mn1-C2 at 86.08(10)°, C1-Mn1-C3 at 88.55(10)° and C2-Mn1-C3 at

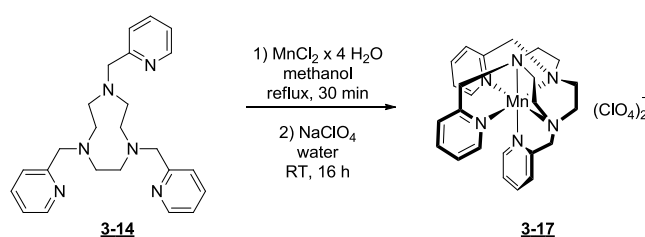
88.79(10)° are all slightly less than 90°. The angles between the coordinated nitrogen atoms are 82.91(8)° for N1-Mn1-N3, 83.55(8)° for N1-Mn1-N2 and 82.71(7)° for N2-Mn1-N3.



**Figure 3.38:** Molecular structure of  $[\text{Mn}(\text{CO})_3(\text{py}_3\text{tacn-}\kappa^3\text{N})]^+$  **3-15** with ellipsoids drawn at the 50% probability level. The hexafluorophosphate counterion in the unit cell is not shown for clarity.

3.2.2.2 Synthesis and characterization of  $[\text{Mn}(\text{py}_3\text{tacn-}\kappa^6\text{N})](\text{ClO}_4)_2$ 

One advantage of the  $\text{py}_3\text{tacn}$  ligand system is the published synthesis of the iCORM product expected to result from complete photolysis of all three carbonyl ligands. Thus, a solution of  $\text{py}_3\text{tacn}$  **3-14** in methanol was degassed with three freeze-pump-thaw cycles. After addition of manganese dichloride tetrahydrate, the mixture was heated to reflux for 30 min. In the report of Wieghardt, the desired compound was isolated as the perchlorate salt for better crystallization and purification. Therefore, sodium perchlorate was added to the reaction mixture to obtain **3-17** as off white needles (Scheme 3.12).<sup>[93]</sup>

Scheme 3.12: Synthesis of **3-17**.

The isolation as the chloride salt, preferred for biological studies was not possible. In particular, purification of  $[\text{Mn}(\text{py}_3\text{tacn-}\kappa^6\text{N})]\text{Cl}_2$  failed because of unidentified byproducts in the reaction mixture, which had the same solubility and crystallization behavior as the main product. Due to the paramagnetic  $3d^5$  manganese(II) center, characterization of  $[\text{Mn}(\text{py}_3\text{tacn-}\kappa^6\text{N})](\text{ClO}_4)_2$  **3-17** was quite difficult as no NMR spectrum could be obtained. In the IR spectrum of **3-17**, three weak bands at 3079, 2891 and 2842  $\text{cm}^{-1}$  are observed, while some weak to medium signals appear at 1609, 1442, 1312, 1016 and 771  $\text{cm}^{-1}$ . Furthermore, one very strong band was observed at 1075  $\text{cm}^{-1}$  (Fig. 3.39). The signals at 3079  $\text{cm}^{-1}$  is due to the aromatic C-H stretching vibrations of the three pyridyl rings while the two signals at 2891 and 2842  $\text{cm}^{-1}$  are due to the aliphatic C-H stretching vibration of the triazacyclononane backbone. The smaller peaks between 1609 and 1016  $\text{cm}^{-1}$  are assigned to the stretching vibrations of the aromatic C-C- and C-N-double bonds.

The very strong band at  $1075\text{ cm}^{-1}$  resulted from the Cl-O stretching vibrations of the perchlorate ions. The C-N stretching vibration of the amine bond is observed at  $771\text{ cm}^{-1}$ .

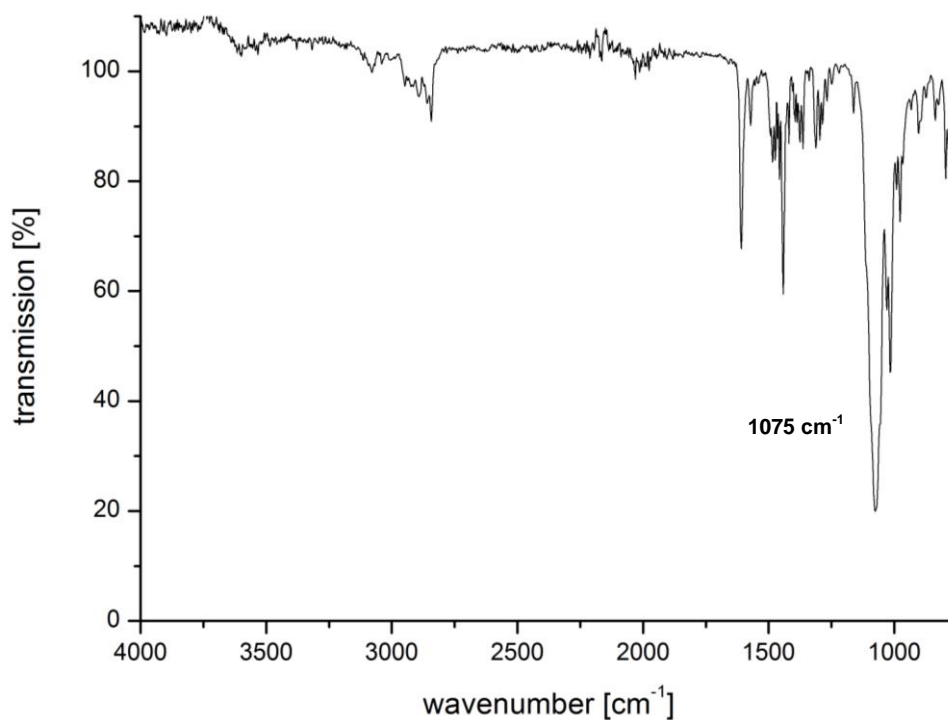


Figure 3.39: ATR-IR spectrum of **3-17**.

The results of the CHN analysis are in line with the values expected for a composition of  $[\text{Mn}(\text{py}_3\text{tacn-}\kappa^6\text{N})](\text{ClO}_4)_2$  and are collected in **Table 3.5**.

Table 3.5: Results of the elemental analysis for  $[\text{Mn}(\text{py}_3\text{tacn-}\kappa^6\text{N})](\text{ClO}_4)_2$  **3-17**.

	C [%]	H [%]	N [%]
<b>found</b>	44.18	4.35	12.56
<b>calculated for <math>\text{C}_{24}\text{H}_{30}\text{ClMnN}_6\text{O}_8</math></b>	43.92	4.61	12.80



### 3.2.3 UV/Vis studies

To study the light-triggered CO-release from  $[\text{Mn}(\text{CO})_3(\text{py}_3\text{tacn-}\kappa^3\text{N})]\text{PF}_6$  **3-15**, absorption spectra at different concentrations were recorded in dimethylsulfoxide to determine the extinction coefficients. At the main absorption band at 365 nm, the extinction coefficient is  $1695 \pm 5 \text{ M}^{-1}\text{cm}^{-1}$ , which is lower than the values of the compounds in the  $[\text{Mn}(\text{CO})_3(\text{L-}\kappa^3\text{N})]\text{Br}$  series at the same wavelength. The compound was stable in the dark in dimethylsulfoxide solution for up to 3.5 h and in phosphate-buffered saline (PBS) in the presence of 60  $\mu\text{M}$  myoglobin and 10 mM dithionite for up to 16 h.

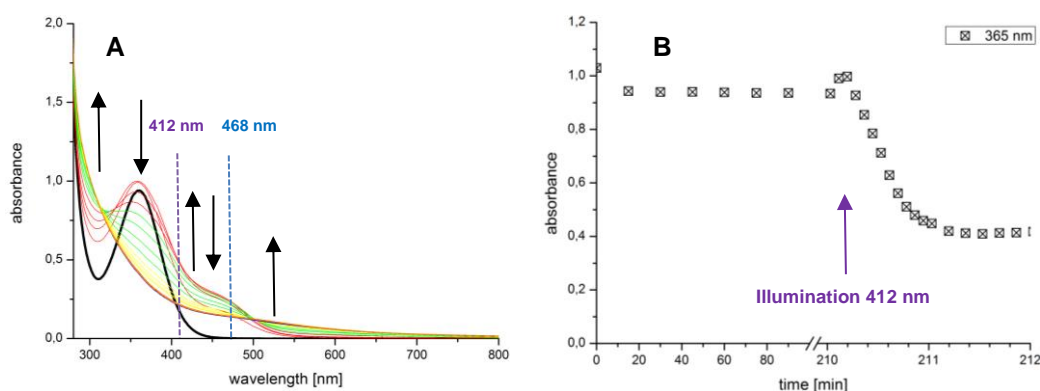


**Figure 3.40:** (A) Changes in the UV/Vis spectra of a DMSO solution of **3-15** illuminated at 412 nm for 20 min. The spectrum recorded before start of the illumination is shown in black. (B) Changes in the absorbance of a solution of **3-15** in DMSO in the dark for 3.5 h and upon subsequent illumination at 365 nm for 2 min.

In the UV/Vis spectrum of **3-15**, several changes are observed upon illumination at 412 nm (**Fig. 3.40A**). Almost immediately, two new shoulders at 300 and 450 nm grow in while the original absorption band at 365 nm decreases in intensity. After 8 min, the shoulder at 450 nm vanishes again and a new band at 550 nm forms. Interestingly, the same effect is also observed upon illumination at 468 nm, although at this wavelength, the absorption is much lower than at 412 nm (**black curve**). The CO-release properties of **3-15** were examined with the myoglobin assay. The compound was stable under these conditions for at least 16 h in the dark (**Fig. 3.40B**). After the dark incubation, the same sample was illuminated at 412 nm. In experiments with a dark incubation time of 1 h, a MbCO concentration of  $(27.7 \pm 6.5) \mu\text{M}$  was

determined with a half-life of 21.6 min (**Fig. 3.41**). Longer dark pre-incubation times of up to 16 h lead to an increase of MbCO to 32.0  $\mu\text{M}$  while the half-life decreased to 10.9 min. The photoactivation at 468 nm and a short dark incubation time of 1 h results in a less efficient release process. The final MbCO concentration decreased to 12.1  $\mu\text{M}$ , while the half-life was extended to 25.3 min in this experiment (**Fig. 3.42**).

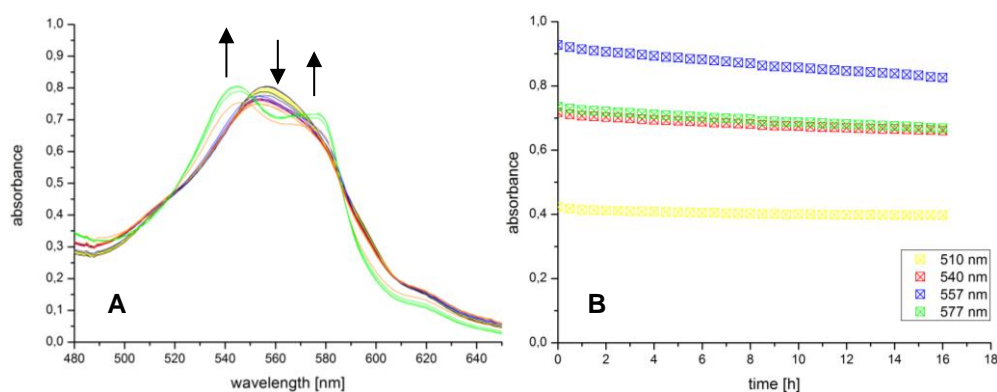


**Figure 3.41:** (A) Changes in the UV/Vis spectra of a solution of **3-15** (10  $\mu\text{M}$ ) in PBS in the presence of myoglobin (60  $\mu\text{M}$ ) and sodium dithionite (10 mM) upon illumination at 412 nm for 2 h. Original spectrum before illumination is shown as a black line. (B) Dark stability trace of solutions of **3-15** (10  $\mu\text{M}$ ) in PBS in the presence of myoglobin (60  $\mu\text{M}$ ) and sodium dithionite (10 mM).

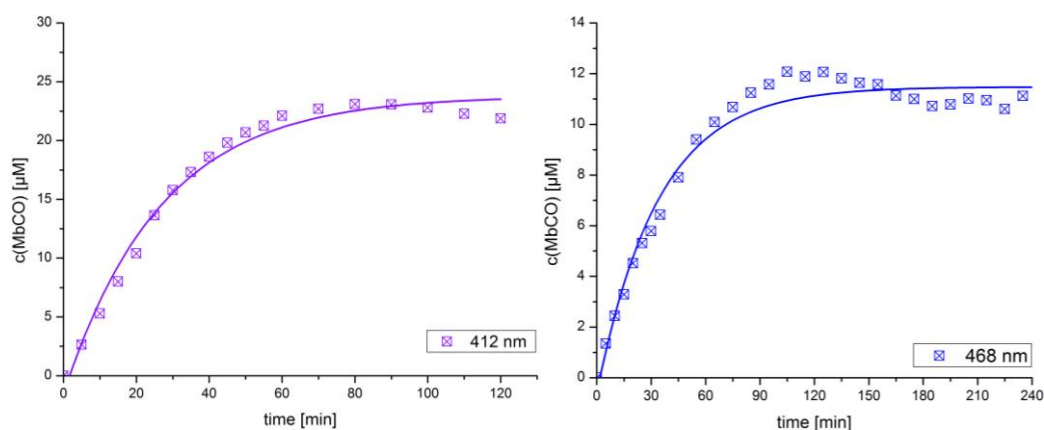


**Figure 3.42:** Concentrations of MbCO generated upon illumination of **3-15** at 412 and 468 nm in PBS in the presence of myoglobin (60  $\mu\text{M}$ ) and sodium dithionite (10 mM).

### 3.2.4 IR studies and DFT calculations

To detect possible intermediates in the photolytic CO release from **3-15** in solution, an IR experiment was carried out the same way as it was done for **3-5** (see section 3.1.6). Briefly, a stock solution of  $[\text{Mn}(\text{CO})_3(\text{py}_3\text{tacn}-\kappa^3\text{N})]\text{PF}_6$  in dimethylsulfoxide was prepared and filled into an IR liquid cell with calcium fluoride windows under exclusion of light. The cell was illuminated at 412 nm and spectra were recorded every 20 s. Later in the experiment, the illumination intervals were increased to 40, 60, 120, 300, and finally 600 s. Distinct changes in the IR spectra could be observed. The three original bands at 2026, 1927 and 1915  $\text{cm}^{-1}$  started to decrease immediately upon exposure to light while two new bands at 1820 and 1829  $\text{cm}^{-1}$  grew in. After 5 min, two additional signals appear at 1861 and 1897  $\text{cm}^{-1}$  which remain stable until the end of the experiment. The weak IR signal of dissolved CO at 2140  $\text{cm}^{-1}$  could not be detected due to the detection limit of the instrument (Fig. 3.43 and 3.44).

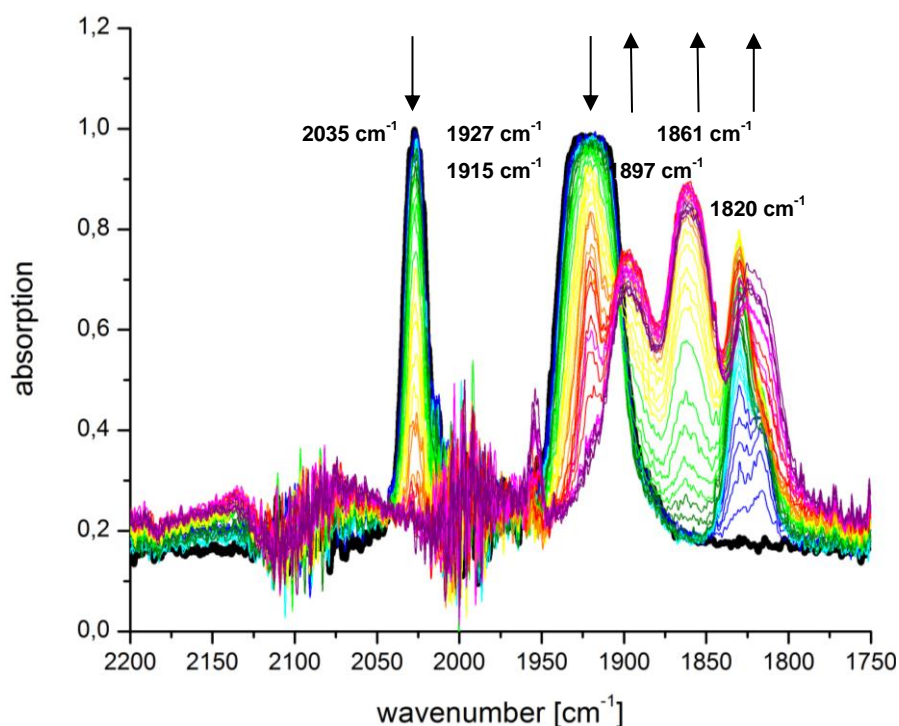
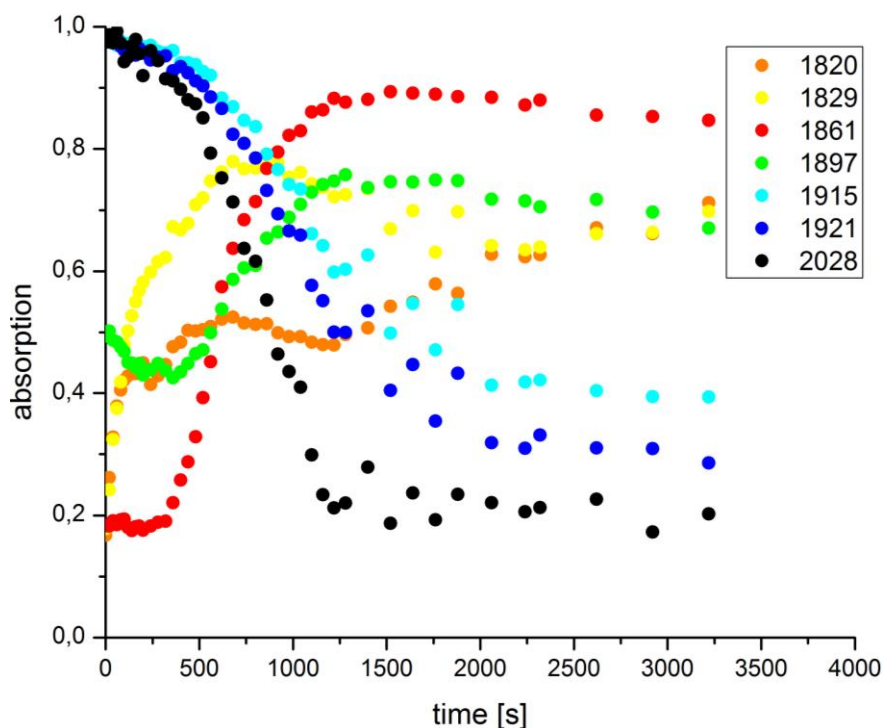


Figure 3.43: Changes in the IR spectrum of a DMSO solution of **3-15** upon illumination at 412 nm from 0-60 min.

To assign these signals to different species, potential iCORM intermediates were constructed from the X-ray structure coordinates of **3-15** and their

geometries optimized with DFT using the BP86 functional and a TZVP basis set together with the COSMO(DMSO) solvation model to the experimental. The DFT model chemistry was verified by comparison of the calculated and experimental CO stretching vibrations (**Fig. 3.45**). With the use of a proper scaling factor of 1.034, the deviation for the symmetric and antisymmetric modes was smaller than 30 cm<sup>-1</sup> for [Mn(CO)<sub>3</sub>(py<sub>3</sub>tacn-κ<sup>3</sup>N)]<sup>+</sup> **3-15** (**A**).



**Figure 3.44:** Time-dependent appearance of the experimental IR traces of a DMSO solution of **3-15** upon illumination at 412 nm for 0-60 min.

Thus, one carbonyl ligand was removed and replaced by a water molecule and the molecule was optimized again. This led to minimum structure **B** with a Mn(CO)<sub>2</sub>(H<sub>2</sub>O)N<sub>3</sub> coordination environment while the three pyridyl groups remain pendant. The calculated scaled CO stretching vibrations are observed at 1911 and 1802 cm<sup>-1</sup>. These are in line with the signals at 1829 and 1820 cm<sup>-1</sup>, observed in the experiment. The calculations also led to a minimum structure **C** with an octahedral Mn(CO)<sub>2</sub>N<sub>4</sub> geometry and a tetracoordinated py<sub>3</sub>tacn ligand with one pyridyl group bound. The calculated scaled CO stretching vibrations for this structure are found at 1918 and 1830 cm<sup>-1</sup>. These two peaks are in good agreement with the experimental stretches found at 1897 and 1861

cm<sup>-1</sup>. Removal of a second carbonyl ligand and replacement with a water molecule results in minimum geometry **D**. For this structure, two different isomers **D1** and **D2** were optimized, which differ in the orientation of the carbonyl and water ligands relative to coordinated pyridine moiety. For **D1**, the carbonyl stretch was calculated at 1780 cm<sup>-1</sup> while for **D2** the carbonyl stretch was significantly higher at 1802 cm<sup>-1</sup>. However, these signals could not be clearly identified in the experiment due to an overlap with the IR bands of the photolysis intermediates **B** and **C**. Next, the water molecule in **D** was removed and replaced by one of the pedant pyridyl groups and the structure optimized again. This led to minimum structure **E** with an octahedral Mn(CO)N<sub>5</sub> geometry. The carbonyl stretching vibration of the only remaining CO ligand is found at 1828 cm<sup>-1</sup>. Removal of the last carbonyl ligand and replacement by a water molecule led to **F**. The replacement of the water molecule by the last pedant pyridyl group and further optimization resulted in minimum structure **G** (Tab. 3.6).

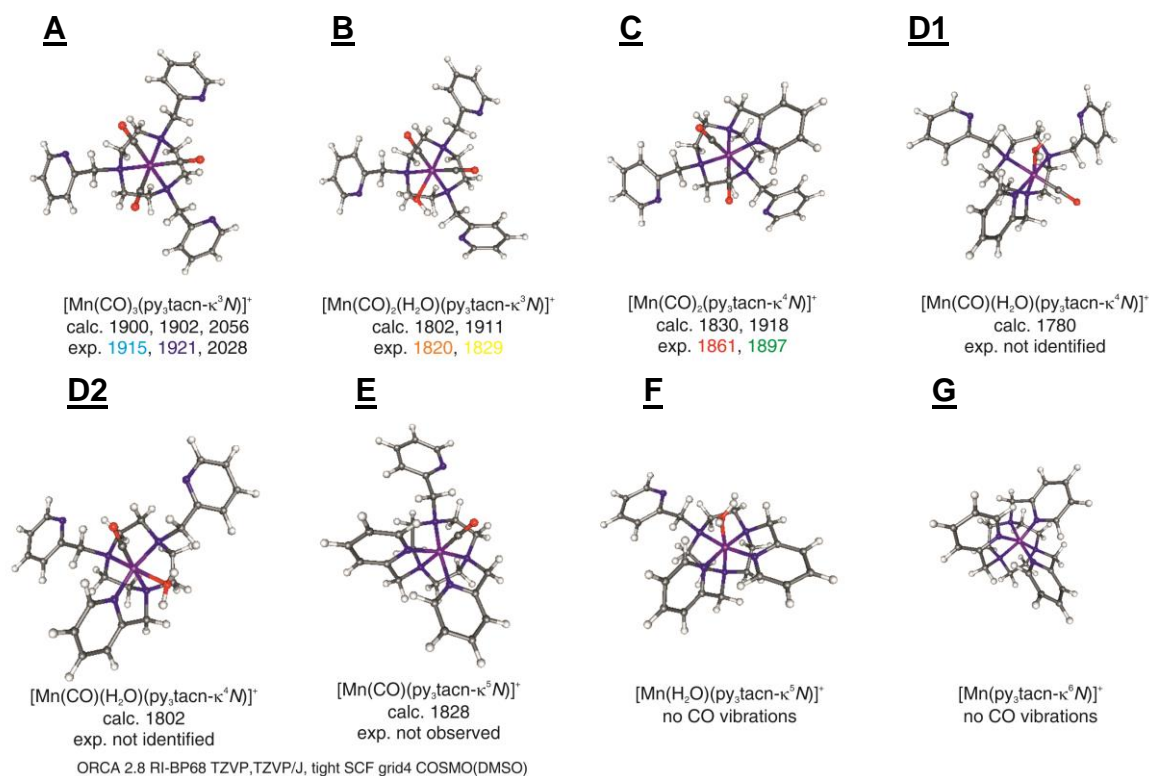


**Figure 3.45:** Structure of the cationic unit of parent compound **3-15** (**A**) and iCORM intermediates **B-G** optimized with BP86 TZVP after subsequent removal of carbonyl ligands and replacement with solvent water or pendant pyridyl group.

Upon the release of CO, the formation of three additional intermediates seems to be possible. The optimized iCORM intermediates  $[\text{Mn}(\text{H}_2\text{O})_2(\text{py}_3\text{tacn-}\kappa^4\text{N})]^+$  and  $[\text{Mn}(\text{H}_2\text{O})_3(\text{py}_3\text{tacn-}\kappa^3\text{N})]^+$  should be found in a non-step-wise release mechanism of the carbonyl ligands. However, these two intermediates did not converge as Mn(I) low spin structures in the DFT-calculations.

The time scale of the first CO released in the IR experiment of **3-15** after the first 20 min is perfectly in line with the release kinetics observed in the myoglobin assay, which showed a half-life of 21.6 min. The second carbonyl ligand should then be released after 60 to 80 min. Due to the overlap of the carbonyl signals of the different intermediates, this process was not clearly identified. The third carbonyl is then released by an oxidative dark process which should lead to the closed shell  $[\text{Mn}(\text{py}_3\text{tacn-}\kappa^6\text{N})]^{2+}$ .

**Table 3.6:** Comparison of experimental and scaled calculated frequencies for compound **A** and potential iCORM intermediates **B-G** resulting from the photolysis of **3-15** at 412 nm.

structure	$\tilde{\nu}_{\text{sym}}(\text{CO}) [\text{cm}^{-1}]$	$\tilde{\nu}_{\text{antisym}}(\text{CO}) [\text{cm}^{-1}]$	$\tilde{\nu}_{\text{antisym}}(\text{CO}) [\text{cm}^{-1}]$
<b>A</b> <sub>exp</sub>	2028	1921	1915
<b>A</b> <sub>calc</sub>	2056	1902	1900
<b>Diff.</b> <sub>calc-exp</sub>	+28	-19	-15
<b>B</b> <sub>exp</sub>	1829	1820	<i>a</i>
<b>B</b> <sub>calc</sub>	1910	1802	<i>a</i>
<b>Diff.</b> <sub>calc-exp</sub>	+81	-18	<i>a</i>
<b>C</b> <sub>exp</sub>	1897	1861	<i>a</i>
<b>C</b> <sub>calc</sub>	1918	1830	<i>a</i>
<b>Diff.</b> <sub>calc-exp</sub>	+21	-31	<i>a</i>
<b>D1</b> <sub>exp</sub>	<i>b</i>	<i>c</i>	<i>c</i>
<b>D1</b> <sub>calc</sub>	1780	<i>c</i>	<i>c</i>
<b>Diff.</b> <sub>calc-exp</sub>	<i>b</i>	<i>c</i>	<i>c</i>
<b>D2</b> <sub>exp</sub>	<i>b</i>	<i>c</i>	<i>c</i>
<b>D2</b> <sub>calc</sub>	1802	<i>c</i>	<i>c</i>
<b>Diff.</b> <sub>calc-exp</sub>	<i>b</i>	<i>c</i>	<i>c</i>
<b>E</b> <sub>exp</sub>	<i>b</i>	<i>c</i>	<i>c</i>
<b>E</b> <sub>calc</sub>	1828	<i>c</i>	<i>c</i>
<b>Diff.</b> <sub>calc-exp</sub>	<i>b</i>	<i>c</i>	<i>c</i>
<b>F</b> <sub>exp</sub>	<i>d</i>	<i>d</i>	<i>d</i>
<b>F</b> <sub>calc</sub>	<i>d</i>	<i>d</i>	<i>d</i>
<b>Diff.</b> <sub>calc-exp</sub>	<i>d</i>	<i>d</i>	<i>d</i>
<b>G</b> <sub>exp</sub>	<i>d</i>	<i>d</i>	<i>d</i>
<b>G</b> <sub>calc</sub>	<i>d</i>	<i>d</i>	<i>d</i>
<b>Diff.</b> <sub>calc-exp</sub>	<i>d</i>	<i>d</i>	<i>d</i>

<sup>a</sup> Dicarbonyl species, only one antisymmetric CO vibrational mode. <sup>b</sup> Not observed, probably overlapped with remaining signals of **A-C**. <sup>c</sup> Monocarbonyl species, only one CO vibrational mode. <sup>d</sup> no CO vibrational mode

ORCA 2.8 RI-BP68 TZVP, TZVP/J, tightSCF grid4 COSMO(DMSO), scaling factor = 1.034

### 3.3 Heterobinuclear manganese/ruthenium PhotoCORMs

#### 3.3.1 Background

For application of PhotoCORMs inside the body, the excitation wavelength should be in the phototherapeutic window from 600-1200 nm since the tissue penetration depth is proportional to the illumination wavelength, and negative effects of energy-rich light on tissue are avoided this way.<sup>[60]</sup> To prepare compounds with longer wavelength absorption, the use of  $\pi$ -systems with large conjugated coligands is one option. As an alternative, the introduction of electron-withdrawing groups or heteroatoms such as sulfur in the ligands has also been established.<sup>[95]</sup> Another way to shift the absorption maximum to higher wavelengths is the use of photosensitizing groups. In particular, transition metal bipyridine complexes are known for their red-shifted absorption maxima.<sup>[96]</sup> Thus, in the present project, an effort was made to coordinate a Ru(II)(bpy)<sub>2</sub> group to a ligand backbone incorporating a second binding pocket for a Mn(I)Br(CO)<sub>3</sub> unit. Upon photoexcitation of the Ru(II) unit, a Ru(III) center is generated while the excess electron is transferred to the bipyridine ligands. Crosstalk between the two metal centers in the complex should then result in electron transfer from the Mn(I) unit to the Ru(III) center. This causes oxidation of the Mn unit to the +II oxidation state together with reduction of the Ru(III) to Ru(II) followed by spontaneous release of the CO ligands as the Mn(II) unit is unable to coordinate carbonyl ligands. To study the influence of the photosensitizing Ru(II) unit, the pure MnBr(CO)<sub>3</sub> complexes were also prepared as controls.



### 3.3.2 Synthesis of the ligands

In this work, the metal precursor  $[\text{Ru}(\text{etx})(\text{tbx})](\text{PF}_6)_2$  **3-18** incorporating a ethyl(2,2':6',2''-terpyridine)-4'-carboxylate (etx) as well as a *N*-((2,2':6',2''-terpyridin)-4'-yl)2,2'-bipyridine-5-carboxamide (tbx) moiety, 3-(pyridin-2-yl)-1,2,4-triazine[5,6-*f*]-1,10-phenanthroline (pytp) **3-19**, 3-(pyridin-2-yl)phenanthro[9,10-*e*]-1,2,4-triazine (pypt) **3-20** and 2,3-di(2-pyridyl)quinoxaline (dpx) **3-21**, were used as bridging ligands for the construction of heterobinuclear PhotoCORMs. The Ru(II)-precursor  $[\text{Ru}(\text{etx})(\text{tbx})](\text{PF}_6)_2$  **3-18** was provided by the group of Prof. Dr. K. Heinze from the Institute of Inorganic and Analytical Chemistry of the Johannes Gutenberg Universität Mainz (Fig. 3.46).

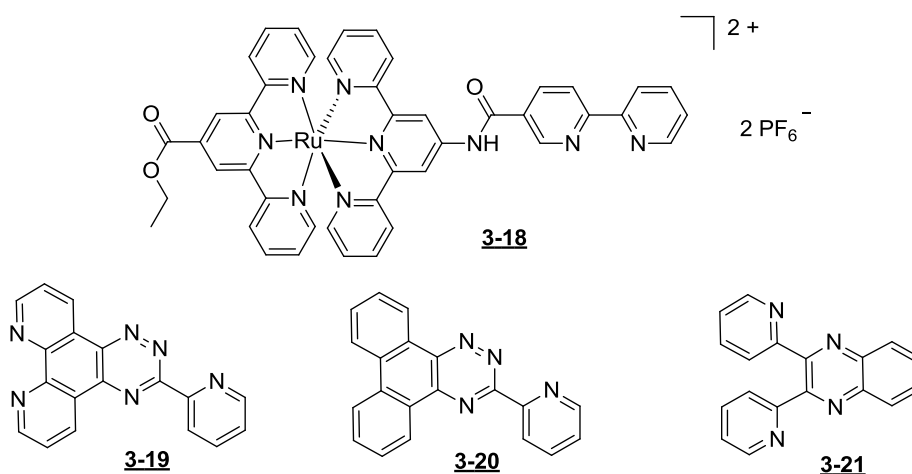
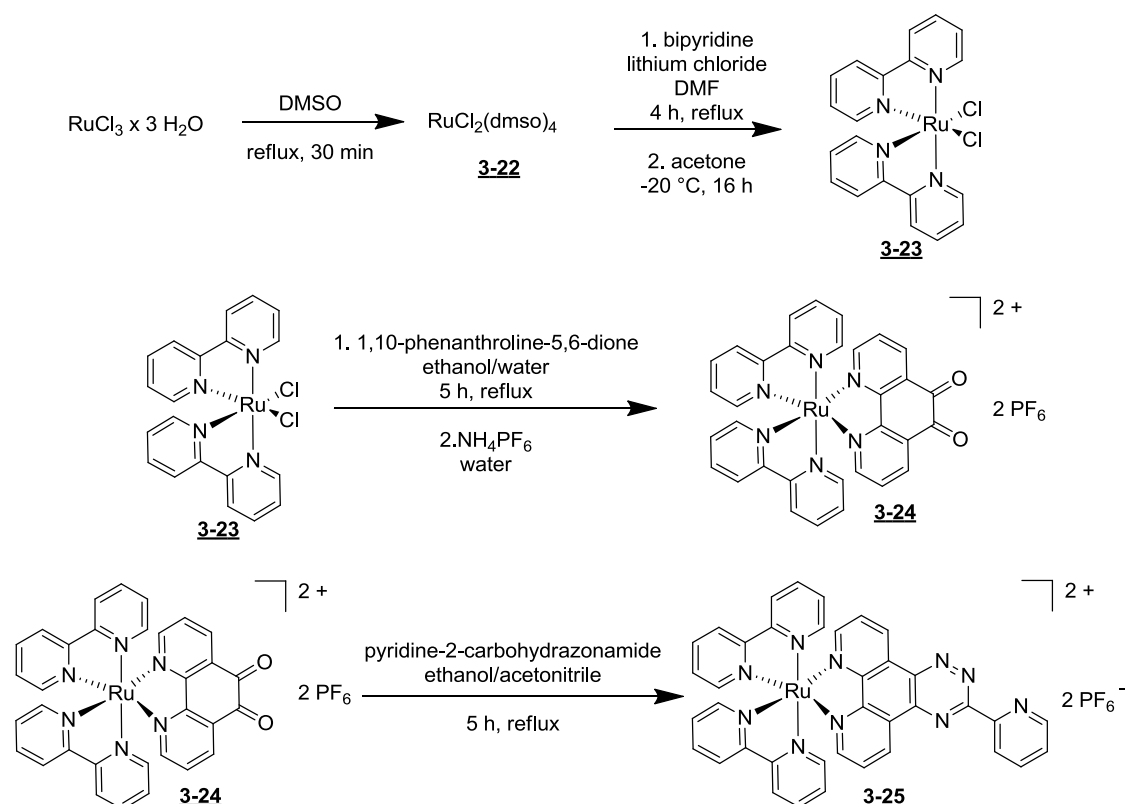


Figure 3.46:  $[\text{Ru}(\text{etx})(\text{tbx})](\text{PF}_6)_2$  **3-18** as well as the ligands pytp **3-19**, pypt **3-20**, and dpx **3-21** used in this work.

In case of the nonsymmetrical pytp system **3-19** the analogous 3-(pyridin-2-yl)phenanthro[9,10-*e*]-1,2,4-triazine (pypt) ligand **3-20** was used for the Mn(I)-CORM to force the Mn(I)Br(CO)<sub>3</sub>-moiety in the right binding pocket. For the symmetric dpx ligand **3-21** this step was not necessary. The 3-(pyridin-2-yl)-1,2,4-triazine[5,6-*f*]-1,10-phenanthroline (pytp) **3-19** and 3-(pyridin-2-yl)phenanthro[9,10-*e*]-1,2,4-triazine (pypt) **3-20** ligands were prepared as described below. The 2,3-di(2-pyridyl)quinoxaline (dpx) **3-21** ligand was prepared by Christoph Schneider in the Schatzschneider group according to the procedure of You *et al.*<sup>[97]</sup>

For the successful synthesis of the heterobinuclear manganese-ruthenium-complexes, the right sequence of reaction is very important. The Ru(II)-moiety has to be coordinated to the ligand backbone first followed by the introduction of the Mn(CO)<sub>3</sub>-moiety, as exploratory experiments showed that introducing the Mn-tricarbonyl group first was not successful. Thus, the ruthenium complex [RuCl<sub>2</sub>(dmsO)<sub>4</sub>] **3-22** was prepared as the initial precursor. Under an inert atmosphere, ruthenium(III) chloride trihydrate was dissolved in degassed dimethylsulfoxide and heated to reflux for 30 min. The mixture was poured into acetone and stored at -20 °C for 16 h. A brownish precipitate was obtained which was washed with acetone and diethylether and dried under vacuum. The product resulted in a yellow powder in moderate yield of 32% (Scheme 3.13).<sup>[98]</sup>



Then, [RuCl<sub>2</sub>(dmsO)<sub>4</sub>] **3-22**, lithium chloride and 2,2'-bipyridine (bpy) were dissolved in degassed *N,N*-dimethylformamide under an inert atmosphere and heated to reflux for 4 h. The violet reaction mixture was poured into acetone and stored at -20 °C for 16 h. A red precipitate formed which was

collected by filtration and extensively washed with cold water, ethanol and diethylether. The product was obtained as a black powder in a moderate yield of 57%. In the  $^1\text{H}$  NMR spectrum, the signals of **3-23** found in the aromatic region have an integral of 2H. At 7.11 and 7.50 ppm, a triplet and a doublet are observed while three additional triplets are found at 7.68, 7.77, and 8.07 ppm. In addition, the spectrum shows three doublets at 8.51, 8.66, and 9.96 ppm (Fig. 3.47).

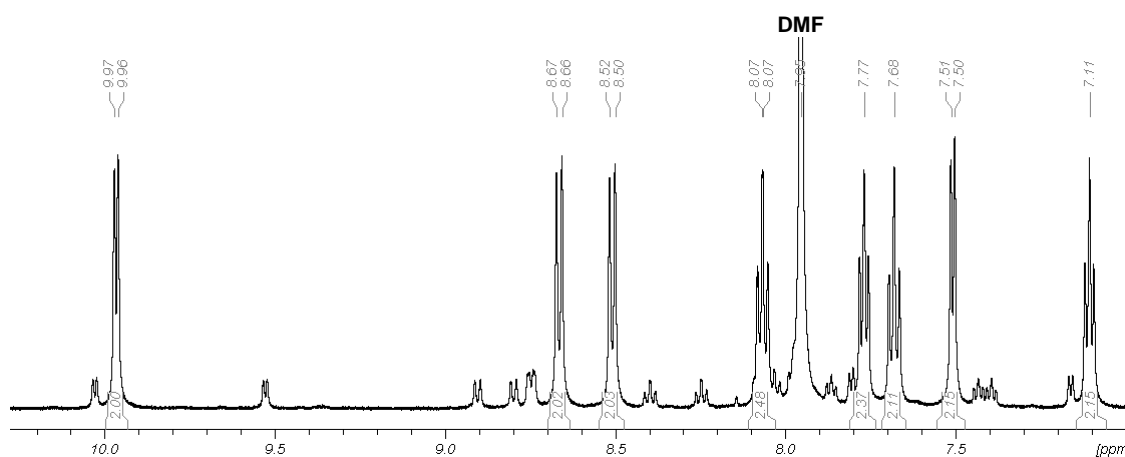


Figure 3.47: Aromatic region of the  $^1\text{H}$  NMR spectrum (500.13 MHz,  $\text{DMSO-d}_6$ ) of **3-23**.

The  $^1\text{H}$  NMR spectrum shows two sets of four signals which are assigned to the protons in the 3-, 4-, 5-, and 6-positions of the pyridine ring in a *trans*-positions and the protons in the 3', 4', 5', and 6'-positions of the pyridine ring in a *cis*-positions to the chloride ligands. The triplet at 7.11 ppm with  $^3J = 5.8$  Hz is due to the two protons in the 4'-positions. At 7.50 ppm with  $^3J = 5.5$  Hz, the doublet of the H3' atoms is observed. The two triplets at 7.68 and 7.77 ppm with  $^3J = 7.1$  Hz each result from the protons in the 4- and 5-positions while the triplet at 8.07 ppm and the doublet at 8.51 ppm with  $^3J = 8.0$  Hz are due to the H5'- and H3-atoms. The two signals with strong downfield shift at 8.66 and 9.96 ppm with  $^3J = 8.0$  and 5.8 Hz result from the protons in the 6'- and 6-positions with direct neighborhood to the ring nitrogen atom, respectively. The  $^1\text{H}$  NMR spectrum also shows some small impurities of a  $[\text{Ru}(\text{bpy})_3]$  byproduct in low concentration as well as the signal of *N,N*-dimethylformamide. Both impurities did not disturb the further reaction processes, and thus no attempt was made to remove them.

The  $^{13}\text{C}\{^1\text{H}\}$  NMR spectrum shows ten signals for **3-23** which are all found in the aromatic region. Four peaks are observed at 122.5, 122.8, 125.3, and 125.3 ppm. With a stronger downfield shift, the spectrum shows signals additional at 133.3, 134.5, 152.0, 153.2, 158.2, and 160.2 ppm (**Fig. 3.48**). The two sets of signals are assigned to the carbon atoms *cis* and *trans* to the chloride ligands. The peaks at 122.5 and 122.8 ppm are due to the carbon atoms in the 3'- and 3-positions while the peaks at 125.3 and 125.3 ppm result from the carbon atoms in the 5'- and 5-positions. The signals at 133.3 and 134.5 ppm are assigned to the C4'- and C4-atoms. The peaks at 152.0, 153.2 ppm result from the C6'- and C6-atoms while the signals at 158.2 and 160.2 ppm are due to the quaternary carbon atoms in the 2'- and 2-positions. The strong downfield shift of the last four signals results from the direct neighboring to the ring nitrogen atoms. The  $^{13}\text{C}\{^1\text{H}\}$  NMR spectrum also shows the three signals of a *N,N*-dimethylformamide impurity.

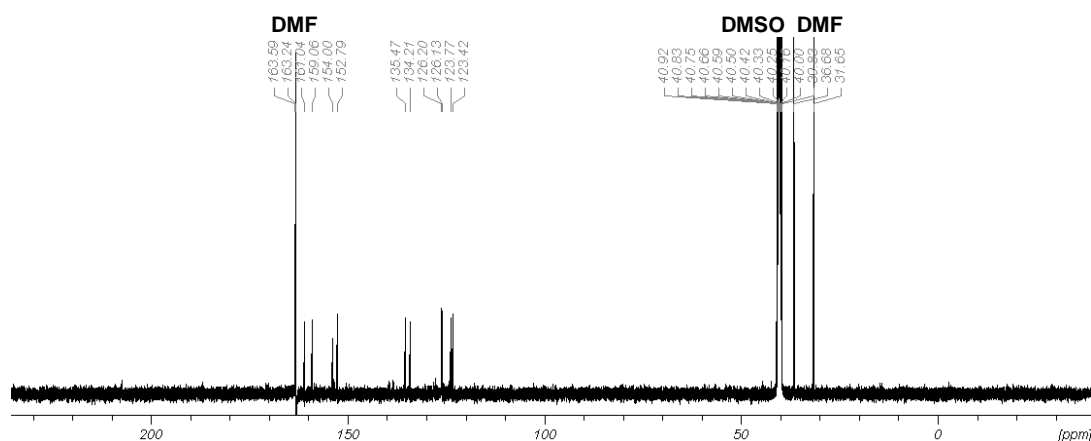


Figure 3.48:  $^{13}\text{C}\{^1\text{H}\}$  NMR spectrum (125.75 MHz,  $\text{DMSO-d}_6$ ) of **3-23**.

To force the Ru(II) moiety into the proper binding pocket, the pytp ligand was prepared directly in the coordination sphere of the ruthenium complex. Thus,  $[\text{RuCl}_2(\text{bpy})_2]$  **3-23** was dissolved under dinitrogen atmosphere in a degassed mixture of ethanol/water (50:50). After addition of 1,10-phenanthroline-5,6-dione (phenox), the mixture was heated to reflux for 3 h. Addition of a saturated aqueous solution of ammonium hexafluorophosphate resulted in formation of an orange precipitate which was collected by filtration, washed with water, cold ethanol and diethylether for purification and dried under

vacuum. The orange powder was obtained in a yield of 55%. The  $^1\text{H}$  NMR spectrum of **3-24** shows a multiplet with an integral of 4H at 7.58–7.63 ppm, and two doublets with an integral of 1H each at 7.82 and 7.83 ppm. At 8.10 and 8.16–8.28 ppm, a doublet and a multiplet with an integral ratio of 2:6 are observed. Two doublets of doublets with integrals of 2H each are found at 8.37 and 8.65 ppm. Further downfield, the spectrum shows a doublet at 8.84 ppm with an integral of 4H (Fig. 3.49).

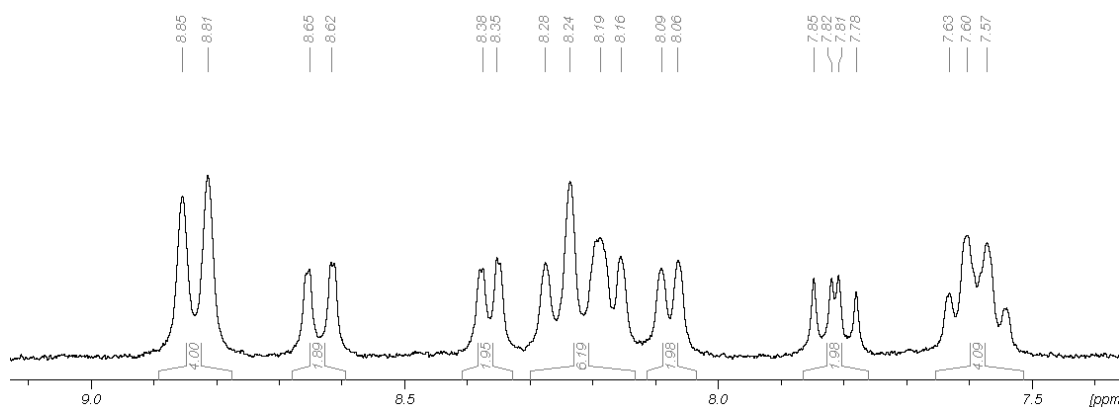


Figure 3.49: Aromatic region of the  $^1\text{H}$  NMR spectrum (acetone- $d_6$ , 500.13 MHz) of **3-24**.

The multiplet at 7.58–7.63 ppm is due to the overlap of the two triplets of the protons in 3- and 3'-positions of the bipyridine ligands. The two doublets at 7.82 and 7.83 ppm with  $^3J = 5.6$  Hz each results from the H4- and H4'-atoms of the 1,10-phenanthroline-5,6-dione (phenox) ligand. The doublet at 8.10 ppm with  $^3J = 5.6$  Hz is assigned to the signal of the H3'-atoms of the bipyridine ligands. The broad multiplet at 8.16–8.28 ppm results from the overlap of the phenox H5- and H5'-atoms as well as the triplet of the bipyridine H4- and H4'-atoms. The doublet of doublet at 8.37 with  $^3J = 5.6$  Hz and  $^4J = 1.4$  Hz is due to the H6- and H6'-protons of the phenox ligand. The doublet of doublets at 8.65 ppm with  $^3J = 8.0$  Hz and  $^4J = 1.4$  Hz results from the H3-protons of the bipyridine ligands. With stronger downfield shift at 8.84 ppm the doublet with  $^3J = 7.9$  Hz of the H6- and H6'-atoms of the bipyridine ligands is found. The  $^{13}\text{C}\{^1\text{H}\}$  NMR spectrum of **3-24** shows 16 signals for the 32 carbon atoms in the complex. All signals appear in the aromatic region. Nine peaks are found at 125.0, 125.0, 128.3, 128.4, 129.3, 131.8, 136.2, 138.8, and 138.9 ppm.

With stronger downfield shift, seven additional signals are observed at 152.4, 152.7, 156.6, 157.2, 157.6, 157.7, and 175.6 ppm. The two peaks at 125.0 ppm result from the carbon atoms in the 3'- and 3-positions of the bipyridine ligands. At 128.3 and 128.4 ppm the signals of the C5'- and C5-atoms are observed while those at 129.3 ppm is due to the C5- and C5'-atoms of the 1, 10-phenanthroline-5, 6-dione (phenox) ligand. The signal of the quaternary phenox C3- and C3'-atoms are found at 131.8 ppm while the signal of the phenox C4- and C4'-atoms are observed at 136.2 ppm. The peaks at 138.8 and 138.9 ppm result from the carbon atoms in the 4'- and 4-positions of the bipyridine ligands. The signals with stronger downfield shifts at 152.4, 152.7 and 156.6 ppm are due to the C6'- and C6-atoms of the bipyridine ligands as well as the C6- and C6'-atoms of the phenox ligand. The quaternary carbon atoms in the 2- and 2'-positions of the phenox ligand are found at 157.2 ppm while the analogous carbon atoms of the bipyridine ligands are observed at 157.6 and 157.7 ppm. The very strong downfield shift of the signal at 175.5 ppm is due to the carbon atoms in the 7- and 7'-positions of the phenox ligand with oxygen double bonds (**Fig. 3.50**).

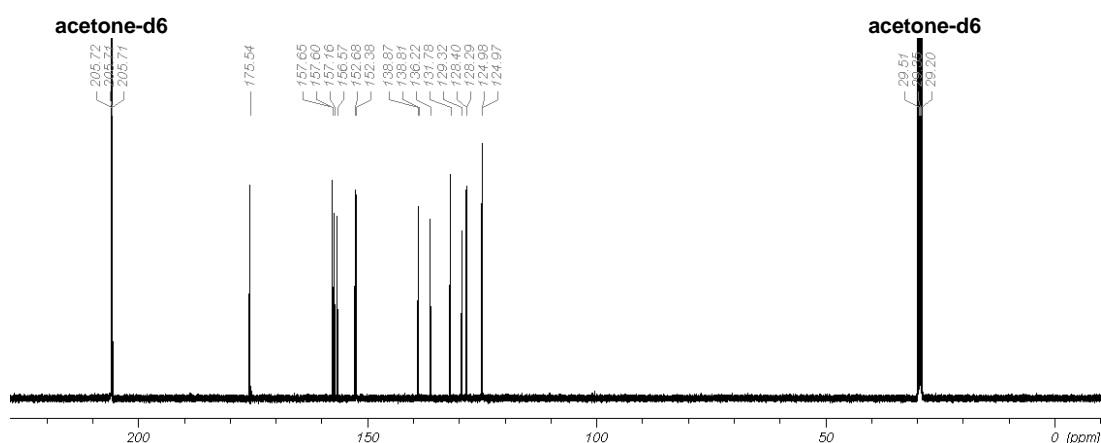
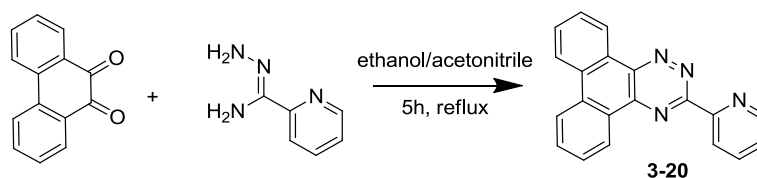
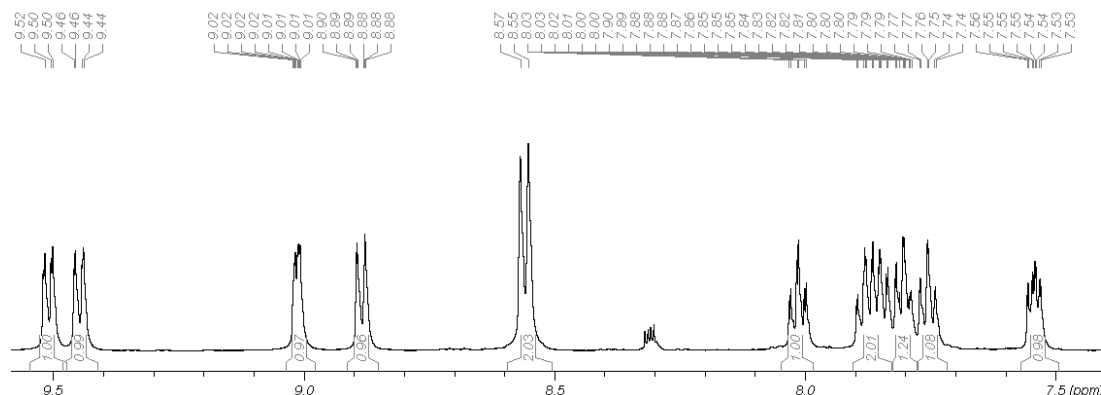


Figure 3.50:  $^{13}\text{C}\{^1\text{H}\}$  NMR spectrum (125.75 MHz, acetone- $d_6$ ) of **3-24**.

For the synthesis of **3-20**, phenanthrene-9,10-dione was dissolved in acetonitrile and a solution of pyridine-2-carbohydrazonamide in ethanol was added. The mixture was heated to reflux for 5 h. After removal of the solvent under vacuum, the product was obtained as brownish yellow powder in an excellent yield of 90% (**Scheme 3.14**).

Scheme 3.14: Synthesis of **3-20**.

In the  $^1\text{H}$  NMR spectrum of **3-20**, 10 signals are found in the aromatic region. At 7.52–7.56 ppm, a multiplet is observed with an integral of 1H. Two triplets with an integral of 1H each are observed at 7.74 and 7.79 ppm. An additional multiplet appears at 7.80–7.90 ppm with an integral of 2H. A further triplet is found at 8.02 ppm as well as two doublets at 8.56 and 8.89 ppm with an integral ratio of 1:2:1. Finally, a multiplet at 9.00–9.03 ppm as well as two doublets at 9.44 and 9.51 ppm have an intensity of 1H each (**Fig. 3.51**).

Figure 3.51: Aromatic region of the  $^1\text{H}$  NMR spectrum (500.13 MHz,  $\text{CDCl}_3$ ) of **3-20**.

The spectrum shows a multiplet at 7.52–7.56 ppm which is assigned to the proton in 5-positions of the pyridine moiety. The two triplets at 7.74 and 7.79 ppm with  $^3J = 7.0$  and  $6.9$  Hz result from the H12- and H12'-atoms of the phenanthrotriazine backbone. The multiplet at 7.80–7.90 ppm results from the overlap of the triplets in the 13- and 13'-positions. The triplet at 8.02 ppm with  $^3J = 7.7$  Hz is assigned to the H4-atom of the pyridine moiety. The doublet of the H11- and H11'-atoms is found at 8.56 ppm with  $^3J = 8.0$  Hz while the doublet at 8.89 ppm with  $^3J = 7.9$  Hz is due to the H14-atom and the multiplet at 9.00–9.03 ppm results from the H14'-atom. The two doublets at 9.44 and 9.51 ppm with  $^3J = 8.0$  and  $7.8$  Hz are assigned to the H3- and H6-protons of the pyridine moiety.

The  $^{13}\text{C}\{^1\text{H}\}$  NMR spectrum of **3-20** shows 20 signals, which are observed at 123.4, 123.4, 124.7, 125.6, 125.7, 127.5, 127.9, 128.2, 128.5, and 129.1 ppm. Additional peaks are found at 131.4, 131.8, 133.0, 134.25, 137.6, 143.7, 145.9, 151.0, 154.1, and 161.0 ppm (Fig. 3.52).

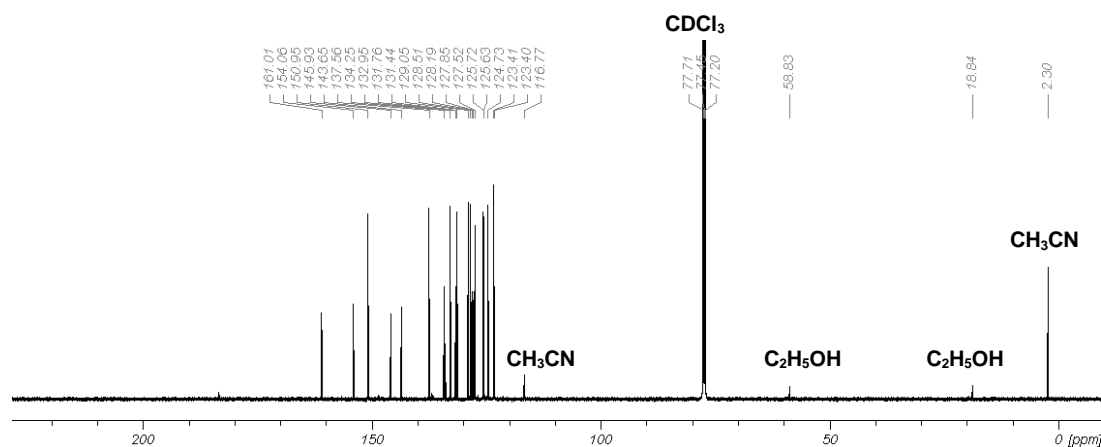


Figure 3.52:  $^{13}\text{C}\{^1\text{H}\}$  NMR spectrum (125.75 MHz,  $\text{CDCl}_3$ ) of **3-20**.

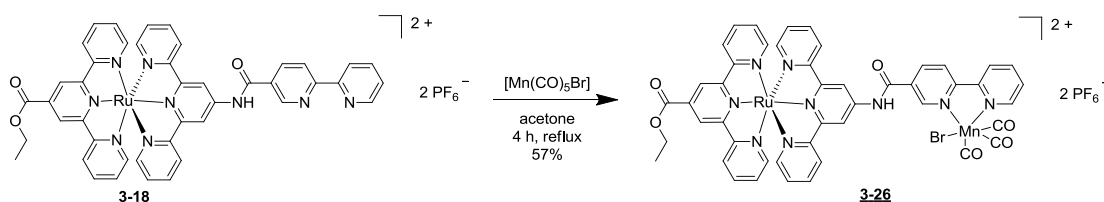
At 123.4 and 123.4 ppm, the signals of the 3-(pyridin-2-yl)phenanthro[9,10-*e*]-1,2,4-triazine (pypt) **3-20** carbon atoms in the 11- and 11'-positions are observed. The signal at 124.7 ppm is due to the C5-atom of the pyridine moiety. The peaks at 125.6 and 125.7 ppm are assigned to the C12- and C12'-atoms while the signals at 127.5 and 127.9 ppm result from the C13- and C13'-atoms. At 128.2 and 131.8 ppm, the signals of the quaternary carbon atoms in the 8- and 9-positions of **3-20** are found. The signals of the C14- and C14'-atoms are observed at 128.5 and 129.1 ppm. The quaternary pypt C7- and C10-atoms are observed at 134.3 and 143.7 ppm. The peaks of the pyridine carbon atom in the 3-, 4-, and 6-positions are found at 131.4, 133.0, and 137.6 ppm while the quaternary C2-atom is found at 154.1 ppm. The signals at 145.9, 151.0, and 161.0 ppm are assigned to the quaternary C6-, C5-, and C3-atoms of the triazine ring. Also some impurities in low concentration are found in the spectrum which, however, did not influence the following reaction.



### 3.3.3 Synthesis of metal complexes

#### 3.3.3.1 Synthesis of $[\text{Ru}(\text{etx})(\text{tbx})\text{MnBr}(\text{CO})_3](\text{PF}_6)_2$

The ruthenium precursor **3-18** was provided by the group of Prof. Dr. K. Heinze from the Institute of Inorganic and Analytical Chemistry of the Johannes Gutenberg Universität Mainz. For the synthesis of the related  $\text{Mn}(\text{CO})_3$  PhotoCORM,  $[\text{Ru}(\text{etx})(\text{tbx})](\text{PF}_6)_2$  **3-18** and manganese pentacarbonyl bromide were dissolved in degassed acetone under an inert atmosphere and exclusion of light. The mixture was heated to reflux for 4 h and, after addition of diethylether, a red precipitate was obtained which was collected by filtration and dried under vacuum. The precipitate was purified on a SepPak C-18 column with water/acetonitrile as eluent. After lyophilization, the product was obtained as a red powder in a moderate yield of 57% (**Scheme 3.15**).



Scheme 3.15: Synthesis of **3-26**.

The IR spectrum of **3-26** shows three very strong bands at 2025, 1928 and 1914  $\text{cm}^{-1}$ , while seven weak to medium bands are found at 1722, 1596, 1457, 1426, 1294, 1252 and 1135  $\text{cm}^{-1}$ . Finally, a very strong band is observed at 834  $\text{cm}^{-1}$  (**Fig. 3.53**). The very strong signal at 2025  $\text{cm}^{-1}$  is due to the symmetric and the two bands at 1928 and 1914  $\text{cm}^{-1}$  due to the antisymmetric C-O stretching vibration of the carbonyl ligands. The C-O stretching vibration of the ester unit appears at 1722  $\text{cm}^{-1}$  while the C-O stretching vibrations of the amide moiety is present at 1596  $\text{cm}^{-1}$ . The medium signals at 1457, 1426, 1294, 1252 and 1135  $\text{cm}^{-1}$  are due to the aromatic C-C and C-N stretching vibrations. The very strong band at 834  $\text{cm}^{-1}$  results from the P-F stretching vibration of  $\text{PF}_6$  counterions.

The  $^1\text{H}$  NMR spectrum of **3-26** shows a triplet at 1.56 ppm as well as a quartet at 4.66 ppm with an integral of 3H and 2H in the aliphatic region of the spectrum. In the aromatic region of the spectrum, two triplets at 7.26 and 7.36 ppm with integrals of 2H each are found while two doublets with an integral of 2H are observed at 7.52 and 7.61 ppm. A triplet with an integral of 1H is found at 7.86 ppm and a multiplet with integral 4H appears at 8.03-8.12 ppm. A doublet and a triplet with integrals of 1H each are observed at 8.30 and 8.38 ppm. The spectrum shows three additional doublets at 8.64, 8.88 and 9.14 ppm with an integral ratio of 2:1:2. At 9.25 and 9.32 ppm a singlet and a doublet with an integral of 1H each are found. Furthermore, the spectrum shows two additional singlets at 9.34 and 9.45 ppm with an integral of 2H each and a doublet at 9.58 ppm with an integral of 1H. Strongly shifted to the downfield at 12.17 ppm, an additional singlet with an integral of 1H is observed (Fig. 3.54).

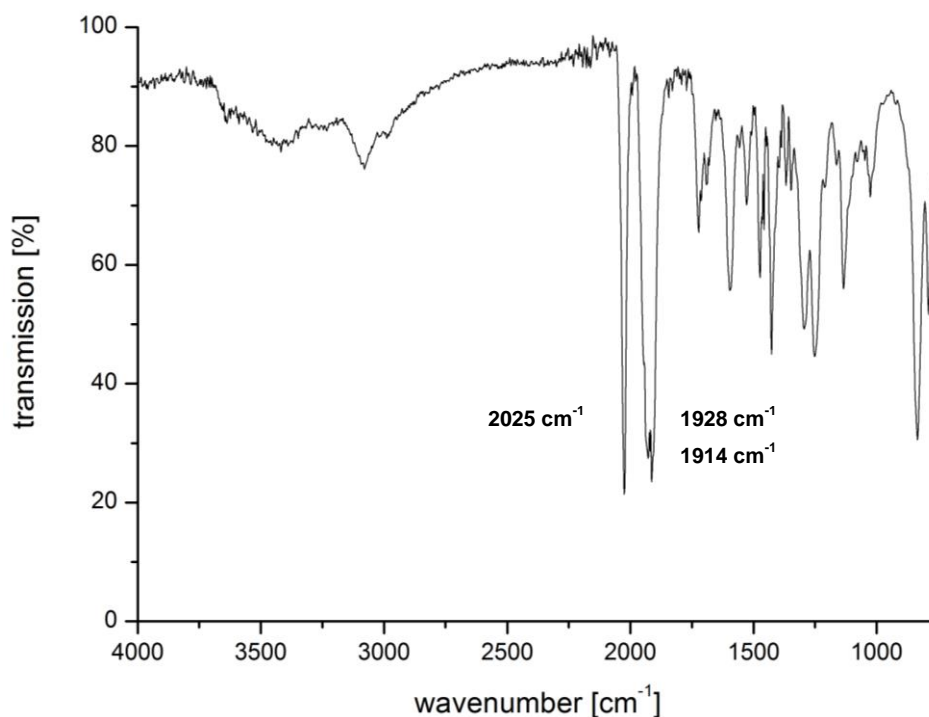


Figure 3.53: ATR-IR spectrum of **3-26**.

The triplet and quartet at 1.56 and 4.66 ppm with  $^3J = 7.0$  and 7.2 Hz result from the protons of the ethyl ester moiety. The aromatic region of the spectrum shows two triplets 7.26 and 7.36 ppm with  $^3J = 6.5$  and 6.2 Hz which

are due to the 4- and 4''- as well as to 5- and 5''-protons of the terpyridine in the tbx ligand. The doublet at 7.52 ppm with  $^3J = 5.5$  Hz are assigned to the 3- and 3''-terpyridine protons of the tbx ligand. Furthermore, the doublet at 7.61 ppm with  $^3J = 5.5$  Hz is due to the 3- and 3''-terpyridine protons of the etx ligand. At 7.86 ppm the triplet with  $^3J = 6.5$  Hz of the 5'-bipyridine proton of the tbx ligand appears. The multiplet at 8.03–8.12 ppm results from the overlap of the signals of the 4-, 4'', 5-, and 5''-terpyridine protons of the etc ligand. The doublet at 8.30 ppm with  $^3J = 5.6$  Hz and the triplet at 8.38 ppm with  $^3J = 7.6$  Hz are due to the bipyridine hydrogen atoms in 3'- and 4'-positions of the tbx ligand. The doublet at 8.64 with  $^3J = 7.9$  Hz results from the terpyridine protons in 6- and 6''-positions of the tbx ligand. The doublet at 8.88 ppm with  $^3J = 9.1$  Hz is assigned to the bipyridine proton in 3-positions of the tbx ligand. At 9.13 ppm the doublet of the terpyridine protons in 6- and 6''-positions with  $^3J = 8.0$  Hz is observed. The singlet at 9.25 ppm is due to the bipyridine proton in the 6-positions of the tbx ligand while the doublet at 9.32 ppm with  $^3J = 5.7$  Hz results from the bipyridine proton in the 4-positions. The singlets at 9.34 and 9.45 ppm are assigned to the hydrogen atoms in the 3'- and 5'-positions of the tbx and etx ligands. The doublet at 9.59 ppm with  $^3J = 5.7$  Hz is due to the bipyridine H6'-atom of the tbx ligand. The singlet with strong downfield shift at 12.17 ppm, results from the amide proton of the tbx ligand.

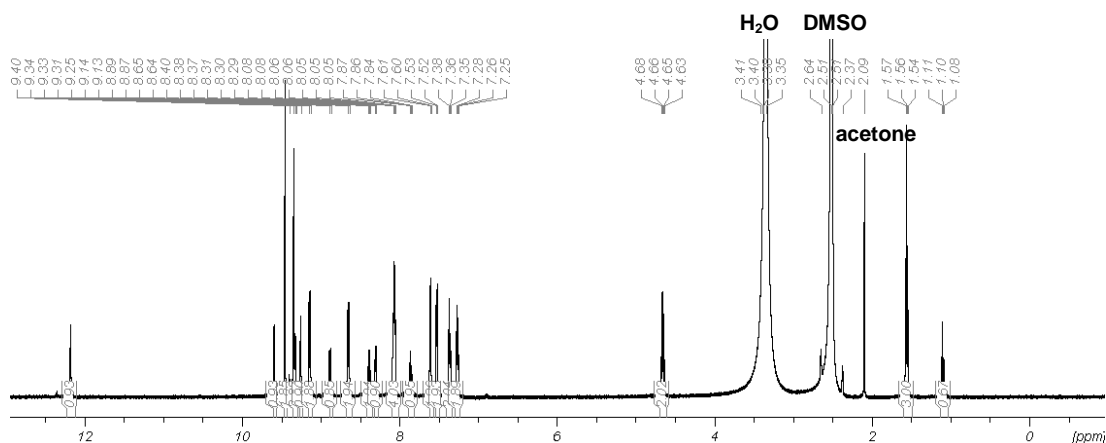


Figure 3.54:  $^1\text{H}$  NMR spectrum (500.13 MHz,  $\text{DMSO-d}_6$ ) of **3-26**.

In the  $^{13}\text{C}\{^1\text{H}\}$  NMR spectrum of **3-26**, 31 carbon signals are observed. In the aliphatic region two peaks are found at 15.2 and 63.3 ppm. In the aromatic region, 28 signals are found between 115.1 and 165.1 ppm. At 213.9 and 222.7 ppm, two peaks with very strong downfield shift are found. Taking into account the equivalence of the carbon atoms in the terpyridine due to symmetry, only 32 signals are expected for the 47 carbon atoms in complex **3-26**. In the aliphatic region of the spectrum, the signals of the ethyl group appear at 15.2 and 63.3 ppm. In the aromatic region of the spectrum, thirteen signals appear which are assigned to the aromatic CH groups with no neighboring ring nitrogen atom at 115.1, 122.0, 123.9, 124.8, 125.4, 125.4, 126.1, 128.4, 128.8, 129.0, 139.1, 139.5, and 140.4 ppm. The signals at 136.5 and 144.23 ppm result from the two quaternary carbon atoms with no neighboring heteroatoms at the etx as well as the bipyridine unit at the tbx ligands. The peaks at 152.8, 153.7, 154.8, and 155.6 ppm are due to the aromatic CH groups with neighboring ring nitrogen atoms. The quaternary seven carbon atoms with neighboring nitrogen atoms appear at 147.0, 155.4, 155.5, 156.8, 157.2, 158.1, and 158.3 ppm. With stronger downfield shift the quaternary ester and amide carbon atoms with oxygen double bonds are observed at 165.1 and 165.1 ppm as well as the signal of the three carbonyl ligands at 213.9 and 222.7 ppm (Fig. 3.55).

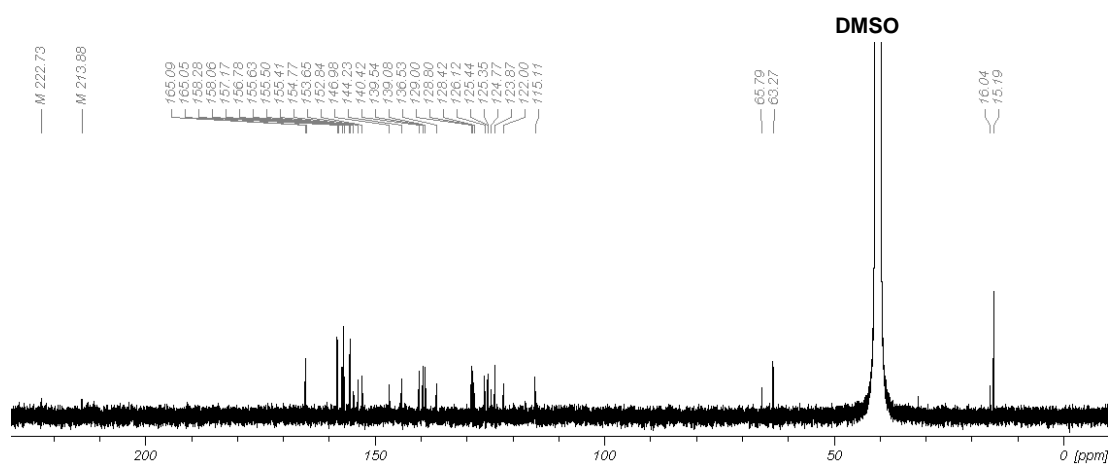
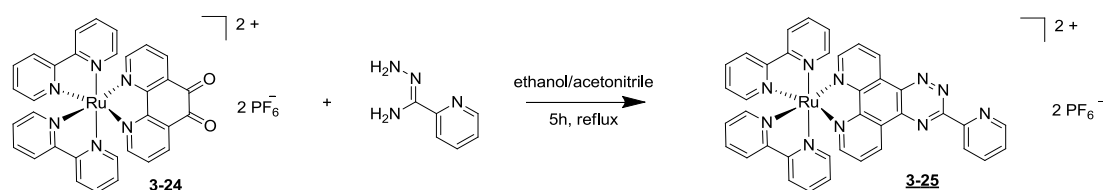


Figure 3.55:  $^{13}\text{C}\{^1\text{H}\}$  NMR spectrum (125.75 MHz, DMSO- $d_6$ ) of **3-26**.

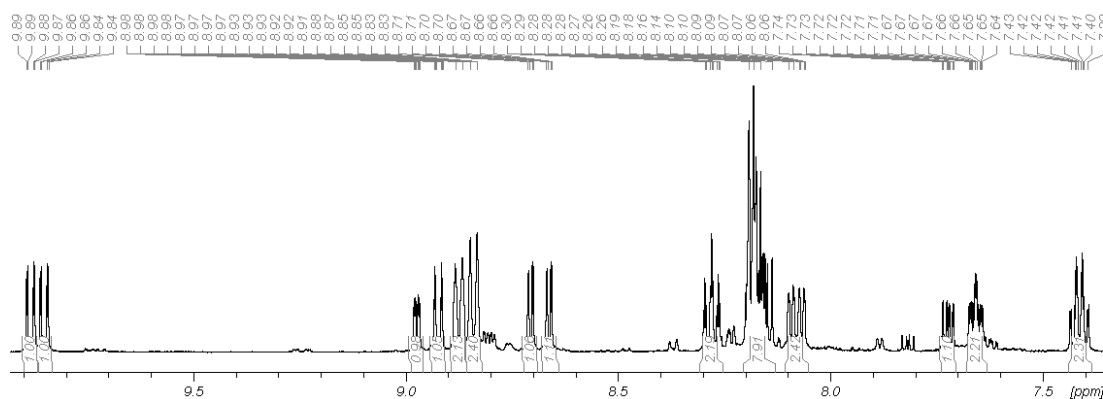
In the positive-mode ESI-MS of **3-26** signals are found at  $m/z = 654.11, 837.17, 972.02, 1056.01$  and  $1201.98$  Da. The spectrum shows a cation at  $m/z = 654.11$  Da with a composition of  $[M-Mn-3CO-Br-C_{11}H_7N_2O-H-2PF_6]^+$ . The signal at  $m/z = 837.17$  Da results from the fragment  $[M-Mn-3CO-Br+H-2PF_6]^+$  which lost the whole Mn(I)-moiety as well as both  $PF_6$  counterions during ionization. At  $m/z = 1056.01$  Da a cation with composition  $[M+H-2PF_6]^+$  is observed while the molecular ion  $[M-PF_6]^+$  appears at  $m/z = 1201.98$  Da.

3.3.3.2 Synthesis of [Ru(bpy)<sub>2</sub>(pytp)](PF<sub>6</sub>)<sub>2</sub>

For the synthesis of the ruthenium precursor [Ru(bpy)<sub>2</sub>(pytp)](PF<sub>6</sub>)<sub>2</sub> **3-25**, [Ru(bpy)<sub>2</sub>(phenox)](PF<sub>6</sub>)<sub>2</sub> **3-24** and pyridine-2-carbohydrazonamide were dissolved in a degassed acetonitrile/ethanol mixture under inert atmosphere and heated to reflux for 5 h. By removal of the solvent, the product was obtained as a red powder in a very good yield of 83% (**Scheme 3.16**).<sup>[99]</sup>

Scheme 3.16: Synthesis of **3-25**.

The <sup>1</sup>H NMR spectrum of **3-25** shows five multiplets at 7.39–7.44, 7.64–7.67, 7.71–7.74, 8.05–8.11 and 8.14–8.20 ppm with an integral ratio of 2:2:1:2:8. A triplet of a triplet is observed at 8.28 ppm with an integral of 2H. Two doublets of a doublet at 8.66 and 8.70 ppm are observed with an integral of 1H each as well as two doublets of 2H at 8.84 and 8.88 ppm. At 8.92 ppm, a doublet of a triplet is found with an integral of 1H while at 8.86–8.89 ppm, a multiplet is observed with an integral of 1H. Strongly shifted downfield, two doublets of a doublet are found at 9.85 and 9.88 ppm with integrals of 1H each (**Fig. 3.56**).

Figure 3.56: Aromatic region of the <sup>1</sup>H NMR spectrum (500.13 MHz, acetone-d<sub>6</sub>) of **3-25**.

The <sup>1</sup>H NMR spectrum of **3-25** shows the signals of the two bipyridine ligands as well as the ones of pytp backbone. The peaks assigned to the bipyridine ligand were detected by comparison with the spectrum of **3-24**. The spectrum

shows eight signals which are assigned to the protons in the 3-, 4-, 5-, and 6-positions of the pyridine ring *trans* to the pytp backbone and the protons in the 3'-, 4'-, 5'-, and 6'-positions of the pyridine ring *cis* to the pytp backbone. However, the multiplet at 7.39-7.44 ppm with an integral of 2H is assigned to the protons in the 4'-positions the multiplet at 7.64-7.67 ppm is due to the ones in the 4-positions. The multiplet at 8.05-8.11 ppm results from the H3'-atoms. The expected triplet of the H5-atoms overlaps with different signals of the pytp backbone. It is found in the unresolved multiplet at 8.14-8.20 ppm with an integral of 7H. The triplet of a triplet at 8.28 ppm with  ${}^3J = 7.9$  Hz,  ${}^4J = 6.4$  Hz and  ${}^5J = 1.6$  Hz is due to the H5'-atoms. The two doublets at 8.84 and 8.88 ppm with  ${}^3J = 8.3$  Hz each result from the H3- and H6'-atoms. At 9.85 and 9.88 ppm two doublets of doublets with  ${}^3J = 8.2$  Hz and  ${}^4J = 1.3$  Hz each are found. Both are due to the protons in the 6-positions of the bipyridine ligands. To separate the signals of the pyridine moiety from the signals of the pytp backbone, the spectrum of **3-25** was compared with the one of **3-24**. Thus, the doublet of doublets of doublets at 7.72 ppm with  ${}^3J = 7.6$  Hz,  ${}^4J = 4.7$  Hz and  ${}^5J = 1.1$  Hz is assigned to the H3-atoms of the pyridine moiety. The signals of the protons in 4-positions of the pyridine moiety as well as the H9-, H9'-, H10-, and H10'-atoms of the backbone are found in the unresolved multiplet at 8.14-8.20 ppm with an integral of 7H. The two doublets of doublets at 8.66 and 8.70 ppm with  ${}^3J = 5.4$  Hz and  ${}^4J = 1.3$  Hz result from the backbone H11'- and H11-atoms adjacent to the Ru(II)-coordinated nitrogen atoms. At 8.92 ppm, a doublet of triplets with  ${}^3J = 7.9$  Hz and  ${}^4J = 1.0$  Hz is found which is due to the protons in 5-positions of the pyridine moiety. The double of doublets of doublets at 8.97 ppm with  ${}^3J = 4.7$  Hz,  ${}^4J = 1.8$  Hz and  ${}^5J = 0.9$  Hz is assigned to the H6-atom of the pyridine moiety ortho to the ring nitrogen atom.

The  $^{13}\text{C}\{^1\text{H}\}$  NMR spectrum of **3-25** shows 35 signals for the 38 carbon atoms contained in the complex. All signals are observed in the aromatic region between 125.3, 163.2 ppm (**Fig. 3.57**).

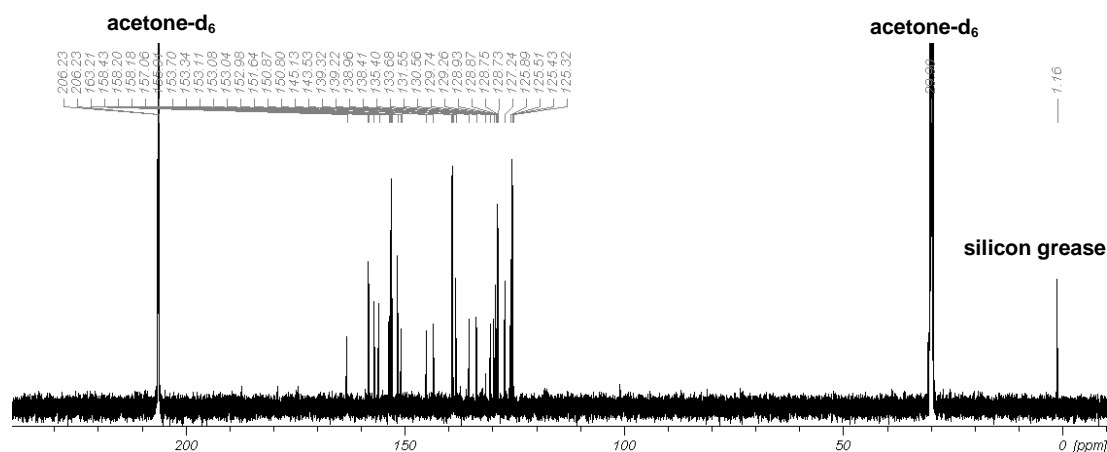


Figure 3.57:  $^{13}\text{C}\{^1\text{H}\}$  NMR spectrum (125.75 MHz, acetone- $\text{d}_6$ ) of **3-25**.

The spectrum of **3-25** shows 18 signals which are assigned to the bipyridine ligands. The eight peaks between 125.3 and 128.9 ppm result from the carbon atoms in the 3-, 3'-, 5-, and 5'-positions not adjacent to the coordinated nitrogen atoms of the bipyridine ligands. With stronger downfield shift the four signals of the C4- and C4'-atoms are found at 138.41, 138.96, 139.22, and 139.32 ppm. The peaks at 153.0, 153.0, 153.1, and 153.1 ppm are due to the carbon atoms in the 6- and 6'-positions adjacent to the nitrogen atoms with Ru(II)-coordination. The two signals at 158.2 ppm are due to the four quaternary carbon atoms in the 2- and 2'-positions. The remaining 17 signals result from the pytp backbone. At 129.3 ppm, a signal, due to the C3- and C5-atoms of the uncoordinated pyridine moiety is found, while the peak of the C4-atom appears at 151.6 ppm. Strongly shifted to the downfield, the two signals adjacent to the pyridine nitrogen are observed. The peak at 157.1 ppm is due to C6- while the one at 158.4 ppm results from the C2-atom. The two signals at 129.7 at 130.6 ppm result from the quaternary carbon atoms not adjacent to nitrogen atoms in the 7- and 7'-positions. At 131.6 and 143.5 ppm the quaternary C5- and C6-atom of the triazine ring are observed. The peaks of the carbon atoms in the 10- and 10'-positions are found at 133.7 and 135.4 ppm while the C9- and C9'-atoms appear at 150.8 and 150.9 ppm. The

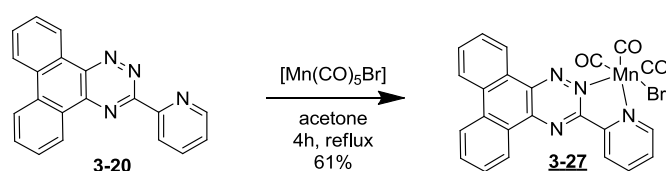


signals of the CH groups, C11- and C11'-atoms adjacent to the Ru(II) coordinated nitrogen are observed at 153.3 and 155.9 ppm while the quaternary C8- and C8'-atoms are assigned to the signals at 145.1 and 153.7 ppm. With strong downfield shift, a signal at 163.2 ppm appears which results from the C3-atom of the triazine ring.

In the positive-mode ESI-MS two signals at  $m/z = 615.07$  Da and  $869.10$  Da are observed. The spectrum shows at  $m/z = 615.07$  Da the sodium chloride adduct with composition of  $[M-2C_{10}H_8N_2+Na+Cl-PF_6]^+$  as well as the molecular ion  $[M-PF_6]^+$  at  $m/z = 869.10$  Da.

3.3.3.3 Synthesis and characterization of  $[\text{MnBr}(\text{CO})_3(\text{pypt})]$ 

As a control, the ruthenium-free complex  $[\text{MnBr}(\text{CO})_3(\text{pypt})]$  **3-27** was synthesized. Therefore, a degassed solution of manganese pentacarbonyl bromide and 3-(pyridin-2-yl)phenanthro[9,10-*e*]-1,2,4-triazine (pypt) in acetone was heated to reflux under nitrogen and exclusion of light for 4 h. Addition of diethylether led to a purple precipitate which was collected by filtration. The product was obtained as a purple powder in a good yield of 61% (**Scheme 3.17**).



**Scheme 3.17:** Synthesis of **3-27**.

The IR spectrum of **3-27** shows a weak band at  $3071\text{ cm}^{-1}$  as well as three very strong bands at  $2026$ ,  $1962$  and  $1906\text{ cm}^{-1}$ . Additional medium to strong bands are found at  $1604$ ,  $1369$  and  $757\text{ cm}^{-1}$  (**Fig. 3.58**).

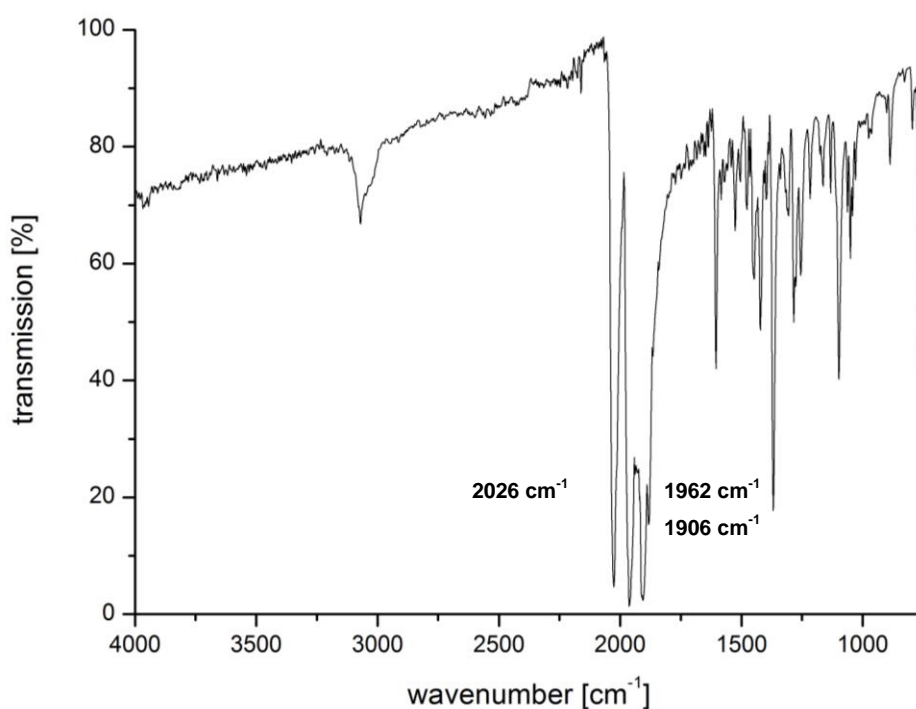


**Figure 3.58:** ATR-IR spectrum of **3-27**.

The band at 3071  $\text{cm}^{-1}$  is due to the C-H stretching vibrations of the ligand backbone. The symmetric C-O stretching vibration appears at 2026  $\text{cm}^{-1}$  while the two bands of the antisymmetric stretching vibrations are found at 1962 and 1906  $\text{cm}^{-1}$  of the *fac*-Mn(CO)<sub>3</sub> unit. The signals at 1604, 1369 and 757  $\text{cm}^{-1}$  result from the aromatic C-C and C-N stretching vibrations.

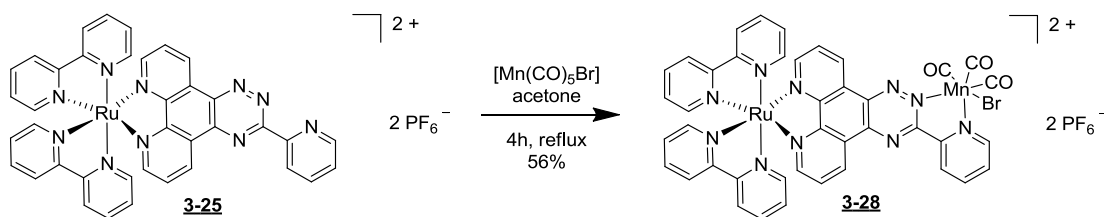
Due to the poor solubility of the complex in any common solvents, NMR spectra could not be recorded. Thus, the purity of the product was established by CHN analysis.

**Table 3.7:** Results of the elemental analysis for [MnBr(CO)<sub>3</sub>(pypt)] **3-27**.

	C [%]	H [%]	N [%]
<b>found</b>	50.83	2.24	10.31
<b>calculated for C<sub>23</sub>H<sub>12</sub>BrMnN<sub>4</sub>O<sub>3</sub> x H<sub>2</sub>O</b>	50.67	2.59	10.28

3.3.3.4 Synthesis and characterization of  $[\text{Ru}(\text{bpy})_2(\text{pytp})\text{MnBr}(\text{CO})_3](\text{PF}_6)_2$ 

As a first example for a heterobinuclear Mn-Ru-PhotoCORM with a Ru(bpy)<sub>2</sub> sensitizing unit, the synthesis of  $[\text{Ru}(\text{bpy})_2(\text{pytp})\text{MnBr}(\text{CO})_3](\text{PF}_6)_2$  **3-28** started from manganese pentacarbonyl bromide and  $[\text{Ru}(\text{bpy})_2(\text{pytp})](\text{PF}_6)_2$  **3-25**. These were dissolved in degassed acetone and heated to reflux for 4 h. For a complete exclusion of light, the use of brown-colored glassware was required. Addition of diethylether led to a formation of a dark red precipitate which was collected by filtration and dried under vacuum. For purification, it was loaded on a SepPak C-18 reversed column and eluted with a water/acetonitrile mixture. After lyophilization, the product was obtained in a moderate yield of 56% as a dark red powder (**Scheme 3.18**).

Scheme 3.18: Synthesis of **3-28**.

The IR spectrum of **3-28** two very strong bands at 2027 and 1927  $\text{cm}^{-1}$ . At 1604, 1466 and 1446  $\text{cm}^{-1}$  additional medium signals are observed while a strong band at 833  $\text{cm}^{-1}$  is found in the spectrum (**Fig. 3.59**).

The two very strong bands at 2027 and 1927  $\text{cm}^{-1}$  are due to the symmetric and antisymmetric C-O stretching vibrations of the *fac*-Mn(CO)<sub>3</sub> unit. The signals at 1604, 1466 and 1446  $\text{cm}^{-1}$  result from the aromatic C-C and C-N stretching vibrations of the ligand backbone as well as the bipyridine moieties. The band at 833  $\text{cm}^{-1}$  shows the P-F stretching vibration of the PF<sub>6</sub> counterions.

The <sup>1</sup>H NMR spectrum of **3-28** was recorded in deuterated acetone (**Fig. 3.60**). It shows two multiplets at 7.34–7.44 and 7.58–7.63 ppm with integrals of 2H each. Also, a doublet at 7.67 ppm and four multiplets 7.70–7.90, 8.00–8.05, 8.09–8.27, and 8.36–8.43 ppm with an integral ratio of 1:4:1:6:2 are found. A triplet of a doublet at 8.50 ppm with an integral of 1H and two multiplets

8.84–8.92 and 9.17–9.21 ppm with integrals of 4H and 1H, respectively are observed in the spectrum. At 9.38 ppm, a doublet with an integral of 2H appears as well as a multiplet at 9.62–9.65 ppm and a doublet at 9.89 ppm with integrals of 1H each.

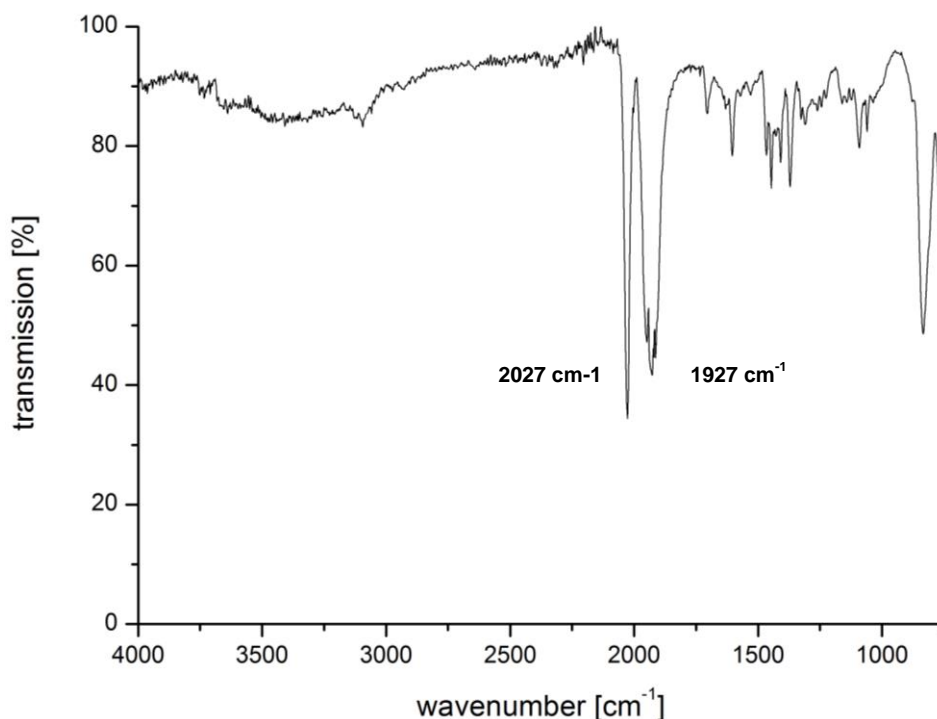


Figure 3.59: ATR-IR spectrum of 3-28.

The  $^1\text{H}$  NMR spectrum of 3-28 shows the signals of the two bipyridine ligands as well as the ones of pytp backbone. The assignment of the peaks was carried out by comparison with the  $^1\text{H}$  NMR spectrum of 3-25. The spectrum shows seven signals which are assigned to the protons in the 3-, 4-, 5-, and 6-position of the pyridine ring *trans* to the pytp backbone and the protons in the 3'-, 4'-, 5'-, and 6'-positions of the pyridine ring *cis* to the pytp backbone. Thus, the two multiplets at 7.34–7.44 and 7.58–7.63 ppm are assigned to the protons in the 4'- and 4-positions. The unresolved multiplet at 7.67–7.90 ppm results from the overlap of the H3'- and H5'-atoms signals of the bipyridine ligands. The triplet at 8.24 ppm with  $^3J = 8.0$  Hz is due to the protons in the 5-positions. The unresolved multiplet at 8.84–8.92 ppm results from the H3- and H6'-atoms. The multiplet at 9.62–9.65 ppm as well as the doublet at 9.89 ppm with  $^3J = 8.3$  Hz are assigned to the H6-atoms. The signals of the pytp



C4-atom appears at 152.6 ppm. With stronger downfield shift the signal for the carbons adjacent to the pyridine nitrogen are observed. The peak at 156.3 ppm is due to the C6-atom while the one at 157.9 ppm results from the C2-atom. The signal at 128.9 ppm results from the quaternary carbon atoms not adjacent to nitrogen atoms in the 7- and 7'-positions. At 133.4 and 143.5 ppm the quaternary C5- and C6-atom of the triazine ring are observed. The signals of the carbon atoms in the 10- and 10'-positions are found at 138.8 and 138.9 ppm while the C9- and C9'-atoms appear at 152.9 ppm. The signal of the CH groups, C11- and C11'-atoms adjacent to the Ru(II) coordinated nitrogen is observed at 157.4 ppm while the quaternary C8- and C8'-atoms are assigned to the signals at 153.0 and 151.2 ppm. Strongly shifted downfield, a signal at 163.1 ppm appears which results from the C3-atom of the triazine ring.

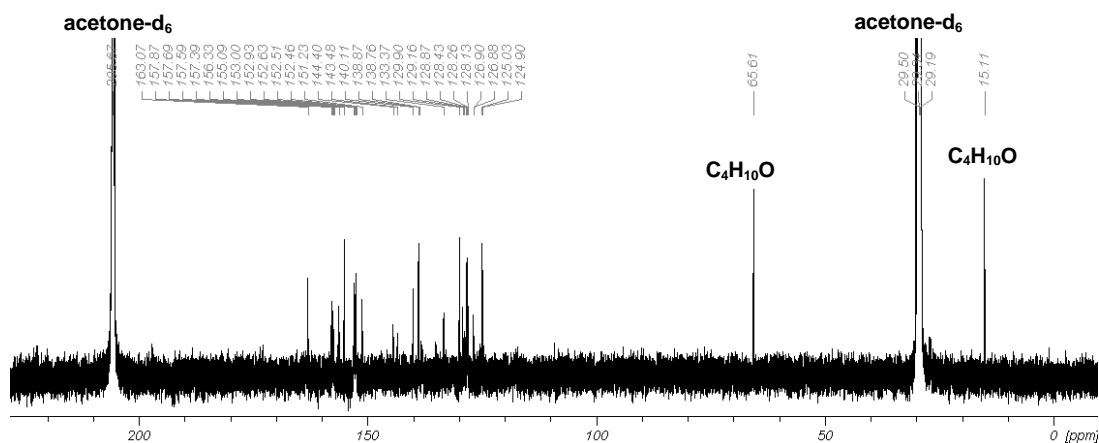
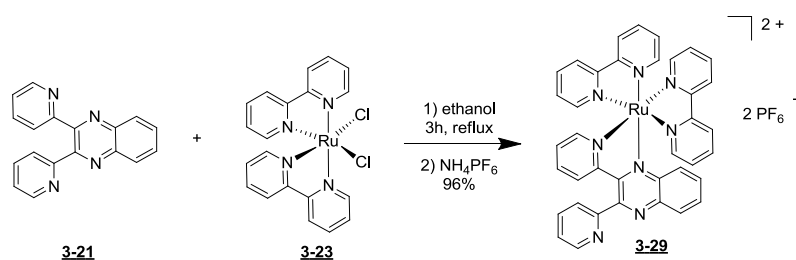


Figure 3.61:  $^{13}\text{C}\{^1\text{H}\}$  NMR (125.75 MHz, acetone- $\text{d}_6$ ) of **3-28**.

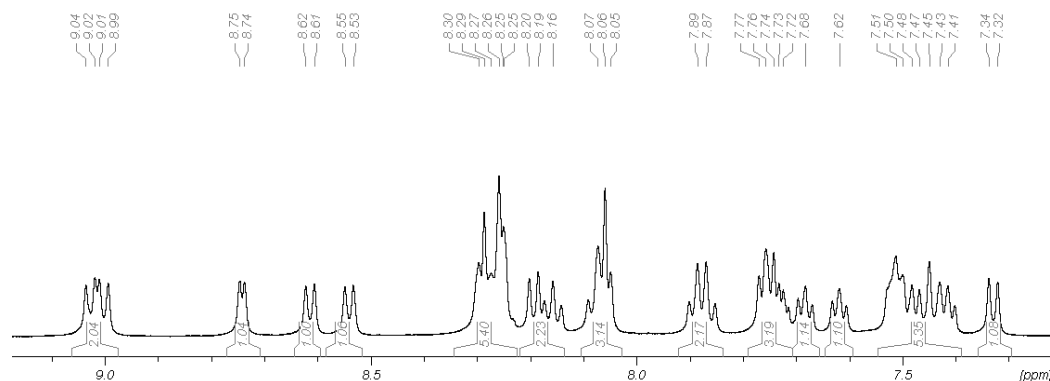
In the positive-mode ESI-MS of **3-28** five signals at  $m/z = 724.13$ ,  $869.10$ ,  $940.96$ ,  $1031.85$ , and  $1088.94$  Da. The spectrum shows a proton adduct at  $m/z = 724.13$  Da with composition  $[\text{M}-\text{Mn}-3\text{CO}-\text{Br}+\text{H}-2\text{PF}_6]^+$ . The signal at  $m/z = 869.10$  Da is due to the fragment  $[\text{M}-\text{Mn}-3\text{CO}-\text{Br}-\text{PF}_6]^+$  which lost the whole manganese moiety as well as one  $\text{PF}_6$  counterion. A dicationic fragment with composition  $[2\text{M}-2\text{PF}_6]^{2+}$  is observed at  $m/z = 940.96$  Da. An additional peak at  $m/z = 1031.85$  Da results from the cation  $[\text{M}-2\text{CO}-\text{PF}_6]^+$  which lost two carbonyl ligands as well as one  $\text{PF}_6$  counterion during ionization. The molecular ion  $[\text{M}-\text{PF}_6]^+$  is observed at  $m/z = 1088.94$  Da.

3.3.3.5 Synthesis of  $[\text{Ru}(\text{bpy})_2(\text{dpx})](\text{PF}_6)_2$ 

The ruthenium(II) complex of 2,3-di(pyridine-2-yl)quinoxaline (dpx) **3-21** was synthesized under an inert atmosphere of dinitrogen. The dpx ligand **3-21** and the ruthenium precursor  $[\text{Ru}(\text{bpy})_2\text{Cl}_2]$  **3-23** were dissolved in degassed ethanol and heated to reflux for 3 h. Addition of an aqueous solution of ammonium hexafluorophosphate resulted in a red precipitate which was collected by filtration and extensively dried under vacuum to obtain the product as red powder in an excellent yield of 96% (**Scheme 3.19**).

Scheme 3.19: Synthesis of **3-29**.

The  $^1\text{H}$  NMR spectrum of **3-29** shows only signals in the aromatic region. At 7.33 ppm, a doublet is found as well as a multiplet at 7.41–7.51 ppm with an integral ratio of 1:5. Two triplets are observed at 7.62 and 7.68 ppm with integral 1H each. The multiplet at 7.71–7.77 ppm has an integral value of 3H, while the quartet at 7.88 ppm has one of 2H. Three additional multiplets are found at 8.05–8.11, 8.13–8.22 and 8.23–8.33 ppm with an integral ratio of 3:2:5. The spectrum shows three doublets at 8.54, 8.62 and 8.74 ppm with integrals of 1H each as well as a multiplet at 8.98–9.05 ppm with an integral of 2H (**Fig. 3.62**).

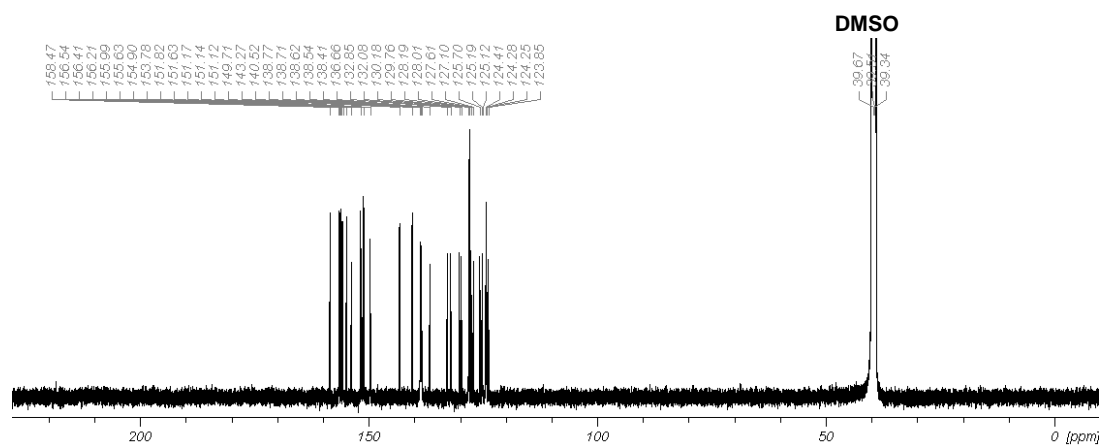
Figure 3.62: Aromatic region of the  $^1\text{H}$  NMR spectrum (500.13 MHz,  $\text{DMSO-d}_6$ ) of **3-29**.



The spectrum shows two sets of signals which are assigned to the protons in the 3-, 4-, 5-, and 6- positions *trans* to the chloride ligands of the pyridine ring and the protons in the 3', 4', 5', and 6'- positions *cis* to the chloride ligands of the pyridine ring. The doublet at 7.33 ppm with  $^3J = 8.3$  Hz is assigned to the H3 atom of the uncoordinated pyridine moiety. The unresolved multiplet at 7.41-7.51 ppm is due to the overlap of the signals of the protons in the 8- and 9-positions of the dpx backbone as well as the H4'-atoms and one of the protons in the 3'-positions of the bipyridine ligands. The signals of the H4-protons are observed as two triplets at 7.62 and 7.68 ppm with  $^3J = 6.7$  and 6.8 Hz. The multiplet at 7.71-7.77 ppm results from the overlap of the H5-signal of the uncoordinated pyridine moiety as well as the H3-atom of the coordinated pyridine arm. Also, the signal of the second H3'-atom of the bipyridine ligands is assigned to this multiplet. The quartet with  $^3J = 8.1$  Hz is due to the H5-atoms of the bipyridine ligands. The unresolved multiplet at 8.05-8.11 ppm results from the overlap of the H4-atom of the uncoordinated as well as the H4- and H5-atoms of the coordinated pyridine moiety. The multiplet at 8.13-8.22 ppm is assigned to the signals of the H5'-atoms of the bipyridine ligands. The unresolved multiplet at 8.23-8.33 ppm results from the overlap of the two signals of the H3- and H6'-atoms of the bipyridine ligands as well as the signal of the H7-atom of the dpx backbone. The three doublets at 8.54, 8.62, and 8.74 ppm with  $^3J = 7.8, 8.1$  and 4.6 Hz are due to the proton in the 10-positions of the dpx backbone and the H6-atoms of the uncoordinated as well as from the coordinated pyridine moiety. The multiplet at 8.98-9.05 ppm results from the overlap of the two bipyridine H6-doublets. In the  $^{13}\text{C}\{^1\text{H}\}$  NMR spectrum of **3-29**, 33 peaks are found for the 38 contained in the complex. All signals appear in the aromatic region of the spectrum. The peaks are found in a range of 124.7 to 159.3 ppm.

To separate the signals of the dpx backbone from the signals of the bipyridine ligands, the spectrum of **3-29** was compared with compound **3-30**. The peaks which appear in both spectra result from the dpx backbone while the remaining signals are due to the bipyridine ligands. Thus, the ten signals at

126.0, 126.1, 128.0, 128.5, 129.1, 131.1, 132.9, 133.7, 139.3, and 139.4 ppm are assigned to the aromatic CH groups not adjacent to nitrogen atoms. The three quaternary carbon atoms not adjacent to the Mn(I)-coordinated nitrogen atoms show peaks at 141.4, 144.1, and 152.7 ppm. The carbon atoms in 6-positions of the uncoordinated and coordinated pyridine moiety are found at 150.6 and 154.7 ppm. The signals at 156.5, 156.9, and 157.3 ppm result from the quaternary carbon atoms adjacent to the nitrogen atoms with manganese(I) coordination. The remaining 15 signals in the spectrum are assigned to the bipyridine ligands. The seven peaks at 124.7, 125.1, 125.1, 125.3, 126.6, 128.9, and 130.6 ppm result from the eight carbon atoms in the 3, 3'-, 5-, and 5'-positions. The signals at 137.5, 139.5, 139.6, and 139.6 ppm have a stronger downfield shift. They are assigned to the C4'- and C4-atoms of the bipyridine ligands. The signal at 152.5 ppm is due to the four carbon atoms in the 6'- and 6-positions while the three signals at 157.1, 157.4, and 159.3 ppm result from the four quaternary C2'- and C2-atoms (**Fig. 3.63**).

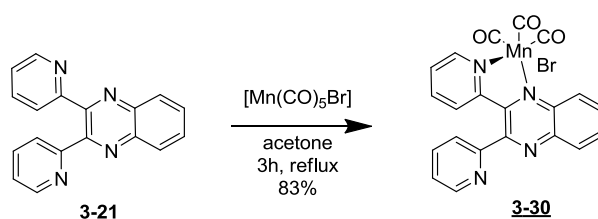


**Figure 3.63:**  $^{13}\text{C}\{^1\text{H}\}$  NMR spectrum (125.75 MHz, DMSO- $d_6$ ) of **3-29**.

In the positive-mode ESI-MS of **3-29** two signals appear at  $m/z = 283.09$  and  $843.11$  Da. The first one is assigned to a fragment with a composition of  $[\text{M}-2\text{C}_{10}\text{H}_8\text{N}_2-\text{H}-2\text{PF}_6]^+$  at  $m/z = 283.09$  Da which has lost the two  $\text{PF}_6$  counterions as well as two bipyridine moieties. The molecular ion  $[\text{M}-\text{PF}_6]^+$  is observed at higher mass.

3.3.3.6 Synthesis of  $[\text{MnBr}(\text{CO})_3(\text{dpx})]$ 

For the synthesis of control compound **3-30**, 2,3-di(pyridin-2-yl)quinoxaline (dpx) **3-21** and manganese pentacarbonyl bromide were dissolved in degassed acetone under inert atmosphere and exclusion of light. The mixture was heated to reflux for 3 h. Addition of diethylether led to formation of a precipitate which was collected by filtration. The product was obtained as a violet powder in a good yield of 83% (**Scheme 3.20**). Recrystallization by slow diffusion of *n*-hexane into a dichloromethane solution of the compound yielded dark red crystals suitable for X-ray structure analysis.

Scheme 3.20: Synthesis of **3-30**.

The IR spectrum of **3-30** shows three very strong signals at 2027, 1938 and 1914  $\text{cm}^{-1}$ . Additional weak to medium bands are found at 1586, 1475, 1355 and 774  $\text{cm}^{-1}$  (**Fig. 3.64**). The sharp signal at 2027  $\text{cm}^{-1}$  is assigned to the symmetric C-O stretching vibration while the two bands at 1938 and 1914  $\text{cm}^{-1}$  are due to the antisymmetric ones of the facially coordinated carbonyl ligands. The peaks at 1586, 1475, 1355 and 774  $\text{cm}^{-1}$  are assigned to the aromatic C-C and C-N stretching vibrations.

The  $^1\text{H}$  NMR spectrum of **3-30** was recorded in  $\text{DMSO-d}_6$  (**Fig. 3.65**). The spectrum only shows signals in the aromatic region. A doublet appears at 7.11 ppm as well as a multiplet at 7.65–7.71 ppm with an integral ratio of 1:2. A triplet and a doublet with integrals of 1H each are found at 7.91 and 8.00 ppm. Two multiplets are observed at 8.11–8.19 ppm and 8.20–8.25 ppm with an integral ratio 2:1. The spectrum shows four doublets at 8.34, 8.71, 8.89 and 9.40 ppm with integrals of 1H each.

The doublet at 7.11 ppm with  $^3J = 8.2$  Hz is assigned to the H3 atom of the uncoordinated pyridine moiety. The multiplet at 7.65–7.71 ppm is due to the

protons in the 8- and 9-positions of the dpx backbone. The triplet at 7.91 ppm with  $^3J = 7.9$  Hz results from the H5-atom of the uncoordinated pyridine moiety. The doublet of the H3-atom of the coordinated pyridine arm with  $^3J = 7.7$  Hz appears at 8.00 ppm. The multiplet at 8.11–8.25 ppm results from the overlap of the signals H4-atom of the uncoordinated as well as the H4 and H5 atoms of the coordinated pyridine moiety. At 8.34 and 8.89 ppm with  $^3J = 8.3$  and 8.1 Hz the doublets of the protons in the 7- and 10-positions of the dpx backbone is observed. The two doublets at 8.71 and 9.40 ppm with  $^3J = 4.7$  and 4.9 Hz result from the H6-atoms of the uncoordinated as well as from the coordinated pyridine moiety.

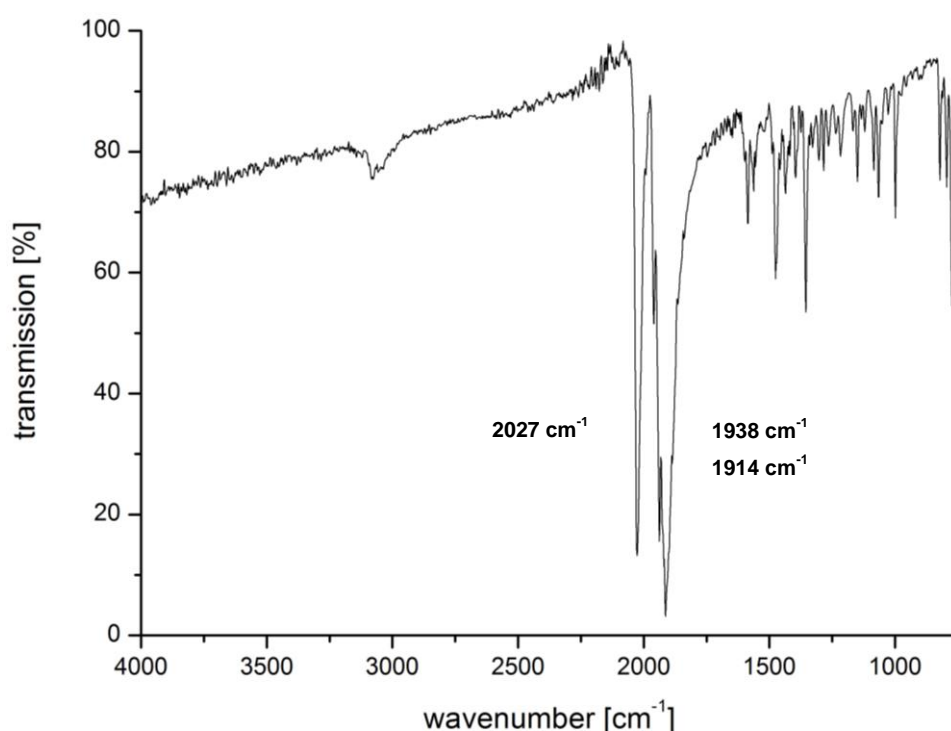


Figure 3.64: ATR-IR spectrum of 3-30.

The  $^{13}\text{C}\{^1\text{H}\}$  NMR spectrum of 3-30 shows 21 signals, 18 are found in the aromatic region between 125.7 and 157.3 ppm. In addition, there are three signals with very strong downfield shift at 221.0, 222.6, and 224.3 ppm (Fig. 3.66).

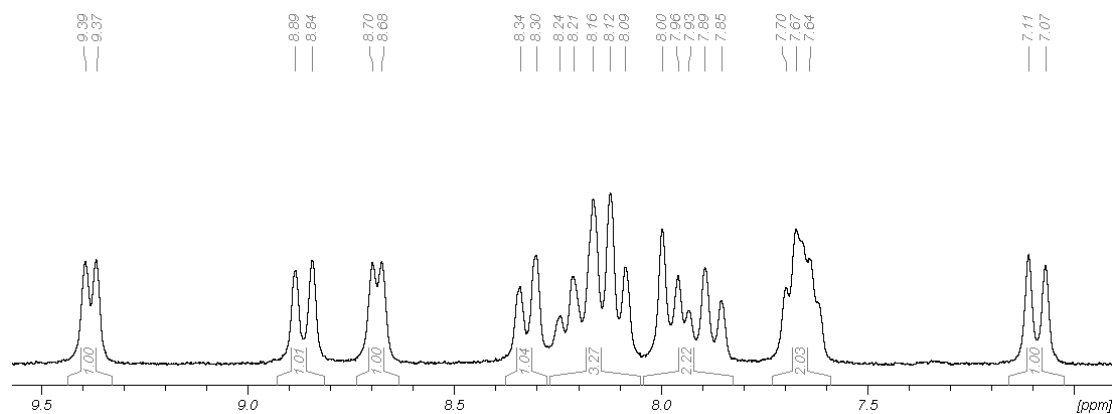


Figure 3.65: Enlargement of the aromatic region of the  $^1\text{H}$  NMR spectrum of **3-30**.

The ten signals at 125.7, 126.2, 127.4, 128.4, 129.4, 131.0, 133.7, 133.8, 138.8, and 138.9 ppm result from the aromatic CH groups not adjacent to nitrogen atoms. The signals of the three quaternary carbon atoms not adjacent to the manganese(I) coordinated nitrogen atoms are found at 141.0, 142.5, and 152.7 ppm. At 150.5 and 154.6 ppm the carbon atoms in the 6-positions of the uncoordinated and coordinated pyridine moiety are observed. The signals at 154.3, 156.7, and 157.3 ppm are due to the quaternary carbon atoms adjacent to the manganese(I) coordinated nitrogen atoms. The signals at 221.0, 222.6, and 224.3 ppm are assigned to the carbon atoms of the carbonyl ligands.

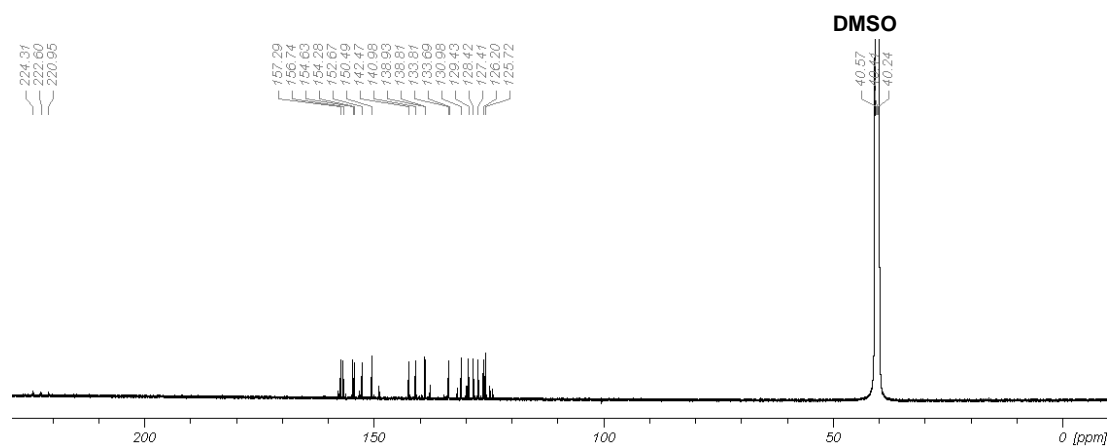


Figure 3.66:  $^{13}\text{C}\{^1\text{H}\}$  NMR spectrum (125.75 MHz,  $\text{DMSO-d}_6$ ) of **3-30**.

In the positive-mode ESI-MS of **3-30**, five peaks at  $m/z = 283.09$ , 420.97, 440.95, 860.91, and 1044.85 are found. The protonated adduct of the dp $x$  ligand shows up at  $m/z = 283.09$  Da as  $[\text{dp}x+\text{H}]^+$ . At  $m/z = 420.97$  Da, the  $[\text{M}-3\text{CO}+\text{H}]^+$  fragment is found which has lost all three carbonyl ligands

during ionization. The sodium adduct of this fragment  $[M-3CO+Na]^+$  is found at  $m/z = 440.95$ . At  $m/z = 860.91$  and  $1044.85$ , sodium cluster ions with compositions of  $[2M-6CO+Na]^+$  and  $[2M+Na]^+$  are observed. The signal of the molecular ion of **3-30** was not detected.

Single crystals of **3-30** suitable for X-ray diffraction were obtained by slow diffusion of *n*-hexane into a dichloromethane solution of the complex. Compound **3-30** crystallizes in the triclinic P-1 space group (Fig. 3.67). The unit cell contains only the  $[MnBr(CO)_3(dpx)]$  moiety.

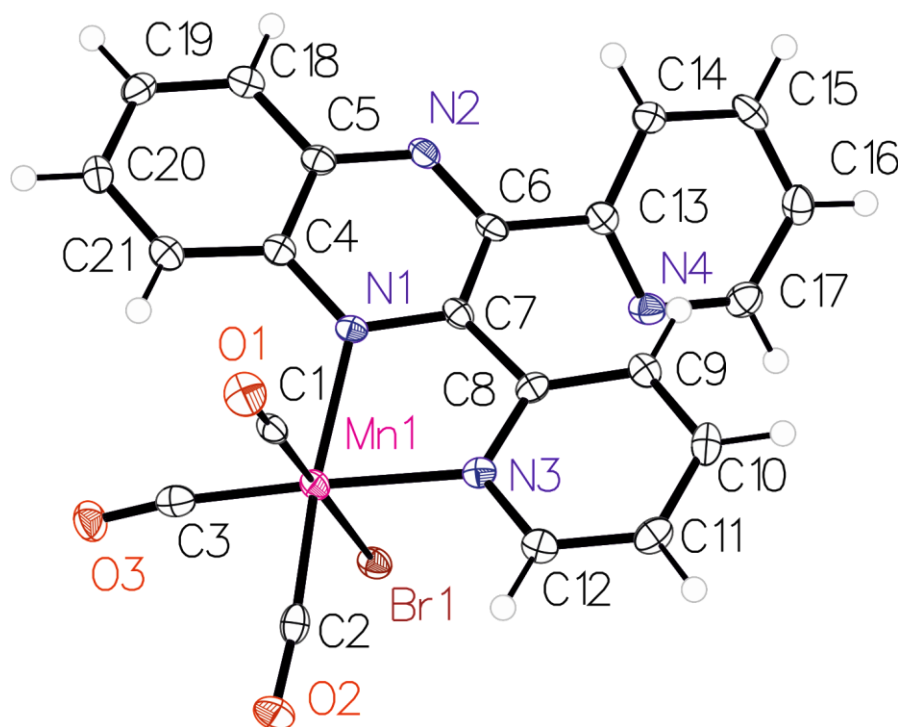


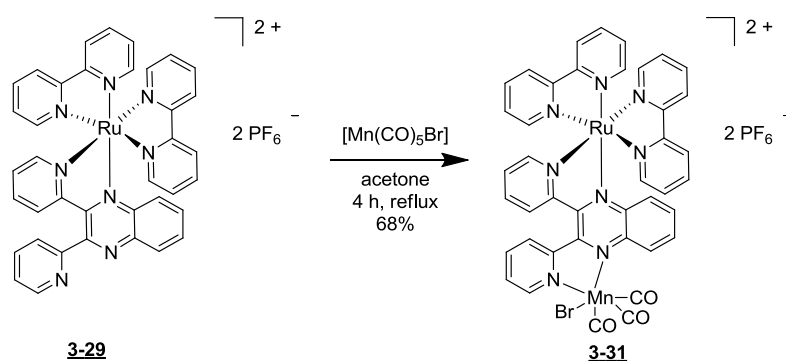
Figure 3.67: Molecular structure of  $[MnBr(CO)_3(dpx)]$  **3-30** with ellipsoids drawn at the 50% probability level.

The manganese(I) center is in an octahedral coordination sphere with a  $MnBrN_2C_3$  ligand environment. The bond lengths between the carbonyl ligands and the manganese(I) center are nearly equal with the values of Mn1-C1 at 1.805(4) Å, Mn1-C2 at 1.798(3) Å and Mn1-C3 at 1.812(4) Å and shorter than the Mn-N bond lengths with Mn1-N1 at 2.076(3) Å, Mn1-N3 at 2.017(3) Å and Mn1-Br1 at 2.5212(6) Å. The angle between bromide ligand and the *trans* carbonyl ligand C1-Mn1-Br1 of 178.68(10)° is close to 180°. The two *trans* angles between the carbonyl ligands and the dpx ligand backbone C2-Mn1-N1 and C3-Mn1-N3 are smaller than C1-Mn1-Br1 angle, but at

175.26(12)° and at 170.84(13)°, still close to linearity. The angles between the carbonyl ligands are C1-Mn1-C2 at 89.65(14)°, C1-Mn1-C3 at 94.53(15)° and C2-Mn1-C3 at 83.80(14)°. Furthermore, the angles between the bromide ligand and the *cis* carbonyl ligands deviate somewhat from 90° with C2-Mn1-Br1 at 89.34(11) and C3-Mn1-Br1 of 86.20(11)°. The angle between the coordinated nitrogen atoms N1-Mn1-N3 is 77.91(10)°. The steric hindrance of the two pyridyl moieties in the dp<sub>x</sub> ligand causes a twisting of the three ring systems of the 2,3-di(2-pyridyl)quinoxaline. The uncoordinated pyridine ring is rotated by 18.6(5)° out of the plane of the quinoxaline, while the bicyclic ring is twisted by 15.0(3)° relative to the coordinated pyridine ring.

3.3.3.7 Synthesis of  $[\text{Ru}(\text{bpy})_2(\text{dpx})\text{MnBr}(\text{CO})_3](\text{PF}_6)_2$ 

For the synthesis of  $[\text{Ru}(\text{bpy})_2(\text{dpx})\text{MnBr}(\text{CO})_3](\text{PF}_6)_2$  **3-31** brown glassware and aluminum foil was used, to prevent photolytic decomposition. Then, manganese pentacarbonyl bromide and  $[\text{Ru}(\text{bpy})_2(\text{dpx})](\text{PF}_6)_2$  **3-29** were dissolved in degassed acetone and heated to reflux for 4 h under an inert atmosphere of dinitrogen. After addition of diethylether and *n*-hexane, black precipitate was obtained which was collected by filtration, dried in vacuum and purified on a SepPak C-18 reversed column with a mixture of water/acetonitrile as the eluent. After lyophilization, the product was obtained as an extremely light-sensitive black powder in a good yield of 68% (**Scheme 3.21**).

Scheme 3.21: Synthesis of **3-31**.

The IR spectrum of **3-31** shows two very strong bands at 2026 and 1928  $\text{cm}^{-1}$ . Three weak signals are observed at 1605, 1466 and 1447  $\text{cm}^{-1}$  as well as one medium band at 833  $\text{cm}^{-1}$  (**Fig. 3.68**). The very strong band at 2026  $\text{cm}^{-1}$  is due to the symmetric while the band at 1928  $\text{cm}^{-1}$  is assigned to the antisymmetric C-O stretching vibration of the carbonyl ligands. The weak signals at 1605, 1466 and 1447  $\text{cm}^{-1}$  result from the aromatic C-C and C-N stretching vibrations. The medium band at 833  $\text{cm}^{-1}$  is assigned to the P-F stretching vibrations of the  $\text{PF}_6$  counterions.

The NMR spectra of **3-31** were recorded in deuterated dichloromethane. In the  $^1\text{H}$  NMR spectrum a multiplet at 7.44-7.48 ppm with integral 3H was observed. Two triplets at 7.54 and 7.61 ppm as well as a multiplet at 7.68-7.73 ppm with integral ratio 1:2:3 are found. At 7.84-8.36 ppm a multiplet



is observed with integral 13H which could not be resolved. The doublet at 8.53 ppm as well as the multiplet at 8.66–8.70 ppm has integrals of 2H each while the two doublets at 8.78 and 9.41 ppm have integrals of 1H each (Fig. 3.69).

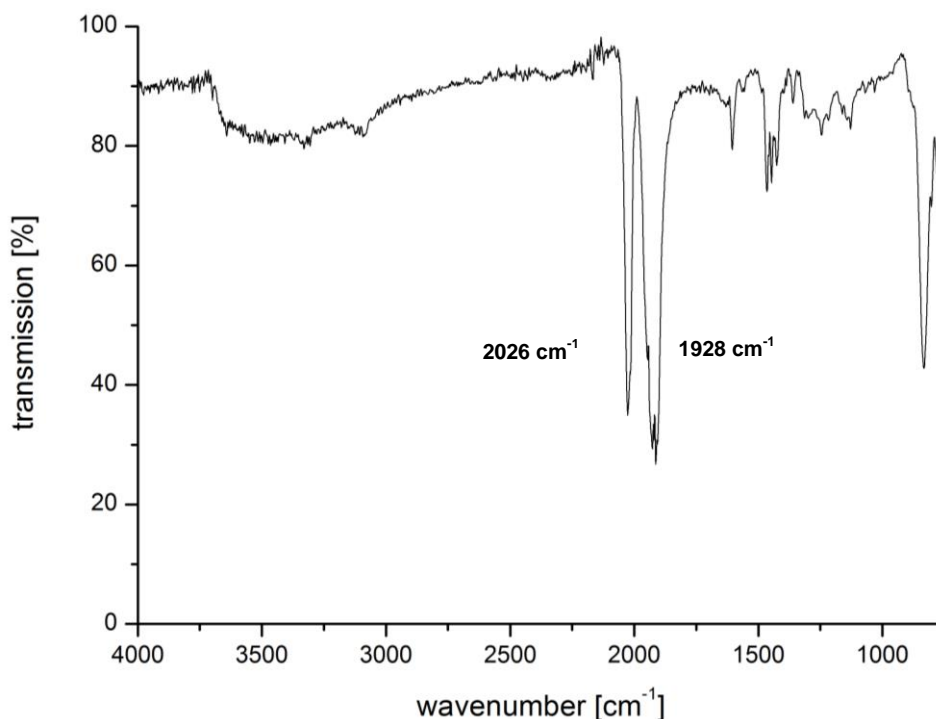


Figure 3.68: ATR-IR spectrum of 3-31.

The  $^1\text{H}$  NMR spectrum is rather complicated. The three multiplets at 7.44–7.48, 7.68–7.73 and 7.84–8.36 ppm cannot be resolved in detail. Thus, the two triplets at 7.54 and 7.61 ppm with  $^3J = 6.6$  and 7.3 Hz cannot be assigned clearly. The doublet at 8.53 ppm with  $^3J = 8.2$  Hz as well as the multiplet at 8.66–8.70 ppm results from the four protons in the 6- and 6'-positions of the bipyridine ligands. The two doublets at 8.78 and 9.41 ppm with  $^3J = 8.6$  and 5.2 Hz are assigned to the H6- and H6'-atoms of the pyridine units of the dpx ligand.

The  $^{13}\text{C}\{^1\text{H}\}$  NMR spectrum of **3-31** shows 39 signals for the 41 carbon atoms contained in the complex. 37 peaks appear in a range of 124.4 to 157.9 ppm while an additional strongly downfield shifted signal appear at 223.7 and 224.2 ppm (Fig. 3.70).

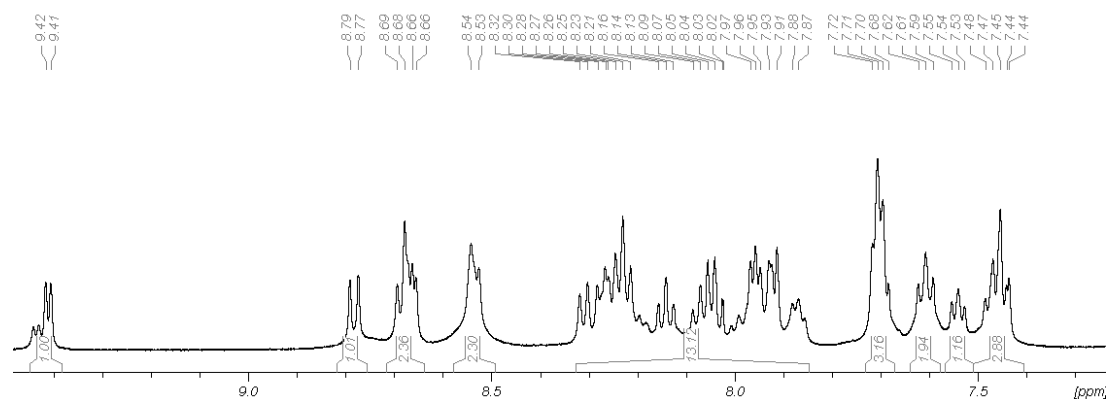


Figure 3.69: Aromatic region of the  $^1\text{H}$  NMR spectrum (500.13 MHz,  $\text{CD}_2\text{Cl}_2$ ) of **3-31**.

The  $^{13}\text{C}\{^1\text{H}\}$  NMR spectrum of **3-31** shows the expected 39 signals. The 22 signals between 124.4 and 139.9 ppm are assigned to the CH groups not adjacent to nitrogen atoms. The signals at 143.3 and 143.7 ppm are due to the quaternary carbon atoms in the 5- and 6-positions of the dpx ligand. The four signals at 151.8, 151.8, 152.1, and 153.2 ppm result from the 6- and 6'-carbon atoms of the bipyridine ligands. Instead of the two expected signals, only one signal is found for the two remaining CH groups at 154.5 ppm. The eight signals at 153.7, 155.7, 156.5, 156.6, 156.9, 157.0, 157.5, and 157.9 ppm result from the remaining quaternary carbon atoms of dpx and bipyridine ligands. With a strong downfield shift at 223.7 and 224.2 ppm, the signals of the carbonyl ligands are observed.

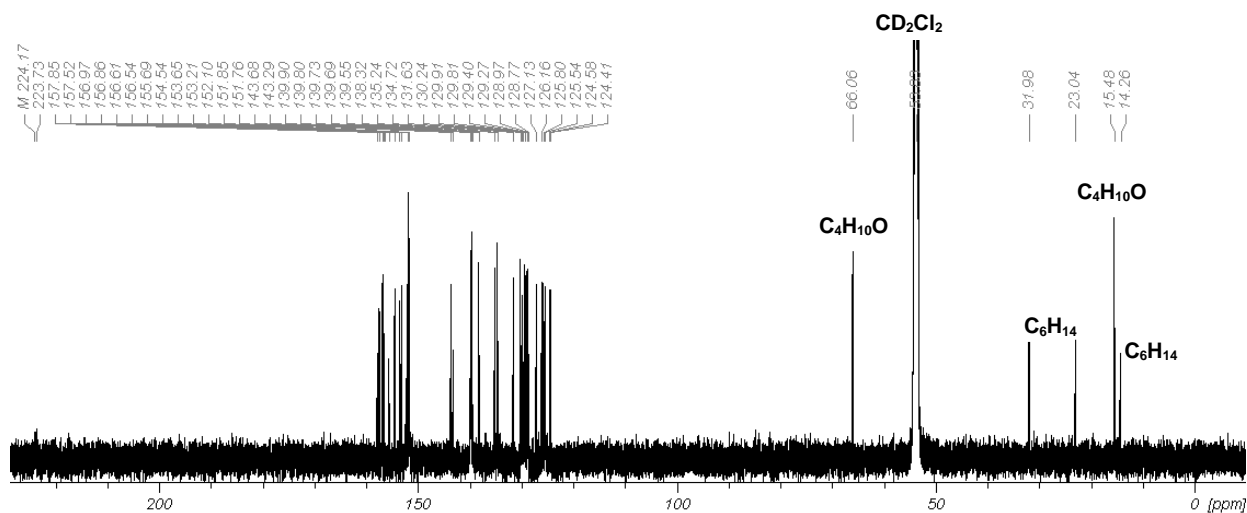


Figure 3.70:  $^{13}\text{C}\{^1\text{H}\}$  NMR spectrum (125.75 MHz,  $\text{CD}_2\text{Cl}_2$ ) of **3-31**.

In the positive-mode ESI-MS of **3-31** six signals at  $m/z = 285.04$ ,  $349.07$ ,  $419.96$ ,  $699.14$ ,  $843.11$ , and  $1062.95$  Da are observed. The spectrum shows a protonated adduct of the dpx ligand at  $m/z = 285.04$  Da with a composition  $[\text{M-Mn}(\text{CO})_3\text{Br-Ru}(\text{C}_{10}\text{H}_8\text{N}_2)_2+\text{H}]^+$ . The dication  $[\text{M-2xPF}_6\text{-Mn}(\text{CO})_3\text{Br}]^{2+}$  is found at  $m/z = 349.07$  Da which lost the whole Mn(I)-moiety as well as both  $\text{PF}_6$  counterions during ionization. The protonated adduct with a composition of  $[\text{M-3xCO-Ru}(\text{C}_{10}\text{H}_8\text{N}_2)_2+\text{H}]^+$  which lost the Ru(II)-unit as well as the three carbonyl ligands appears at  $m/z = 419.96$  Da. At  $m/z = 699.14$  Da a fragment with composition  $[\text{M-2xPF}_6\text{-Mn}(\text{CO})_3\text{Br-H}]^+$  is observed. The cation  $[\text{M-PF}_6\text{-Mn}(\text{CO})_3\text{Br}]^+$  which lost the Mn(I)-moiety as well as one  $\text{PF}_6$  counterion during ionization is found at  $m/z = 843.11$  Da. The spectrum shows the molecular ion  $[\text{M-PF}_6]^+$  at  $m/z = 1062.95$  Da.

### 3.3.4 Photophysical studies of Mn(I)-Ru(II)-PhotoCORMs

As a starting point for the photophysical study of the series of heterobinuclear Mn(I)-Ru(II)-complexes, the absorption spectra of the different complexes **3-18** and **3-25** to **3-31** were recorded and a concentration series prepared to calculate the extinction coefficients. All UV/Vis spectra were measured in dimethylsulfoxide, with the exception of [Ru(bpy)<sub>2</sub>(dpx)MnBr(CO)<sub>3</sub>](PF<sub>6</sub>)<sub>2 **3-31**, which was measured in dichloromethane due to its poor stability in dimethylsulfoxide (Tab. 3.8).</sub>

Table 3.8: Absorption maxima and extinction coefficients of compound **3-18** and **3-25** to **3-31** in different solvents.

<i>compound</i>	<i>solvent</i>	$\lambda_{max}$ [nm]	$\epsilon_{\lambda_{max}}$ [M <sup>-1</sup> cm <sup>-1</sup> ]
<b>3-18</b>	DMSO	500	19000 ± 2000
<b>3-26</b>	DMSO	500	24000 ± 5300
<b>3-25</b>	DMSO	450	15000 ± 600
<b>3-27</b>	DMSO	480	5400 ± 600
<b>3-28</b>	DMSO	450	19000 ± 2700
<b>3-29</b>	DMSO	525	7200 ± 400
<b>3-30</b>	DMSO	500	2600 ± 300
<b>3-31</b>	CH <sub>2</sub> Cl <sub>2</sub>	585	11000 ± 1200

The introduction of the MnBr(CO)<sub>3</sub> moiety to the bpy binding pocket of the tbx ligand in **3-18** resulted in broadening of the main absorption band at 500 nm, the intensity of which increased by about 20%. In case of the pytp compounds **3-25** and **3-28** the extinction coefficient of the main absorption band increases from 15000 ± 600 to 19000 ± 2700 M<sup>-1</sup>cm<sup>-1</sup> while the extinction coefficient of the pytp manganese compound **3-27** has a value of 5400 ± 600 M<sup>-1</sup>cm<sup>-1</sup>. The absorption maxima of **3-25** and **3-28** are found at 450 nm, and the one of the comparable Mn(I)-complex **3-27** is even 30 nm higher, due to the difference in the ligand-backbone of **3-27** and **3-28**. With exchange of the MnBr(CO)<sub>3</sub> moiety of **3-30** by the Ru(bpy)<sub>2</sub> unit in the binding pocket of the dpx ligand resulting in compound **3-29**, the absorption band is shifted by 25 nm to the red region of the spectrum while the extinction

coefficient increases by a factor of 3. For the heterobinuclear complex **3-31** the maximum is red shifted by 85 nm to 585 nm in comparison to the pure manganese compound **3-30** with an extinction coefficient of  $11000 \pm 1200 \text{ M}^{-1}\text{cm}^{-1}$ . According to the experiments, the influence of the Ru(II)-moiety is observed in the difference of the extinction coefficients. While the Mn(I)-compounds **3-27** and **3-30** have values of  $5400 \pm 600$  and  $2600 \pm 300 \text{ M}^{-1}\text{cm}^{-1}$  the values become  $19000 \pm 2700$  and  $11000 \pm 1200 \text{ M}^{-1}\text{cm}^{-1}$ , being four times higher for the heterobinuclear Mn(I)-Ru(II)-PhotoCORMs **3-28** and **3-31**. The highest extinction coefficient was found for **3-26** due to the Ru(etc)(tbx) moiety which seems to be a better photosensitizer than the Ru(bpy)<sub>2</sub> units in **3-28** and **3-31**. The most red-shifted absorption maximum of the three heterobinuclear complexes is found for **3-31** and 85 nm higher than for **3-26** and even 135 nm higher than for **3-28** (Fig. 3.71).

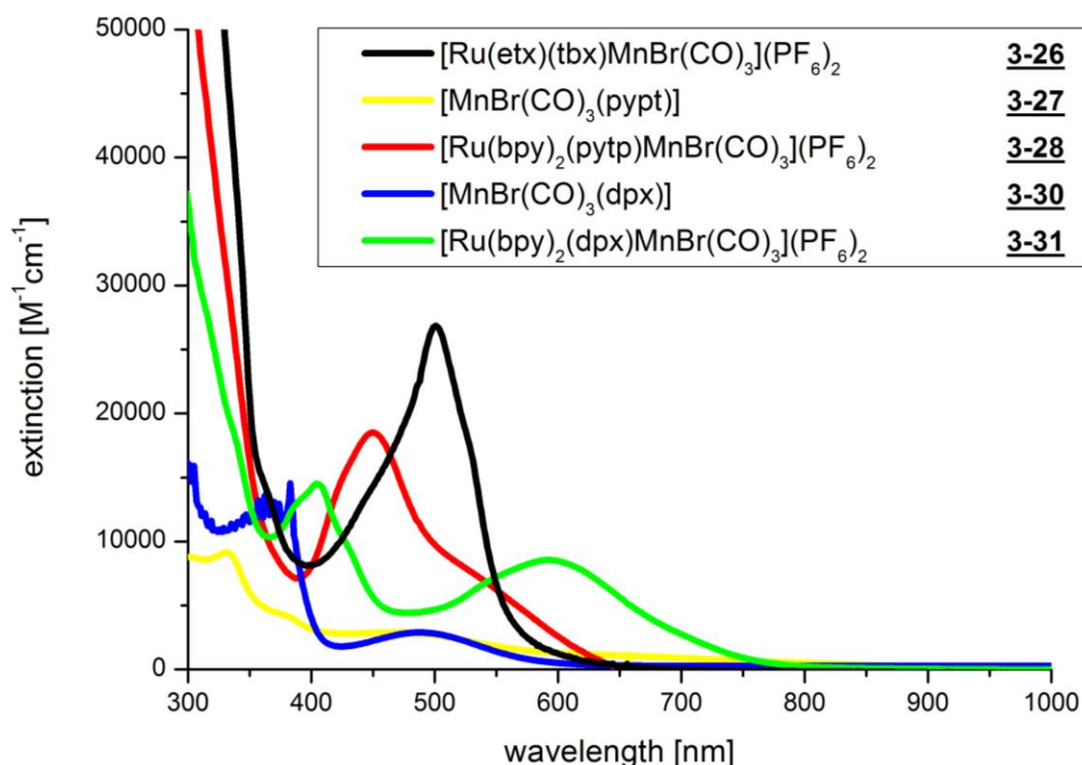


Figure 3.71: UV/Vis spectra of **3-26**, **3-27**, **3-29**, **3-30** in DMSO and **3-31** in  $\text{CH}_2\text{Cl}_2$ .

The availability of the proper light sources limited the choice of excitation wavelength for further photophysical studies. Thus, photolysis experiments of compounds 3-26, 3-27, 3-29, 3-30, and 3-31 were carried out at 412, 468, 525, and 660 nm which are collected in **Table 3.9**.

**Table 3.9:** Selected illumination wavelengths of the PhotoCORMs 3-26, 3-27, 3-29, 3-30 and 3-31.

<i>compound</i>	$\lambda_{max}$ [nm]	$\lambda_{illumination}$ [nm]
<u>3-26</u>	500	468/525
<u>3-27</u>	480	412/468
<u>3-28</u>	450	468
<u>3-30</u>	500	468
<u>3-31</u>	585	468/525/660

3.3.4.1 Photolytic CO release from  $[\text{Ru}(\text{etx})(\text{tbx})\text{MnBr}(\text{CO})_3](\text{PF}_6)_2$ 

To study the CO-release properties of **3-26**, first the dark stability of the compound was assessed in a UV/Vis experiment. Thus, a solution of dithionite-reduced myoglobin in PBS was added to a cuvette, followed by a solution of **3-26** in dimethylsulfoxide. The total concentrations were 60  $\mu\text{M}$  of myoglobin, 10 mM of dithionite and 10  $\mu\text{M}$  of CORM **3-26**. The cuvette was placed in a UV/Vis spectrometer and spectra were recorded every 30 min (**Fig. 3.72**).

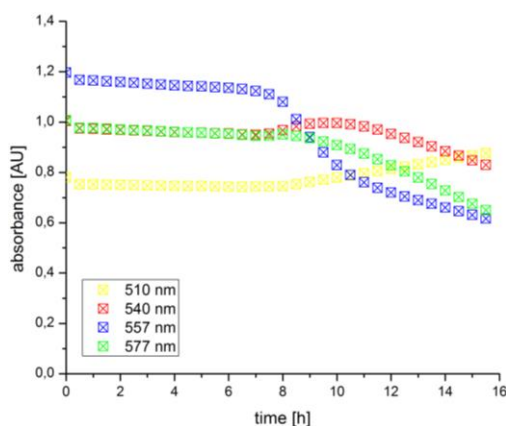


**Figure 3.72:** Change of absorbance at 510, 540, 557, and 577 nm with dark incubation time of a solution of **3-26** (10  $\mu\text{M}$ ) in PBS in the presence of myoglobin (60  $\mu\text{M}$ ) and sodium dithionite (10 mM).

The recorded UV/Vis spectra show no changes of absorbance at the detected wavelengths at 510, 540, 557, and 577 nm up to 7 h in the dark. After this time period a significant decrease in absorbance at 540, 557 and 577 nm is observed while the absorbance at 510 nm increases marginally. Thus, the experiment shows the stability of **3-26** for 7 h in phosphate-buffered myoglobin solutions, followed by an unidentified dark reaction of the compound. Then, CO-release behavior was studied by the myoglobin assay. Thus, solutions were prepared the same way as in the dark experiment and then illuminated with wavelengths of 468 and 525 nm (**Fig. 3.73**).

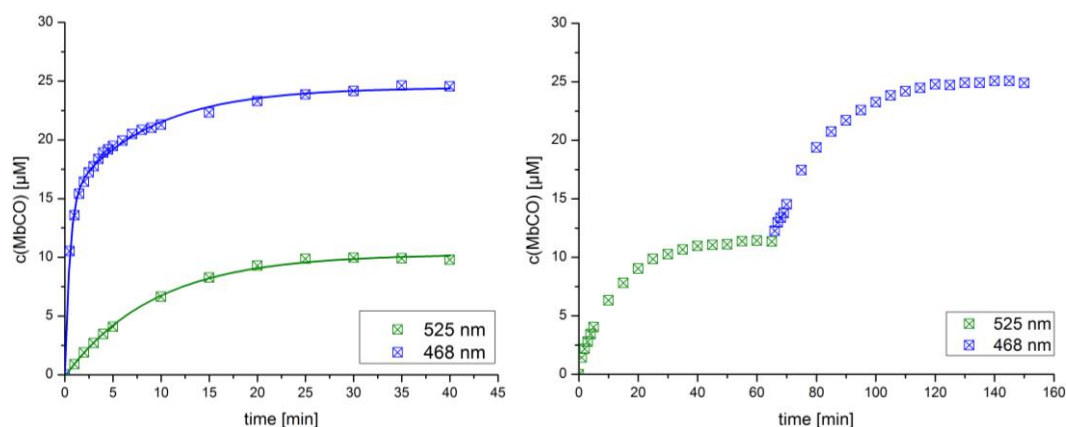


**Figure 3.73:** Concentrations of MbCO upon illumination of PhotoCORM **3-26** (10  $\mu\text{M}$ ) in PBS in the presence of myoglobin (60  $\mu\text{M}$ ) and sodium dithionite (10 mM), (left) at a single wavelength of 468 or 525 nm and (right) consecutive illumination first at 525 nm for 65 min and then at 468 nm for 85 min.

When illuminated at 468 nm, **3-26** releases ( $22.6 \pm 0.5$ )  $\mu\text{M}$  ( $2.3 \pm 0.1$  eq.) of carbon monoxide with a very short half-life of 1.3 min. The concentration of MbCO decreases to ( $10.6 \pm 0.1$ )  $\mu\text{M}$  ( $1.1 \pm 0.01$  eq.), when switching to a longer wavelength of 525 nm while the half-life increases by almost a factor of 10 to 8.5 min. Thus, the exchange of the light source to illumination wavelengths of 525 nm makes the process less efficient. In a further experiment a solution was illuminated consecutively first at 525 nm until the concentration of the generated MbCO reaches a plateau level at ( $10.6 \pm 0.1$ )  $\mu\text{M}$  ( $1.1 \pm 0.01$  eq.) and then at 468 nm. The change of the light source to a shorter wavelength of 468 nm results in the release of a second equivalent of CO. Thus, this dual-wavelength illumination showed the direct influence of the selected light source on the efficacy of the photolysis as well as the possibility of a dose control of the CO released.



3.3.4.2 Photolytic CO release from [MnBr(CO)<sub>3</sub>(pypt)]

To study the dark stability of **3-27**, a solution of dithionite-reduced, myoglobin in phosphate-buffered saline (PBS) was prepared, and a solution of **3-27** (10  $\mu$ M) in dimethylsulfoxide was added the same was as described above (see Section 3.3.4.1). Then, UV/Vis spectra were taken every 30 min (Fig. 3.74).

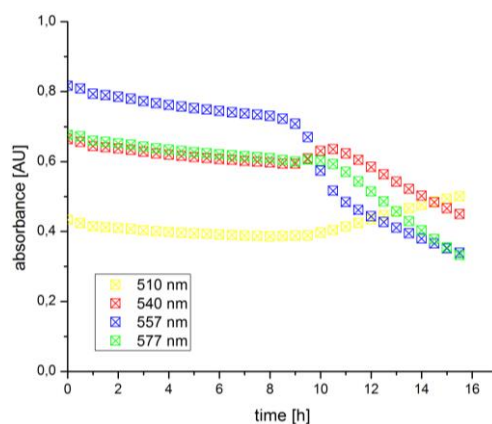


**Figure 3.74:** Change of absorbance at 510, 540, 557, and 577 nm with dark incubation time of a solution of **3-27** (10  $\mu$ M) in PBS in the presence of myoglobin (60  $\mu$ M) and sodium dithionite (10 mM).

The experiment showed similar results for **3-27** as seen for compound **3-26**. For 8 h no significant changes of absorbance at the detected wavelengths at 510, 540, 557, and 577 nm were observed. After 8 h, the absorbance decreases rapidly at 540, 557, and 577 nm until the end of the experiment at 16 h while the absorbance detected at 510 nm slightly increases. In the myoglobin assay no significant concentrations of generated MbCO were detected with an illumination wavelength at 468 nm. Also, by change of the light source to shorter wavelength of 412 nm, no absorption bands for the MbCO were observed in the recorded UV/Vis spectra. This might result from the bad solubility of **3-27** in common solvents. This assumption is confirmed by small amounts of precipitate found in the cuvette after the experiments.

3.3.4.3 Photolytic CO release from  $[\text{Ru}(\text{bpy})_2(\text{pytp})\text{MnBr}(\text{CO})_3](\text{PF}_6)_2$ 

As starting point for the photophysical studies of  $[\text{Ru}(\text{bpy})_2(\text{pytp})\text{MnBr}(\text{CO})_3](\text{PF}_6)_2$  **3-28**, a dark experiment was carried out the same way as for the compounds **3-26** and **3-27**. As seen before, the absorbances at the detected wavelengths at 510, 540, 557 and 577 nm show no changes and therefore stability of **3-28** in the dark for 8 h, followed by an unidentified dark reaction (**Fig. 3.75**).

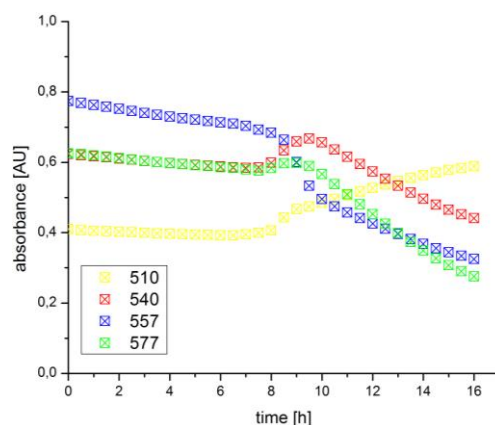


**Figure 3.75:** Change of absorbance at 510, 540, 557, and 577 nm with dark incubation time of a solution of **3-28** (10  $\mu\text{M}$ ) in PBS in the presence of myoglobin (60  $\mu\text{M}$ ) and sodium dithionite (10 mM).

The absorption maximum of **3-28** is found at 450 nm. Thus, an illumination light source of 468 nm was used in the myoglobin assay. In the experiments a concentration of  $(22.5 \pm 1.4) \mu\text{M}$  ( $2.3 \pm 0.1$  eq.) generated MbCO was detected. The half-life of the liberation process is 4.8 min. This fast releasing kinetics is due to the high extinction coefficient of  $19000 \pm 2700 \text{ M}^{-1}\text{cm}^{-1}$ . (**Fig. 3.76**).

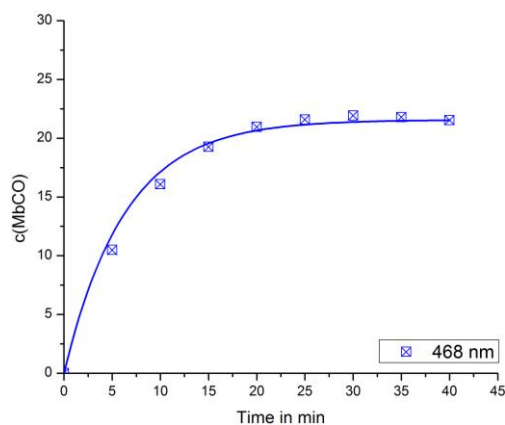


**Figure 3.76:** Concentrations of MbCO upon illumination of PhotoCORM **3-28** (10  $\mu\text{M}$ ) in PBS in the presence of myoglobin (60  $\mu\text{M}$ ) and sodium dithionite (10 mM)

3.3.4.4 Photolytic CO release from  $[\text{MnBr}(\text{CO})_3(\text{dpx})]$ 

The photo triggered CO-release from  $[\text{MnBr}(\text{CO})_3(\text{dpx})]$  **3-30** was followed with the standard myoglobin assay. Initially, studies of the dark stability of **3-30** in dimethylsulfoxide solution in the presence of reduced myoglobin were carried out. Thus, UV/Vis spectra of the solution were recorded every 30 min for a time period of 18 h (**Fig. 3.77**).

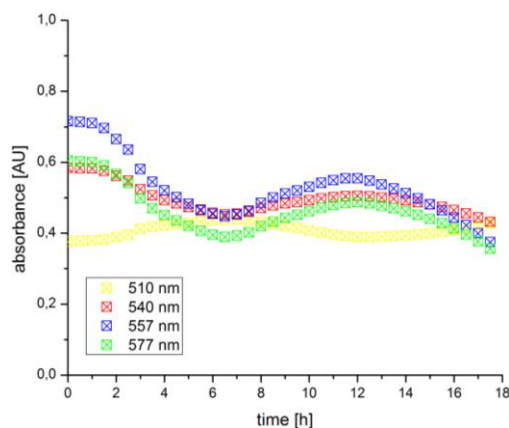


**Figure 3.77:** Change of absorbance at 510, 540, 557, and 577 nm during dark incubation of a solution of **3-30** (10  $\mu\text{M}$ ) in PBS in the presence of myoglobin (60  $\mu\text{M}$ ) and sodium dithionite (10 mM).

The absorption bands of myoglobin at 510, 540, 557 and 577 nm undergo pronounced changes already after 1 h. While the absorbance at 540, 557, and 577 nm decrease during the next 6 h, then follows a slight increase for an additional 4 h. Then, again towards the end of the experiment the absorbance decreases. At 510 nm, a reversed behavior is observed. The so far unknown dark reaction starts earlier in this experiment than was observed for compounds **3-26** to **3-28**. This indicates that solutions of **3-30** in dimethylsulfoxide are not stable under the conditions of the myoglobin assay. For the photo-triggered CO-release from **3-30**, an illumination wavelength of 468 nm was used in the standard myoglobin assay.

In this experiment an amount of  $(16.3 \pm 0.1) \mu\text{M}$  MbCO was detected after 80 min which translates to  $1.6 \pm 0.01$  equivalents of carbon monoxide released from compound **3-30**. The plateau level was reached after 120 min with a half-life of 19.7 min (**Fig. 3.78**).

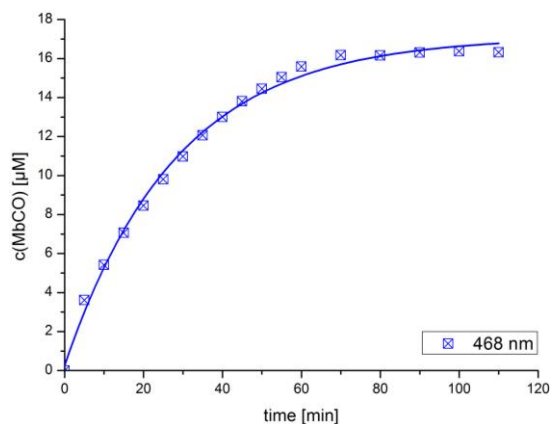


**Figure 3.78:** Concentration of MbCO formed during illumination of PhotoCORM **3-30** ( $10 \mu\text{M}$ ) in PBS in the presence of myoglobin ( $60 \mu\text{M}$ ) and sodium dithionite ( $10 \text{mM}$ ).

3.3.4.5 Photolytic CO release from  $[\text{Ru}(\text{bpy})_2(\text{dpx})\text{MnBr}(\text{CO})_3](\text{PF}_6)_2$ 

According to the absorption maximum,  $[\text{Ru}(\text{bpy})_2(\text{dpx})\text{MnBr}(\text{CO})_3](\text{PF}_6)_2$  **3-31** seems to be the most promising complex in the series of heterobinuclear Mn(I)-Ru(II)-PhotoCORMs. Compound **3-31** has an absorption maximum at 585 nm with an extinction coefficient of  $11000 \pm 1200 \text{ M}^{-1}\text{cm}^{-1}$  in  $\text{CH}_2\text{Cl}_2$ . However, the poor stability of **3-31** in dimethylsulfoxide was already observed during characterization of the compound, where  $^1\text{H}$  NMR spectra recorded in deuterated dimethylsulfoxide showed several signals of decomposition products. Thus, the decomposition of **3-31** in dimethylsulfoxide was studied by UV/Vis spectroscopy over 16 h. Spectra were recorded every 30 min and spectral changes at the two characteristic absorption maxima at 410 and 585 nm were recorded over incubation time (Fig. 3.79).

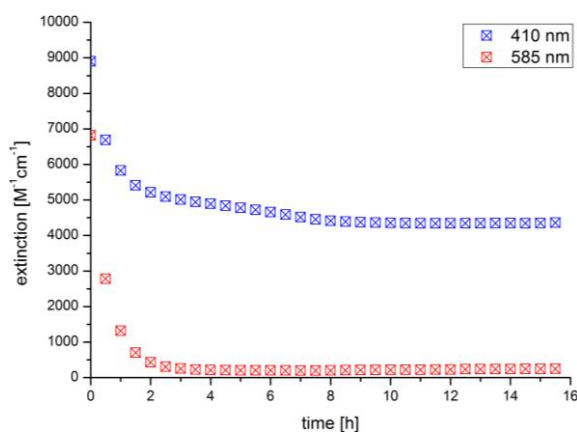
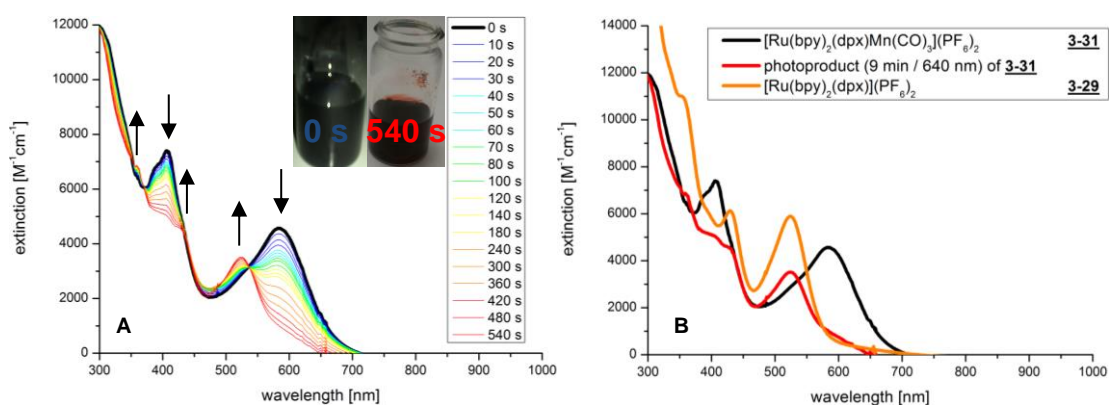


Figure 3.79: Change of absorbance at 510, 540, 557, and 577 nm with dark incubation time of a solution of **3-31** (0.13 mM) in DMSO.

The experiment showed complete decomposition of **3-31** over 2 h. Visual inspection also showed that dimethylsulfoxide as well as dichloromethane solutions of **3-31** change their color from blackish blue via purple to dark red over a time period of 10 min just under normal daylight. In the dark this transformation required several hours for dimethylsulfoxide solutions while the solutions of **3-31** in dichloromethane showed stability over weeks. Thus, for the photolysis experiments, an illumination wavelength of 660 nm was selected. The photolytic process was followed by UV/Vis spectroscopy and

spectra were recorded in intervals of 10, 20, and later 60 s. The spectral changes upon the illumination are shown in **Figure 3.80A**. While the main bands of **3-31** at 407 and 585 nm decrease to a plateau level, new absorption bands at 355, 430, and 530 nm grow in until the end of the experiment. These three signals are also found in the UV/Vis spectrum of **3-29**, which indicates the complete loss of the Mn(I)-moiety during photolysis. The overlay of the UV/Vis spectra of **3-31** and its photoproduct as well as **3-29**, shows the photolytic transformation of compound **3-31** to **3-29** (**Fig. 3.80B**).



**Figure 3.80:** (A) Changes in the UV/Vis spectra of a solution of **3-31** in DMSO illuminated at 660 nm for 9 min. The spectrum before start of illumination is highlighted in black. (B) UV/Vis spectra of **3-31**, **3-29** and the photoproduct of **3-31** in DMSO.

The CO release from **3-31** was also studied with the standard myoglobin assay. To explore the dark stability of **3-31**, a dimethylsulfoxide solution was added to an aqueous dithionite-reduced, buffered myoglobin solution and UV/Vis spectra were recorded every 30 min (**Fig. 3.81**).

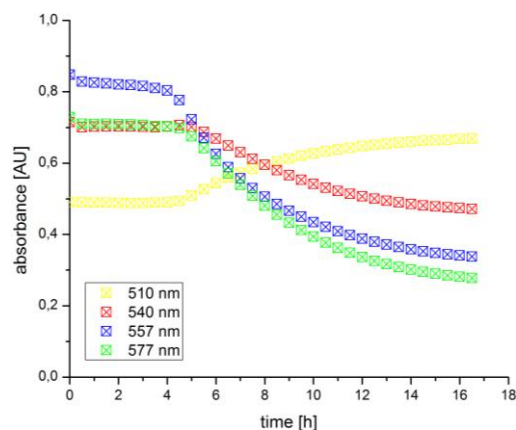


**Figure 3.81:** Change of absorbance at 510, 540, 557, and 577 nm with dark incubation time of a solution of **3-31** (10  $\mu$ M) in PBS in the presence of myoglobin (60  $\mu$ M) and sodium dithionite (10 mM).

At wavelengths of 510, 540, 557, and 577 nm, no changes were observed for 4 h demonstrating the dark stability of **3-31** over this time period. An illumination wavelength of 468, 525, and 660 nm was used for the measurements. Photoactivation at 468 nm led to a release of  $(14.5 \pm 7.5) \mu\text{M}$  ( $1.5 \pm 0.8$  eq.) of CO with a half-life of 12.9 min. Upon illumination at 525 nm,  $(7.1 \pm 2.5) \mu\text{M}$  ( $0.7 \pm 0.3$  eq.) of MbCO formed with a half-life of the complex of 15.0 min. At 660 nm,  $(5.5 \pm 2.3) \mu\text{M}$  ( $0.6 \pm 0.2$  eq.) of carbon monoxide were released with a half-life of 14.0 min. Thus, variation of the light source from 468 to 525 nm decreased the amount of MbCO formed by about 50%. The use of 660 nm excitation only marginal further reduced the concentration of MbCO generated while the half-life increases from 13 to 15 min upon longer wavelength excitation (**Fig. 3.82**).

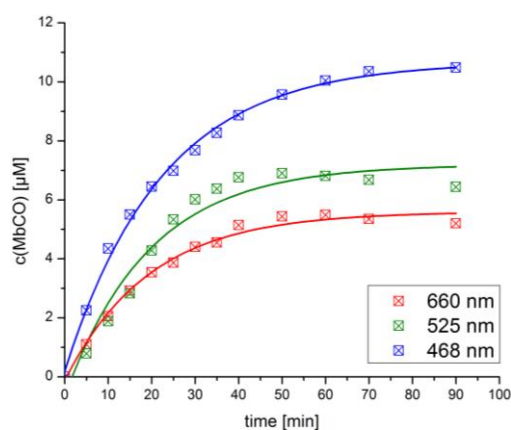


**Figure 3.82:** Concentration of MbCO formed upon illumination of **3-31** ( $10 \mu\text{M}$ ) in PBS in the presence of myoglobin ( $60 \mu\text{M}$ ) and sodium dithionite ( $10 \text{mM}$ ) at an excitation wavelength of 468, 525, or 660 nm.

However, the photolysis under the conditions of the myoglobin assay is less efficient than in dimethylsulfoxide. This is likely due to the reducing conditions resulting from the addition of sodium dithionite, which might interfere with the oxidation of the  $\text{Mn}(\text{CO})_3$  unit to  $\text{Mn}(\text{II})$ , which however is essential for release of all three carbonyl ligands.

#### 3.3.4.6 Comparison of the CO release from Mn(I)-Ru(II)-PhotoCORMs

Three different Mn(CO)<sub>3</sub>-Ru(II) PhotoCORMs were prepared together with control compounds only incorporating Mn(CO)<sub>3</sub> or Ru(II) moieties. These are based on 3-(pyridin-2-yl)-1,2,4-triazine[5,6-*f*]-1,10-phenanthroline (pytp) **3-19**, 3-(pyridin-2-yl)phenanthro[9,10-*e*]-1,2,4-triazine (pypt) **3-20** 2,3-di(2-pyridyl)quinoxaline (dpx) **3-21** ligands as well as the metal precursor [Ru(etx)(tbx)](PF<sub>6</sub>)<sub>2</sub> **3-18**. In contrast to the Mn(I)-PhotoCORMs **3-5** to **3-8** as well as **3-15** and **3-16** discussed above which were stable, a lack of long term stability in the presence of dithionite reduced myoglobin was found for all Mn(I)-Ru(II)-PhotoCORMs as well as for the pure Mn(CO)<sub>3</sub> control compounds of the series. The instability could result from the negatively charged bromide ligand of the MnBr(CO)<sub>3</sub>-unit which might undergo side reactions involving myoglobin, dithionite and even the manganese(I) core. In the long term stable complexes **3-5** to **3-8**, **3-15**, and **3-16** no charged ligands are present which gives a hint that the bromide ligand is involved in the side reactions.

The most efficient CO release was found in the Ru(tpy)<sub>2</sub> unit containing compound **3-26**. For the experiments with 468 nm as illumination wavelength it released 2.3 ± 0.1 equivalents. The observed half-life of 1.3 min was the shortest of all compounds discussed in this work. Upon changing of the light source to 525 nm the released CO equivalents decreased to 1.1 ± 0.1. With a half-life of 7.2 min compound **3-26** releases CO faster than most of the other compounds of the series. The very fast CO release may result from the higher extinction coefficient of 24000 ± 5300 M<sup>-1</sup>cm<sup>-1</sup> for this Ru(tpy)<sub>2</sub> containing compound compared with the Ru(bpy)<sub>2</sub> containing complexes in the series. Due to solubility problems no results were obtained in the myoglobin assay for compound **3-27**. [Ru(bpy)<sub>2</sub>(pytp)MnBr(CO)<sub>3</sub>](PF<sub>6</sub>)<sub>2</sub> **3-28** is the complex with the lowest absorption maximum in the series. Thus, in experiments with higher wavelength light sources than 468 nm, no significant carbon monoxide release was obtained. With illumination at 468 nm a release of 2.3 ± 0.1 equivalents of CO were found. The half-life of **3-28** is with 4.8 min quite fast



which results from the high extinction coefficient of  $19000 \pm 2700 \text{ M}^{-1}\text{cm}^{-1}$ . The manganese complex  $[\text{MnBr}(\text{CO})_3(\text{dpx})]$  **3-30** showed the release of  $(1.6 \pm 0.01)$  equivalents of CO with an illumination wavelength at 468 nm. For this compound the longest half-life with 19.7 min in the series was observed. This results from the lowest extinction coefficient of  $2600 \pm 300 \text{ M}^{-1}\text{cm}^{-1}$  due to the missing Ru(II) unit. This might be the reason why no significant CO release was found for higher wavelengths such as 525 nm which are still covered by the absorption maximum.  $[\text{Ru}(\text{bpy})_2(\text{dpx})\text{MnBr}(\text{CO})_3](\text{PF}_6)_2$  **3-31** is the complex with the highest absorption maximum in the series at 585 nm and extension of the absorption band to nearly 750 nm. This makes the compound very promising for the usage of illumination wavelengths which fit into the phototherapeutic window from 600 to 1200 nm. Therefore, the myoglobin assay was performed with 468, 525, and 660 nm as excitation wavelengths. The most efficient carbon monoxide release was found for the energy rich 468 nm light source. At this wavelength,  $1.5 \pm 0.8$  equivalents of CO were detected with a half-life of 12.9 min. A change of the light source to 525 nm or 660 nm led to a decrease in liberated CO equivalents to  $0.7 \pm 0.3$  and  $0.6 \pm 0.2$  while the half-lives elongated slightly to 15.0 and 14.0 min (**Tab. 3.10**).

**Table 3.10:** Concentrations of MbCO, equivalents of CO and half-lives in different assays of **3-26** to **3-31**.

	$\lambda_{\text{max}} [\text{nm}]$	$\lambda_{\text{illumination}} [\text{nm}]$	$c(\text{MbCO}) [\mu\text{M}]^a$	CO [eq.]	$t_{1/2} [\text{min}]$
<b>3-26</b>	500	468	$22.6 \pm 0.5$	$2.3 \pm 0.1$	1.3
<b>3-26</b>	500	525	$10.6 \pm 1.2$	$1.1 \pm 0.1$	7.2
<b>3-27</b>	480	412	-	-	-
<b>3-28</b>	450	468	$22.5 \pm 1.4$	$2.3 \pm 0.1$	4.8
<b>3-30</b>	500	468	$16.3 \pm 0.1$	$1.6 \pm 0.01$	19.7
<b>3-31</b>	585	468	$14.5 \pm 7.5$	$1.5 \pm 0.8$	12.9
<b>3-31</b>	585	525	$7.1 \pm 2.5$	$0.7 \pm 0.3$	15.0
<b>3-31</b>	585	660	$5.5 \pm 2.3$	$0.6 \pm 0.2$	14.0

<sup>a</sup>  $c(\text{MbCO})_{\text{max}} = 30 \mu\text{M}$

However, the experiments showed that the efficiency of the carbon monoxide release correlates with the extinction coefficient and the excitation wavelength. A high extinction coefficient generally results in short half-lives of the complexes in the photolysis. Illumination at 468 nm causes efficient CO release with short half-lives in a range of 1.3 to 19.7 min. The use of a 525 nm or 660 nm light source leads to a decrease of the number of CO equivalents released and a longer the half-life of the liberation processes. In particular **3-26** has some interesting features to control the CO release. Experiments showed that a change of the light source from 525 nm to 468 nm after reaching the plateau level at one CO equivalent resulted in the release of one further equivalent. Thus, a stepwise release of carbon monoxide triggered by the chosen light source is possible for this compound which might give rise to a dose control of the liberated CO in clinical applications.

### 3.4 Mixed CO/NO-releasing molecules

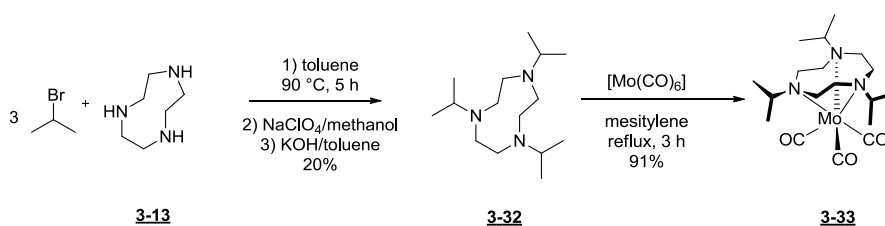
#### 3.4.1 Synthesis of ligands and metal complexes

In addition to carbon monoxide, nitric oxide is also known as an important small signaling molecule in the human body and there is extensive cross-talk between the signaling pathways triggered by these two molecules. However, so far, researchers have focused on molecules exclusively releasing either CO or NO. Thus, the preparation of metal complexes carrying both carbonyl and nitrosyl ligands in the coordination sphere of a single metal center with the possibility to liberate either CO or NO selectively by different trigger mechanisms would be of considerable interest. As a starting point to the exploration of mixed CO/NO-releasing molecules, the known compound  $[\text{Mo}(\text{CO})_2(\text{NO})(i\text{Pr}_3\text{tacn})]\text{PF}_6$ , with  $i\text{Pr}_3\text{tacn} = 1,4,7$ -triisopropyl-1,4,7-triazacyclonane as the coligand was selected from the literature, published in 1994 by Wieghardt *et al.* as a precursor to the first example of a nitrosyl(oxo)molybdenum(0) complex.<sup>[100]</sup>

Synthesis of the  $i\text{Pr}_3\text{tacn}$  ligand started with reaction of 1,4,7-triazacyclononane (tacn) **3-13** with isopropyl bromide in toluene at 90 °C for 5 h in the presence of potassium hydroxide (**Scheme 3.21**). After removal of the solvent, the compound was precipitated as the perchlorate salt for purification. The free ligand **3-32** was then obtained as a colorless oil by stirring a solution of the perchlorate salt in toluene in the presence of potassium hydroxide followed by removal of the solvent. The low yield of 20% is due to by the formation of mono- and disubstituted side-products which however can be separated from the main product by precipitation as the perchlorate salt.

The  $^1\text{H}$  NMR spectrum of **3-32** shows a doublet at 0.97 ppm, a singlet at 2.64 ppm, and a septet at 2.87 ppm with integrals of 18H, 12H, and 3H, respectively. In the  $^{13}\text{C}\{^1\text{H}\}$  NMR spectrum, peaks are observed at 18.3, 52.8, and 54.4 ppm. In the  $^1\text{H}$  NMR, the singlet at 2.64 ppm is due to the six equivalent methylene groups of the triazacyclononane backbone. The doublet

at 0.97 ppm and the septet at 2.87 ppm both show a splitting of  $^3J = 6.6$  Hz and are assigned to the methyl and methine protons of the three equivalent isopropyl moieties, respectively. The  $^{13}\text{C}\{^1\text{H}\}$  NMR signals at 18.3 and 52.8 ppm are also due to the methyl and methine units, respectively, while the peak at 54.4 ppm results from the six equivalent carbon atoms of the triazacyclononane ring. To introduce the molybdenum carbonyl moiety, the *i*Pr<sub>3</sub>tacn ligand and molybdenum hexacarbonyl were then dissolved in degassed mesitylene and heated to reflux for 3 h. The product was obtained as a brownish-yellow precipitate in very good yield (**Scheme 3.21**).<sup>[101]</sup>



**Scheme 3.21:** Synthesis of *i*Pr<sub>3</sub>tacn ligand **3-32** and its molybdenum tricarbonyl complex **3-33**.

The IR spectrum of **3-33** shows two very strong bands at 1888 and 1727  $\text{cm}^{-1}$  with additional weaker signals observed at 1443, 1388, 1123, and 1066  $\text{cm}^{-1}$ . The spectrum is dominated by the symmetric and antisymmetric stretching vibrations of the facial  $\text{Mo}(\text{CO})_3$  unit at 1888 and 1727  $\text{cm}^{-1}$ , respectively. The weak bands between 1443 and 1066  $\text{cm}^{-1}$  are due to the CH stretching vibrations of the isopropyl groups (**Fig. 3.83**).

The  $^1\text{H}$  NMR spectrum of **3-33** shows a doublet at 1.29 ppm with an integral of 18H and  $^3J = 6.4$  Hz and a singlet at 2.70 ppm with an integral of 12H in addition to the water and dimethylsulfoxide solvent peaks. The doublet at 1.29 ppm is assigned to the methyl groups of the isopropyl moieties while the singlet at 2.70 ppm is due to the signals of the triazacyclononane backbone. The expected septet of the methine groups at 3.27 ppm is only partly discernible due to overlap with the solvent water peak. Apparently, coordination of the ligand to the  $\text{Mo}(\text{CO})_3$  moiety leads to a downfield shift of all  $^1\text{H}$  NMR signals. The spectrum shows small impurities at 1.05 and 2.20 ppm which, however, do not influence further reaction steps (**Fig. 3.84**).

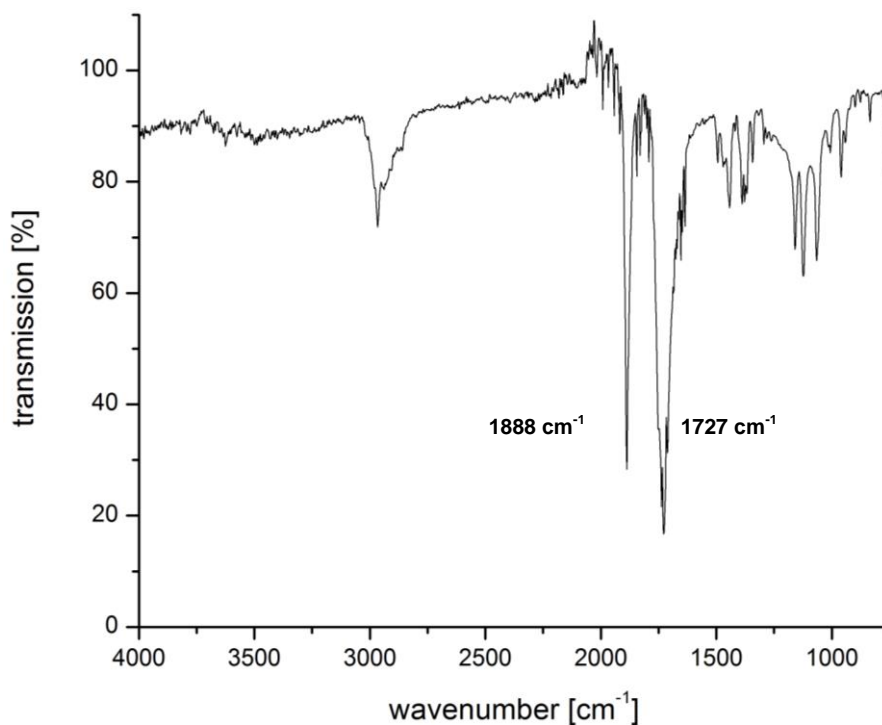


Figure 3.83: ATR-IR spectrum of **3-33**.

The  $^{13}\text{C}\{^1\text{H}\}$  NMR spectrum of **3-33** shows three peaks at 19.2, 54.4, 61.7, and 229.0 ppm. The peak at 19.2 ppm is assigned to the methyl carbon atoms of the equivalent isopropyl groups while the signal at 61.7 ppm is due to the methine groups, which coincidentally overlap with the ring methylene signals of the ligand. The signals for the six carbons of the triazacyclononane backbone are found at 54.4 ppm. At 229.0 ppm, the resonance of the three equivalent carbonyl carbon atoms *fac*- $\text{Mo}(\text{CO})_3$  moiety is observed.

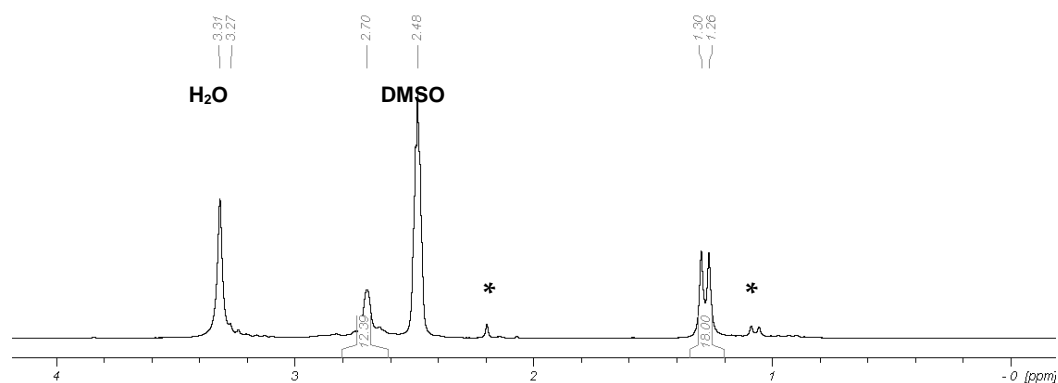
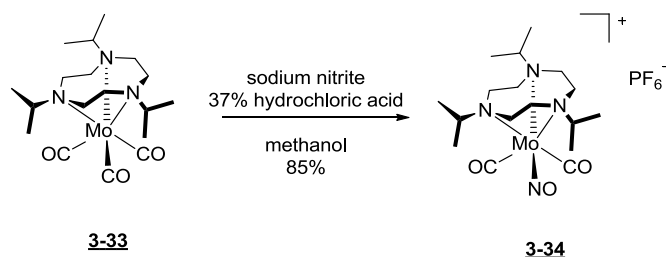


Figure 3.84:  $^1\text{H}$  NMR spectrum (199.93 MHz,  $\text{DMSO-d}_6$ ) of **3-33**. The asterisk marks the signals of a small impurity.

To introduce the nitrosyl ligand, a suspension of **3-33** and sodium nitrite in methanol was stirred at room temperature while concentrated hydrochloric acid was added dropwise, resulting in a clear yellow solution. The solvent was then removed and the residue dissolved in water. Addition of a saturated solution of potassium hexafluorophosphate in water led to precipitation of product **3-34** as a yellow solid in good yield (**Scheme 3.22**).<sup>[100]</sup>



**Scheme 3.22:** Synthesis of mixed ligand carbonyl/nitrosyl complex **3-34**.

The IR spectrum of **3-34** shows three very strong peaks at 2018, 1939, and 1912  $\text{cm}^{-1}$  as well as strong signals at 1643 and 829  $\text{cm}^{-1}$ . The peak at 2018  $\text{cm}^{-1}$  is assigned to the symmetric C-O stretching vibration of the *cis*-Mo(CO)<sub>2</sub> moiety. Instead of one expected band for the antisymmetric C-O stretching vibration, two bands at 1939 and 1912  $\text{cm}^{-1}$  are present. The splitting is due to solid-state packing effects and is not observed in solution IR experiments. The peak at 1643  $\text{cm}^{-1}$  results from the N-O stretching vibration of the nitrosyl ligand, which also shows a slight splitting due to packing effects. The strong signal at 829  $\text{cm}^{-1}$  is due to the P-F stretch of the hexafluorophosphate counterion (**Fig. 3.85**).

The <sup>1</sup>H NMR of **3-34** shows three doublets at 1.30, 1.40 and 1.42 ppm with an integral of 6H each and <sup>3</sup>J = 6.6, 6.5, and 6.5 Hz, respectively. Furthermore, three multiplets are observed at 2.88-2.94, 3.00-3.06, and 3.07-3.13 ppm with integrals of 2H, 4H, and 6H, respectively, as well as two septets at 3.21 and 3.53 ppm with integrals of 1H and 2H (**Fig. 3.86**).

The three methyl groups of the isopropyl moieties are inequivalent due to the *trans*-orientation to either the carbonyl or nitrosyl ligands. Thus, the signal at 1.30 ppm results from the six protons of the two methyl groups of the isopropyl moiety in *trans* position to the nitrosyl ligand. The two doublets at

1.40 and 1.42 ppm result from the four methyl groups of the remaining isopropyl moieties which are not completely identical due to the slightly twisted triazacyclononane backbone (see below). The three multiplets at 2.88-2.94, 3.00-3.06, and 3.07-3.13 ppm belong to the inequivalent methylene groups of the triazacyclononane backbone. The two septets at 3.21 and 3.53 ppm with coupling constants of  $^3J = 6.6$  and 6.5 Hz are assigned to the three methine protons of the isopropyl moieties.

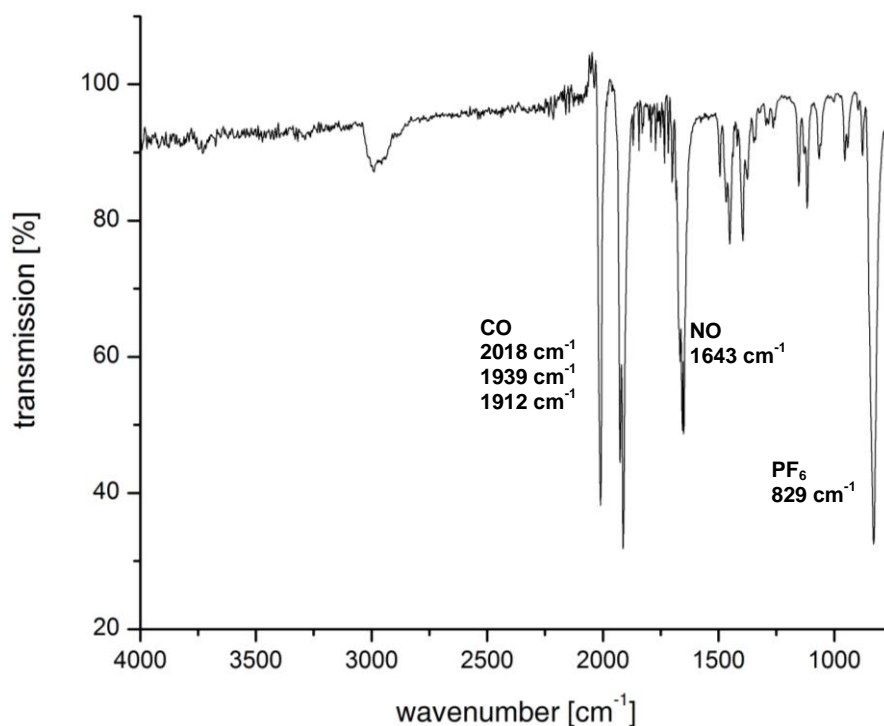


Fig. 3.85: ATR-IR spectrum of **3-34**.

The  $^{13}\text{C}\{^1\text{H}\}$  NMR of **3-34** shows eight peaks at 19.6, 19.7, 19.9, 52.4, 53.1, 62.9, 64.9, and 223.3 ppm. The signals at 19.6, 19.7, and 19.9 ppm are due to the inequivalent methyl carbon atoms of the three isopropyl moieties while the signals at 62.9 and 64.9 ppm are assigned to the methine groups. At 52.4 and 53.1 ppm the signals of the triazacyclononane backbone are found. The strongly downfield-shifted signal at 223.3 ppm stems from the two chemically equivalent carbonyl carbon atoms.

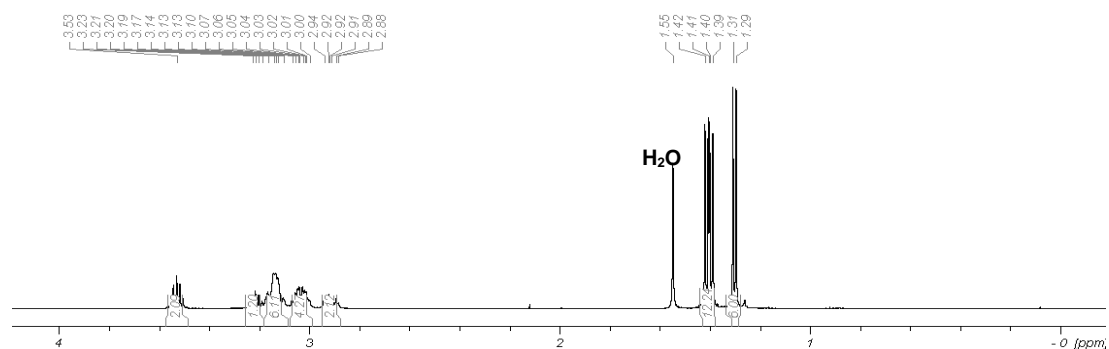


Figure 3.86:  $^1\text{H}$  NMR spectra (500.13 MHz,  $\text{CD}_2\text{Cl}_2$ ) of **3-34**.

In the positive-mode ESI mass spectrum of **3-34**, seven signals at  $m/z = 225.98$ ,  $268.02$ ,  $295.05$ ,  $339.10$ ,  $381.16$ ,  $411.16$ , and  $439.16$  Da are observed. All signals show the typical isotope pattern of molybdenum with seven peaks for the  $^{92}\text{Mo}$ ,  $^{94}\text{Mo}$ ,  $^{95}\text{Mo}$ ,  $^{96}\text{Mo}$ ,  $^{97}\text{Mo}$ ,  $^{98}\text{Mo}$ , and  $^{100}\text{Mo}$  isotopes in an intensity ratio of about 1.7:1:1.7:1.7:1:2.5:1. The peak at  $m/z = 225.98$  Da fits with a composition of  $[\text{M}-2\text{CO}-\text{NO}-3(\text{C}_3\text{H}_7)-\text{PF}_6]^+$ . The species at  $m/z = 268.02$  Da matches with a formula of  $[\text{M}-2\text{CO}-\text{NO}-2(\text{C}_3\text{H}_7)-\text{PF}_6]^+$  which has lost both carbonyl ligands, the nitrosyl ligand and two of the three isopropyl groups as well as the  $\text{PF}_6^-$  counterion. The peak at  $m/z = 295.05$  Da is assigned to the cation  $[\text{M}-\text{CO}-\text{NO}-2(\text{C}_3\text{H}_7)-\text{PF}_6]^+$ . The signal at  $m/z = 339.10$  Da is due to a fragment with the composition  $[\text{M}-\text{CO}-\text{NO}-\text{C}_3\text{H}_7-\text{PF}_6]^+$ . At  $m/z = 381.16$  Da, a species assigned to  $[\text{M}-\text{CO}-\text{NO}-\text{PF}_6]^+$  is found, which has lost one carbonyl as well as the nitrosyl ligand and the  $\text{PF}_6^-$  counterion during ionization. At  $m/z = 411.16$  Da, the fragment  $[\text{M}-\text{CO}-\text{PF}_6]^+$  is observed. Finally, at  $m/z = 439.16$  Da, the molecular ion  $[\text{M}-\text{PF}_6]^+$  is found. Thus, the CO and NO ligands as well as all isopropyl groups are labile and lead to fragmentation even under ESI conditions.

Single crystals of **3-34** could be obtained by slow diffusion of *n*-hexane into a solution of the complex in dichloromethane. Although this compound is known in the literature for some time, its X-ray crystal structure was not reported to date and thus a structure determination was undertaken. Compound **3-34** crystallizes in the orthorhombic space group *Pbca*. The unit cell contains the cationic  $[\text{Mo}(\text{CO})_2(\text{NO})(i\text{Pr}_3\text{tacn})]^+$  moiety as well as the hexafluorophosphate counter ion (Fig. 3.87). The molybdenum(0) center is in



an octahedral coordination environment with a  $\text{MoC}_2\text{N}_4$  ligand sphere. The NO ligand and one of the two carbonyl groups are disordered over two positions. The bond lengths with the molybdenum(0) center are  $\text{Mo1-N1a/C2b}$  at  $1.880(2)$  Å and  $\text{Mo1-C2a/N1b}$  at  $1.956(2)$  Å. The distance between the fixed carbonyl ligand and the molybdenum(0) center  $\text{Mo-C1}$  is  $1.963(2)$  Å. The Mo-N bond lengths to the *iPr*<sub>3</sub>tacn ligand range from  $2.3016(16)$  Å for  $\text{Mo1-N4}$  to  $2.3105(16)$  Å for  $\text{Mo1-N3}$  and are nearly equal.

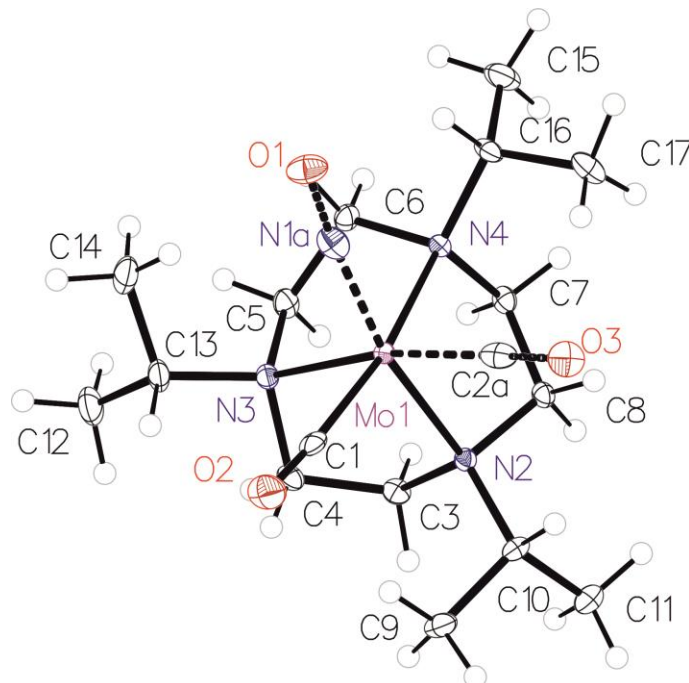


**Figure 3.87:** One of the two possible configurations of the molecular structure of the cationic unit of **3-34** with ellipsoids drawn at the 50% probability level. N1a and C2a are disordered and the positions of both atoms can be exchanged. The hexafluorophosphate counterion is not shown for clarity.

The bond angles of the disordered ligands are  $\text{Mo1-N1a/C2b-O1}$  at  $175.36(17)^\circ$  and  $\text{Mo1-N1b/C2a-O1}$  at  $177.24(17)^\circ$ . This nearly linear arrangement is an indicator of the electronic structure of the nitrosyl ligand and the molybdenum center.<sup>[102]</sup> The angle close to  $180^\circ$  supports an assignment as a  $\text{Mo}(0)$  center coordinated to a positively charged  $\text{NO}^+$  ligand.<sup>[103]</sup> In contrast, binding of a neutral nitrosyl radical ligand to a molybdenum(I) center would be expected to result in a bent structure with a Mo-N-O angle of  $125^\circ$ - $155^\circ$ .<sup>[104]</sup> A search of the CCDC database revealed several other compounds with a  $\text{Mo}(\text{CO})_2(\text{NO})\text{N}_3$  coordination environment. Interestingly, all of these complexes are coordinated by aromatic nitrogen

ligands such as bis(pyrazolyl)methane, while compound **3-34** is the only one structurally characterized so far with an aliphatic ligand backbone. However, the prominent bond lengths as well as the Mo-N1-O1 angles are quite similar for all compounds. The Mo-C bond lengths range between 1.90(1) and 2.05(2) Å while the distance between the Mo center and the nitrosyl N atoms varies from 1.75(3) to 1.89(1) Å. The Mo-N bond lengths to the ligand backbone are between 2.165(3) and 2.27(1) Å. The Mo-N1-O1 angles of the reported compounds are all close to 180° and thus support the Mo(0)-NO<sup>+</sup> formulation for all compounds. However, the CCDC research showed that disorder of carbonyl and nitrosyl ligands is common. With exception of ZIJXIZ and YOFWAR, all structures listed show disordered CO and NO ligands in their coordination sphere (**Tab. 3.11**).

**Table 3.11:** Comparison of important bond lengths (Å) and nitrosyl angle (°) of **3-34** and other compounds with a Mo(CO)<sub>2</sub>(NO)N<sub>3</sub> core structure from the CCDC database.

CCDC code	Mo-C1	Mo-C2a/N1b	Mo-N1a/C2b	Mo-N2	Mo-N3	Mo-N4	Mo-N-O
<b>3-34</b>	1.963(2)	1.956(2)	1.880(2)	2.3026(16)	2.3105(16)	2.3016(16)	175.27(17) 177.24(17)
ZIJXIZ <sup>[105]</sup>	1.932(5)	1.912(4)	1.894(5)	2.219(4)	2.210(4)	2.209(4)	178.0(4)
HUTRUJ <sup>[106]</sup>	<sup>a</sup>	<sup>a</sup>	<sup>a</sup>	2.219(3)	2.213(3)	2.219(3)	<sup>a</sup>
JIQLIE <sup>[107]</sup>	<sup>a</sup>	<sup>a</sup>	<sup>a</sup>	2.219(8)	2.264(7)	2.219(6)	<sup>a</sup>
JIQLOK <sup>[107]</sup>	<sup>a</sup>	<sup>a</sup>	<sup>a</sup>	2.249(4)	2.211(5)	2.230(5)	<sup>a</sup>
LIFJIT <sup>[108]</sup>	<sup>a</sup>	1.912(4)	<sup>a</sup>	2.225(3)	2.225(3)	2.225(3)	<sup>a</sup>
QODCER <sup>[109]</sup>	2.05(2)	2.05(2)	1.81(3)	2.216(13)	2.216(13)	2.216(13)	<sup>b</sup>
	1.95(2)	1.95(2)	1.75(3)	2.185(12)	2.185(12)	2.185(12)	<sup>b</sup>
YAGPOL <sup>[110]</sup>	1.90(1)	1.93(1)	1.89(1)	2.27(1)	2.23(1)	2.26(1)	174(1)
YOFWAR <sup>[111]</sup>	2.005(4)	1.986(4)	1.789(3)	2.165(3)	2.260(3)	2.240(3)	178.81(22)

<sup>a</sup> X-ray data was not of sufficient quality to distinguish between nitrosyl and carbonyl ligands.

<sup>b</sup> values were not reported.

### 3.4.2 UV/Vis studies

A dilution series of  $[\text{Mo}(\text{CO})_2(\text{NO})(i\text{Pr}_3\text{tacn})]\text{PF}_6$  **3-34** in dimethylsulfoxide was prepared and the extinction coefficient determined at 350 nm as  $\epsilon_\lambda = 265 \pm 15 \text{ M}^{-1}\text{cm}^{-1}$ . In addition, there is a main band at 285 nm and two shoulders at 400 and 480 nm. The UV/Vis spectrum of **3-34** in dimethylsulfoxide was then monitored over 16 h in the dark in 30 min intervals. No changes in the position and intensity of the absorption maxima was observed, which demonstrates the extended stability of **3-34** in dimethylsulfoxide under exclusion of light (**Fig. 3.88**).

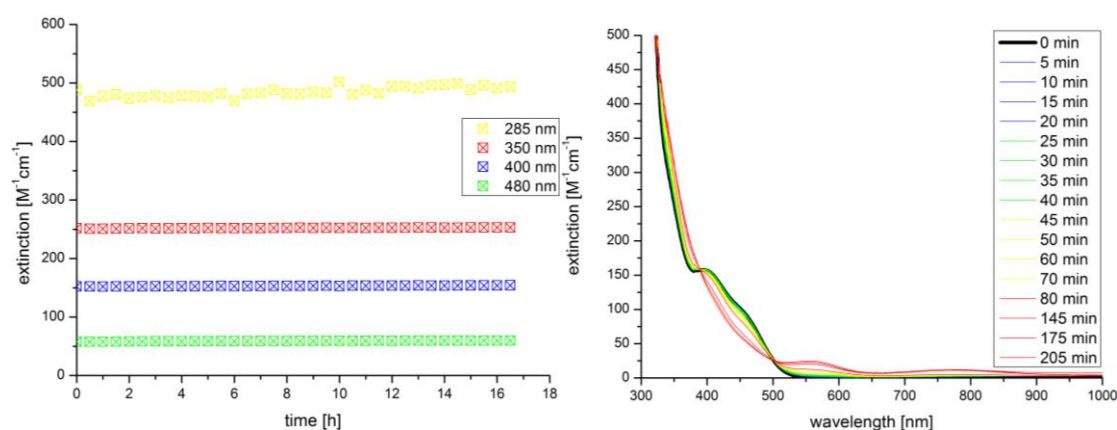


**Figure 3.88:** Changes in extinction at 285, 350, 400 and 480 nm of **3-34** in DMSO solution for 0-16 h in the dark (left) and upon illumination at 254 nm for 0-205 min (right). The initial spectrum before illumination is shown in black.

Upon illumination of a dimethylsulfoxide solution of **3-34** at 254 nm with an UV hand lamp, the intensity of the band at 400 nm as well as the shoulder at 480 nm slowly decreased to a plateau level over the first 80 min. In addition, after 25 min of illumination time, two new weak absorption bands at 580 nm and 780 nm slowly grew in which remained until the end of the experiment. The assignment of the absorption bands was done with the aid of TDDFT calculations and is described in the next section.

To study the potential CO release from  $[\text{Mo}(\text{CO})_2(\text{NO})(i\text{Pr}_3\text{tacn})]\text{PF}_6$  **3-34**, the standard myoglobin assay was used. Thus, myoglobin was dissolved in phosphate-buffered saline (PBS) and reduced by addition of an aqueous solution of sodium dithionite, followed by addition of a stock solution of metal complex **3-34** in dimethylsulfoxide. The final concentrations in the

cuvette were 60  $\mu\text{M}$  of myoglobin, 10 mM of dithionite and 10  $\mu\text{M}$  of **3-34**. UV/Vis spectra were recorded every 30 min for 16 h while the solution was kept in the dark and the absorption at 510, 540, 557 and 577 nm was then plotted versus incubation time. No changes in the absorbance occurred over the first 13 h. Only towards the end of the incubation period, a slight decrease of all four bands was observed, which could be indicative of decomposition and precipitation of the protein upon extended incubation (**Fig. 3.89**).

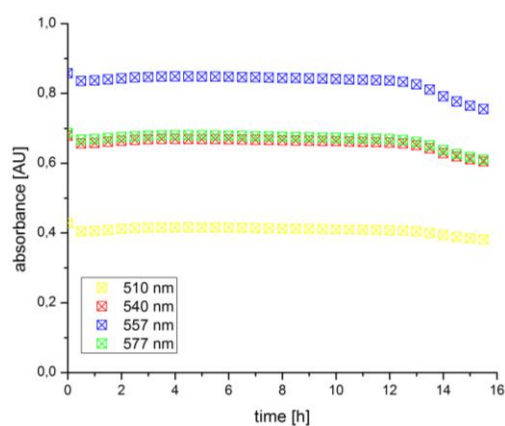


**Figure 3.89:** Changes in the absorbance at 510, 540, 557 and 577 nm of **3-34** (10  $\mu\text{M}$ ) in PBS in the presence of myoglobin (60  $\mu\text{M}$ ) and dithionite (10 mM) while kept in the dark.

Illumination of a freshly prepared solution of **3-34** in the presence of myoglobin at 254 nm for 60 min resulted in a decrease of the intensity at 510 nm, 540, 557 and 577 nm. An extended illumination for an additional 2 h led to further changes in the UV/Vis spectrum. Two shoulders were observed at 540 and 577 nm while the absorption maximum at 557 nm decreased in intensity. The shoulders at 540 and 577 nm are due to generation of MbCO. However, as myoglobin seems to decompose upon exposure to with high-energy UV light, the concentration of MbCO could not be determined accurately from this experiment (**Fig. 3.90**).

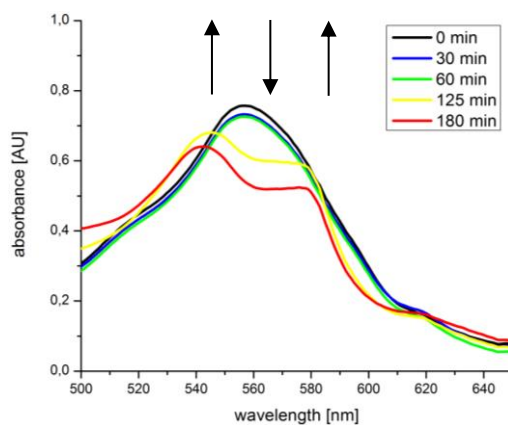


**Figure 3.90:** Changes in the UV/Vis spectrum of **3-34** (10 μM) in PBS in the presence of myoglobin (60 μM) and dithionite (10 mM) under illumination at 254 nm for 0-180 min.

The results of the myoglobin assay show that **3-34** is not suitable as a photoactivatable CORM due to the risk of tissue damage upon prolonged UV light exposure. The MbNO absorption bands at 421, 548 and 579 nm were not observed in the myoglobin assay. Thus, compound **3-34** does not act as an NO-releasing molecule under these conditions.<sup>[112]</sup>

### 3.4.3 Solution IR studies and DFT/TDDFT calculations

To detect possible intermediates in the photolytic release of CO and/or NO from **3-34** in solution, an IR experiment under UV illumination was carried out. Thus, a 16 mM stock solution of  $[\text{Mo}(\text{CO})_2(\text{NO})(i\text{Pr}_3\text{tacn})]\text{PF}_6$  **3-34** in acetonitrile was prepared which was transferred to a liquid IR cell with calcium fluoride windows under exclusion of light. The cell was illuminated at 254 nm and vibrational spectra were recorded every 2 min. Later in the experiment, the illumination intervals were increased to 5, 10 and then 30 min and distinct changes in the IR spectra were observed. The three original bands at 2022, 1931 and 1671  $\text{cm}^{-1}$  started to disappear almost immediately upon exposure to light while two new bands at 1894 and 1613  $\text{cm}^{-1}$  grew in. After 60 min of illumination time, the band at 1613  $\text{cm}^{-1}$  had further shifted to 1598  $\text{cm}^{-1}$  while the signal at 1894  $\text{cm}^{-1}$  decreased in intensity to nearly zero again. In addition, the very weak IR signal of dissolved CO at 2140  $\text{cm}^{-1}$  was detected in very low intensity (Figs. 3.91 and 3.92).

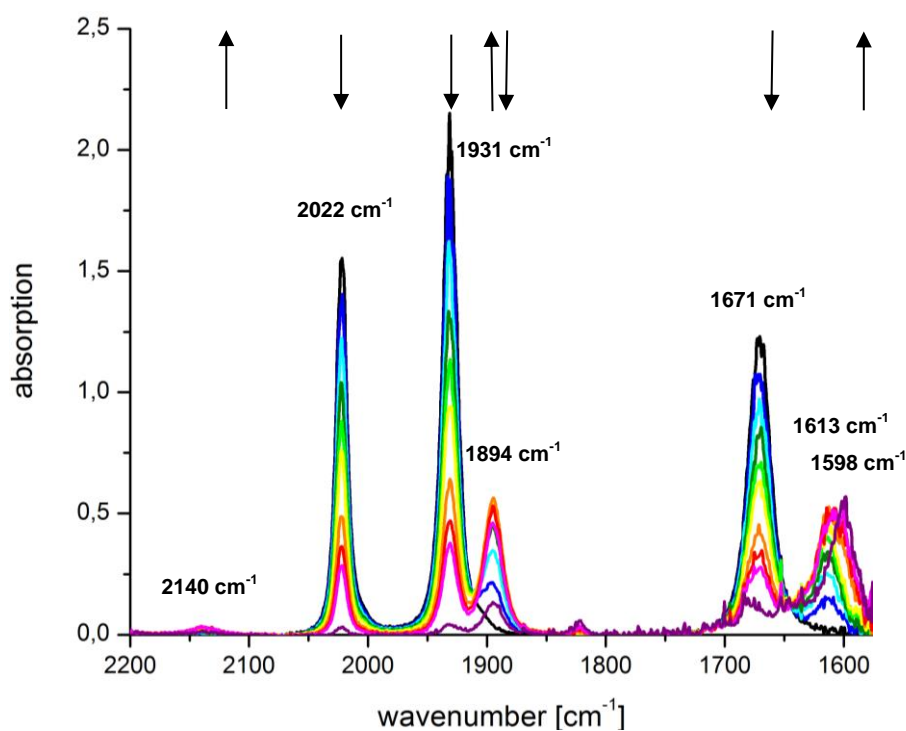
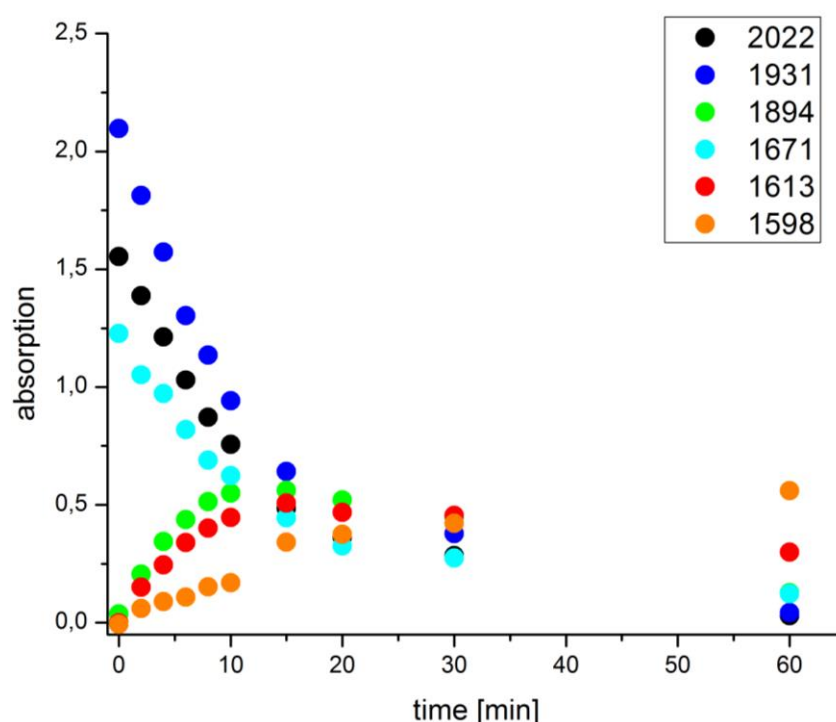


Figure 3.91: Changes in the IR spectrum of **3-34** (16 mM) in acetonitrile upon illumination at 254 nm for 0-60 min.

To assign these signals, potential intermediates resulting from the photolysis of **3-34** were constructed from the X-ray structure coordinates of the parent compound and their geometries optimized with DFT using the BP86 functional and a TZVP basis set with the COSMO solvation model in acetonitrile. The CO and NO stretching vibrations calculated at the same level of theory were then compared to the experimental values (**Fig. 3.93** and **Tab. 3.12**). The DFT model chemistry was verified by comparison of the calculated and experimental CO and NO stretching vibrations of **3-34**.



**Figure 3.92:** Appearance and disappearance of the different CO and NO stretching vibrations of **3-34** and its photoproducts with increasing illumination time upon photolysis at 254 nm.

With the use of a proper scaling factor of 1.018, the deviation between experimental and calculated values for the symmetric and antisymmetric CO stretching modes was smaller than  $33\text{ cm}^{-1}$  for  $[\text{Mo}(\text{CO})_2(\text{NO})(i\text{Pr}_3\text{tacn})]^+$  **3-34** (**A**), which is within the normal limits of this methodology. For all optimized structures, the calculated CO stretching modes are lower while the calculated NO stretch is higher than the experimental value.<sup>[29],[78]</sup> During the whole photolysis experiment, bands for the NO stretching vibration in the range of  $1600$  to  $1700\text{ cm}^{-1}$  were detected. Thus, nitrosyl-free intermediates **B**, **E**, and **F**

are unlikely to form and were excluded from analysis with only the nitrosyl compounds **C** and **D** further considered. The scaled calculated NO and CO stretching vibrations of **C** are at 1647 and 1886  $\text{cm}^{-1}$ , respectively. These values match quite well with the two signals of the first photolysis intermediate observed at 1613 and 1894  $\text{cm}^{-1}$  (**Fig 3.91**). In particular, the sign and magnitude of deviation compare very well with those found for **A**. For structure **D**, the calculated NO stretch appears at 1584  $\text{cm}^{-1}$ . This also matches well with the signal at 1598  $\text{cm}^{-1}$  observed upon extended photolysis. Thus, it can be concluded from the IR experiments and DFT calculations that photolysis of **3-34** leads to consecutive release of the two carbonyl ligands, which are replaced by acetonitrile solvent molecules while the NO remains bound under these conditions. This is also in line with the results of the myoglobin assay.

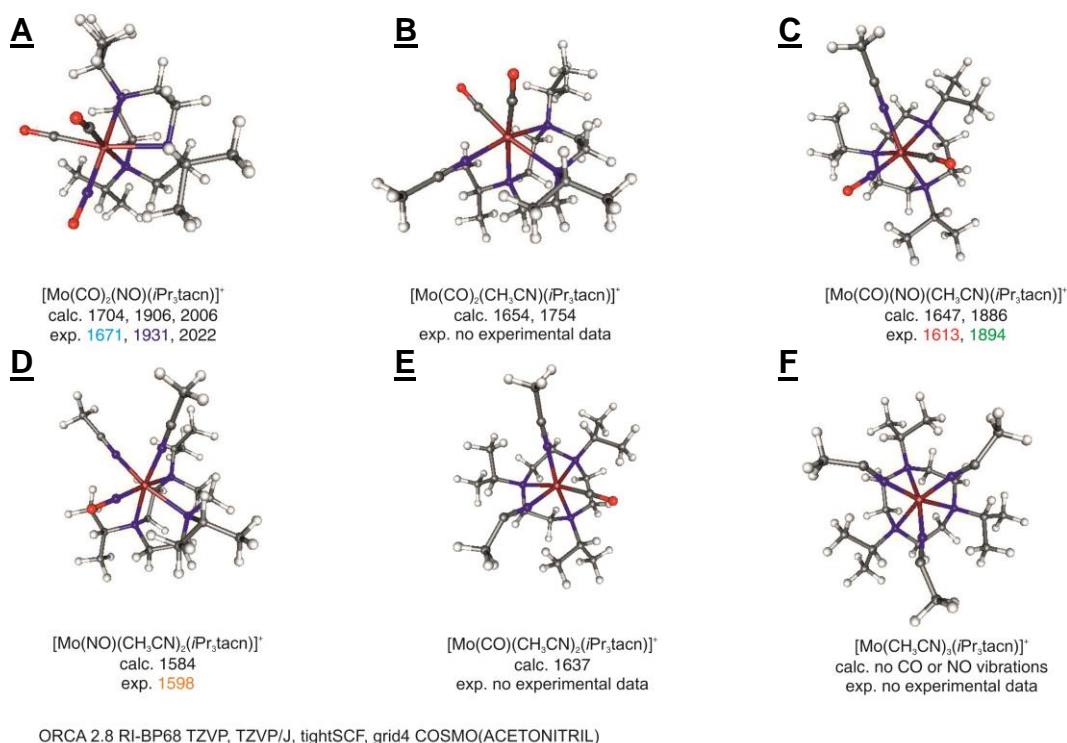


**Figure 3.93:** Structure of the cationic unit of parent compound **3-34** (**A**) and potential intermediates **B-F** resulting from CO and/or NO release optimized with DFT at the BP86 TZVP level of theory with comparison of calculated and experimental NO and CO stretching vibrations.



The first 45 singlet excited states of  $[\text{Mo}(\text{CO})_2(\text{NO})(i\text{Pr}_3\text{tacn})]^+$  **3-34** (**A**) as well as the ones of the relevant intermediates **C** and **D** were calculated with TDDFT using the B3LYP functional and the same basis set as for the geometry optimization and frequency calculations, including the acetonitrile solvent in the COSMO model (**Tab. 3.13**). For parent structure **A**, the main transitions are from the HOMO, HOMO-1 or HOMO-2 orbitals to the LUMO to LUMO+5 orbitals. With exception of state 8, which is of ILCT character from the nitrosyl to the carbonyl ligands, all others are MLCT transitions from the low-spin  $3d^6$  molybdenum(0) center to either the nitrosyl or both nitrosyl and carbonyl ligands.

**Table 3.12:** Comparison of experimental and calculated scaled CO and NO vibrational frequencies for compound **3-34** (**A**) and potential photolysis products **B-F**.

structure	$\tilde{\nu}_{\text{sym}}(\text{CO}) [\text{cm}^{-1}]$	$\tilde{\nu}_{\text{antisym}}(\text{CO}) [\text{cm}^{-1}]$	$\tilde{\nu}(\text{NO}) [\text{cm}^{-1}]$
<b>A</b> <sub>exp</sub>	2022	1931	1671
<b>A</b> <sub>calc</sub>	2006	1906	1704
<b>Diff.</b> <sub>calc-exp</sub>	-16	-25	+33
<b>B</b> <sub>exp</sub>	<i>a</i>	<i>a</i>	<i>b</i>
<b>B</b> <sub>calc</sub>	1754	1654	<i>b</i>
<b>Diff.</b> <sub>calc-exp</sub>	<i>a</i>	<i>a</i>	<i>b</i>
<b>C</b> <sub>exp</sub>	1894	<i>c</i>	1613
<b>C</b> <sub>calc</sub>	1886	<i>c</i>	1647
<b>Diff.</b> <sub>calc-exp</sub>	-8	<i>c</i>	34
<b>D</b> <sub>exp</sub>	<i>d</i>	<i>d</i>	1598
<b>D</b> <sub>calc</sub>	<i>d</i>	<i>d</i>	1584
<b>Diff.</b> <sub>calc-exp</sub>	<i>d</i>	<i>d</i>	-14
<b>E</b> <sub>exp</sub>	<i>a</i>	<i>e</i>	<i>e</i>
<b>E</b> <sub>calc</sub>	1637	<i>e</i>	<i>e</i>
<b>Diff.</b> <sub>calc-exp</sub>	<i>a</i>	<i>e</i>	<i>e</i>
<b>F</b> <sub>exp</sub>	<i>f</i>	<i>f</i>	<i>f</i>
<b>F</b> <sub>calc</sub>	<i>f</i>	<i>f</i>	<i>f</i>
<b>Diff.</b> <sub>calc-exp</sub>	<i>f</i>	<i>f</i>	<i>f</i>

*a* Not observed. *b* Dicarbonyl species, no NO vibrational mode. *c* Monocarbonyl-nitrosyl species, only one CO vibrational mode. *d* Mononitrosyl species, no CO vibrational modes. *e* Monocarbonyl species, only one CO vibrational mode, no NO vibrational mode. *f* no CO or NO vibrational modes.

**Table 3.13:** Energies (in nm), oscillator strength ( $f_{osc}$ ), main orbital contributions, and type of transitions involved in the most important singlet excitations for  $[\text{Mo}(\text{CO})_2(\text{NO})(i\text{Pr}_3\text{tacn})]^+$  **3-34** calculated with TDDFT

#	state <sup>a</sup>	$\lambda$ (nm)	$f_{osc}$	Main transitions <sup>b</sup>	Type of transitions	
<b>A</b>	1	441	0.0012	113 → 114 (99%)	MLCT (Mo → NO)	
	3	396	0.0020	112 → 114 (54%) 113 → 115 (30%)	MLCT (Mo → NO)	
	5	343	0.0012	111 → 115 (82%)	MLCT (Mo → NO, CO)	
	6	288	0.0172	113 → 117 (84%)	MLCT (Mo → NO, CO)	
	7	277	0.0172	113 → 116 (37%) 113 → 119 (28%)	MLCT (Mo → NO, CO)	
	8	271	0.0107	112 → 116 (68%)	ILCT (NO → CO)	
	<b>C</b>	1	512	0.0031	117 → 118 (99%)	MLCT (Mo → NO, CO)
		4	347	0.0021	116 → 118 (45%) 117 → 119 (51%)	MLCT (Mo → NO, CO)
5		329	0.0025	115 → 119 (48%) 117 → 121 (24%)	MLCT (Mo → NO, CO)	
6		315	0.0108	115 → 119 (42%) 117 → 121 (21%)	MLCT (Mo → NO, CO)	
8		274	0.0243	117 → 123 (20%)	MLCT (Mo → NO, CO, CH <sub>3</sub> CN)	
9		271	0.0155	116 → 120 (29%)	MLCT (Mo → NO, CO, CH <sub>3</sub> CN)	
10		263	0.0132	117 → 124 (25%)	MLCT (Mo → NO, CO, CH <sub>3</sub> CN)	
12		251	0.0478	115 → 120 (33%)	MLCT (Mo → NO, CO, CH <sub>3</sub> CN) ILCT (NO → CO, CH <sub>3</sub> CN)	
<b>D</b>		1	567	0.0019	121 → 122 (97%)	MLCT (Mo → NO, CH <sub>3</sub> CN)
		2	524	0.0019	121 → 123 (96%)	MLCT (Mo → NO, CH <sub>3</sub> CN)
	3	383	0.0012	121 → 124 (35%)	MLCT (Mo → NO, CH <sub>3</sub> CN)	
	5	365	0.0080	121 → 128 (25%) 121 → 132 (33%)	MLCT (Mo → NO, CH <sub>3</sub> CN)	
	6	350	0.0022	119 → 123 (46%) 120 → 122 (25%)	MLCT (Mo → NO, CH <sub>3</sub> CN)	
	7	346	0.0012	119 → 122 (21%) 120 → 123 (45%)	MLCT (Mo → NO, CH <sub>3</sub> CN)	
	8	330	0.0051	121 → 124 (32%) 121 → 126 (39%)	MLCT (Mo → CH <sub>3</sub> CN)	
	9	326	0.0148	121 → 128 (43%)	MLCT (Mo → CH <sub>3</sub> CN)	
	10	298	0.0101	121 → 131 (27%)	MLCT (Mo → CH <sub>3</sub> CN)	
	11	300	0.1800	121 → 125 (45%)	MLCT (Mo → CH <sub>3</sub> CN)	
	15	271	0.0664	120 → 124 (48%)	MLCT (Mo → CH <sub>3</sub> CN) ILCT (NO → CH <sub>3</sub> CN)	
	16	265	0.0960	119 → 124 (20%) 120 → 125 (26%)	MLCT (Mo → CH <sub>3</sub> CN) ILCT (NO → CH <sub>3</sub> CN)	

<sup>a</sup> Only transitions with an oscillator strength > 0.001 in the 250 to 600 nm range are reported.<sup>b</sup> Only contributions > 20% are listed.

In monocarbonyl-nitrosyl photolysis product **C**, the main transitions are from the HOMO, HOMO-1 or HOMO-2 into the LUMO to LUMO+6. In state 12, an ILCT contribution from the nitrosyl to the carbonyl and acetonitrile ligands is found while all other main transitions have MLCT character. In states 8, 9, 10, and 12, electron density is transferred from the Mo(0) center to the nitrosyl, carbonyl and acetonitrile ligands, while in states 1, 4, 5, and 6, charge is shifted from the metal center to the nitrosyl and carbonyl ligands exclusively. In mononitrosyl complex **D**, the main transitions are also from HOMO, HOMO-1 or HOMO-2 orbitals to LUMO to LUMO+10. Only state 16 has an ILCT contribution from the nitrosyl to the acetonitrile ligands. All other main transitions are exclusively of MLCT character. The charge transfer in states 1 to 7 occurs from the molybdenum to the nitrosyl and acetonitrile ligands, respectively, while in states 8 to 11 as well as 15, the electron density is transferred from the metal center to the acetonitrile ligands.

The absorption bands obtained from the TDDFT calculations match very well with the experimental data of the photolysis followed by UV/Vis spectroscopy, which was shown in the last section (**Fig. 3.88**). In the experimental spectrum, the strong main absorption band of the parent compound **3-34** appears in a range of 250 - 350 nm while two additional shoulders are found at 400 and 480 nm. For the optimized structure **A**, intense absorption bands are calculated at 271, 277, 288, and 343 nm. Also, significant absorption bands at 396 and 441 nm are found. During the photolysis experiments, the shoulders at 400 and 480 nm decrease in intensity while a new absorption band grows in at 520 nm. This change in the absorption spectrum is also calculated for the optimized structure **C** which shows no significant absorption bands between 400-500 nm, but a new weak band at 512 nm. Upon extended illumination, the absorption band at 520 nm broadens to higher wavelengths and reaches a maximum of 580 nm. This is also found in the calculated UV/Vis spectrum of the postulated photoproduct **D** which shows absorption bands at 524 and 567 nm.

In summary, both, the calculated IR vibrations and UV/Vis absorption bands support the consecutive light-triggered release of the two carbonyl ligands while the NO remains tightly bound.

The IR experiments show that compound 3-34 is not suitable as a dual-mode CO/NO releaser since the nitrosyl ligand remains tightly bound to the metal center even upon prolonged exposure to UV light. Furthermore, use as a PhotoCORM will also be not advised since the high-energy 254 nm UV light required for photolytic CO release will likely be harmful to cells.

## 4 Conclusion

### 4.1 English version

Since its discovery as a small signaling molecule in the human body, researchers have tried to utilize the beneficial cytoprotective properties of carbon monoxide in therapeutic applications. Initial work focused on the controlled direct application of CO gas. However, to circumvent the disadvantages of this method such as requirement for special equipment, hospitalization of the patient and the risk of overdosing, metal-carbonyl complexes were developed as *CO-releasing molecules* (CORMs) which are able to deliver CO in a tissue-specific manner. However, upon the release of CO from the metal coordination sphere, complex fragments termed *inactivated CORMs* (iCORMs) with free coordination sites remain which can undergo nonspecific follow-up reactions under physiological conditions.

Thus, the first aim of the present thesis was the coordination of tetradentate ligands such as tris(2-pyridylmethyl)amine (tpa), bis(2-pyridylmethyl)(2-quinolylmethyl)amine (bpqa), bis(2-quinolylmethyl)(2-pyridylmethyl)amine (bqpa) and tris(2-quinolylmethyl)amine (tmqa) in a tridentate facial manner to a *fac*-Mn(CO)<sub>3</sub> moiety previously established as a *photoactivatable CO-releasing molecule* (PhotoCORM). The desired coordination of the pedant donor group upon photolytic CO release at 365 nm was demonstrated by UV/Vis-, IR- und <sup>1</sup>H NMR experiments and verified by DFT calculations. All complexes of the series showed long-term dark stability in phosphate-buffered saline (PBS), but released between two and three equivalents of carbon monoxide with half-lives of around 5-10 minutes upon illumination at 365 nm. Although the photolytic properties of the complexes were quite similar besides the differences in type of heteroaromatic ligands, the determination of the log*P* values showed an increase of lipophilicity with the number of quinoline groups, which might enable tissue-specific uptake. A significant cellular manganese uptake as well as the binding of CO released

upon photolysis to the cytochrome *c* oxidases in *E. coli* cells was demonstrated for  $[\text{Mn}(\text{CO})_3(\text{tpa})]^+$ . Furthermore, this complex exhibited photoinduced bactericidal activity when the cells were grown in succinate-containing medium and thus unable to change their metabolism to mixed acid fermentation.

In the second part of the project, the hexadentate ligand 1,4,7-tris(2-pyridylmethyl)-1,4,7-triazacyclononane ( $\text{py}_3\text{tacn}$ ) was coordinated to a facial  $\text{Mn}(\text{CO})_3$  moiety. The resulting  $[\text{Mn}(\text{CO})_3(\text{py}_3\text{tacn-}\kappa^3\text{N})]^+$  complex has one pedant donor group per labile carbonyl ligand and thus is a significant improvement over the 1<sup>st</sup> generation tpa-complexes. The metal-codigand *inactivated CORM* (iCORM) fragment expected to be generated upon complete photolytic CO release,  $[\text{Mn}(\text{py}_3\text{tacn-}\kappa^6\text{N})]^{2+}$ , was synthesized independently and will serve as a well-defined negative control in upcoming biological tests. The corresponding CORM has long-term dark stability in pure dimethylsulfoxide or phosphate-buffered myoglobin solution, with three equivalents of CO released with a half-life of 22 minutes upon illumination at 412 nm. The photolysis was also followed by IR spectroscopy and the intermediates, in line with a stepwise release of carbon monoxide, and occupation of vacated sites by the pedant pyridine group were verified by DFT calculations.

Due to possible tissue damage by energy-rich light and the inverse correlation of tissue penetration depth and illumination wavelength, the absorption maxima of PhotoCORMs should ideally be in the phototherapeutic window between 600 and 1200 nm. Thus, in the third part of this work, a series of heterobinuclear  $\text{Mn}(\text{CO})_3/\text{Ru}(\text{bpy})_2$  PhotoCORMs was prepared to shift the absorption of these compounds into the red region of the UV/Vis spectrum. For the synthesis of such Mn(I)/Ru(II) complexes, the bridging ligands 2,3-di(2-pyridyl)quinoxaline (dpx) and 3-(pyridin-2-yl)-1,2,4-triazine[5,6-f]-1,10-phenanthroline (pytp) were prepared and the two binding pockets subsequently filled with a  $\text{Ru}(\text{bpy})_2$  and a *fac*- $\text{Mn}(\text{CO})_3$  moiety. The resulting two heterobinuclear metal complexes  $[\text{Ru}(\text{bpy})_2(\text{dpx})\text{MnBr}(\text{CO})_3]^{2+}$  and

$[\text{Ru}(\text{bpy})_2(\text{pytp})\text{MnBr}(\text{CO})_3]^{2+}$  as well as  $[\text{Ru}(\text{etx})(\text{tbx})\text{MnBr}(\text{CO})_3]^{2+}$  with  $\text{etx}$  = ethyl(2,2':6',2''-terpyridine)-4'-carboxylate and  $\text{tbx}$  = *N*-((2,2':6',2''-terpyridin)-4'-yl)2,2'-bipyridine-5-carboxamide which was prepared by a metal precursor provided by the group of Prof. Dr. Katja Heinze showed a significant shift of the main absorption bands to higher wavelengths as well as two times higher extinction coefficients than the analogous mononuclear Mn(I) compounds. However, both the Mn(I)/Ru(II) and Mn(I) complexes had a reduced stability in phosphate-buffered myoglobin solution even in the absence of light. The efficiency of the CO-release from  $[\text{Ru}(\text{etx})(\text{tbx})\text{MnBr}(\text{CO})_3]^{2+}$  and  $[\text{Ru}(\text{bpy})_2(\text{dpx})\text{MnBr}(\text{CO})_3]^{2+}$  could be controlled by proper choice of the excitation wavelength. A change from 468 to 525 nm or even 660 nm led to a decrease of the number of CO equivalents released from two to one and an elongation of the half-lives.

Finally, since nitric oxide also serves as a small messenger molecule in the human body with its signaling pathways interacting with those of CO, a mixed-ligand CO/NO metal complex was sought.  $[\text{Mo}(\text{CO})_2(\text{NO})(i\text{Pr}_3\text{tacn})]^+$  with *iPr*<sub>3</sub>tacn = 1,4,7-triisopropyl-1,4,7-triazacyclonane was selected from the literature and its molecular structure determined by single crystal diffraction, demonstrating the presence of an NO<sup>+</sup> ligand in the coordination sphere as indicated by a MO-N-O angle close to 180°. Photolysis of  $[\text{Mo}(\text{CO})_2(\text{NO})(i\text{Pr}_3\text{tacn})]^+$  required high-energy UV light, which prevented a quantification of the CO release due to photolytic decomposition of the myoglobin. However, solution IR experiments showed that the complex lost the two carbon monoxide ligands upon illumination at 254 nm while the NO remained tightly bound to the metal. The structures observed of the intermediates were also verified by DFT calculations.

In conclusion, in this project, four different classes of novel transition metal-based *photoactivatable CO-releasing molecules* (PhotoCORMs) were prepared and studied. The first group incorporated one additional free donor group per LMn(CO)<sub>3</sub> moiety but varied in the number of coordinated pyridyl and quinolinyl groups which allows the control of the lipophilicity of these

compounds. As an extension of this concept, the second series incorporated one free donor group per labile carbonyl ligand which gives rise to well-defined photolysis products that can be independently prepared and assayed. The third class was based on a Ru(II) photosensitizer unit connected to a MnBr(CO)<sub>3</sub> PhotoCORM moiety. This shifts the absorption maximum from 500 nm to about 585 nm in [Ru(bpy)<sub>2</sub>(dpx)MnBr(CO)<sub>3</sub>]<sup>2+</sup>. Finally, a first mixed-ligand CO/NO carrier molecule was evaluated for its photolytic behavior. However, while the carbonyl ligands were photolabile at low excitation wavelengths, release of the NO ligand was not observed under the conditions studied.

In a next step, detailed studies on the bioactivity of the different classes of PhotoCORMs need to be carried out with partner groups from biochemistry to fully explore their biomedical potential.



## 4.2 Deutsche Version

Seit der Entdeckung als von Kohlenstoffmonoxid *small signaling molecule* im menschlichen Körper stehen seine zellschützenden Eigenschaften im Interesse der Forschung, die für therapeutische Anwendungen nutzbar gemacht werden könnten. Anfangs lag hierbei der Fokus auf einer kontrollierten Verabreichung von gasförmigem Kohlenstoffmonoxid. Um die Nachteile dieser Methode, wie beispielsweise spezielle klinische Ausrüstung sowie das Risiko einer Überdosierung zu umgehen wurden Metallkomplexe mit CO-Liganden als *CO-releasing molecules* (CORMs) entwickelt, welche in der Lage sind Kohlenstoffmonoxid gewebespezifisch im Körper abzugeben. Durch die Freisetzung von CO aus der Koordinationssphäre eines Metallzentrums entstehen jedoch auch Komplexfragmente, sogenannte *inactivated CORMs* (iCORMs), welche unter physiologischen Bedingungen unbekannte Folgereaktionen eingehen können. Deshalb bestand das erste Ziel der vorliegenden Doktorarbeit darin, die tetradentaten Liganden Tris(2-pyridylmethyl)amin (tpa), Bis(2-pyridylmethyl)(2-quinolylmethyl)amin (bpqa), Bis(2-quinolyl-methyl)(2-pyridylmethyl)amin (bqpa) und Tris(2-quinolylmethyl)amin (tmqa) an eine faciale  $\text{Mn}(\text{CO})_3$  Einheit zu koordinieren, deren Komplexe dann als *photoactivatable CO-releasing molecules* (PhotoCORM) fungieren sollten. Die Koordination der zusätzlichen Donorgruppe im Zuge der photolytischen CO Freisetzung wurde am Beispiel von  $[\text{Mn}(\text{CO})_3(\text{tpa})]^+$  durch UV/Vis-, IR- und  $^1\text{H}$  NMR-Experimente gezeigt und durch DFT-Rechnungen untermauert. Alle Verbindungen der Serie zeigten in Phosphat-Puffer eine hohe Stabilität im Dunkeln. Durch Photoaktivierung bei einer Wellenlänge von 365 nm konnten aus den Komplexen zwei bis drei Äquivalente CO mit einer Halbwertszeit um 10 Minuten freigesetzt werden. Obwohl die photolytischen Eigenschaften der Komplexe sehr ähnlich waren, steigt die Lipophilie angegeben durch den  $\log P$ -Wert mit steigender Anzahl der im Komplex enthaltenen Quinolin-Gruppen an, was die Gewebeaufnahme erleichtern sollte. Für  $[\text{Mn}(\text{CO})_3(\text{tpa})]^+$  konnte ein deutlicher Anstieg der intrazellulären Mangankonzentration sowie die

Bindung von freigesetztem CO an die Cytochrom *c*-Oxidase in *E. coli* beobachtet werden. Auch zeigte diese Verbindung eine photoinduzierte Toxizität gegenüber diesen Bakterienkulturen, solange diese in Succinat-haltigem Nährmedium gezüchtet wurden und somit nicht in der Lage waren ihren Stoffwechsel auf die „mixed acid fermentation“ umzustellen.

Im zweiten Teil der Arbeit sollte dann der hexadentate Ligand 1,4,7-Tris(2-pyridylmethyl)-1,4,7-triazacyclonane (py<sub>3</sub>tacn) an eine faciale Mn(CO)<sub>3</sub>-Einheit koordiniert werden. Der resultierende [Mn(CO)<sub>3</sub>(py<sub>3</sub>tacn-κ<sup>3</sup>N)]<sup>+</sup> Komplex verfügt über eine freie Donorgruppe für jeden Kohlenstoffmonoxid-Liganden. Das Metall-Coligand-Fragment, [Mn(py<sub>3</sub>tacn-κ<sup>6</sup>N)]<sup>2+</sup>, welches als photolytisches Endprodukt erwartet wird, wurde über einen separaten Syntheseweg hergestellt und wird als Negativkontrolle in kommenden biologischen Testreihen eingesetzt werden. Untersuchungen zur CO-Freisetzung aus [Mn(CO)<sub>3</sub>(py<sub>3</sub>tacn-κ<sup>3</sup>N)]<sup>+</sup> zeigten, dass die Verbindung sowohl in Dimethylsulfoxid als auch in gepuffertem Myoglobin im Dunkeln lange Zeit stabil ist. Bei Belichtung mit 412 nm können aus dem Komplex etwa drei Äquivalente CO mit einer Halbwertszeit von 22 Minuten freigesetzt werden. Der Photolyseprozess wurde auch mittels IR-Spektroskopie verfolgt und die Zwischenstufen, welche Hinweis auf eine stufenweise Abgabe der CO-Liganden wie auch die Besetzung der freien Koordinationsstellen durch die freien Pyridingruppen gaben, durch DFT Rechnungen belegt.

Aufgrund der Möglichkeit von Gewebeschädigungen durch kurzwelliges UV-Licht und den inversen Zusammenhang von Gewebeeindringtiefe und Belichtungswellenlänge, sollte das Absorptionsmaximum eines PhotoCORMs idealerweise im phototherapeutischen Fenster zwischen 600 und 1200 nm liegen. Deshalb wurden im dritten Teil dieser Arbeit heterobinukleare Mn(CO)<sub>3</sub>/Ru(bpy)<sub>2</sub> PhotoCORMs hergestellt, um die Absorption der Verbindungen in den roten Bereich des sichtbaren Spektrums zu verschieben. Für die Synthese der Mn(I)/Ru(II) PhotoCORMs wurden 2,3-Di(2-pyridyl)quinoxalin (dpx) und 3-(pyridin-2-yl)-1,2,4-triazin[5,6-*f*]-1,10-phenanthrolin (pytp) als verbrückende Liganden verwendet, wobei zunächst

eine Bindungstasche mit Ru(bpy)<sub>2</sub> und anschließend die zweite mit Mn(CO)<sub>3</sub> gefüllt wurden. Die zwei resultierenden heterobinukleare Metallkomplexe [Ru(bpy)<sub>2</sub>(dpx)MnBr(CO)<sub>3</sub>]<sup>2+</sup> und [Ru(bpy)<sub>2</sub>(pytp)MnBr(CO)<sub>3</sub>]<sup>2+</sup> sowie [Ru(etx)(tbx)MnBr(CO)<sub>3</sub>]<sup>2+</sup>, mit etx = Ethyl(2,2':6',2''-terpyridin)-4'-carboxylat und tbx = N-((2,2':6',2''-Terpyridin)-4'-yl)2,2'-bipyridin-5-carboxamid, welcher aus einer Ruthenium-Vorstufe aus der Arbeitsgruppe von Prof. Dr. Katja Heinze synthetisiert wurde zeigten eine deutliche Verschiebung der intensivsten Absorptionsbande zu höheren Wellenlängen und eine Verdopplung der Extinktionskoeffizienten im Vergleich zu den analogen mononuklearen Mn(I)-Verbindungen. Jedoch konnte sowohl für die Mn(I)/Ru(II)- als auch für die Mn(I)-Komplexe selbst unter Lichtausschluss eine Zersetzung in gepuffertem Myoglobin festgestellt werden. Die Effizienz der CO-Freisetzung aus [Ru(etx)(tbx)MnBr(CO)<sub>3</sub>]<sup>2+</sup> und [Ru(bpy)<sub>2</sub>(dpx)MnBr(CO)<sub>3</sub>]<sup>2+</sup> lässt sich durch die Wahl einer geeigneten Anregungswellenlänge kontrollieren. Durch den Wechsel von 468 zu 525 nm oder sogar 660 nm wurde die Anzahl der freigesetzten CO-Äquivalente von zwei auf eins reduziert. Auch konnte eine Verlängerung der Halbwertszeiten festgestellt werden.

Da Stickstoffmonoxid ebenfalls als *small messenger molecule* im menschlichen Körper bekannt ist, dessen Signalwege mit denen von CO interagieren, wurde ein gemischter CO/NO-Metallkomplex gesucht. [Mo(CO)<sub>2</sub>(NO)(iPr<sub>3</sub>tacn)]<sup>+</sup> mit iPr<sub>3</sub>tacn = 1,4,7-triisopropyl-1,4,7-triazacyclonon wurde aus der Literatur ausgewählt und synthetisiert. Die molekulare Struktur der Verbindung konnte erstmals durch Röntgenbeugung am Einkristall aufgeklärt werden und enthält mit einem Mo-N-O Winkel von 180° das Stickstoffmonoxids als NO<sup>+</sup>-Liganden. Das energiereiche UV-Licht, welches zur Photolyse von [Mo(CO)<sub>2</sub>(NO)(iPr<sub>3</sub>tacn)]<sup>+</sup> benötigt wurde, führte unter den Bedingungen des Myoglobin-Assay jedoch zu einer Zersetzung des Proteins. Durch Photolyse-Experimente in Acetonitril, welche mit IR-Spektroskopie verfolgt wurden, konnte jedoch die Freisetzung der beiden CO-Liganden durch Belichtung mit 254 nm beobachtet werden während der Nitrosyl-Ligand an das

Metallzentrum gebunden blieb. Die gefundenen Photolyseprodukte konnten auch mittels DFT-Rechnungen identifiziert werden.

Zusammengefasst wurden im Rahmen dieser Doktorarbeit vier verschiedene Klassen von Übergangsmetallbasierten *photoactivatable CO-releasing molecules* (PhotoCORMs) hergestellt und untersucht. Die erste Gruppe von Molekülen verfügt über eine zusätzliche freie Donorgruppe pro *fac*-Mn(CO)<sub>3</sub>-Einheit, variiert aber in der Anzahl der koordinierten Pyridyl- und Quinolinyl-Einheiten, wodurch die Lipophilie der Verbindungen eingestellt werden kann. Die Verbindungen der zweiten Generation beinhalten eine freie Donorgruppe pro labilen Carbonyl-Liganden. Dies führt zu wohldefinierten photolytischen Endprodukten, welche auch separat hergestellt und getestet werden können. Die dritte Klasse basiert auf Ru(II)-Photosensitizern, die an eine MnBr(CO)<sub>3</sub>-PhotoCORM-Einheit angebunden wurden. Dies hat im Fall von  $[\text{Ru}(\text{bpy})_2(\text{dpx})\text{MnBr}(\text{CO})_3]^{2+}$  eine Verschiebung des Absorptionsmaximums von 500 nm zu 585 nm zur Folge. Schließlich konnte ein gemischtes CO/NO-Trägermolekül erstmals auf seine photolytischen Eigenschaften untersucht werden. Während beide CO-Liganden in  $[\text{Mo}(\text{CO})_2(\text{NO})(i\text{Pr}_3\text{tacn})]^+$  labil waren, konnte eine Freisetzung des NO-Liganden unter den vorliegenden Bedingungen nicht beobachtet werden. In der Weiterführung dieses Projekts sollten detaillierte Studien zur biologischen Aktivität der verschiedenen PhotoCORMs durchgeführt werden um das volle biomedizinische Potential dieser Verbindungen zu ermitteln.

## 5 Experimental section

### 5.1 General procedures and instrumentation

#### General

All reactions were carried out in oven-dried Schlenk glassware under an atmosphere of pure argon or pure dinitrogen when necessary. Light was excluded by use of brown glassware with a < 450 nm cut-off or wrapping of the apparatus in aluminium foil for all syntheses. Dichloromethane, diethyl ether, *N,N*-dimethylformamide and *n*-hexane were dried over 4 Å molecular sieves while acetonitrile, ethanol, and methanol were dried over 3 Å molecular sieves and degassed by applying the freeze-pump-thaw method with at least two cycles of applied vacuum. Otherwise, chemicals were used as commercially received. The ligand precursors 1,10-phenanthroline-5,6-dione (phenox), pyridine-2-carbohydrazonamide as well as the ligand 2,3-di(pyridin-2-yl)quinoxaline (dpx) were available from the Master thesis project of Christoph Schneider.<sup>[113]</sup> The [Ru(etx)(tbx)](PF<sub>6</sub>)<sub>2</sub> complex was provided the group of Prof. Dr. Katja Heinze from the Institute of Inorganic and Analytical Chemistry, Johannes-Gutenberg-Universität Mainz. All other chemicals were obtained from commercial sources and used without further purification.

### **NMR spectroscopy**

NMR spectra were recorded on Bruker Avance 200 ( $^1\text{H}$  at 199.93 MHz,  $^{13}\text{C}$  at 50.27 MHz,  $^{19}\text{F}$  at 188.12 MHz and  $^{31}\text{P}$  at 80.93 MHz), DRX 300 ( $^1\text{H}$  at 300.13 MHz and  $^{13}\text{C}$  at 75.47 MHz) or Avance 500 ( $^1\text{H}$  at 500.13 MHz and  $^{13}\text{C}$  at 125.75 MHz) spectrometers. Chemical shifts are indicated downfield relative to tetramethylsilane (TMS) and are referenced relative to the residual signal of the solvent.<sup>[114]</sup> The multiplicity of the signals is given as singlet (s), doublet (d), triplet (t), quartet (q), septet (sept) or multiplet (m). Coupling constants  $J$  are given in Hz. Spectra were analyzed with the TopSpin V 3.2 software.

### **UV/Vis spectroscopy**

Absorption spectra were recorded with an Agilent 8453 UV/Vis diode array spectrophotometer in quartz cuvettes ( $d = 1$  cm).

### **CHN analysis**

The elemental composition of most of the samples was determined with a vario MICRO cube analyzer from Elementar Analysensysteme GmbH, Hanau. The elemental composition of halogenated samples was determined with an EA 3000 Elemental Analyser from HEKAtech GmbH, Wegberg.

### **IR spectroscopy**

IR spectra of pure solid samples were recorded with a Nicolet 380 FT-IR spectrometer equipped with a SMART iTR ATR unit. The spectra were recorded in the range from 4000 to 750  $\text{cm}^{-1}$  with 32 scans per sample. Photolysis experiments were carried out with a Jasco FT/IR-4100 spectrometer using a flow-cell holder equipped with calcium fluoride windows ( $d = 4$  mm) and a Teflon spacer ( $d = 0.5$  mm). The spectra were recorded in the range from 4000 to 600  $\text{cm}^{-1}$  with 12 scans per measurement. Peak intensities are marked as very strong (vs), strong (s), medium (m), weak (w), or broad (br).

### Single crystal X-ray structure analysis

The X-ray diffraction data for  $[\text{Mn}(\text{CO})_3(\text{tpa})]\text{Br}$  **3-5** was collected on a Bruker X8-APEX II diffractometer with a CCD area detector and multi-layer mirror-monochromated  $\text{MoK}\alpha$  radiation by Thomas Kramer from the group of Prof. Dr. Holger Braunschweig. All other data were collected by Christoph Nagel on an Bruker FR591 Apex II diffractometer with a rotating anode, CCD area detector, and multi-layer mirror-monochromated  $\text{MoK}\alpha$  radiation. The structures were solved using direct methods, refined with the OLEX2<sup>[115]</sup> or SHELX<sup>[116]</sup> software packages and expanded using Fourier techniques.<sup>[115-116]</sup> For each structure, all non-hydrogen atoms were refined anisotropically, all hydrogen atoms were assigned to idealized geometric positions, and the latter also included in the structure factors calculations. The disorder of one CO and the NO group in  $[\text{Mo}(\text{CO})_2(\text{NO})(i\text{Pr}_3\text{tacn})]\text{PF}_6$  was treated with the EXYZ command of the OLEX2<sup>[115]</sup> software package which places carbon and nitrogen atoms in the same position at 50:50 occupancy.

### ESI mass spectrometry

All mass spectra were recorded on a Bruker micrOTOF ESI mass spectrometer by Prof. Dr. Ulrich Schatzschneider. The solvent flow rate was  $240 \mu\text{L h}^{-1}$  with a nebulizer pressure of 0.3 bar and a dry gas flow rate of  $4 \text{ L min}^{-1}$  at a temperature of  $180 \text{ }^\circ\text{C}$ .

### Density functional theory calculations

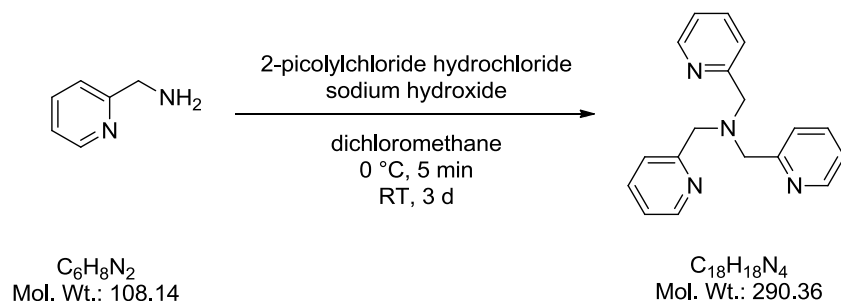
All DFT calculations were carried out by Prof. Dr. Ulrich Schatzschneider on the Linux cluster of the Leibniz-Rechenzentrum (LRZ) in Munich with ORCA version 2.8,<sup>[117]</sup> using the BP86 functional with the resolution-of-the-identity (RI) approximation, a def2-TZVP/def2-TZVP/J basis set,<sup>[118]</sup> the tightscf and grid4 options, and the COSMO solvation model with dimethylsulfoxide or acetonitrile as the solvent for geometry optimizations. Graphics were created with gOpenmol.<sup>[119]</sup>

## 5.2 Synthetic procedures

### 5.2.1 Synthesis of the ligands

#### 5.2.1.1 Synthesis of tris(2-pyridylmethyl)amine (tpa)<sup>[120]</sup>

USC-CN001

**3-1**

2-Pyridylmethylchloride hydrochloride (9.83 g, 60 mmol) was dissolved in deionized water (25 mL) and cooled with an ice bath. After addition of 5.3 M sodium hydroxide (11 mL), the reaction mixture was stirred for 5 min. Then, a solution of 2-pyridylmethanamine (3.09 mL, 3.24 g, 30 mmol) in dichloromethane (50 mL) was added and the ice bath was removed. After 3 d of stirring, additional 5.3 M sodium hydroxide (11 mL) was added at once. The reaction mixture was then immediately washed with 4.4 M sodium hydroxide (25 mL) and the organic phase separated and dried over magnesium sulfate. After removal of the solvent under vacuum, the brown residue was extracted with hot diethylether (75 mL) and allowed to crystallize overnight at 8 °C. The product was obtained as white needles after recrystallization from diethylether (75 mL).

**Yield:** 2.28 g (5.72 mmol, 26%)

**IR:** 3015 (m), 2816 (m), 1588 (vs), 1570 (s), 1474 (vs), 1438 (vs)  $\text{cm}^{-1}$ .

**<sup>1</sup>H NMR** ( $\text{CDCl}_3$ , 199.93 MHz):  $\delta$  = 3.93 (s, 6H,  $\text{CH}_2$ ), 7.12-7.19 (m, 3H,  $H_4$ ), 7.54-7.72 (m, 6H,  $H_3+H_5$ ), 8.54 (d,  $^3J$  = 4.8 Hz, 3H,  $H_6$ ) ppm.

**<sup>13</sup>C{<sup>1</sup>H} NMR** ( $\text{CDCl}_3$ , 50.27 MHz):  $\delta$  = 60.0 ( $\text{CH}_3$ ), 122.0 (C5), 123.0 (C3), 136.4 (C4), 149.1 (C6), 159.5 (C2) ppm.

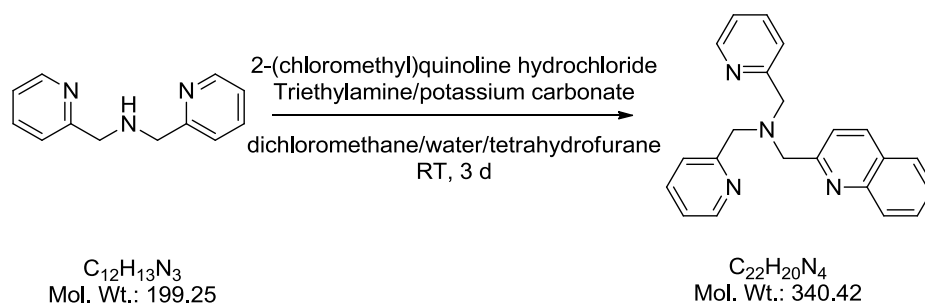


**Elemental analysis (%):**

calculated (C <sub>18</sub> H <sub>18</sub> N <sub>4</sub> ):	C: 74.46	H: 6.25	N: 19.30
found:	C: 74.58	H: 6.21	N: 19.50

5.2.1.2 Synthesis of bis(2-pyridylmethyl)(2-quinolylmethyl)amine (bpqa)<sup>[84]</sup>

USC-CN068

3-2

To a solution of 2-(chloromethyl)quinoline hydrochloride (0.22 g, 1.00 mmol) in deionized water (1 mL) was added a saturated solution of potassium carbonate (152 mg, 1.10 mmol) in water (1 mL). To this suspension, dichloromethane (2 mL) was added to obtain a clear solution. The aqueous phase was discarded and tetrahydrofuran (10 mL), triethylamine (0.2 mL) and bis(2-pyridylmethyl)amine (200 mg, 1.00 mmol) were added and stirred for 3 d at room temperature. The solvent was then removed under vacuum and the brown residue purified by column chromatography (1x10 cm) using alumina (neutral aluminium oxide 90, standardized, Brockmann grade 1, Merck) as the stationary phase and ethyl acetate as the eluent. The product was obtained as a white to yellowish solid material.

**Yield:** 85.0 mg (0.25 mmol, 25%).

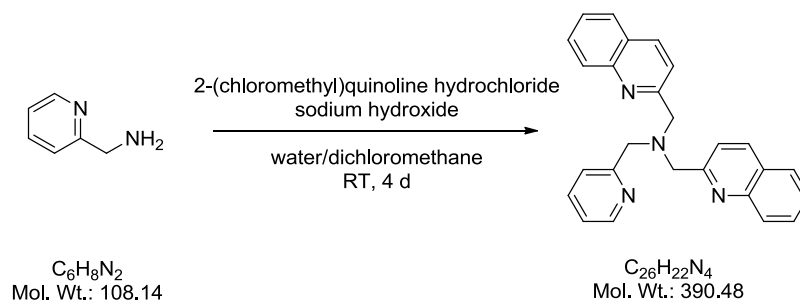
**IR:** 3014 (w), 2978 (w), 2813 (m), 1590 (vs), 1475 (s), 1435 (s), 1121 (m), 824 (s), 762 (vs)  $\text{cm}^{-1}$ .

**<sup>1</sup>H NMR** ( $\text{CDCl}_3$ , 199.93 MHz):  $\delta$  = 3.92 (s, 4H,  $\text{CH}_2$ ), 4.04 (s, 2H,  $\text{CH}_2$ ), 7.08-7.18 (m, 2H,  $\text{H}_4(\text{py})$ ), 7.44-7.82 (m, 8H,  $\text{H}_3/5(\text{py})+\text{H}_3/8/9/10(\text{qui})$ ), 8.04 (d,  $^3J$  = 8.5 Hz, 1H,  $\text{H}_7(\text{qui})$ ), 8.12 (d,  $^3J$  = 8.5 Hz, 1H,  $\text{H}_4(\text{qui})$ ), 8.52 (d,  $^3J$  = 4.8 Hz, 2H,  $\text{H}_6(\text{py})$ ) ppm.



5.2.1.3 Synthesis of bis(2-quinolylmethyl)(2-pyridylmethyl)amine (bqpa)<sup>[84]</sup>

USC-CN060

**3-3**

2-(Chloromethyl)quinoline hydrochloride (2.00 g, 9.34 mmol) was dissolved in deionized water (5 mL) and cooled in an ice bath. After addition of 5.3 M sodium hydroxide (5 mL), the reaction mixture was stirred for 5 min. Then, a solution of 2-pyridylmethylamine (0.50 mL, 3.24 g, 30 mmol) in dichloromethane (10 mL) was added and the ice bath was removed. Over 4 d of stirring, additional 5.3 M sodium hydroxide (5 mL) was added in small portions. The reaction mixture was then washed with 4.4 M sodium hydroxide (10 mL) and the organic phase separated and dried over magnesium sulfate. After removal of the solvent under vacuum, the brown residue was treated with diethylether (45 mL), which caused the precipitation of a white solid. The precipitate was collected by filtration and dried in vacuum. The product was obtained as a white powder.

**Yield:** 493.0 mg (1.26 mmol, 14%).

**IR:** 3059 (w), 2816 (w), 1601 (m), 1503 (s), 1426 (s), 1116 (m), 994 (m), 825 (s), 756 (s)  $\text{cm}^{-1}$ .

**<sup>1</sup>H NMR** ( $\text{CDCl}_3$ , 500.13 MHz):  $\delta$  = 3.99 (s, 2H,  $\text{CH}_2$ ), 4.11 (s, 4H,  $\text{CH}_2$ ), 7.15 (ddd,  $^3J$  = 7.4 Hz,  $^4J$  = 4.9 Hz,  $^5J$  = 1.3 Hz, 1H,  $H4(\text{py})$ ), 7.50 (ddd,  $^3J$  = 8.1 Hz,  $^4J$  = 6.9 Hz,  $^5J$  = 1.2 Hz, 2H,  $H8(\text{qui})$ ), 7.61 (d,  $^3J$  = 7.9 Hz, 1H,  $H3(\text{py})$ ), 7.66-7.68 (m, 3H,  $H9(\text{qui}) + H4(\text{py})$ ), 7.77 (d,  $^3J$  = 8.5 Hz, 2H,  $H3(\text{qui})$ ), 7.80 (d,  $^3J$  = 8.2 Hz, 2H,  $H10(\text{qui})$ ), 8.08 (d,  $^3J$  = 8.3 Hz, 2H,  $H7(\text{qui})$ ), 8.14 (d,  $^3J$  = 8.5 Hz, 2H,  $H4(\text{qui})$ ), 8.56 (d,  $^3J$  = 4.8 Hz, 1H,  $H6(\text{py})$ ) ppm.

$^{13}\text{C}\{^1\text{H}\}$  NMR ( $\text{CDCl}_3$ , 125.75 MHz):  $\delta$  = 60.5 ( $\text{CH}_2(\text{py})$ ), 61.1 ( $\text{CH}_2(\text{qui})$ ), 121.1 ( $\text{C}3(\text{qui})$ ), 122.1 ( $\text{C}5(\text{py})$ ), 123.3 ( $\text{C}3(\text{py})$ ), 126.2 ( $\text{C}8(\text{qui})$ ), 127.4 ( $\text{C}5(\text{qui})$ ), 127.5 ( $\text{C}7(\text{qui})$ ), 129.1 ( $\text{C}10(\text{qui})$ ), 129.4 ( $\text{C}9(\text{qui})$ ), 136.4 ( $\text{C}4(\text{qui})+\text{C}4(\text{py})$ ), 147.6 ( $\text{C}6(\text{qui})$ ), 149.2 ( $\text{C}6(\text{py})$ ), 159.2 ( $\text{C}2(\text{py})$ ), 160.1 ( $\text{C}2(\text{qui})$ ) ppm.

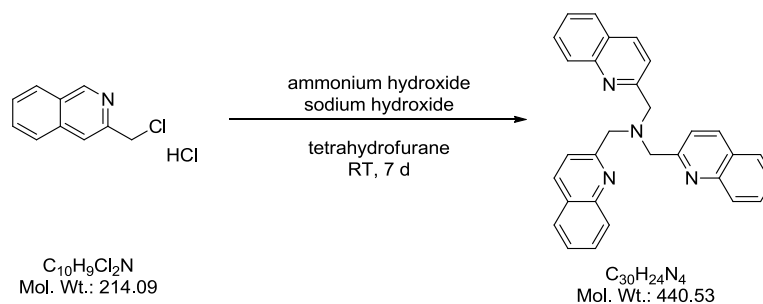
**Elemental analysis (%):**

calculated ( $\text{C}_{26}\text{H}_{22}\text{N}_4$ ):      C: 79.97      H: 5.68      N: 14.35

found:                              C: 79.69      H: 5.84      N: 14.34

5.2.1.4 Synthesis of tris(2-quinolylmethyl)amine (tmqa)<sup>[84]</sup>

USC-CN046

**3-4**

To a solution of 2-(chloromethyl)quinoline hydrochloride (1.09 g, 4.50 mmol) and 25% ammonium hydroxide (1.50 mmol, 3.85 mL) in tetrahydrofuran (20 mL) was added solid sodium hydroxide (0.18 g, 4.50 mmol). The mixture was stirred for 7 d at room temperature. The white precipitate formed was collected by filtration and collected. After removal of the solvent under vacuum, an oily brown residue was obtained, which was dissolved in dichloromethane and washed with water (10 mL). The solution was dried over magnesium sulfate and the solvent was removed under vacuum. The resulting white powder was combined with the collected precipitate to obtain the product as a white powder.

**Yield:** 222 mg (0.50 mmol, 34%).

**IR:** 3054 (w), 2842 (w), 1601 (s), 1427 (s), 1120 (s), 827 (vs), 766 (vs)  $\text{cm}^{-1}$ .

**<sup>1</sup>H NMR** ( $\text{CDCl}_3$ , 500.13 MHz):  $\delta$  = 4.13 (s, 6H,  $\text{CH}_2$ ), 7.47 - 7.51 (m, 3H,  $\text{H}_9(\text{qui})$ ), 7.65 - 7.70 (m, 3H,  $\text{H}_8(\text{qui})$ ), 7.74 (d,  $^3J$  = 8.7 Hz, 3H,  $\text{H}_3(\text{qui})$ ), 7.77 (d,  $^3J$  = 8.1 Hz, 3H,  $\text{H}_7(\text{qui})$ ), 8.06 (d,  $^3J$  = 8.7 Hz, 3H,  $\text{H}_{10}(\text{qui})$ ), 8.12 (d,  $^3J$  = 8.5 Hz, 3H,  $\text{H}_4(\text{qui})$ ) ppm.

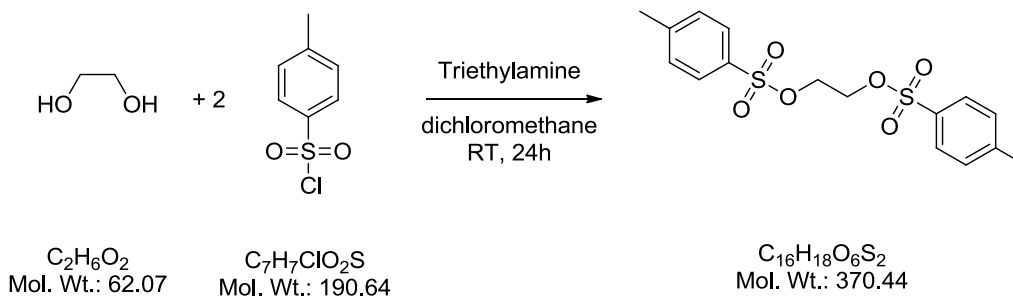
**<sup>13</sup>C{<sup>1</sup>H} NMR** ( $\text{CDCl}_3$ , 125.75 MHz):  $\delta$  = 61.3 ( $\text{CH}_2$ ), 121.4 ( $\text{C}_3(\text{qui})$ ), 126.4 ( $\text{C}_8(\text{qui})$ ), 127.5 ( $\text{C}_4(\text{qui})$ ), 127.6 ( $\text{C}_{10}(\text{qui})$ ), 129.2 ( $\text{C}_6(\text{qui})$ ), 129.6 ( $\text{C}_7(\text{qui})$ ), 136.5 ( $\text{C}_4(\text{qui})$ ), 147.7 ( $\text{C}_5(\text{qui})$ ), 160.1 ( $\text{C}_2(\text{qui})$ ) ppm.

**Elemental analysis (%):**

calculated ( $\text{C}_{30}\text{H}_{24}\text{N}_4$ ) $\times \text{H}_2\text{O}$ :	C: 78.58	H: 5.72	N: 12.22
found:	C: 78.65	H: 5.62	N: 11.76

5.2.1.5 Synthesis of ethylene-glycol ditosylate<sup>[121]</sup>

USC-CN018



A solution of tosyl chloride (27.5 g, 0.14 mol) and triethylamine (14.5 g, 0.14 mol) in dichloromethane (200 mL) was cooled to 0 °C with an ice bath and then ethylene glycol (8 g, 0.06 mol) was added over a 1 h period. The ice bath was removed and the reaction mixture was stirred for another 24 h. After pouring the reaction mixture into water (1 L), it was extracted with dichloromethane (3x100 mL). The organic layer was dried over magnesium sulfate and filtered. Removal of the solvent under vacuum gave the product as colorless to brownish needles.

**Yield:** 23.5 g (0.06 mol, 92%).

**IR:** 1597 (m), 1358 (vs), 1175 (vs), 1036 (m), 1016 (m), 912 (s), 767 (s)  $\text{cm}^{-1}$ .

**<sup>1</sup>H NMR** ( $\text{CDCl}_3$ , 199.93 MHz):  $\delta$  = 2.45 (s, 6H,  $\text{CH}_3$ ), 4.18 (s, 4H,  $\text{CH}_2$ ), 7.33 (d,  $^3J$  = 8.6 Hz, 4H,  $\text{H}3/5$ ), 7.73 (d,  $^3J$  = 8.3 Hz, 4H,  $\text{H}2/6$ ) ppm.

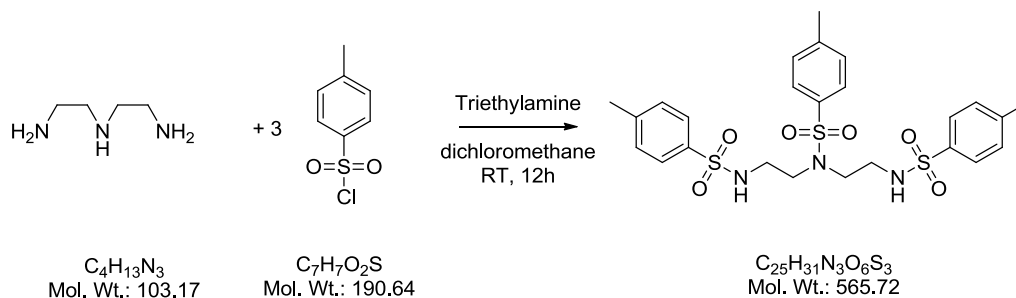
**<sup>13</sup>C{<sup>1</sup>H} NMR** ( $\text{CDCl}_3$ , 50.27 MHz):  $\delta$  = 21.8 ( $\text{CH}_3$ ), 66.8 ( $\text{CH}_2$ ), 128.1 ( $\text{C}3/5$ ), 130.1 ( $\text{C}2/6$ ), 132.4 ( $\text{C}4$ ), 145.4 ( $\text{C}1$ ) ppm.

**Elemental analysis (%)**:

calculated ( $\text{C}_{25}\text{H}_{31}\text{O}_6\text{S}_3$ ):	C: 51.88	H: 4.90	S: 17.31
found:	C: 51.31	H: 5.00	S: 17.08

5.2.1.6 Synthesis of diethylene triamine-*N,N',N''* tritosylate<sup>[121]</sup>

USC-CN010

**3-9**

A solution of diethylene triamine (8.0 g, 0.08 mol) and triethylamine (25.2 g, 0.25 mol) in dichloromethane (350 mL) was cooled to 0 °C with an ice bath and tosyl chloride (45.8 g, 0.24 mol) was added. The reaction mixture was allowed to warm to room temperature and stirred for 12 h. After removal of the solvent under vacuum the product was obtained as a white powder.

**Yield:** 40.4 g (0.07 mol, 89%).

**IR:** 3283 (s), 2032 (vs), 1599 (w), 1444 (w), 1333 (s), 1153 (vs), 1092 (m) 1077 (m), 812 (m)  $\text{cm}^{-1}$ .

**$^1\text{H}$  NMR** ( $\text{CDCl}_3$ , 199.93 MHz):  $\delta$  = 2.43 (s, 9H,  $\text{CH}_3$ ), 3.15 (m, 8H,  $\text{CH}_2$ ), 7.31 (d,  $^3J$  = 8.2 Hz, 6H,  $\text{H}_{3/5}$ ), 7.61 (d,  $^3J$  = 8.5 Hz, 2H,  $\text{H}_{2/6}$ ) 7.76 (d,  $^3J$  = 8.3 Hz, 4H,  $\text{H}_{2/6}$ ) ppm.

**$^{13}\text{C}\{^1\text{H}\}$  NMR** ( $\text{CDCl}_3$ , 50.27 MHz):  $\delta$  = 21.5 ( $\text{CH}_3$ ), 50.8 ( $\text{CH}_2$ ), 127.1 ( $\text{C}_{3/5}$ ), 127.3 ( $\text{C}_{3/5}$ ), 129.8 ( $\text{C}_{2/6}$ ), 130.0 ( $\text{C}_{2/6}$ ), 134.6 ( $\text{C}_4$ ), 136.7 ( $\text{C}_4$ ), 143.6 ( $\text{C}_1$ ), 144.2 ( $\text{C}_1$ ) ppm.

**Elemental analysis (%):**

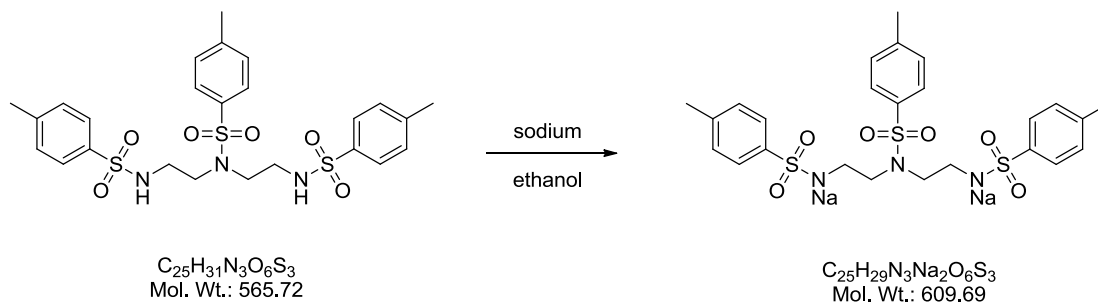
calculated ( $\text{C}_{25}\text{H}_{31}\text{N}_3\text{O}_6\text{S}_3$ ) x ( $\text{CH}_2\text{Cl}_2$ ):

	C: 47.99	H: 5.11	N: 6.46	S: 14.78
found:	C: 48.90	H: 5.19	N: 6.62	S: 14.92



5.2.1.7 Synthesis of disodium diethylene triamine-*N,N',N''* tritosylate<sup>[122]</sup>

USC-CN047

**3-10**

Sodium metal (1.5 g, 0.07 mol) was added in small amounts to anhydrous ethanol (250 mL) with rigorous stirring. Diethylene triamine-*N,N',N''*-tritosylate (31.8 g, 0.06 mol) was dissolved in this mixture and additional sodium metal (1.5 g, 0.07 mol) was added. The sealed flask was cooled to 0 °C. The product precipitated as a white powder which was collected by filtration and dried under vacuum at 50 °C.

**Yield:** 32.0 g (0.05 mol, 95%).

**IR:** 1306 (w), 1185 (vs), 1153 (s), 1121 (vs), 1079 (m), 810 (m)  $\text{cm}^{-1}$ .

**$^1\text{H}$  NMR** (DMSO- $d_6$ , 199.93 MHz):  $\delta$  = 2.30 (s, 9H,  $\text{CH}_3$ ), 2.62 (m, 4H,  $\text{CH}_2$ ), 2.84 (m, 4H,  $\text{CH}_2$ ), 7.10 (d,  $^3J$  = 8.0 Hz, 4H,  $\text{H}_3/5$ ), 7.28 (d,  $^3J$  = 8.4 Hz, 2H,  $\text{H}_3/5$ ), 7.45 (d,  $^3J$  = 8.0 Hz, 6H,  $\text{H}_2/6$ ) ppm.

**$^{13}\text{C}\{^1\text{H}\}$  NMR** (DMSO- $d_6$ , 50.27 MHz)  $\delta$  = 20.7 ( $\text{CH}_3$ ), 45.2 ( $\text{CH}_2$ ), 51.0 ( $\text{CH}_2$ ), 126.1 ( $\text{C}_3/5$ ), 126.5 ( $\text{C}_3/5$ ), 128.0 ( $\text{C}_2/6$ ), 129.4 ( $\text{C}_2/6$ ), 137.0 ( $\text{C}_4$ ), 137.4 ( $\text{C}_4$ ), 142.2 ( $\text{C}_1$ ), 145.4 ( $\text{C}_1$ ) ppm.

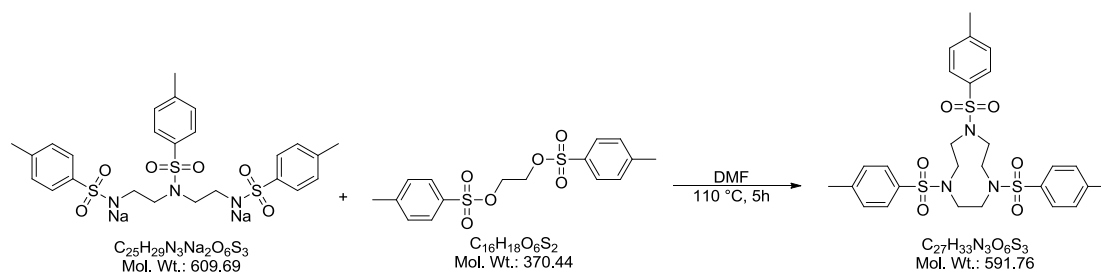
**Elemental analysis (%):**

calculated ( $\text{C}_{25}\text{H}_{29}\text{Na}_2\text{N}_3\text{O}_6\text{S}_3$ )  $\times \text{H}_2\text{O}$ :

	C: 47.84	H: 4.98	N: 6.69	S: 15.32
found:	C: 48.11	H: 4.78	N: 6.89	S: 15.66

5.2.1.8 Synthesis of 1,4,7-triazacyclonane-*N,N',N''* tritosylate<sup>[122]</sup>

USC-CN050

**3-11**

Disodium diethylene triamine-*N,N',N''* tritosylate (38.0 g, 0.06 mol) was dissolved in anhydrous *N,N*-dimethylformamide (250 mL) and heated to 110 °C. To this mixture, a solution of ethylene-glycol ditosylate (23.0 g, 0.06 mol) in anhydrous *N,N*-dimethylformamide (125 mL) was added dropwise over 2 h. After complete addition, the reaction mixture was stirred for 3 h at 110 °C. After cooling to room temperature, the solution was poured into water (1.5 L) and the crude product precipitated as an off-white mass which was collected by filtration and washed with water (100 mL). The product was obtained as a white powder after recrystallization from boiling ethanol (500 mL).

**Yield:** 32.0 g (0.05 mol, 90%).

**IR:** 1334 (s), 1317 (vs), 1149 (vs), 1088 (m), 995 (s), 815 (m) cm<sup>-1</sup>.

**<sup>1</sup>H NMR** (CDCl<sub>3</sub>, 199.93 MHz): δ = 2.43 (s, 9H, CH<sub>3</sub>), 3.42 (s, 12H, CH<sub>2</sub>), 7.32 (d, <sup>3</sup>J = 8.0 Hz, 6H, H<sub>3/5</sub>), 7.70 (d, <sup>3</sup>J = 8.3 Hz, 6H, H<sub>2/6</sub>) ppm.

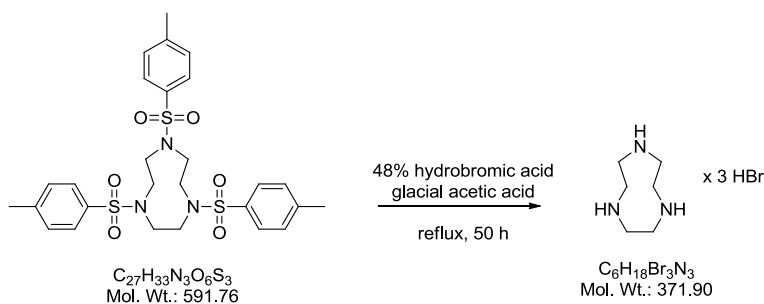
**<sup>13</sup>C{<sup>1</sup>H} NMR** (CDCl<sub>3</sub>, 50.27 MHz): δ = 21.5 (CH<sub>3</sub>), 51.9 (CH<sub>2</sub>), 127.5 (C<sub>3/5</sub>), 129.9 (C<sub>2/6</sub>), 134.6 (C<sub>4</sub>), 143.9 (C<sub>1</sub>) ppm.

**Elemental analysis (%):**

calculated (C <sub>27</sub> H <sub>33</sub> N <sub>3</sub> O <sub>6</sub> S <sub>3</sub> ):	C: 54.80	H: 5.62	N: 7.10	S: 16.26
found:	C: 54.57	H: 5.56	N: 7.43	S: 15.80

5.2.1.9 Synthesis of 1,4,7-triazacyclonane-trihydrobromide<sup>[122]</sup>

USC-CN051

**3-12**

1,4,7-Triazacyclonane-*N,N',N''* tritosylate (32.0 g, 0.05 mol), 48% hydrobromic acid (150 mL) and glacial acetic acid (85 mL) were slowly heated to reflux. The suspension turned into a dark brown solution after 20 h. After additional 30 h at reflux, the mixture was allowed to cool to room temperature. The crude product was obtained by precipitation with ethanol (50 mL) and diethylether (100 mL). The brownish product was collected by filtration, washed with ethanol and diethylether and dried under vacuum. It was directly used without further purification in the next step.

**Yield:** 7.85 g (0.02 mol, 42%)

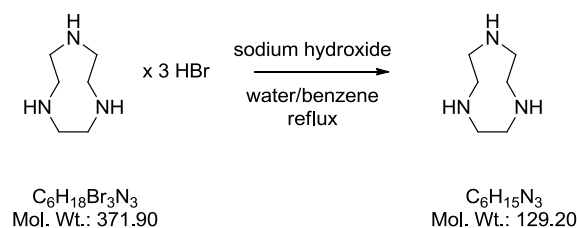
**IR:** 2860 (s), 2769 (s), 2460 (m), 1584 (m), 1447 (m), 1407 (m), 1337 (s), 1157 (s), 1087 (w), 940 (m)  $\text{cm}^{-1}$ .

**$^1\text{H}$  NMR** ( $\text{D}_2\text{O}$ , 199.93 MHz):  $\delta = 3.53$  (s, 12H,  $\text{CH}_2$ ) ppm.

**$^{13}\text{C}\{^1\text{H}\}$  NMR** ( $\text{D}_2\text{O}$ , 50.27 MHz):  $\delta = 42.4$  ( $\text{CH}_2$ ) ppm.

5.2.1.10 Synthesis of 1,4,7-triazacyclonane (tacn)<sup>[122]</sup>

USC-CN052

**3-13**

1,4,7-Triazacyclonane-trihydrobromide (7.28 g, 0.02 mol) was dissolved in deionized water (11 mL) and cooled to 0 °C with an ice bath. To this mixture, a solution of sodium hydroxide (2.31 g, 0.06 mol) in as little water as possible was added in small portions. The reaction mixture was then filtered and benzene (20 mL) was added to the filtrate. After removal of the water with a Dean-Stark trap, the benzene was evaporated. The product was obtained by distillation (10<sup>-2</sup> mbar, 30 – 50 °C) as a clear colorless liquid which crystallized upon cooling to room temperature. The product was stored under dinitrogen in the refrigerator at 8 °C.

**Yield:** 934 mg (7.23 mmol, 37%).

**IR:** 3358 (m), 3332 (m), 2885 (s), 2862 (s), 2785 (s), 1467 (m), 1352 (m), 1157 (m), 1075 (m), 986 (w) cm<sup>-1</sup>.

**<sup>1</sup>H NMR** (CDCl<sub>3</sub>, 199.93 MHz): δ = 2.77 (s, 12H, CH<sub>2</sub>) ppm.

**<sup>13</sup>C{<sup>1</sup>H} NMR** (CDCl<sub>3</sub>, 50.27 MHz): δ = 47.6 (CH<sub>2</sub>) ppm.

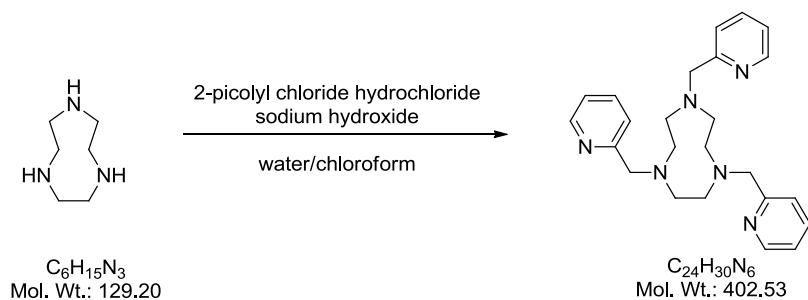
**Elemental analysis (%):**

calculated (C<sub>6</sub>H<sub>15</sub>N<sub>3</sub>):      C: 55.78      H: 11.70      N: 32.52

found:                              C: 55.40      H: 11.71      N: 32.44

5.2.1.11 Synthesis of *N,N',N''* tris(2-picolyl)-1,4,7-triazacyclonane (py<sub>3</sub>tacn)<sup>[93]</sup>

USC-CN053

**3-14**

2-Pyridylmethyl chloride hydrochloride (1.53 g, 9.30 mmol) was added to an aqueous solution (8 mL) of 1,4,7-triazacyclonane (0.40 g, 3.10 mmol). Solid sodium hydroxide (~2 g) was added to the suspension in small amounts at room temperature with stirring until a clear red solution was obtained (pH ~ 11). The solution was extracted with chloroform (5 x 10 mL) and the organic phase washed with cold water and dried over calcium oxide. The product was obtained as extremely hygroscopic red oil after removal of the solvent under vacuum.

**Yield:** 1.16 g (2.88 mmol, 93%).

**<sup>1</sup>H NMR** (CDCl<sub>3</sub>, 199.93 MHz): δ = 2.87 (s, 12H, CH<sub>2</sub>), 3.80 (s, 6H, CH<sub>2</sub>), 7.08-7.15 (m, 3H, H<sub>4</sub>), 7.48 (d, <sup>3</sup>J = 7.7 Hz, 3H, H<sub>3</sub>), 7.63 (t, <sup>3</sup>J = 7.6 Hz, 3H, H<sub>5</sub>), 8.48 (d, <sup>3</sup>J = 4.9 Hz, 3H, H<sub>6</sub>) ppm.

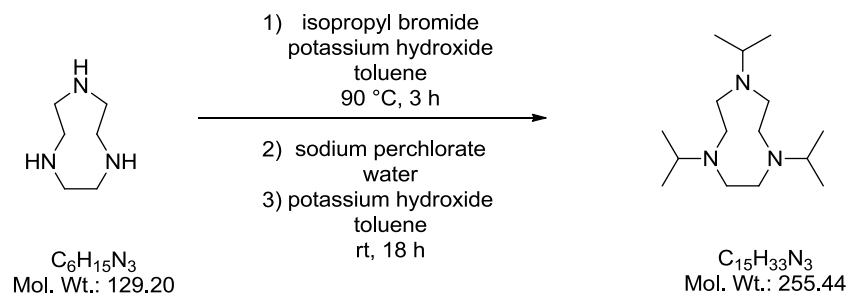
**<sup>13</sup>C{<sup>1</sup>H} NMR** (CDCl<sub>3</sub>, 50.27 MHz): δ = 55.8 (CH<sub>2</sub>), 64.8 (CH<sub>2</sub>), 121.8 (C<sub>3</sub>), 123.18 (C<sub>4</sub>), 136.2 (C<sub>5</sub>), 148.9 (C<sub>6</sub>), 160.5 (C<sub>2</sub>) ppm.

**Elemental analysis (%)**:

calculated (C <sub>24</sub> H <sub>30</sub> N <sub>6</sub> ) x NaOH x H <sub>2</sub> O:	C: 62.59	H: 7.22	N: 18.25
found:	C: 62.63	H: 7.04	N: 17.74

5.2.1.12 Synthesis of 1,4,7-triisopropyl-1,4,7-triazacyclonane (*iPr<sub>3</sub>tacn*)<sup>[101]</sup>

USC-CN063

**3-32**

Isopropyl bromide (1.28 g, 0.01 mol) was added to a toluene solution (8 mL) of 1,4,7-triazacyclonane (0.40 g, 3.10 mmol). The reaction mixture was stirred at 90 °C. Over time, a yellowish oil separated from the solution. Then, potassium hydroxide (0.60 g, 0.01 mol) was added and the mixture was stirred for 5 h at 90 °C. The precipitated potassium bromide was filtered off and the filtrate extracted with toluene (5 x 5 mL). The organic phases were combined and the toluene was removed under vacuum. The resulting yellow oil, containing mono-, di- and tri-substituted 1,4,7-triazacyclonane, was dissolved in methanol (6 mL) and solid sodium perchlorate (0.80 g, 6.53 mmol) was added with stirring, followed by water (4 mL) in small amounts until turbidity was observed. The mono-hydro perchlorate salt of the tri-substituted 1,4,7-triazacyclonane precipitated as colorless crystals after several hours at 8 °C, while other species remained dissolved. To obtain the free ligand, the mono-hydro perchlorate salt (250 mg, 0.70 mmol) was dissolved in toluene (5 mL) and solid potassium hydroxide (100 mg, 1.78 mmol) was added in small amounts. The mixture was then stirred at room temperature for 18 h. The precipitated potassium perchlorate was collected by filtration and the toluene phase was dried over magnesium sulfate. The product was obtained as colorless oil after removal of the solvent.

**Yield:** 158 mg (0.62 mmol, 20%).

**IR:** 2968 (m), 2850 (w), 1470 (m), 1390 (m), 1367 (m), 1074 (vs)  $\text{cm}^{-1}$ .

**$^1\text{H}$  NMR** ( $\text{CDCl}_3$ , 199.93 MHz):  $\delta$  = 0.97 (d,  $^3J$  = 6.6 Hz, 18H,  $\text{CH}_3$ ), 2.64 (s, 6H,  $\text{CH}_2$ ), 2.87 (sept,  $^3J$  = 6.6 Hz, 3H, CH) ppm.

**$^{13}\text{C}\{^1\text{H}\}$  NMR** ( $\text{CDCl}_3$ , 50.27 MHz):  $\delta$  = 18.3 ( $\text{CH}_3$ ), 52.8 ( $\text{CH}_2$ ), 54.4 (CH) ppm.

**Elemental analysis (%):**

calculated ( $\text{C}_{15}\text{H}_{34}\text{ClN}_3\text{O}_4$ ):            C: 50.76            H: 9.37            N: 11.84

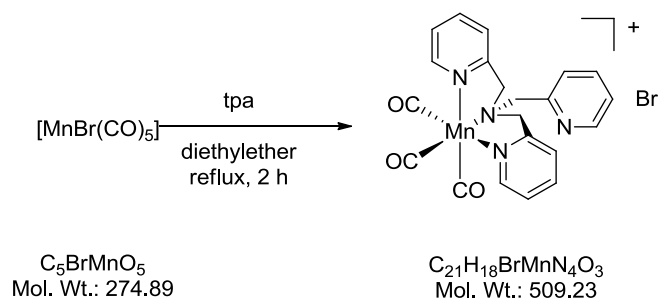
found:    C: 45.47            H: 9.14            N: 12.18

The large deviation in the elemental analysis is probably caused by water and salt impurities which, however, did not interfere with the next synthetic step.

## 5.2.2 Synthesis of PhotoCORMs with tetradentate ligands

5.2.2.1 Synthesis of  $[\text{Mn}(\text{CO})_3(\text{tpa}-\kappa^3\text{N})]\text{Br}$ 

USC-CN028

3-5

Under argon, tris(2-pyridylmethyl)amine (1.57 g, 3.93 mmol) and manganese pentacarbonyl bromide (1.08 g, 4.00 mmol) were heated to reflux for 2 h in degassed diethylether (125 mL). The crude product precipitated from the solution, was collected by filtration, washed with diethylether (20 mL) and dried under vacuum to result in a yellow powder. Colorless crystals suitable for X-ray structure analysis were obtained by slow diffusion of diethylether into a dichloromethane solution of the compound.

**Yield:** 1.86 g (3.65 mmol, 92%).

**IR:** 3016 (w), 2032 (vs), 1961 (vs), 1905 (vs), 1606 (w), 1586 (w), 1449 (w), 1427 (w), 779 (s), 772 (s)  $\text{cm}^{-1}$ .

**$^1\text{H}$  NMR** (DMSO- $d_6$ , 300.13 MHz):  $\delta$  = 4.36 (d,  $^2J$  = 17 Hz, 2H,  $\text{CH}_2$ ), 4.95 (s, 2H,  $\text{CH}_2$ ), 5.25 (d,  $^2J$  = 16.9 Hz, 2H,  $\text{CH}_2$ ), 7.39-7.50 (m, 4H,  $H_{3/4}$  (py)), 7.54 (m, 1H,  $H_4$  (py)), 7.82-7.92 (m, 3H,  $H_{4/5}$  (py)), 8.00 (td,  $^3J$  = 7.2 Hz,  $^4J$  = 5.1 Hz, 1H,  $H_5$  (py)), 8.74 (d,  $^3J$  = 5.4 Hz, 1H,  $H_6$  (py)), 8.89 (d,  $^3J$  = 5.4 Hz, 1H,  $H_6$  (py)) ppm.

**$^{13}\text{C}\{^1\text{H}\}$  NMR** (DMSO- $d_6$ , 75.47 MHz):  $\delta$  = 67.1 ( $\text{CH}_2$ ), 71.3 ( $\text{CH}_2$ ), 122.7 (C5), 124.1 (C5), 125.3 (C3), 126.2 (C3), 137.4 (C4), 139.5 (C4), 149.4 (C6), 152.1 (C6), 153.3 (C2), 160.4 (C2), 218.6 (CO) ppm.

**Elemental analysis (%):**

calculated ( $\text{C}_{21}\text{H}_{18}\text{BrMnN}_4\text{O}_3$ ):	C: 49.53	H: 3.56	N: 11.00
found:	C: 49.70	H: 3.31	N: 11.04

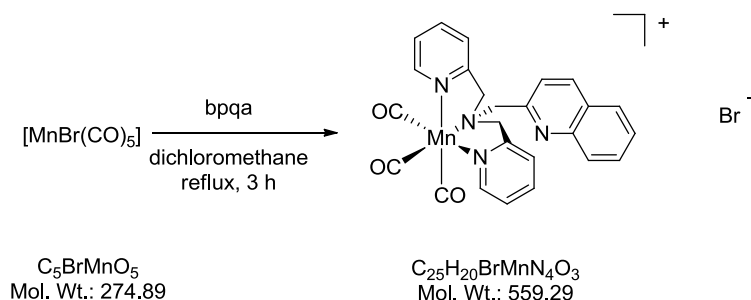


**ESI-MS:**

m/z: 345.09 [M-3CO-Br]<sup>+</sup>, 429.08 [M-Br]<sup>+</sup>, 939.07 [2M-Br]<sup>+</sup>.

5.2.2.2 Synthesis of  $[\text{Mn}(\text{bpqa}-\kappa^3\text{N})(\text{CO})_3]\text{Br}$ 

USC-CN069

**3-6**

Under dinitrogen, bis(2-pyridylmethyl)(2-quinolylmethyl)amine (bpqa) (85.0 mg, 0.25 mmol) and manganese pentacarbonyl bromide (70 mg, 0.25 mmol) were heated to reflux for 3 h in degassed dichloromethane (10 mL). After cooling to room temperature, the product was precipitated with diethylether (10 mL), collected by filtration, and dried under vacuum. It was obtained as a yellow powder.

**Yield:** 44 mg (0.08 mmol, 32%).

**IR:** 2027 (vs), 1921 (vs), 1913 (vs), 1609 (w), 1596 (w), 1440 (w), 1428 (w), 838 (s), 760 (m)  $\text{cm}^{-1}$ .

**$^1\text{H}$  NMR** (DMSO- $d_6$ , 500.13 MHz):  $\delta$  = 4.64 (d,  $^2J$  = 17.0 Hz, 2H,  $\text{CH}_2$ ), 5.22 (s, 2H,  $\text{CH}_2$ ), 5.31 (d,  $^2J$  = 17.0 Hz, 2H,  $\text{CH}_2$ ), 7.46 (t,  $^3J$  = 6.5 Hz, 2H,  $H_4$  (py)), 7.50 (d,  $^3J$  = 7.7 Hz, 2H,  $H_3$  (py)), 7.70 (t,  $^3J$  = 6.8 Hz, 1H,  $H_8$  (qui)), 7.84 (t,  $^3J$  = 7.4 Hz, 1H,  $H_9$  (qui)), 7.88 – 7.95 (m, 3H,  $H_5$  (py),  $H_{10}$  (qui)), 8.03 (d,  $^3J$  = 8.4 Hz, 1H,  $H_3$  (qui)), 8.08 (d,  $^3J$  = 8.0 Hz, 1H,  $H_7$  (qui)), 8.55 (d,  $^3J$  = 8.4 Hz, 1H,  $H_4$  (qui)), 8.93 (d,  $^3J$  = 5.5 Hz, 2H,  $H_2$  (py)) ppm.

**$^{13}\text{C}\{^1\text{H}\}$  NMR** (DMSO- $d_6$ , 125.75 MHz):  $\delta$  = 67.4 ( $\text{CH}_2$ ), 71.3 ( $\text{CH}_2$ ), 122.7 ( $\text{C}_5$  (py)), 122.8 ( $\text{C}_3$  (qui)), 125.3 ( $\text{C}_3$  (py)), 127.2 ( $\text{C}_8$  (qui)), 127.2 ( $\text{C}_5$  (qui)), 127.9 ( $\text{C}_7$  (qui)), 129.0 ( $\text{C}_{10}$  (qui)), 130.0 ( $\text{C}_9$  (qui)), 137.2 ( $\text{C}_4$  (qui)), 139.5 ( $\text{C}_4$  (py)), 146.8 ( $\text{C}_6$  (qui)), 152.1 ( $\text{C}_6$  (py)), 154.6 ( $\text{C}_2$  (qui)), 160.7 ( $\text{C}_2$  (py)), 218.5 (CO), 218.6 (CO) ppm.

**Elemental analysis (%):**

calculated (C<sub>25</sub>H<sub>20</sub>BrMnN<sub>4</sub>O<sub>3</sub>): C: 53.69 H: 3.60 N: 10.02

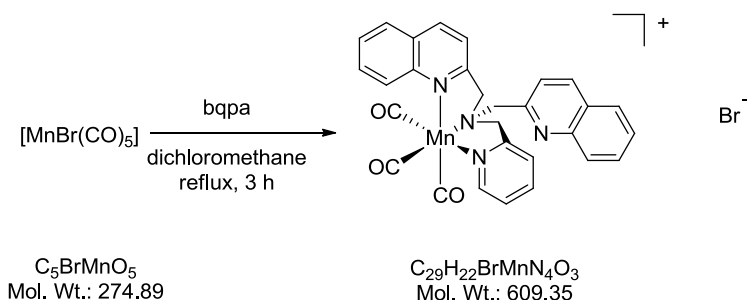
found: C: 53.50 H: 4.40 N: 9.24

**ESI-MS:**

m/z: 284.02 [M-3CO-C<sub>9</sub>H<sub>7</sub>N+H<sub>2</sub>O-Br]<sup>+</sup>, 395.11 [M-3CO-Br]<sup>+</sup>, 479.09 [M-Br]<sup>+</sup>.

5.2.2.3 Synthesis of  $[\text{Mn}(\text{CO})_3(\text{bqpa}-\kappa^3\text{N})]\text{Br}$ 

USC-CN062

3-7

Under dinitrogen, bis(2-quinolylmethyl)(2-pyridylmethyl)amine (bqpa) (100.0 mg, 0.25 mmol) and manganese pentacarbonyl bromide (70 mg, 0.25 mmol) were heated to reflux for 3 h in degassed dichloromethane (10 mL). After cooling to room temperature, the crude yellow product was precipitated with diethylether (10 mL), collected by filtration, and dried under vacuum. The product was purified by column chromatography (50 × 4 cm) on silica gel (silica gel 60; 0.063-0.200 mm, Merck) as the stationary phase and methanol/dichloromethane (20:80 v/v) as the eluent. From the first fraction, the product was obtained as a yellow powder after removal of the solvent under vacuum.

**Yield:** 56 mg (0.09 mmol, 25%)

**IR:** 2026 (vs), 1913 (vs), 1600 (w), 1504 (w), 1431 (w), 1428 (w), 825 (w), 761 (w)  $\text{cm}^{-1}$ .

**$^1\text{H}$  NMR** (DMSO- $d_6$ , 500.13 MHz):  $\delta$  = 4.35 (d,  $^2J$  = 17.8 Hz, 1H,  $\text{CH}_2$ ), 5.05 (d,  $^2J$  = 17.4 Hz, 1H,  $\text{CH}_2$ ), 5.20 (d,  $^2J$  = 17.8 Hz, 1H,  $\text{CH}_2$ ), 5.30 (s, 2H,  $\text{CH}_2$ ), 5.63 (d,  $^2J$  = 17.5 Hz, 1H,  $\text{CH}_2$ ), 7.50 (d,  $^3J$  = 8.3 Hz, 1H,  $H_{10}$  (qui)), 7.56 (t,  $^3J$  = 6.1 Hz, 1H,  $H_4$  (py)), 7.67 (t,  $^3J$  = 6.7 Hz, 1H,  $H_3$  (py)), 7.73 – 7.82 (m, 4H,  $H_8$  (qui)),  $H_5$  (py)), 7.88 (d,  $^3J$  = 8.5 Hz, 1H,  $H_7$  (qui)), 7.55 – 8.08 (m, 3H,  $H_9$  (qui),  $H_3$  (qui)), 8.16 (d,  $^3J$  = 7.0 Hz, 1H,  $H_3$  (qui)), 8.53 (d,  $^3J$  = 8.6 Hz, 1H,  $H_7$  (qui)), 8.58 (d,  $^3J$  = 8.7 Hz, 1H,  $H_4$  (qui)), 8.64 (d,  $^3J$  = 8.6 Hz, 1H,  $H_4$  (qui)), 9.22 (d,  $^3J$  = 4.9 Hz, 1H,  $H_2$  (py)) ppm.

**Elemental analysis (%):**

calculated (C<sub>29</sub>H<sub>22</sub>BrMnN<sub>4</sub>O<sub>3</sub>) x 3 (H<sub>2</sub>O):

C: 52.50      H: 4.25      N: 8.45

found:

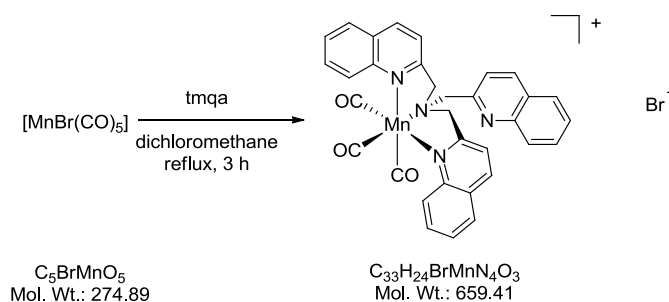
C: 53.03      H: 4.06      N: 8.61

**ESI-MS:**

m/z: 334.04 [M-3CO-C<sub>9</sub>H<sub>7</sub>N+H<sub>2</sub>O-Br]<sup>+</sup>, 445.12 [M-3CO-Br]<sup>+</sup>, 529.11 [M-Br]<sup>+</sup>.

5.2.2.4 Synthesis of  $[\text{Mn}(\text{CO})_3(\text{tmqa}-\kappa^3\text{N})]\text{Br}$ 

USC-CN048

**3-8**

Under dinitrogen, tris(2-quinolylmethyl)amine (tmqa) (100.0 mg, 0.23 mmol) and manganese pentacarbonyl bromide (62 mg, 0.23 mmol) were heated to reflux for 3 h in degassed dichloromethane (10 mL). After cooling to room temperature, the crude yellow product was precipitated with diethylether (10 mL), collected by filtration, and dried under vacuum. The product was obtained as a yellow powder. Colorless crystals suitable for X-ray structure analysis were obtained by slow diffusion of *n*-hexane into a dichloromethane solution of the compound.

**Yield:** 84 mg (0.13 mmol, 56%)

**IR:** 2026 (vs), 1935 (vs), 1913 (vs), 1600 (w), 1514 (w), 1432 (w), 823 (w), 780 (w), 750 (w)  $\text{cm}^{-1}$ .

**$^1\text{H}$  NMR** (DMSO- $d_6$ , 500.13 MHz):  $\delta$  = 4.95 (d,  $^2J$  = 18.4 Hz, 2H,  $\text{CH}_2$ ), 5.42 (s, 2H,  $\text{CH}_2$ ), 5.60 (d,  $^2J$  = 18.5 Hz, 2H,  $\text{CH}_2$ ), 7.48 (d,  $^3J$  = 7.9 Hz, 1H,  $H_8$  (qui)), 7.60 - 7.73 (m, 4H,  $H_8$ ,  $H_9$ ,  $H_{10}$  (qui)), 7.75 - 7.80 (m, 2H,  $H_9$  (qui)), 7.87 - 7.96 (m, 3H,  $H_3$  (qui)),  $H_{10}$  (qui)), 8.04 (d,  $^3J$  = 7.6 Hz, 1H,  $H_7$  (qui)), 8.19 (d,  $^3J$  = 8.1 Hz, 2H,  $H_3$  (qui)), 8.39 (d,  $^3J$  = 8.7 Hz, 2H,  $H_7$  (qui)), 8.53 (d,  $^3J$  = 8.2 Hz, 1H,  $H_4$  (qui)), 8.64 (d,  $^3J$  = 8.4 Hz, 2H,  $H_4$  (qui)) ppm.

$^{13}\text{C}\{^1\text{H}\}$  NMR (DMSO- $d_6$ , 125.75 MHz):  $\delta$  = 68.4 (CH<sub>2</sub>), 69.3 (CH<sub>2</sub>), 119.7 (C3 (qui)), 122.7 (C3 (qui)), 126.0 (C8, C5 (qui)), 127.1 (C8 (qui)), 127.6 (C5 (qui)), 128.0 (C7 (qui)), 128.4 (C10 (qui)), 128.5 (C7 (qui)), 129.9 (C9 (qui)), 130.0 (C10 (qui)), 132.2 (C9 (qui)), 137.2 (C4 (qui)), 140.5 (C4 (qui)), 146.5 (C6 (qui)), 147.0 (C6 (qui)), 155.2 (C2 (qui)), 165.4 (C2 (qui)), 218.4 (CO), 219.8 (CO) ppm.

**Elemental analysis (%):**

calculated (C<sub>33</sub>H<sub>24</sub>BrMnN<sub>4</sub>O<sub>3</sub>) x 2 H<sub>2</sub>O:

C: 56.99      H: 4.06      N: 8.06

found:                      C: 56.33      H: 3.72      N: 7.76

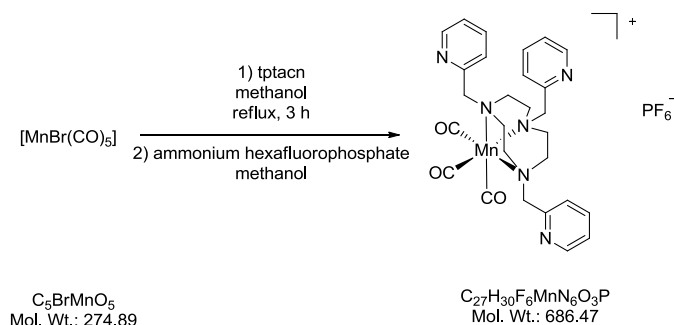
**ESI-MS:**

m/z: 384.05 [M-3CO-C<sub>9</sub>H<sub>7</sub>N+H<sub>2</sub>O-Br]<sup>+</sup>, 495.14 [M-3CO-Br]<sup>+</sup>, 579.12 [M-Br]<sup>+</sup>.

## 5.2.3 Synthesis of PhotoCORMs with hexadentate ligands

5.2.3.1 Synthesis of  $[\text{Mn}(\text{CO})_3(\text{py}_3\text{tacn-}\kappa^3\text{N})]\text{X}$ Synthesis of  $[\text{Mn}(\text{CO})_3(\text{py}_3\text{tacn-}\kappa^3\text{N})]\text{PF}_6$ 

USC-CN054

**3-15**

Under dinitrogen, manganese pentacarbonyl bromide (275.0 mg, 1.00 mmol) was added to a degassed solution of *N,N',N''*-tris-(2-pyridylmethyl)-1,4,7-triazacyclonane (402.0 mg, 1.00 mmol) in methanol (80 mL) and heated to reflux for 3 h. The resulting yellow solution was cooled to room temperature and the product precipitated as a yellow crystalline solid by addition of a saturated solution of ammonium hexafluorophosphate (200 mg, 1.38 mmol) in methanol (3 mL). The yellow product was collected by filtration and dried in vacuum extensively. Colorless crystals suitable for X-ray structure analysis were obtained by slow diffusion of *n*-hexane into a dichloromethane solution of the compound.

**Yield:** 281 mg (0.41 mmol, 62%).

**IR:** 2028 (vs), 1921 (vs), 1592 (w), 1440 (w), 1025 (w), 831 (s), 739 (w)  $\text{cm}^{-1}$ .

**$^1\text{H}$  NMR** ( $\text{CDCl}_3$ , 199.93 MHz):  $\delta$  = 2.75 (m, 6H,  $\text{CH}_2$ ), 3.84 (m, 6H,  $\text{CH}_2$ ), 4.70 (s, 6H,  $\text{CH}_2$ ), 7.36 (m, 3H,  $H5(\text{py})$ ), 7.48 (d,  $^3J$  = 6.4 Hz, 3H,  $H3(\text{py})$ ), 7.80 (td,  $^3J$  = 8.6 Hz,  $^4J$  = 0.9 Hz, 3H,  $H4(\text{py})$ ), 8.62 (d,  $^3J$  = 4.9 Hz, 3H,  $H6(\text{py})$ ) ppm.

**$^{13}\text{C}\{^1\text{H}\}$  NMR** ( $\text{CDCl}_3$ , 50.27 MHz):  $\delta$  = 55.1 ( $\text{CH}_2$ ), 69.7 ( $\text{CH}_2$ ), 124.3 ( $\text{C5}(\text{py})$ ), 126.5 ( $\text{C3}(\text{py})$ ), 137.3 ( $\text{C4}(\text{py})$ ), 150.0 ( $\text{C6}(\text{py})$ ), 152.2 ( $\text{C2}(\text{py})$ ) ppm.



**Elemental analysis (%):**

calculated (C<sub>27</sub>H<sub>30</sub>F<sub>6</sub>MnN<sub>6</sub>O<sub>3</sub>P) x CH<sub>3</sub>OH:

C: 46.81      H: 4.77      N: 11.70

found:

C: 46.62      H: 4.81      N: 11.42

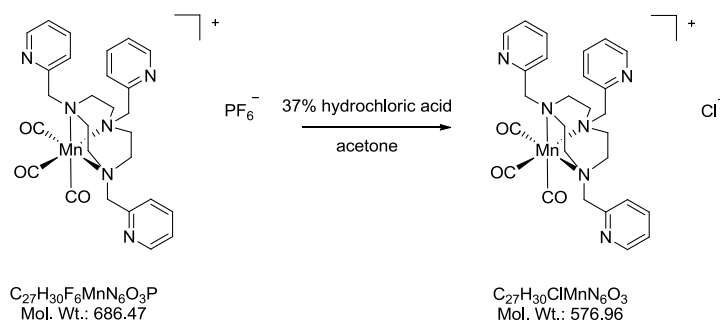
**ESI-MS:**

m/z: 365.14 [M-3CO-C<sub>6</sub>H<sub>6</sub>N-PF<sub>6</sub>]<sup>+</sup>, 383.15 [M-3CO-C<sub>6</sub>H<sub>6</sub>N+H<sub>2</sub>O-PF<sub>6</sub>]<sup>+</sup>,

541.17 [M-PF<sub>6</sub>]<sup>+</sup>.

Synthesis of  $[\text{Mn}(\text{CO})_3(\text{py}_3\text{tacn-}\kappa^3\text{N})]\text{Cl}$ 

USC-CN067

**3-16**

$[\text{Mn}(\text{CO})_3(\text{py}_3\text{tacn-}\kappa^3\text{N})]\text{PF}_6$  (0.34 g, 0.49 mmol) was dissolved in a minimum amount of acetone (5 mL). To this solution, 37% hydrochloric acid was added dropwise (1.00 mL). The yellow product which precipitated was collected by filtration and dried under vacuum.

**Yield:** 231 mg (0.40 mmol, 82%).

**IR:** 2014 (vs), 1912 (vs), 1680 (w), 1591 (w), 1441 (w), 790 (w), 737 (w)  $\text{cm}^{-1}$ .

**$^1\text{H}$  NMR** (DMSO- $d_6$ , 500.13 MHz):  $\delta$  = 2.77 (d,  $^3J$  = 7.9 Hz, 6H,  $\text{CH}_2$ ), 3.76 (d,  $^3J$  = 7.9 Hz, 6H,  $\text{CH}_2$ ), 4.74 (s, 6H,  $\text{CH}_2$ ), 7.49 (t,  $^3J$  = 4.8 Hz, 3H,  $\text{H}5(\text{py})$ ), 7.75 (d,  $^3J$  = 7.7 Hz, 3H,  $\text{H}3(\text{py})$ ), 7.94 (td,  $^3J$  = 7.7 Hz,  $^4J$  = 1.4 Hz, 3H,  $\text{H}4(\text{py})$ ), 8.68 (d,  $^3J$  = 4.8 Hz, 3H,  $\text{H}6(\text{py})$ ) ppm.

**$^{13}\text{C}\{^1\text{H}\}$  NMR** (DMSO- $d_6$ , 125.75 MHz):  $\delta$  = 55.1 ( $\text{CH}_2$ ), 69.7 ( $\text{CH}_2$ ), 124.3 ( $\text{C}5(\text{py})$ ), 126.5 ( $\text{C}3(\text{py})$ ), 137.3 ( $\text{C}4(\text{py})$ ), 150.0 ( $\text{C}6(\text{py})$ ), 152.2 ( $\text{C}2(\text{py})$ ) ppm.

**Elemental analysis (%):**

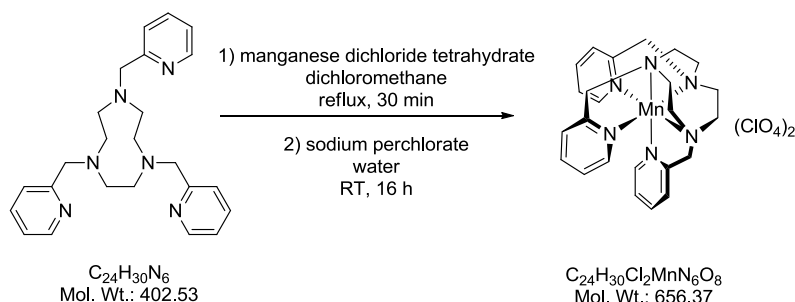
calculated ( $\text{C}_{27}\text{H}_{30}\text{ClMnN}_6\text{O}_3$ )  $\times$  1.5  $\text{H}_2\text{O}$ :

C: 53.69      H: 5.51      N: 13.91

found:                      C: 53.50      H: 5.34      N: 14.16

5.2.3.2 Synthesis of  $[\text{Mn}(\text{py}_3\text{tacn-}\kappa^6\text{N})](\text{ClO}_4)_2$ <sup>[93]</sup>

USC-CN056

**3-17**

To a degassed solution of *N,N',N''* tris(2-pyridylmethyl)-1,4,7-triazacyclonane ( $\text{py}_3\text{tacn}$ ) (0.40 g, 1.00 mmol) in methanol (40 mL), manganese dichloride tetrahydrate (0.20 g, 1.02 mmol) was added and heated to 60 °C for 30 min. Then, solid sodium perchlorate monohydrate (0.30 g, 2.55 mmol) was added, and the solution was cooled to 5 °C for 16 h. The off-white product which precipitated was collected by filtration, washed with ethanol (5 mL) and diethylether (10 mL), and dried under vacuum.

**Yield:** 416 mg (0.63 mmol, 65%)

**IR:** 1609 (m), 1442 (m), 1076 (s), 1016 (m)  $\text{cm}^{-1}$ .

**$^1\text{H}$  NMR /  $^{13}\text{C}\{^1\text{H}\}$  NMR:** No NMR spectra were recorded due to the paramagnetic nature of the  $3d^5$  manganese(II) complex.

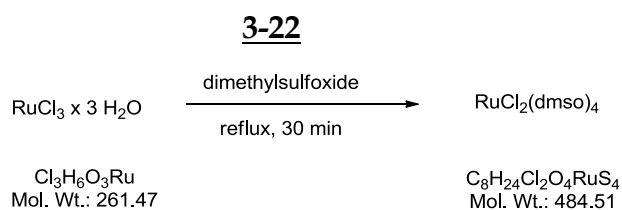
**Elemental analysis (%):**

calculated ( $\text{C}_{24}\text{H}_{30}\text{Cl}_2\text{MnN}_6\text{O}_8$ ):	C: 43.92	H: 4.61	N: 12.80
found:	C: 44.18	H: 4.35	N: 12.56

## 5.2.4 Synthesis of heterobinuclear manganese/ruthenium-PhotoCORMs

5.2.4.1 Synthesis of  $[\text{RuCl}_2(\text{dmsO})_4]$ <sup>[98]</sup>

USC CN002



A degassed solution of ruthenium(III) chloride trihydrate (1.00 g, 3.82 mmol) in dimethylsulfoxide (16 mL) was heated to reflux for 30 min. After cooling to room temperature, the reaction mixture was poured into acetone (60 mL) and stored at -20 °C for 16 h. The precipitated product was collected by filtration, washed with acetone (20 mL) and diethylether (60 mL) and dried under vacuum to result in a yellow powder. The different sets of signals in the  $^1\text{H}$  and  $^{13}\text{C}\{^1\text{H}\}$  NMR are due to the different isomers of the complex which result from either oxygen or sulfur coordination of the dimethylsulfoxide ligands.

**Yield:** 590 mg (1.22 mmol, 32%)

**IR:** 3028 (w), 2920 (w), 1403 (w), 1120 (vs), 1093 (vs), 1017 (vs), 916 (vs)  $\text{cm}^{-1}$ .

**$^1\text{H}$  NMR** (DMSO- $d_6$ , 199.93 MHz):  $\delta = 2.72$  (s, 6H,  $\text{CH}_3$ ), 3.39 (s, 6H,  $\text{CH}_3$ ), 3.47 (s, 6H,  $\text{CH}_3$ ), 3.49 (s, 6H,  $\text{CH}_3$ ) ppm.

**$^{13}\text{C}\{^1\text{H}\}$  NMR** (DMSO- $d_6$ , 50.27 MHz):  $\delta = 45.1$  ( $\text{CH}_3$ ), 45.4, ( $\text{CH}_3$ ), 45.8 ( $\text{CH}_3$ ), 46.4 ( $\text{CH}_3$ ), 47.2 ( $\text{CH}_3$ ), 47.5 ( $\text{CH}_3$ ) ppm.

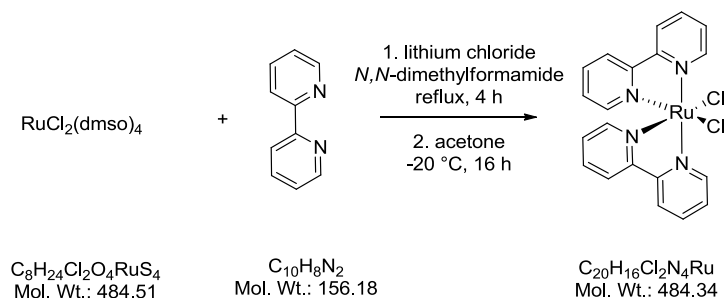
**Elemental analysis (%)**:

calculated ( $\text{C}_8\text{H}_{24}\text{Cl}_2\text{O}_4\text{RuS}_4$ ):

	C: 19.83	H: 4.99	S: 26.47
found:	C: 21.28	H: 5.39	S: 26.72

5.2.4.2 Synthesis of  $[\text{RuCl}_2(\text{bpy})_2]$ <sup>[123]</sup>

USC CN080

**3-23**

Under dinitrogen, lithium chloride (3.20 g, 75.48 mmol) was added to a solution of  $[\text{RuCl}_2(\text{dmsO})_4]$  (700 mg, 1.44 mmol) and 2,2' bipyridine (bpy) (480 mg, 3.07 mmol) in degassed *N,N*-dimethylformamide (16 mL). The solution was heated to reflux for 4 h. After cooling to room temperature, the violet reaction mixture was poured into acetone (200 mL) and stored overnight at -20 °C. The red precipitate was collected by filtration and washed with cold water until the filtrate became colorless. The product was washed with cold ethanol (5 mL) and diethylether (60 mL) to obtain a black powder which was dried extensively under vacuum.

**Yield:** 400 mg (0.83 mmol, 57%)

**IR:** 3070 (m), 1600 (m), 1442 (s), 1418 (s), 1308 (m), 1266 (m), 1017 (m), 763 (s)  $\text{cm}^{-1}$ .

**$^1\text{H}$  NMR** (DMSO- $d_6$ , 500.13 MHz):  $\delta$  = 7.11 (t,  $^3J$  = 5.8 Hz, 2H, CH), 7.50 (d,  $^3J$  = 5.5 Hz, 2H, CH), 7.68 (t,  $^3J$  = 7.1 Hz, 2H, CH), 7.77 (t,  $^3J$  = 7.1 Hz, 2H, CH), 8.07 (t,  $^3J$  = 8.0 Hz, 2H, CH), 8.51 (d,  $^3J$  = 8.0 Hz, 2H, CH), 8.66 (d,  $^3J$  = 8.0 Hz, 2H, CH), 9.96 (d,  $^3J$  = 5.8 Hz, 2H, CH) ppm.

**$^{13}\text{C}\{^1\text{H}\}$  NMR** (DMSO- $d_6$ , 125.75 MHz):  $\delta$  = 122.5 (CH), 122.8, (CH), 125.3 (CH), 125.3 (CH), 133.3 (CH), 134.5 (CH), 152.0 (CH), 153.2 (CH), 158.2 ( $\text{C}_q$ ), 160.2 ( $\text{C}_q$ ) ppm.

**Elemental analysis (%):**

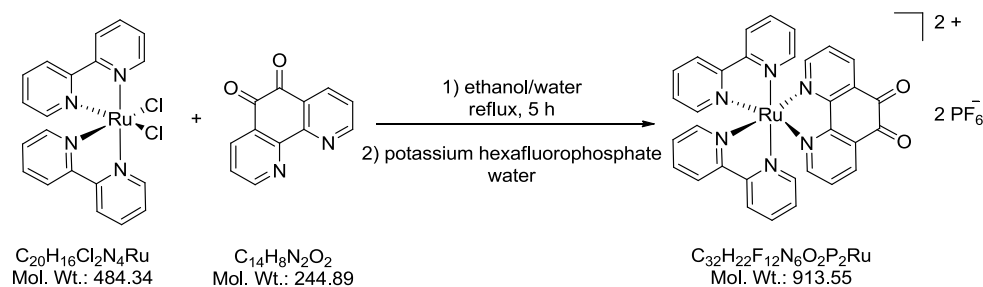
calculated (C<sub>20</sub>H<sub>16</sub>Cl<sub>2</sub>N<sub>4</sub>Ru):      C: 49.60      H: 3.33      N: 11.57

found:                                      C: 38.14      H: 4.63      N: 9.65

The large deviation in the elemental analysis is probably caused by water and salt impurities which, however, did not interfere with the next synthetic step.

5.2.4.3 Synthesis of  $[\text{Ru}(\text{bpy})_2(\text{phenox})](\text{PF}_6)_2$ <sup>[99]</sup>

USC CN081

**3-24**

Under dinitrogen, 1,10-phenanthroline-5,6-dione (phenox) (150 mg, 0.72 mmol) and  $[\text{RuCl}_2(\text{bpy})_2]$  (312 mg, 0.66 mmol) were dissolved in a degassed mixture of ethanol/water (50:50) and heated to reflux for 3 h. The mixture was cooled to room temperature and a saturated aqueous solution of potassium hexafluorophosphate (60 mL) was added to obtain an orange precipitate. The precipitate was collected by filtration, washed with water (10 mL), cold ethanol (10 mL) and diethylether (20 mL). After drying under vacuum the product was obtained as an orange powder.

**Yield:** 330 mg (0.36 mmol, 55%)

**IR:** 1704 (w), 1447 (w), 1428 (w), 834 (vs)  $\text{cm}^{-1}$ .

**$^1\text{H}$  NMR** (DMSO- $d_6$ , 500.13 MHz):  $\delta = 7.58 - 7.63$  (m, 4H, CH), 7.82 (d,  $^3J = 5.6$  Hz, 1H, CH), 7.83 (d,  $^3J = 5.6$  Hz, 1H, CH), 8.10 (d,  $^3J = 5.6$  Hz, 2H, CH), 8.18 - 8.28 (m, 6H, CH), 8.37 (dd,  $^3J = 5.6$  Hz,  $^4J = 1$  Hz, 2H, CH), 8.65 (dd,  $^3J = 8.0$  Hz,  $^4J = 1.4$  Hz, 2H, CH), 8.84 (d,  $^3J = 7.9$  Hz, 4H, CH) ppm.

**$^{13}\text{C}\{^1\text{H}\}$  NMR** (DMSO- $d_6$ , 125.75 MHz):  $\delta = 125.0$  (CH), 125.0 (CH), 128.3 (CH), 128.4 (CH), 129.3 (CH), 131.8 ( $\text{C}_q$ ), 136.2 (CH), 138.8 (CH), 138.9 (CH), 152.4 (CH), 152.7 (CH), 156.6 (CH), 157.2 ( $\text{C}_q$ ), 157.6 ( $\text{C}_q$ ), 157.7 ( $\text{C}_q$ ), 175.5 (CO) ppm.

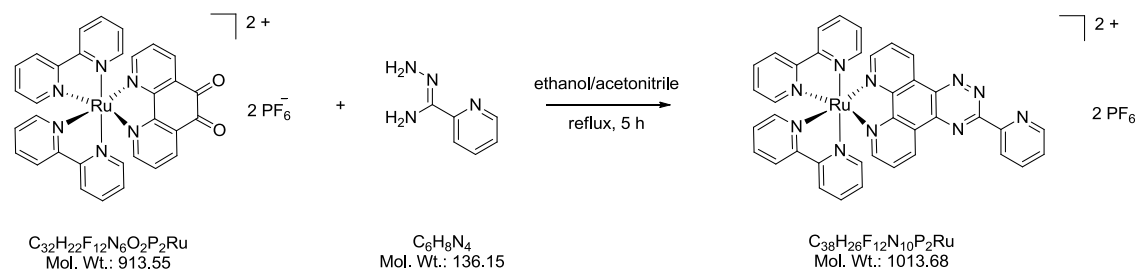
**Elemental analysis (%):**

calculated ( $\text{C}_{32}\text{H}_{22}\text{F}_{12}\text{N}_6\text{O}_2\text{P}_2\text{Ru}$ )  $\times$  0.8  $\text{KPF}_6$   $\times$   $\text{H}_2\text{O}$ :

	C: 35.63	H: 2.24	N: 7.79
found:	C: 35.43	H: 2.57	N: 7.84

5.2.4.4 Synthesis of  $[\text{Ru}(\text{bpy})_2(\text{pytp})](\text{PF}_6)_2$ <sup>[99]</sup>

USC CN082

**3-25**

$[\text{Ru}(\text{bpy})_2(\text{phenox})](\text{PF}_6)_2$  (200 mg, 0.22 mmol) was dissolved in acetonitrile (20 mL) and a solution of pyridine-2-carbohydrazonamide (34 mg, 0.24 mmol) in ethanol (6 mL) added. The mixture was sparged with dinitrogen and then heated to reflux for 5 h. The mixture was cooled to room temperature and the solvent was removed under vacuum to obtain the product as a red powder which was dried extensively under vacuum.

**Yield:** 186 mg (0.18 mmol, 83%)

**IR:** 3087 (w), 1604 (w), 1466 (m), 1446 (m), 1370 (m), 829 (vs)  $\text{cm}^{-1}$ .

**$^1\text{H}$  NMR** (DMSO- $d_6$ , 500.13 MHz):  $\delta$  = 7.39 – 7.44 (m, 2H, CH), 7.64 – 7.67 (m, 2H, CH), 7.72 (ddd,  $^3J$  = 7.6 Hz,  $^4J$  = 4.7 Hz,  $^5J$  = 1.1 Hz, 1H, CH), 8.05 – 8.11 (m, 2H, CH), 8.14 – 8.20 (m, 7H, CH), 8.28 (tt,  $^3J$  = 7.9 Hz,  $^4J$  = 6.4 Hz,  $^5J$  = 1.6 Hz, 2H, CH), 8.66 (dd,  $^3J$  = 5.4 Hz,  $^4J$  = 1.3 Hz, 1H, CH), 8.70 (dd,  $^3J$  = 5.4 Hz,  $^4J$  = 1.3 Hz, 1H, CH), 8.84 (d,  $^3J$  = 8.3 Hz, 2H, CH), 8.88 (d,  $^3J$  = 8.3 Hz, 2H, CH) 8.92 (dt,  $^3J$  = 7.9 Hz,  $^4J$  = 1.0 Hz, 1H, CH), 8.97 (ddd,  $^3J$  = 4.7 Hz,  $^4J$  = 1.8 Hz,  $^5J$  = 0.9 Hz, 1H, CH), 9.85 (dd,  $^3J$  = 8.2 Hz,  $^4J$  = 1.3 Hz, 1H, CH), 9.88 (dd,  $^3J$  = 8.2 Hz,  $^4J$  = 1.3 Hz, 1H, CH), ppm.

**$^{13}\text{C}\{^1\text{H}\}$  NMR** (DMSO- $d_6$ , 125.75 MHz):  $\delta$  = 125.3 (CH), 125.4 (CH), 125.5 (CH), 127.2 (CH), 128.7 (CH), 128.8 (CH), 128.9 (CH), 128.9 (CH), 129.3 (CH), 129.7 (C<sub>q</sub>), 130.6 (C<sub>q</sub>), 131.6 (C<sub>q</sub>), 133.7 (CH), 135.4 (CH), 138.4 (CH), 139.0 (CH), 139.2 (CH), 139.3 (CH), 143.5 (C<sub>q</sub>), 145.1 (C<sub>q</sub>), 150.8 (CH), 150.9 (CH), 151.6 (CH), 153.0 (CH), 153.0 (CH), 153.1 (CH), 153.1 (CH), 153.3 (CH), 153.7 (C<sub>q</sub>), 155.9 (CH), 157.1 (CH), 158.2 (C<sub>q</sub>), 158.2 (C<sub>q</sub>), 158.4 (C<sub>q</sub>), 163.2 (C<sub>q</sub>) ppm.



**Elemental analysis (%):**

calculated ( $C_{38}H_{26}F_{12}N_{10}P_2Ru$ ) x 5  $H_2O$ : C: 41.35 H: 3.29 N: 12.69

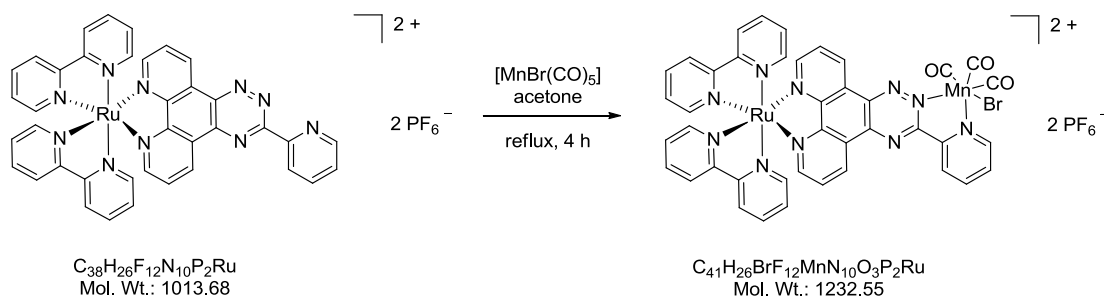
found: C: 40.95 H: 2.88 N: 12.63

**ESI-MS:**

m/z: 615.07  $[M-2xC_{10}H_8N_2+Na+Cl-PF_6]^+$ , 869.10  $[M-PF_6]^+$ .

5.2.4.5 Synthesis of  $[\text{Ru}(\text{bpy})_2(\text{pytp})(\text{MnBr}(\text{CO})_3)](\text{PF}_6)_2$ 

USC CN078

**3-28**

Under dinitrogen and very careful exclusion of light,  $[\text{Ru}(\text{bpy})_2(\text{pytp})](\text{PF}_6)_2$  (150 mg, 0.15 mmol) and manganese pentacarbonyl bromide (45 mg, 0.16 mmol) were dissolved in degassed acetone (30 mL) and heated to reflux for 4 h. The mixture was concentrated in vacuum and diethylether (20 mL) was added to obtain a dark red precipitate, which was collected by filtration and dried in vacuum. The resulting dark red powder was dissolved in a water/acetonitrile mixture (35:65 v/v) and loaded on a reversed-phase column (Waters SepPak C-18, 5 g). After washing the column with a water/acetonitrile mixture (3 x 10 mL, 98:2 v/v), the product was eluted using a water/acetonitrile mixture (5 mL, 35:65 v/v) and pure acetonitrile (2 mL) and lyophilized to obtain a dark red powder which was dried extensively under vacuum.

**Yield:** 104 mg (0.08 mmol, 56%)

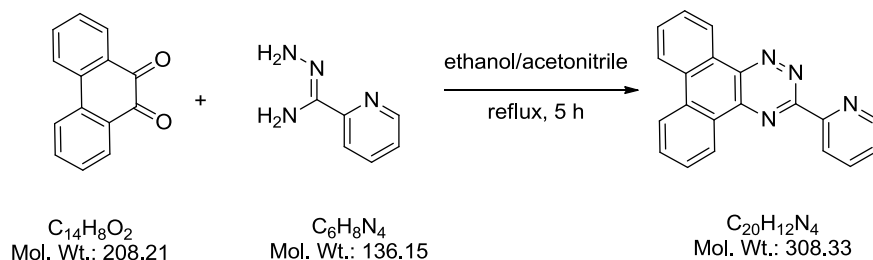
**IR:** 3094 (w), 2027 (vs), 1927 (vs), 1604 (m), 1466 (m), 1446 (m), 833 (s)  $\text{cm}^{-1}$ .

**$^1\text{H}$  NMR** (Acetone- $d_6$ , 500.13 MHz):  $\delta$  = 7.34 – 7.44 (m, 2H, CH), 7.58 – 7.63 (m, 2H, CH), 7.67 – 7.90 (m, 4H, CH), 8.02 (ddd,  $^3J$  = 7.4 Hz,  $^4J$  = 5.7 Hz,  $^5J$  = 1.6 Hz, 1H, CH), 8.09 – 8.20 (m, 4H, CH), 8.24 (t,  $^3J$  = 8.0 Hz, 2H, CH), 8.36 – 8.43 (m, 2H, CH), 8.50 (td,  $^3J$  = 7.8 Hz,  $^4J$  = 1 Hz, 1H, CH), 8.84 – 8.92 (m, 4H, CH), 9.17 – 9.21 (m, 1H, CH), 9.38 (d,  $^3J$  = 5.5 Hz, 2H, CH), 9.62 – 9.65 (m, 1H, CH), 9.89 (d,  $^3J$  = 8.3 Hz, 1H, CH), ppm.



5.2.4.6 Synthesis of 3-(pyridin-2-yl)phenanthro[9,10-*e*]-1,2,4-triazine (pypt)<sup>[99]</sup>

USC CN084

**3-20**

The synthesis of 3-(pyridin-2-yl)phenanthro[9,10-*e*]-1,2,4-triazine was carried out analogous to the synthesis of [Ru(bpy)<sub>2</sub>(pytp)](PF<sub>6</sub>)<sub>2</sub>. Phenanthrene-9,10-dione (208 mg, 1.00 mmol) was dissolved in acetonitrile (120 mL) and then, a solution of pyridine-2-carbohydrazonamide (136 mg, 1.00 mmol) in ethanol (30 mL) was added and heated to reflux for 5 h. The mixture was cooled to room temperature and the solvent was removed in vacuum extensively to obtain the product as brownish yellow powder.

**Yield:** 278 mg (0.90 mmol, 90%)

**IR:** 3057 (w), 1606 (m), 1452 (m), 1404 (s), 1368 (vs), 758 (vs) cm<sup>-1</sup>.

**<sup>1</sup>H NMR** (CDCl<sub>3</sub>, 500.13 MHz): δ = 7.52 – 7.56 (m, 1H, CH), 7.74 (t, <sup>3</sup>J = 7.0 Hz, 1H, CH), 7.79 (t, <sup>3</sup>J = 6.9 Hz, 1H, CH), 7.80 – 7.90 (m, 2H, CH), 8.02 (t, <sup>3</sup>J = 7.7 Hz, 1H, CH), 8.56 (d, <sup>3</sup>J = 8.0 Hz, 2H, CH), 8.89 (d, <sup>3</sup>J = 7.9 Hz, 1H, CH), 9.00 – 9.03 (m, 1H, CH), 9.44 (d, <sup>3</sup>J = 8.0 Hz, 1H, CH), 9.51 (d, <sup>3</sup>J = 7.8 Hz, 1H, CH) ppm.

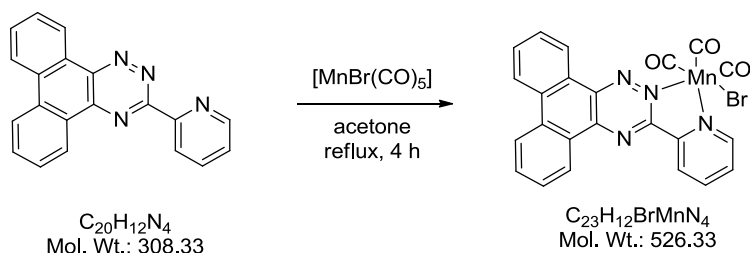
**<sup>13</sup>C{<sup>1</sup>H} NMR** (CDCl<sub>3</sub>, 125.75 MHz): δ = 123.4 (CH), 123.4 (CH), 124.7 (CH), 125.6 (CH), 125.7 (CH), 127.5 (CH), 127.9 (CH), 128.2 (C<sub>q</sub>), 128.5 (CH), 129.1 (CH), 131.4 (CH), 131.8 (C<sub>q</sub>), 133.0 (CH), 134.3 (C<sub>q</sub>), 137.6 (CH), 143.7 (C<sub>q</sub>), 145.9 (C<sub>q</sub>), 151.0 (C<sub>q</sub>), 154.1 (C<sub>q</sub>), 161.0 (C<sub>q</sub>) ppm.

**Elemental analysis (%):**

calculated (C <sub>20</sub> H <sub>12</sub> N <sub>4</sub> ) × 0.5 H <sub>2</sub> O:	C: 75.70	H: 4.13	N: 17.65
found:	C: 76.10	H: 4.31	N: 17.90

5.2.4.7 Synthesis of  $[\text{MnBr}(\text{CO})_3(\text{pypt})]$ 

USC CN085

3-27

Under dinitrogen and exclusion of light, manganese pentacarbonyl bromide (106 mg, 0.39 mmol) and 3-(pyridin-2-yl)phenanthro[9,10-*e*]-1,2,4-triazine (pypt) (120 mg, 0.39 mmol) was dissolved in degassed acetone (50 mL) and heated to reflux for 4 h. The mixture was concentrated under vacuum and diethylether (40 mL) was added. A purple solid precipitated which was collected by filtration and dried in vacuum. The product was obtained as a purple powder which was extensively dried under vacuum.

**Yield:** 125 mg (0.90 mmol, 62%)

**IR:** 3071 (w), 2026 (vs), 1962 (vs), 1906 (vs), 1604 (m), 1369 (vs), 757 (s)  $\text{cm}^{-1}$ .

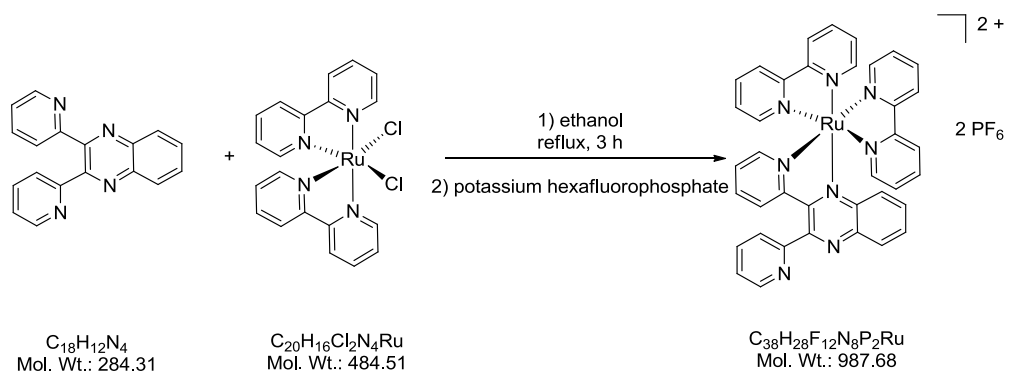
**$^1\text{H}$  NMR /  $^{13}\text{C}\{^1\text{H}\}$  NMR** Because of the poor solubility of the compound in any common solvents, no NMR spectra could be obtained.

**Elemental analysis (%):**

calculated ( $\text{C}_{23}\text{H}_{12}\text{BrMnN}_4\text{O}_3$ ) $\times$ $\text{H}_2\text{O}$ :	C: 50.67	H: 2.59	N: 10.28
found:	C: 50.83	H: 2.24	N: 10.31

5.2.4.8 Synthesis of  $[\text{Ru}(\text{bpy})_2(\text{dpx})](\text{PF}_6)_2$ 

USC CN087

**3-29**

Under dinitrogen, 2,3-di(pyridine-2-yl)quinoxaline (dpx) (110 mg, 0.39 mmol) and  $[\text{Ru}(\text{bpy})_2\text{Cl}_2]$  (175 mg, 0.36 mmol) were dissolved in degassed ethanol (60 mL) and heated to reflux for 3 h. The mixture was concentrated under vacuum and a saturated aqueous solution of potassium hexafluorophosphate (20 mL) was added to obtain a red precipitate, which was collected by filtration and extensively dried under vacuum to obtain the product as a red powder.

**Yield:** 340 mg (0.34 mmol, 96%)

**IR:** 3124 (w), 1603 (w), 1467 (m), 1446 (m), 832 (s)  $\text{cm}^{-1}$ .

**$^1\text{H}$  NMR** (DMSO- $d_6$ , 500.13 MHz):  $\delta$  = 7.33 (d,  $^3J$  = 8.3 Hz, 1H, CH), 7.41 – 7.51 (m, 5H, CH), 7.62 (t,  $^3J$  = 6.7 Hz, 1H, CH), 7.68 (t,  $^3J$  = 6.8 Hz, 1H, CH), 7.71 – 7.77 (m, 3H, CH), 7.88 (q,  $^3J$  = 8.1 Hz, 2H, CH), 8.05 – 8.11 (m, 3H, CH), 8.13 – 8.22 (m, 2H, CH), 8.23 – 8.33 (m, 5H, CH), 8.54 (d,  $^3J$  = 7.8 Hz, 1H, CH), 8.62 (d,  $^3J$  = 8.1 Hz, 1H, CH), 8.74 (d,  $^3J$  = 4.6 Hz, 1H, CH), 8.98 – 9.05 (m, 2H, CH), ppm.

**$^{13}\text{C}\{^1\text{H}\}$  NMR** (DMSO- $d_6$ , 125.75 MHz):  $\delta$  = 124.7 (CH), 125.1 (CH), 125.1 (CH), 125.3 (CH), 126.0 (CH), 126.1 (CH), 126.6 (CH), 128.0 (CH), 128.5 (CH), 128.9 (CH), 129.1 (CH), 130.6 (CH), 131.1 (CH), 132.9 (CH), 133.7 (CH), 137.5 (CH), 139.3 (CH), 139.4 (CH), 139.5 (CH), 139.6 (CH), 139.6 (CH), 141.4 ( $\text{C}_q$ ), 144.1 ( $\text{C}_q$ ), 150.6 (CH), 152.5 (CH), 152.7 ( $\text{C}_q$ ), 154.7 (CH), 156.5 ( $\text{C}_q$ ), 156.9 ( $\text{C}_q$ ), 157.1 ( $\text{C}_q$ ), 157.3 ( $\text{C}_q$ ), 157.4 ( $\text{C}_q$ ), 159.3 ( $\text{C}_q$ ) ppm.

**Elemental analysis (%):**

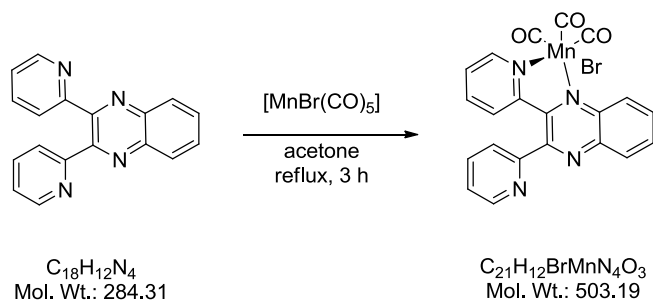
calculated ( $C_{38}H_{28}F_{12}N_8P_2Ru$ ) x 2  $KPF_6$ : C: 33.66 H: 2.08 N: 8.26  
found: C: 33.56 H: 2.45 N: 8.64

**ESI-MS:**

m/z: 283.09  $[M-2(C_{10}H_8N_2)-H-2PF_6]^+$ , 843.11  $[M-PF_6]^+$

5.2.4.9 Synthesis of  $[\text{MnBr}(\text{CO})_3(\text{dpx})]$ 

USC CN089

**3-30**

Under dinitrogen and careful exclusion of light, manganese pentacarbonyl bromide (274 mg, 1.00 mmol) and 2,3-di(pyridin-2-yl)quinoxaline (dpx) (284 mg, 1.00 mmol) were dissolved in degassed acetone (50 mL) and heated to reflux for 3 h. The mixture was concentrated under vacuum and diethylether (20 mL) was added to obtain a violet precipitate. The precipitate was collected by filtration and dried under vacuum to obtain the product as a violet powder. Dark red crystals suitable for X-ray structure analysis were obtained by slow diffusion of *n*-hexane into a dichloromethane solution of the compound.

**Yield:** 418 mg (0.83 mmol, 83%)

**IR:** 2027 (vs), 1938 (vs), 1914 (vs), 1586 (w), 1475 (w), 1355 (m), 774 (m)  $\text{cm}^{-1}$ .

**$^1\text{H}$  NMR** (DMSO- $d_6$ , 500.13 MHz):  $\delta$  = 7.11 (d,  $^3J$  = 8.2 Hz, 1H, CH), 7.65 – 7.71 (m, 2H, CH), 7.91 (t,  $^3J$  = 7.9 Hz, 1H, CH), 8.00 (d,  $^3J$  = 7.7 Hz, 1H, CH), 8.11–8.25 (m, 3H, CH), 8.34 (d,  $^3J$  = 8.3 Hz, 1H, CH), 8.71 (d,  $^3J$  = 4.7 Hz, 1H, CH), 8.89 (d,  $^3J$  = 8.1 Hz, 1H, CH), 9.40 (d,  $^3J$  = 4.9 Hz, 1H, CH) ppm.

**$^{13}\text{C}\{^1\text{H}\}$  NMR** (DMSO- $d_6$ , 125.75 MHz):  $\delta$  = 125.7 (CH), 126.2 (CH), 127.4 (CH), 128.4 (CH), 129.4 (CH), 131.0 (CH), 133.7 (CH), 133.8 (CH), 138.8 (CH), 138.9 (CH), 141.0 ( $\text{C}_q$ ), 142.5 ( $\text{C}_q$ ), 150.5 (CH), 152.8 ( $\text{C}_q$ ), 154.3 ( $\text{C}_q$ ), 154.6 (CH), 156.7 ( $\text{C}_q$ ), 157.3 ( $\text{C}_q$ ), 221.0 (CO), 222.6 (CO), 224.3 (CO) ppm.



**Elemental analysis (%):**

calculated (C<sub>21</sub>H<sub>12</sub>BrMnN<sub>4</sub>O<sub>3</sub>): C: 50.13 H: 2.40 N: 11.13

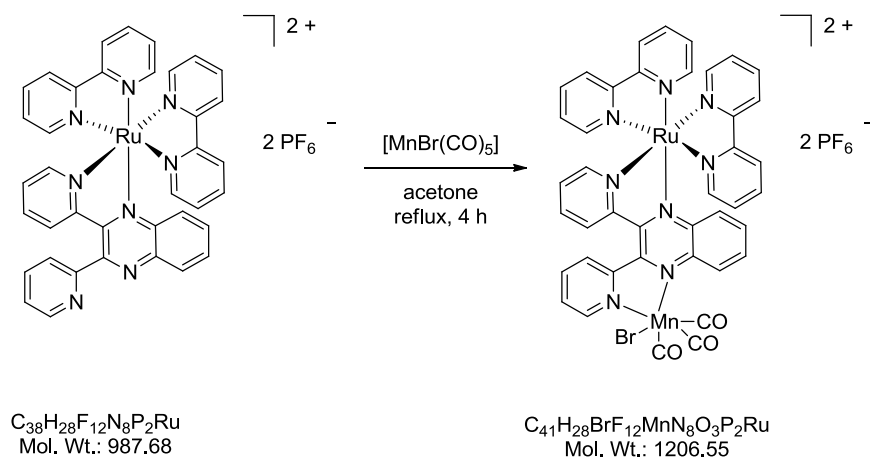
found: C: 50.26 H: 2.54 N: 10.96

**ESI-MS:**

m/z: 283.09 [M-Mn-3CO-Br+H]<sup>+</sup>, 420.97 [M-3CO+H]<sup>+</sup>, 440.95 [M-3CO+Na]<sup>+</sup>,  
860.91 [2M-6CO+Na]<sup>+</sup>, 1044.85 [2M+Na]<sup>+</sup>

5.2.4.9 Synthesis of  $[\text{Ru}(\text{bpy})_2(\text{dpx})(\text{MnBr}(\text{CO})_3)](\text{PF}_6)_2$ 

USC CN088

**3-31**

Under dinitrogen and careful exclusion of light, manganese pentacarbonyl bromide (58 mg, 0.21 mmol) and  $[\text{Ru}(\text{bpy})_2(\text{dpx})](\text{PF}_6)_2$  (200 mg, 0.20 mmol) were dissolved in degassed acetone (50 mL) and heated to reflux for 4 h. The mixture was concentrated in vacuum and diethylether (20 mL) was added to obtain a black precipitate. The precipitate was collected by filtration and dried under vacuum to obtain a black powder which was dissolved in a mixture of water and acetonitrile (35:65 v/v) and loaded on a reversed phase column (Waters SepPak C-18, 5 g). After washing the column with a water/acetonitrile mixture (3 x 10 mL, 98:2 v/v), the product was eluted using a water/acetonitrile mixture (5 mL, 35:65 v/v) and pure acetonitrile (2 mL) and lyophilized to obtain a black powder which was extensively dried under vacuum.

**Yield:** 164 mg (0.14 mmol, 68%)

**IR:** 2026 (vs), 1928 (vs), 1605 (w), 1466 (w), 1447 (w), 833 (m)  $\text{cm}^{-1}$ .

**$^1\text{H}$  NMR** ( $\text{CD}_2\text{Cl}_2$ , 500.13 MHz):  $\delta$  = 7.44 – 7.48 (m, 3H, CH), 7.54 (t,  $^3J$  = 6.6 Hz, 1H, CH), 7.61 (t,  $^3J$  = 7.3 Hz, 2H, CH), 7.68 – 7.73 (m, 3H, CH), 7.84 – 8.36 (m, 13H, CH), 8.53 (d,  $^3J$  = 8.2 Hz, 2H, CH), 8.66 – 8.70 (m, 2H, CH), 8.78 (d,  $^3J$  = 8.6 Hz, 1H, CH), 9.41 (d,  $^3J$  = 5.2 Hz, 1H, CH) ppm.

$^{13}\text{C}\{^1\text{H}\}$  NMR ( $\text{CD}_2\text{Cl}_2$ , 125.75 MHz):  $\delta$  = 124.4 (CH), 124.6 (CH), 125.5 (CH), 125.8 (CH), 126.2 (CH), 127.1 (CH), 128.8 (CH), 129.0 (CH), 129.3 (CH), 129.4 (CH), 129.8 (CH), 129.9 (CH), 130.2 (CH), 131.6 (CH), 134.7 (CH), 135.2 (CH), 138.3 (CH), 139.6 (CH), 139.7 (CH), 139.7 (CH), 139.8 (CH), 139.9 (CH), 143.3 ( $\text{C}_q$ ), 143.7 ( $\text{C}_q$ ), 151.8 (CH), 151.9 (CH), 152.1 (CH), 153.2 (CH), 153.7 ( $\text{C}_q$ ), 154.5 (CH), 155.7 ( $\text{C}_q$ ), 156.5 ( $\text{C}_q$ ), 156.6 ( $\text{C}_q$ ), 156.9 ( $\text{C}_q$ ), 157.0 ( $\text{C}_q$ ), 157.5 ( $\text{C}_q$ ), 157.9 ( $\text{C}_q$ ), 223.7 (CO), 224.2 (CO) ppm.

**Elemental analysis (%):**

calculated ( $\text{C}_{41}\text{H}_{28}\text{BrF}_{12}\text{MnN}_8\text{O}_3\text{P}_2\text{Ru}$ )  $\times$  3  $\text{H}_2\text{O}$ :

C: 39.06      H: 2.72      N: 8.89

found:

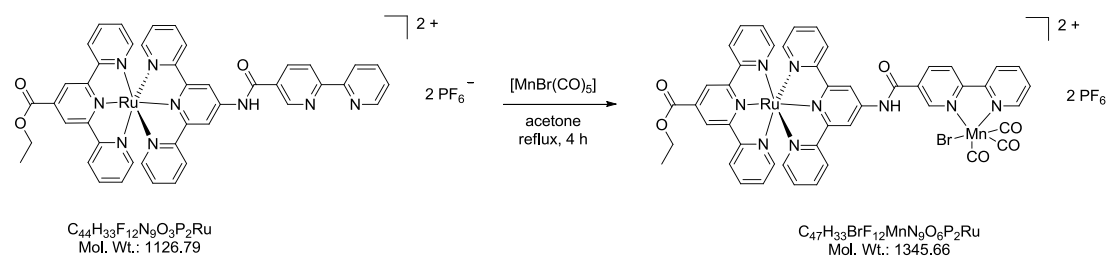
C: 39.45      H: 2.84      N: 8.87

**ESI-MS:**

m/z: 285.04  $[\text{M-Mn-3CO-Br-Ru-2}(\text{C}_{10}\text{H}_8\text{N}_2)+\text{H}]^+$ , 349.07  $[\text{M-Mn-3CO-Br-2PF}_6]^{2+}$ , 419.96  $[\text{M-3CO-Ru-2}(\text{C}_{10}\text{H}_8\text{N}_2)+\text{H}]^+$ , 699.14  $[\text{M-Mn-3CO-Br+H-2PF}_6]^+$ , 843.11  $[\text{M-Mn-3CO-Br-PF}_6]^+$ , 1062.95  $[\text{M-PF}_6]^+$

5.2.4.10 Synthesis of [Ru(etx)(tbx)(MnBr(CO)<sub>3</sub>)](PF<sub>6</sub>)<sub>2</sub>

USC CN086

**3-26**

Under dinitrogen and careful exclusion of light, manganese pentacarbonyl bromide (22 mg, 0.08 mmol) and [Ru(etx)(tbx)](PF<sub>6</sub>)<sub>2</sub> (87 mg, 0.08 mmol) were dissolved in degassed acetone (40 mL) and heated to reflux for 4 h. The mixture was concentrated under vacuum and diethylether (20 mL) was added to obtain a red precipitate. The precipitate was collected by filtration and dried under vacuum to obtain a red powder. This was dissolved in a mixture of water and acetonitrile (35:65 v/v) and loaded on a reversed-phase column (Waters SepPak C-18, 5 g). After washing the column with a mixture of water and acetonitrile (3 x 10 mL, 98:2 v/v), the product was eluted using a water/acetonitrile mixture (5 mL, 35:65 v/v) and pure acetonitrile (2 mL) and lyophilized to obtain a red powder which was extensively dried under vacuum.

**Yield:** 50 mg (0.04 mmol, 57%)

**IR:** 2025 (vs), 1928 (vs), 1914 (vs), 1722 (w), 1596 (m), 1457 (m), 1426 (m), 1294 (m), 1252 (m), 1135 (m), 834 (vs) cm<sup>-1</sup>.

**<sup>1</sup>H NMR** (DMSO-d<sub>6</sub>, 500.13 MHz): δ = 1.56 (t, <sup>3</sup>J = 7.0 Hz, 3H, CH<sub>3</sub>), 4.66 (q, <sup>3</sup>J = 7.2 Hz, 2H, CH<sub>2</sub>), 7.26 (t, <sup>3</sup>J = 6.5 Hz, 2H, CH), 7.36 (t, <sup>3</sup>J = 6.2 Hz, 2H, CH), 7.52 (d, <sup>3</sup>J = 5.5 Hz, 2H, CH), 7.61 (d, <sup>3</sup>J = 5.5 Hz, 2H, CH), 7.86 (t, <sup>3</sup>J = 6.5 Hz, 1H, CH), 8.03 – 8.12 (m, 4H, CH), 8.30 (d, <sup>3</sup>J = 5.6 Hz, 1H, CH), 8.38 (t, <sup>3</sup>J = 7.6 Hz, 1H, CH), 8.64 (d, <sup>3</sup>J = 7.9 Hz, 2H, CH), 8.88 (d, <sup>3</sup>J = 9.1 Hz, 1H, CH), 9.13 (d, <sup>3</sup>J = 8.0 Hz, 2H, CH), 9.25 (s, 1H, CH), 9.32 (d, <sup>3</sup>J = 5.7 Hz, 1H, CH), 9.34 (s, 2H, CH), 9.45 (s, 2H, CH), 9.59 (d, <sup>3</sup>J = 5.7 Hz, 1H, CH), 12.17 (s, 1H, NHCO) ppm.

$^{13}\text{C}\{^1\text{H}\}$  NMR (DMSO- $d_6$ , 125.75 MHz):  $\delta$  15.2 (CH<sub>2</sub>), 63.3 (CH<sub>3</sub>), 115.1 (CH), 122.0 (CH), 123.9 (CH), 124.8 (CH), 125.4 (CH), 125.4 (CH), 126.1 (CH), 128.4 (CH), 128.8 (CH), 129.0 (CH), 136.5 (C<sub>q</sub>), 139.1 (CH), 139.5 (CH), 140.4 (CH), 144.2 (C<sub>q</sub>), 147.0 (C<sub>q</sub>), 152.8 (CH), 153.7 (CH), 154.8 (CH), 155.4 (C<sub>q</sub>), 155.5 (C<sub>q</sub>), 155.6 (CH), 156.8 (C<sub>q</sub>), 157.2 (C<sub>q</sub>), 158.1 (C<sub>q</sub>), 158.3 (C<sub>q</sub>), 165.1 (C<sub>q</sub>), 165.1 (C<sub>q</sub>), 213.9 (CO), 222.7 (CO) ppm.

**Elemental analysis (%):**

calculated (C<sub>47</sub>H<sub>33</sub>BrF<sub>12</sub>MnN<sub>9</sub>O<sub>6</sub>P<sub>2</sub>Ru) x 0.5 EtOH:

C: 42.56      H: 2.77      N: 9.12

found:

C: 42.32      H: 3.10      N: 9.17

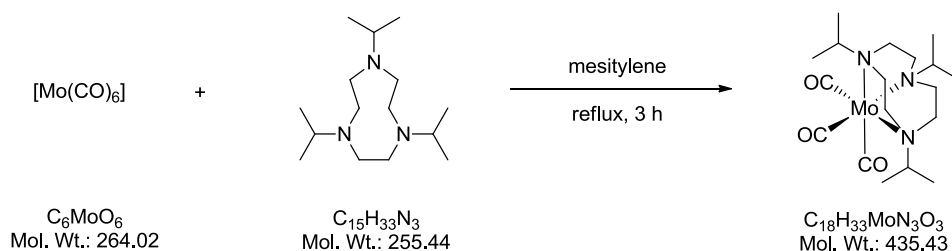
**ESI-MS:**

m/z: 654.11 [M-Mn-3CO-Br-C<sub>11</sub>H<sub>7</sub>N<sub>2</sub>O+H-2PF<sub>6</sub>]<sup>+</sup>, 837.17 [M-Mn-3CO-Br+H-2PF<sub>6</sub>]<sup>+</sup>, 972.02 [M-3CO+H-2PF<sub>6</sub>]<sup>+</sup>, 1056.01 [M+H-2PF<sub>6</sub>]<sup>+</sup>, 1201.98 [M-PF<sub>6</sub>]<sup>+</sup>

## 5.2.5 Synthesis of mixed CO/NO-releasing molecules

5.2.5.1 Synthesis of  $[\text{Mo}(\text{CO})_3(\text{iPr}_3\text{tacn})]$ <sup>[101]</sup>

USC-CN070

**3-33**

Under dinitrogen, molybdenum hexacarbonyl (81 mg, 0.31 mmol) and 1,4,7-triisopropyl-1,4,7-triazacyclonane (80 mg, 0.31 mmol) were dissolved in degassed mesitylene (10 mL) and heated to reflux for 3 h. The precipitated brownish product was collected by filtration and dried under vacuum at 50 °C.

**Yield:** 122 mg (0.28 mmol, 91%).

**IR:** 2966 (w), 1888 (vs), 1727 (vs), 1443 (w), 1388 (w), 1123 (w), 1066 (w)  $\text{cm}^{-1}$ .

**$^1\text{H}$  NMR** (DMSO- $d_6$ , 199.93 MHz):  $\delta$  = 1.29 (d,  $^3J$  = 6.4 Hz, 18H,  $\text{CH}_3$ ), 2.70 (s, 12H,  $\text{CH}_2$ ), 3.27 (m, 3H,  $\text{CH}$ ) ppm. The multiplet of the methine protons at 3.27 ppm partly overlaps with the solvent water peak at 3.31 ppm.

**$^{13}\text{C}\{^1\text{H}\}$  NMR** (DMSO- $d_6$ , 50.27 MHz):  $\delta$  = 19.2 ( $\text{CH}_3$ ), 54.4 ( $\text{CH}_2$ ), 61.7 ( $\text{CH}$ ), 229.0 ( $\text{CO}$ ) ppm.

**Elemental analysis (%):**

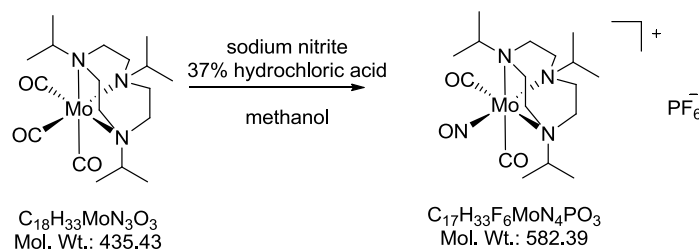
calculated ( $\text{C}_{18}\text{H}_{33}\text{MoN}_3\text{O}_3$ ) : C: 49.65 H: 7.64 N: 9.65

found: C: 41.51 H: 6.59 N: 8.03

The large deviation in the elemental analysis is probably caused by water and salt impurities which, however, did not interfere with the next synthetic step.

5.2.5.2 Synthesis of  $[\text{Mo}(\text{CO})_2(\text{NO})(i\text{Pr}_3\text{tacn})]\text{PF}_6$ <sup>[100]</sup>

USC-CN071

**3-34**

$[\text{Mo}(\text{CO})_3(i\text{Pr}_3\text{tacn})]$  (100 mg, 0.23 mmol) and sodium nitrite (30 mg, 0.43 mmol) were dissolved in methanol (10 mL). To this suspension, 37% hydrochloric acid (1 mL) was added to obtain a yellow solution. The solvent was then immediately removed under vacuum and the residue dissolved in deionized water (30 mL). After addition of a solution of potassium hexafluorophosphate (0.03 mg, 0.16 mmol) in deionized water (1 mL), the yellow product that precipitated was collected by filtration and dried under vacuum for several days. Yellow crystals suitable for X-ray structure analysis were obtained by slow diffusion of *n*-hexane into a dichloromethane solution of the compound.

**Yield:** 113 mg (0.19 mmol, 84%)

**IR:** 2978 (w), 2018 (vs), 1939 (s), 1912 (vs), 1672 (m), 1643 (s), 1467 (w), 1116 (w), 1060 (w), 829 (vs)  $\text{cm}^{-1}$ .

**$^1\text{H}$  NMR** ( $\text{CD}_2\text{Cl}_2$ , 500.13 MHz):  $\delta$  = 1.30 (d,  $^3J$  = 6.6 Hz, 6H,  $\text{CH}_3$ ), 1.40 (d,  $^3J$  = 6.5 Hz, 6H,  $\text{CH}_3$ ), 1.42 (d,  $^3J$  = 6.5 Hz, 6H,  $\text{CH}_3$ ), 2.88 - 2.94 (m, 2H,  $\text{CH}_2$ ), 3.00 - 3.06 (m, 4H,  $\text{CH}_2$ ), 3.07 - 3.13 (m, 6H,  $\text{CH}_2$ ), 3.21 (sept,  $^3J$  = 6.6 Hz, 1H, CH), 3.53 (sept,  $^3J$  = 6.5 Hz, 2H, CH), ppm.

**$^{13}\text{C}\{^1\text{H}\}$  NMR** ( $\text{CD}_2\text{Cl}_2$ , 125.27 MHz):  $\delta$  = 19.6 ( $\text{CH}_3$ ), 19.7 ( $\text{CH}_3$ ), 19.9 ( $\text{CH}_3$ ), 52.4 ( $\text{CH}_2$ ), 53.1 ( $\text{CH}_2$ ), 62.9 (CH), 64.9 (CH), 223.3 (CO) ppm.

**Elemental analysis (%):**

calculated ( $\text{C}_{17}\text{H}_{33}\text{F}_6\text{MoN}_4\text{O}_3\text{P}$ ) x $\text{H}_2\text{O}$ :	C: 34.01	H: 5.88	N: 9.33
found:	C: 34.37	H: 5.62	N: 9.23

**ESI-MS:**

m/z: 225.98 [M-2CO-NO-3(C<sub>3</sub>H<sub>7</sub>)-PF<sub>6</sub>]<sup>+</sup>, 268.02 [M-2CO-NO-2(C<sub>3</sub>H<sub>7</sub>)-PF<sub>6</sub>]<sup>+</sup>,  
295.05 [M-CO-NO-2(C<sub>3</sub>H<sub>7</sub>)-PF<sub>6</sub>]<sup>+</sup>, 339.10 [M-CO-NO-C<sub>3</sub>H<sub>7</sub>-PF<sub>6</sub>]<sup>+</sup>, 381.16 [M-  
CO-NO-PF<sub>6</sub>]<sup>+</sup>, 411.16 [M-CO-PF<sub>6</sub>]<sup>+</sup>, 439.16 [M-PF<sub>6</sub>]<sup>+</sup>



### 5.3 Myoglobin assay

For preparation of the myoglobin stock solution, horse skeletal muscle myoglobin (Sigma Aldrich, M0630) (~250 mg) was dissolved in phosphate-buffered saline (PBS) (0.1 M, ~10 mL) to give a dark brown solution. Any non-dissolved solid particles were collected by filtration and a UV/Vis spectra was taken. The concentration was calculated from the Lambert-Beer law at the absorption band at 557 nm using  $\epsilon_{(557\text{nm})} = 13.8 \text{ M}^{-1}\text{cm}^{-1}$ . Then, in a 1 cm quartz cuvette, the stock solution of myoglobin was diluted with 0.1 M phosphate-buffered saline (PBS) (pH = 7.4) to a total 890  $\mu\text{L}$ , to obtain a total concentration of 60  $\mu\text{M}$  in the cuvette. The solution was then degassed by bubbling with argon or dinitrogen and then reduced by addition of an excess of sodium dithionite solution (10 mM, 100  $\mu\text{L}$ ) in the same solvent to give a total volume of 990  $\mu\text{L}$ . The metal complex sample (~ 1 mg) was dissolved in dimethylsulfoxide. Then, 10  $\mu\text{L}$  of this stock solution was added to the myoglobin solution to give a final concentration of 10  $\mu\text{M}$  of metal complex, 1 mM of sodium dithionite and 60  $\mu\text{M}$  of myoglobin with  $A_{557 \text{ nm}} < 1$ . The solutions were illuminated under argon or dinitrogen either with a custom-made 15 LED cluster at 660 nm (Kingbright Elec. Co., 6000 mcd, part. no. BL0106-15-39), 525 nm (Kingbright Elec. Co., 6500 mcd, part. no. L-34ZGC), 468 nm (Kingbright Elec. Co., 5000 mcd, part. no. BL0106-15-299), 412 nm (UV-LEDs, model YDG-504VC, Kingbright Elec. Co., Taipei, Taiwan, part. no. 181000-05) or an UV hand lamp at 365 nm (LF-206.LS, 6 W, UVITEC Cambridge). The cuvettes were positioned perpendicular to the light source at a distance of 3 cm. The photoactivation was interrupted at regular intervals to record UV/Vis spectra on an Agilent 8453 UV/Vis diode array spectrophotometer. Dark control experiments were carried out under the same conditions over a period of 12-20 h. For these experiments, spectra were recorded automatically at regular time intervals of 10 or 30 min. The concentration of carboxymyoglobin (MbCO) was calculated from changes in the Q-band absorption at 540 nm as shown in eq. (2) with  $\epsilon_{(540\text{nm})}(\text{MbCO}) = 15 \text{ M}^{-1}\text{cm}^{-1}$ .<sup>[124]</sup> These values were then numerically corrected

for deviations at the isosbestic point at 510 nm for  $A(t = 0)$  as described by Fairlamb.<sup>[87]</sup> The half-lives and the number of CO equivalents released were obtained from an exponential fit of a plot of  $c(\text{MbCO})$  versus illumination time using Origin.

$$c(\text{MbCO}) = \left( \frac{A(t)}{l} - \frac{A(t=0)}{l} \right) \times \frac{1}{\varepsilon_{540 \text{ nm}}(\text{MbCO}) - \frac{A(t=0)}{c_0(\text{Mb}) \times l}} \quad (2)$$

## 5.4 Photolysis with NMR detection

Photolysis experiments were carried out on a Bruker Advance 200 spectrometer ( $^1\text{H}$  at 199.93 MHz). A stock solution of  $[\text{Mn}(\text{CO})_3(\text{tpa})]\text{Br}$  (65.10 mg, 0.12 mmol) in deuterated dimethylsulfoxide (4.50 mL) was prepared and degassed for 20 min by bubbling with dinitrogen under exclusion of light. Six NMR tubes were then each filled with the same volume of stock solution (0.70 mL) and five of them were illuminated with a 365 nm UV hand lamp (LF-206.LS, 6 W, UVITEC Cambridge) for 10, 20, 30, 40, and 50 min. The last sample was immediately placed in the 200 MHz NMR spectrometer without illumination.  $^1\text{H}$  NMR spectra of every sample were recorded at the end of each illumination period.

## 5.5 Photolysis with IR detection

Experiments were carried out on a Jasco FT/IR-4100 spectrometer using a flow-cell holder equipped with calcium fluoride windows ( $d = 4$  mm) and a Teflon spacer ( $d = 0.5$  mm). A stock solution of the compound in dimethylsulfoxide (0.01 M, 1 mL) was prepared and filled into the IR liquid cell under exclusion of light. The cell was illuminated with a 412 nm LED cluster (UV-LEDs, model YDG-504VC, Kingbright Elec. Co., Taipei, Taiwan, part. no. 181000-05) or a 365 nm UV hand held lamp (LF-206.LS, 6 W, UVITEC Cambridge) and spectra were taken every 20 s. Later during the experiment, the illumination interval was increased to 40, 60, 120, 300, and 600 s, respectively.

## 5.6 Determination of the *n*-octanol/water partition coefficient

The  $\log P_{7.4}$  values were determined by the “shake-flask” method. For saturation of the phases, equal volumes of phosphate buffered saline (PBS) (10 mM, pH 7.4) and *n*-octanol were shaken on a lab shaker (IKA KS 130 basic) for 72 h. Then, 750  $\mu\text{L}$  of each phase and 10  $\mu\text{L}$  of a sample stock solution in dimethylsulfoxide (10 mg/mL) were transferred to an Eppendorf tube and shaken on a lab vortexer (VWR Analogue Vortexer) for 15 min. For separation of the phases, the mixture was centrifuged (5 min, 3000 rpm) and UV/Vis spectra of both phases were taken from aliquots of 500  $\mu\text{L}$ .  $\log P_{7.4}$  values were then calculated from eq. 3.<sup>[66]</sup>

$$\log P_{7.4} = \log \left( \frac{A_{\text{octanol (300 nm)}}}{A_{\text{PBS (300 nm)}}} \right) \quad (2)$$

## 5.7 Biological assays

### 5.7.1 *Escherichia coli* growth condition

All biological assays were carried out in the group of Prof. Dr. Robert K. Poole at the Department of Molecular Biology and Biotechnology, University of Sheffield, by Samantha McLean. For all bacterial studies, the strain *Escherichia coli* K12 derivative MG1655 was used. For whole cell spectral measurements, cells were grown in Luria broth and a glucose- or succinate-limited Evans medium was used for manganese analysis and growth inhibition experiments. Cells were grown at 37 °C with shaking at 200 rpm. Cultures (20 mL) were grown in side-arm flasks (250 mL) for the growth inhibition experiments. The optical density was measured using a Klett-Summerson photoelectric colorimeter (Klett Manufacturing Co.) fitted with a number 66 red filter.

### 5.7.2 Whole-cell UV/Vis spectroscopy

Bacterial cultures (600 ml) were harvested after growth to mid-exponential phase and washed with phosphate buffered saline (PBS). Then, the cells were resuspended to an approximate OD<sub>600</sub> of 50. Difference spectra were taken of cells reduced by sodium dithionite alone versus cells reduced and incubated with [Mn(CO)<sub>3</sub>(tpa)]Br **3-5** (100 μM) for 20 min at room temperature. During incubation, cell suspensions were illuminated with a 365 nm UV hand lamp (UVIlite LF-206LS, 6 W, UVItec Ltd, Cambridge, UK). The measurements were carried out on an Olis RSM1000 dual-beam rapid scanning monochromator in CLARITY mode (On-Line Instrument Systems).

### 5.7.3 Manganese uptake analysis

Samples of cells were taken after growth to mid-exponential phase both prior to and at regular intervals after incubation with [Mn(CO)<sub>3</sub>(tpa)]Br **3-5** (50 μM). The manganese content was then measured in triplicate using ICP-MS.

## 6 References

- [1] R. Motterlini, L. E. Otterbein, *Nat. Rev. Drug discovery* **2010**, *9*, 728-743.
- [2] B. Wegiel, D. J. Gallo, K. G. Raman, J. M. Karlsson, B. Ozanich, B. Y. Chin, E. Tzeng, S. Ahmad, A. Ahmed, C. J. Baty, L. E. Otterbein, *Circ. Res.* **2010**, *121*, 537-548.
- [3] C. L. Hartsfield, I. F. McMurtry, D. D. Ivy, K. G. Morris, S. Vidmar, D. M. Rodman, K. A. Fagan, *Am. J. Physiol. Heart Circ. Physiol.* **2004**, *287*, H2009-H2015.
- [4] B. S. Zuckerbraun, B. Y. Chin, B. Wegiel, T. R. Billiar, E. Czimadia, J. Rao, L. Shimoda, E. Ifedigbo, S. Kanno, L. E. Otterbein, *J. Exp. Med.* **2006**, *203*, 2109-2119.
- [5] A. Wilks, M. Ikeda-Saito, *Acc. Chem. Res.* **2014**.
- [6] B. E. Mann, *Organometallics* **2012**, *31*, 5728-5735.
- [7] S. W. Ryter, J. Alam, A. M. K. Choi, *Physiol. Rev.* **2006**, *86*, 583-650.
- [8] R. Motterlini, P. Sawle, J. Hammad, B. E. Mann, T. R. Johnson, C. J. Green, R. Foresti, *Pharmacol. Res.* **2013**, *68*, 108-117.
- [9] S. Hou, S. H. Heinemann, T. Hoshi, *Physiol.* **2009**, *24*, 26-35.
- [10] J. Boczkowski, J. J. Poderoso, R. Motterlini, *Trends Biochem. Sci.* **2006**, *31*, 614-621.
- [11] R. Wang, L. Wu, *JBC* **1997**, *272*, 8222-8226.
- [12] S. Hou, R. Xu, S. H. Heinemann, T. Hoshi, *PNAS* **2008**, *105*, 4039-4043.
- [13] S. Hou, M. F. Reynolds, F. T. Horrigan, S. H. Heinemann, T. Hoshi, *Acc. Chem. Res.* **2006**, *39*, 918-924.
- [14] S. Hou, R. Xu, S. H. Heinemann, T. Hoshi, *Nat. Struct. Mol. Biol.* **2008**, *15*, 403-410.
- [15] H. P. Kim, S. W. Ryter, A. M. Choi, *Ann. Rev. Pharmacol. Toxicol.* **2006**, *46*, 411-449.
- [16] S. E. J. Williams, P. Wootton, H. S. Mason, J. Bould, D. E. Iles, D. Riccardi, C. Peers, P. J. Kemp, *Science* **2004**, *306*, 2093-2097.
- [17] R. Schubert, M. T. Nelson, *TRENDS Pharmacol. Sci.* **2001**, *22*, 505-511.
- [18] E. R. Derbyshire, M. A. Marletta, *Ann. Rev. Biochem.* **2012**, *81*, 533-559.
- [19] N. Schallner, C. C. Romao, J. Biermann, W. A. Lagreze, L. E. Otterbein, H. Buerkle, T. Loop, U. Goebel, *PloS One* **2013**, *8*, e60672-.
- [20] S. W. Ragsdale, L. Yi, G. Bender, N. Gupta, Y. Kung, L. Yan, T. A. Stich, T. Doukov, L. Leichert, P. M. Jenkins, C. M. Bianchetti, S. J. George, S. P. Cramer, R. D. Britt, U. Jakob, J. R. Martens, G. N. Phillips, Jr., C. L. Drennan, *Biochem. Soc. Trans.* **2012**, *40*, 501-507.
- [21] M. Desmard, K. S. Davidge, O. Bouvet, D. Morin, D. Roux, R. Foresti, J. D. Ricard, E. Denamur, R. K. Poole, P. Montravers, R. Motterlini, J. Boczkowski, *FASEB J.* **2009**, *23*, 1023-1031.
- [22] J. L. Wilson, H. E. Jesse, B. Hughes, V. Lund, K. Naylor, K. S. Davidge, G. M. Cook, B. E. Mann, R. K. Poole, *Antioxid. Redox Signaling* **2013**, *19*, 497-509.

- [23] H. Bai, M. D. Rolfe, W. Jia, S. Coakley, R. K. Poole, J. Green, M. Holcombe, *PLoS Comput. Biol.* **2014**, *10*, e1003595.
- [24] H. E. Jesse, T. L. Nye, S. McLean, J. Green, B. E. Mann, R. K. Poole, *Biochim. Biophys. Acta* **2013**, *1834*, 1693-1703.
- [25] K. S. Davidge, G. Sanguinetti, C. H. Yee, A. G. Cox, C. W. McLeod, C. E. Monk, B. E. Mann, R. Motterlini, R. K. Poole, *J. Biol. Chem.* **2009**, *284*, 4516-4524.
- [26] M. Tinajero-Trejo, K. J. Denby, S. E. Sedelnikova, S. A. Hassoubah, B. E. Mann, R. K. Poole, *J. Biol. Chemistry* **2014**, *289*, 29471-29482.
- [27] N. Rana, S. McLean, B. E. Mann, R. K. Poole, *Microbiology* **2014**, *160*, 2771-2779.
- [28] J. S. Ward, J. M. Lynam, J. Moir, I. J. S. Fairlamb, *Chem. Eur. J.* **2014**, *20*, 15061-15068.
- [29] C. Nagel, S. McLean, R. K. Poole, H. Braunschweig, T. Kramer, U. Schatzschneider, *Dalton Trans.* **2014**, *43*, 9986-9997.
- [30] C. C. Romao, W. A. Blattler, J. D. Seixas, G. J. Bernardes, *Chem. Soc. Rev.* **2012**, *41*, 3571-3583.
- [31] R. Motterlini, B. E. Mann, F. R., *Expert Opin. Invest. Drugs* **2005**, *14*, 1305-1318.
- [32] R. Motterlini, J. E. Clark, R. Foresti, P. Sarathchandra, B. E. Mann, C. J. Green, *Circ. Res.* **2002**, *90*, 17e-24.
- [33] R. Foresti, J. Hammad, J. E. Clark, T. R. Johnson, B. E. Mann, A. Friebe, C. J. Green, R. Motterlini, *Br. J. Pharmacol.* **2004**, *142*, 453-460.
- [34] R. Motterlini, P. Sawle, J. Hammad, S. Bains, R. Alberto, R. Foresti, C. J. Green, *FASEB J.* **2005**, *19*, 284-286.
- [35] I. J. S. Fairlamb, A. K. Duhme-Klair, J. M. Lynam, B. E. Moulton, C. T. O'Brien, P. Sawle, J. Hammad, R. Motterlini, *Bioorganic & medicinal chemistry letters* **2006**, *16*, 995-998.
- [36] W. Strohmeier, *Angew. Chem.* **1963**, *75*, 453 - 454.
- [37] W. Strohmeier, *J. Organomet. Chem.* **1975**, *94*, 273 - 280.
- [38] W. Strohmeier, F.-J. Müller, *Chem. Ber.* **1969**, *102*, 3614 - 3615.
- [39] T. R. Johnson, B. E. Mann, I. P. Teasdale, H. Adams, R. Foresti, C. J. Green, R. Motterlini, *Dalton Trans.* **2007**, 1500-1508.
- [40] U. Schatzschneider, *Br. J. Pharmacol.* **2015**, *172*, 1638-1650..
- [41] I. J. S. Fairlamb, J. M. Lynam, B. E. Moulton, I. E. Taylor, A. K. Duhme-Klair, P. Sawle, R. Motterlini, *Dalton Trans.* **2007**, 3603-3605.
- [42] F. Zobi, L. Kromer, B. Spingler, R. Alberto, *Inorg. Chem.* **2009**, *48*, 8965-8970.
- [43] F. Zobi, A. Degonda, M. C. Schaub, A. Y. Bogdanova, *Inorg. Chem.* **2010**, *49*, 7313-7322.
- [44] F. Zobi, O. Blacque, R. A. Jacobs, M. C. Schaub, A. Y. Bogdanova, *Dalton Trans.* **2012**, *41*, 370-378.
- [45] F. Zobi, L. Quaroni, G. Santoro, T. Zlateva, O. Blacque, B. Sarafimov, M. C. Schaub, A. Y. Bogdanova, *J. Med. Chem.* **2013**, *56*, 6719-6731.
- [46] T. J. Haley, F. D. Cartwright, *J. Pharm. Sci.* **1968**, *57*, 321-323.

- [47] S. Botov, E. Stamellou, S. Romanski, M. Guttentag, R. Alberto, J.-M. Neudörfl, B. Yard, H.-G. Schmalz, *Organometallics* **2013**, *32*, 3587-3594.
- [48] S. Romanski, B. Kraus, M. Guttentag, W. Schlundt, H. Rucker, A. Adler, J. M. Neudorfl, R. Alberto, S. Amslinger, H. G. Schmalz, *Dalton Trans.* **2012**, *41*, 13862-13875.
- [49] S. Romanski, B. Kraus, U. Schatzschneider, J. M. Neudorfl, S. Amslinger, H. G. Schmalz, *Angew. Chem. Int. Ed. Engl.* **2011**, *50*, 2392-2396.
- [50] S. Romanski, H. Rucker, E. Stamellou, M. Guttentag, J. M. Neudörfl, R. Alberto, S. Amslinger, B. Yard, H. G. Schmalz, *Organometallics* **2012**, *31*, 5800-5809.
- [51] U. Schatzschneider, *Inorg. Chim. Acta* **2011**, *374*, 19-23.
- [52] S. B. Brown, E. A. Brown, I. Walker, *The Lancet Oncology* **2004**, *5*, 497-508.
- [53] J. F. Lovell, T. W. B. Liu, J. Chen, G. Zheng, *Chem. Rev.* **2010**, *110*, 2839-2857.
- [54] G. C. Ellis-Davies, *Nat. Methods* **2007**, *4*, 619-628.
- [55] K. L. Ciesinski, K. L. Haas, M. G. Dickens, Y. T. Tesema, K. J. Franz, *J. Am. Chem. Soc.* **2008**, *130*, 12246-12247.
- [56] M. Salierno, E. Marceca, D. S. Peterka, R. Yuste, R. Etchenique, *J. Inorg. Biochem.* **2010**, *104*, 418-422.
- [57] M. Salierno, C. Fameli, R. Etchenique, *Eur. J. Inorg. Chem.* **2008**, *2008*, 1125-1128.
- [58] G. Stochel, A. Wanat, E. Kuli, Z. Stasicka, *Coord. Chem. Rev.* **1998**, *171*, 203-220.
- [59] R. D. Rimmer, H. Richter, P. C. Ford, *Inorg. Chem.* **2010**, *49*, 1180-1185.
- [60] P. Agostinis, K. Berg, K. A. Cengel, T. H. Foster, A. W. Girotti, S. O. Gollnick, S. M. Hahn, M. R. Hamblin, A. Juzeniene, D. Kessel, M. Korbelik, J. Moan, P. Mroz, D. Nowis, J. Piette, B. C. Wilson, J. Golab, *CA-Cancer J. Clin.* **2011**, *61*, 250-281.
- [61] R. D. Rimmer, A. E. Pierri, P. C. Ford, *Coord. Chem. Rev.* **2012**, *256*, 1509-1519.
- [62] K. Meister, J. Niesel, U. Schatzschneider, N. Metzler-Nolte, D. A. Schmidt, M. Havenith, *Angew. Chem. Int. Ed. Engl.* **2010**, *49*, 3310-3312.
- [63] H. Pfeiffer, M. Dragoun, A. Prokop, U. Schatzschneider, *Z. Anorg. Allg. Chem.* **2013**, *639*, 1568-1576.
- [64] H. Pfeiffer, T. Sowik, U. Schatzschneider, *J. Organomet. Chem.* **2013**, *734*, 17-24.
- [65] H.-M. Berends, P. Kurz, *Inorg. Chim. Acta* **2012**, *380*, 141-147.
- [66] P. C. Kunz, W. Huber, A. Rojas, U. Schatzschneider, B. Spingler, *Eur. J. Inorg. Chem.* **2009**, *2009*, 5358-5366.
- [67] C. S. Jackson, S. Schmitt, Q. P. Dou, J. J. Kodanko, *Inorg. Chem.* **2011**, *50*, 5336-5338.
- [68] I. Chakraborty, S. J. Carrington, P. K. Mascharak, *ChemMedChem* **2014**.
- [69] I. Chakraborty, S. J. Carrington, P. K. Mascharak, *Acc. Chem. Res.* **2014**.



- [70] M. A. Gonzalez, S. J. Carrington, N. L. Fry, J. L. Martinez, P. K. Mascharak, *Inorg. Chem.* **2012**, *51*, 11930-11940.
- [71] M. A. Gonzalez, N. L. Fry, R. Burt, R. Davda, A. Hobbs, P. K. Mascharak, *Inorg. Chem.* **2011**, *50*, 3127-3134.
- [72] M. A. Gonzalez, S. J. Carrington, I. Chakraborty, M. M. Olmstead, P. K. Mascharak, *Inorg. Chem.* **2013**, *52*, 11320-11331.
- [73] M. A. Gonzalez, M. A. Yim, S. Cheng, A. Moyes, A. J. Hobbs, P. K. Mascharak, *Inorg. Chem.* **2012**, *51*, 601-608.
- [74] V. P. L. Velásquez, T. M. A. Jazzazi, A. Malassa, H. Görls, G. Gessner, S. H. Heinemann, M. Westerhausen, *Eur. J. Inorg. Chem.* **2012**, *2012*, 1072-1078.
- [75] R. D. Rimmer, H. Richter, P. C. Ford, *Inorg. Chem.* **2010**, *49*, 1180-1185.
- [76] P. R. Gil, W. J. Parak, *ACS Nano* **2008**, *2*, 2200-2205.
- [77] H. Pfeiffer, A. Rojas, J. Niesel, U. Schatzschneider, *Dalton Trans.* **2009**, 4292-4298.
- [78] P. Govender, S. Pai, U. Schatzschneider, G. S. Smith, *Inorg. Chem.* **2013**, *52*, 5470-5478.
- [79] L. Henry, C. Schneider, B. Mützel, P. V. Simpson, C. Nagel, K. Fucke, U. Schatzschneider, *Chem. Commun.* **2014**, *50*, 15692-15695.
- [80] G. Dordelmann, H. Pfeiffer, A. Birkner, U. Schatzschneider, *Inorg. Chem.* **2011**, *50*, 4362-4367.
- [81] H. Maeda, *Bioconjugate Chem.* **2010**, *21*, 797-802.
- [82] P. Govender, B. Therrien, G. S. Smith, *Eur. J. Inorg. Chem.* **2012**, *2012*, 2853-2862.
- [83] F. Mohr, J. Niesel, U. Schatzschneider, C. W. Lehmann, *Z. Anorg. Allg. Chem.* **2012**, *638*, 543-546.
- [84] N. Wei, N. N. Murthy, Q. Chen, J. Zubieta, K. D. Karlin, *Inorg. Chem.* **1994**, *33*, 1953-1965.
- [85] Z. Tyeklar, R. R. Jacobson, N. Wei, N. N. Murthy, J. Zubieta, K. D. Karlin, *J. Am. Chem. Soc.* **1993**, *115*, 2677-2689.
- [86] K. Meister, J. Niesel, U. Schatzschneider, N. Metzler-Nolte, D. A. Schmidt, M. Havenith, *Angew. Chem. Int. Ed.* **2010**, *49*, 3310-3312.
- [87] A. J. Atkin, J. M. Lynam, B. E. Moulton, P. Sawle, R. Motterlini, N. M. Boyle, M. T. Pryce, I. J. S. Fairlamb, *Dalton Trans.* **2011**, *40*, 5755-5761.
- [88] P. D. Leeson, B. Springthorpe, *Nat. Rev. Drug Discovery* **2007**, *6*, 881-890.
- [89] P. D. Leeson, *Nature* **2012**, *481*, 455-456.
- [90] C. A. Lipinski, F. Lombardo, B. W. Dominy, P. J. Feeney, *Adv. Drug Delivery Rev.* **2001**, *46*, 3-26.
- [91] P. Rudolf, F. Kanal, J. Knorr, C. Nagel, J. Niesel, T. Brixner, U. Schatzschneider, P. Nuernberger, *J. Phys. Chem. Lett.* **2013**, *4*, 596-602.
- [92] H.-M. Berends, P. Kurz, *Inorg. Chim. Acta* **2012**, *380*, 141-147.
- [93] K. Wieghardt, E. Schöffmann, B. Nuber, J. Weiss, *Inorg. Chem.* **1986**, *25*, 4877 - 4883.
- [94] K. Wieghardt, W. Schmidt, B. Nuber, J. Weiss, *Chem. Ber.* **1979**, 2220-2230.

- [95] S. J. Carrington, I. Chakraborty, J. M. Bernard, P. K. Mascharak, *ACS Med. Chem. Lett.* **2014**, *5*, 1324-1328.
- [96] D. J. Charboneau, N. A. Piro, W. S. Kassel, T. J. Dudley, J. J. Paul, *Polyhedron* **2015**, *91*, 18-27.
- [97] L. You, E. J. Cho, J. Leavitt, L. C. Ma, G. T. Montelione, E. V. Anslyn, R. M. Krug, A. Ellington, J. D. Robertus, *Bioorg. Med. Chem. Lett.* **2011**, *21*, 3007-3011.
- [98] I. P. Evans, A. Spencer, G. Wilkinson, *Dalton Trans.* **1973**, 204-209.
- [99] A. M. Downward, E. G. Moore, R. M. Hartshorn, *Chem. Commun.* **2011**, *47*, 7692-7694.
- [100] J. Bohmer, G. Haselhorst, K. Wieghardt, B. Nuber, *Angew Chem* **1994**, *106*, 1556-1559.
- [101] G. Haselhorst, S. Stoetzel, A. Strassburger, W. Walz, K. Wieghardt, B. Nuber, *Dalton Trans.* **1993**, 83.
- [102] S. P. Semproni, W. S. McNeil, R. A. Baillie, B. O. Patrick, C. F. Campana, P. Legzdins, *Organometallics* **2010**, *29*, 867-875.
- [103] A. J. Włodarczyk, P. P. Romańczyk, S. S. Kurek, W. Nitek, J. A. McCleverty, *Polyhedron* **2008**, *27*, 783-796.
- [104] A. K. Gallien, D. Schaniel, T. Woike, P. Klufers, *Dalton Trans.* **2014**, *43*, 13278-13292.
- [105] A. Włodarczyk, R. M. Richardson, M. D. Ward, J. A. McCleverty, M. H. B. Hursthouse, S. J. Coles, *Polyhedron* **1996**, *15*, 27-35.
- [106] A. L. Rheingold, L. N. Zakharov, S. Trofimenko, *Inorg. Chem.* **2003**, *42*, 827-833.
- [107] J. A. Campo, J. A. McCleverty, C. M. J. V. Heras, E. Pinilla, A. Monge, J. A. McCleverty, *Dalton Trans.* **1998**, 3065-3070.
- [108] J. C. Jeffery, S. S. Kurek, J. A. McCleverty, E. Psillakis, R. M. Richardson, M. D. Ward, A. Włodarczyk, *Dalton Trans.* **1994**, 2559-2563.
- [109] N. C. Harden, J. C. Jeffery, J. A. McCleverty, L. H. Rees, M. D. Ward, *New J. Chem.* **1998**, *22*, 661-663.
- [110] M. Cano, J. V. Heras, A. Monge, E. Gutierrez, C. J. Jones, S. L. W. McWhinnied, J. A. McCleverty, *Dalton Trans.* **1992**, 2435-2438.
- [111] K.-B. Shiu, J. S.-T. Lin, D.-W. Fung, T.-J. Chan, S.-M. Peng, M.-C. Cheng, J. L. Chou, *Inorg. Chem.* **1995**, *34*, 854-863.
- [112] S. J. Millar, B. W. Mos, M. H. Stevensonab, *Meat Science* **1996**, *42*, 277-288.
- [113] C. Schneider, *MSc. Thesis*, Julius-Maximilians-Universität Würzburg (Würzburg), **2012**.
- [114] G. R. Fulmer, A. J. M. Miller, N. H. Sherden, H. E. Gottlieb, A. Nudelman, B. M. Stoltz, J. E. Bercaw, K. I. Goldberg, *Organometallics* **2010**, *29*, 2176-2179.
- [115] O. V. Dolomanov, L. J. Bourhis, R. J. Gildea, J. A. K. Howard, H. Puschman, *J. Appl. Cryst.* **2009**, *339* - 341.
- [116] G. M. Sheldrick, *Acta Crystallogr., Sec. A: Found. Adv.* **2008**, *64*, 112-122.
- [117] F. Neese, *WIRES: Computational Molecular Science* **2012**, *2*, 73-78.
- [118] A. Schäfer, H. Horn, R. Ahlrichs, *J. Chem. Phys.* **1992**, *97*, 2571.

- [119] F. Weigend, R. Ahlrichs, *Phys. Chem. Chem. Phys.* **2005**, 7, 3297-3305.
- [120] Z. Tyeklar, R. R. Jacobson, N. Wei, N. N. Murthy, J. Zubieta, K. D. Karlin, *J. Am. Chem. Soc.* **1993**, 115, 2677-2689.
- [121] J. Kang, J. H. Jo, *Bull. Korean Chem. Soc.* **1403**, 24, 1403-1406.
- [122] K. Wieghardt, W. Schmidt, B. Nuher, J. Weiss, *Chem. Ber.* **1979**, 112, 2220-2230.
- [123] C. E. McCusker, J. K. McCusker, *Inorg. Chem.* **2011**, 50, 1656-1669.
- [124] E. Antonini, M. Brunori, *Hemoglobin and Myoglobin in Their Reactions with Ligands*, Vol. 21, North-Holland Pub. Co, Amsterdam, **1971**.

## 7 Appendices

### Calculation of CO equivalents released

$$A(t) = \varepsilon_{540nm}(Mb) \cdot c(Mb) \cdot l + \varepsilon_{540nm}(MbCO) \cdot c(MbCO) \cdot l$$

$$c(Mb) + c(MbCO) = c_0(Mb)$$

$$A(t) = \varepsilon_{540nm}(Mb) \cdot c_0(Mb) \cdot l - \varepsilon_{540nm}(Mb) \cdot c(MbCO) \cdot l + \varepsilon_{540nm}(MbCO) \cdot c(MbCO) \cdot l$$

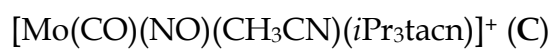
$$\frac{A(t)}{l} = \frac{A(t=0)}{c_0(Mb) \cdot l} \cdot c_0(Mb) + c(MbCO) \left( \varepsilon_{540nm}(MbCO) - \frac{A(t=0)}{c_0(Mb) \cdot l} \right)$$

$$\Leftrightarrow \frac{A(t)}{l} = \frac{A(t=0)}{l} + c(MbCO) \left( \varepsilon_{540nm}(MbCO) - \frac{A(t=0)}{c_0(Mb) \cdot l} \right)$$

$$\Leftrightarrow c(MbCO) \left( \varepsilon_{540nm}(MbCO) - \frac{A(t=0)}{c_0(Mb) \cdot l} \right) = \frac{A(t)}{l} - \frac{A(t=0)}{l}$$

$$\Leftrightarrow c(MbCO) = \left( \frac{A(t)}{l} - \frac{A(t=0)}{l} \right) \frac{1}{\varepsilon_{540nm}(MbCO) - \frac{A(t=0)}{c_0(Mb) \cdot l}}$$



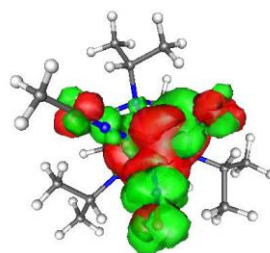
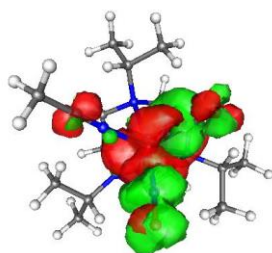
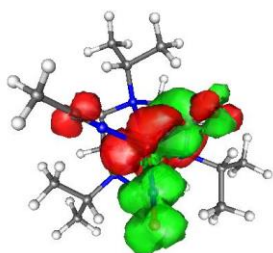


State:

1

4

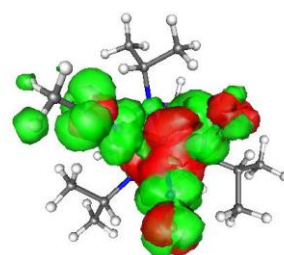
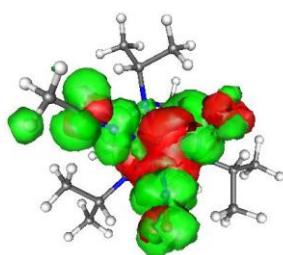
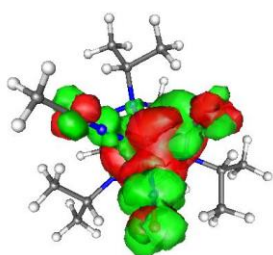
5



6

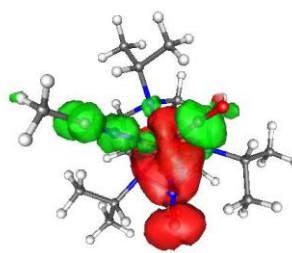
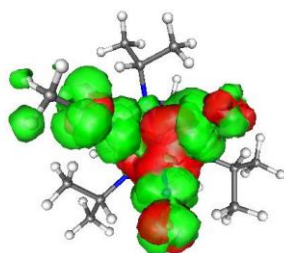
8

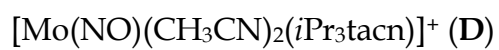
9



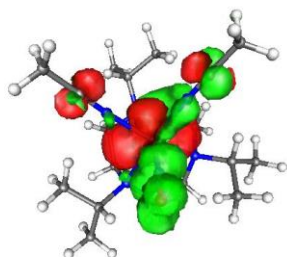
10

12

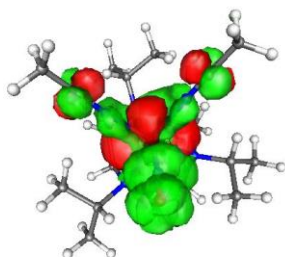




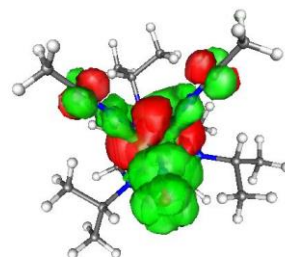
State: 1



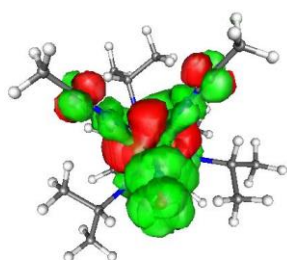
2



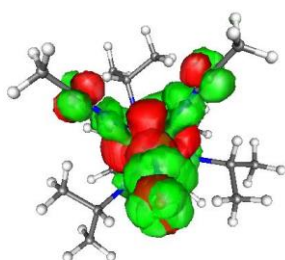
3



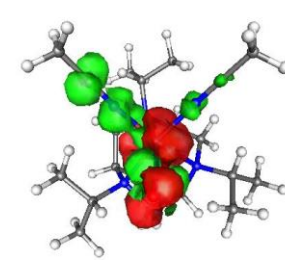
5



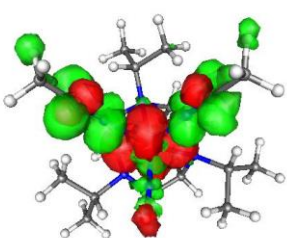
6



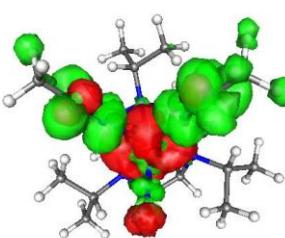
7



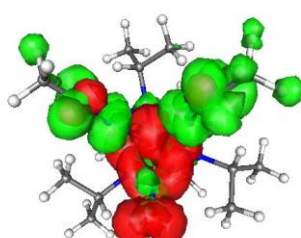
10



11



15



16

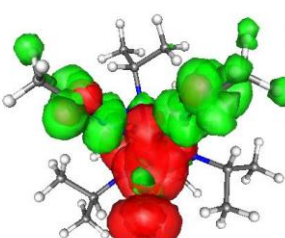


Table 7.1: Crystallographic data for **3-5**

<i>[Mn(CO)<sub>3</sub>(tpa)]Br</i>	<b>3-5</b>
<b>Empirical formula</b>	C <sub>21</sub> H <sub>18</sub> BrMnN <sub>4</sub> O <sub>3</sub>
<b>Molecular weight [g/mol]</b>	509.23
<b>Temperature [K]</b>	100(2)
<b>Wavelength Mo-K<math>\alpha</math> [Å]</b>	0.71073
<b>Crystal size [mm]</b>	0.31 x 0.25 x 0.16
<b>Crystal system, space group</b>	monoclinic, <i>P</i> <sub>2</sub> <sub>1</sub> / <i>n</i>
<b>a [Å]</b>	12.520(11)
<b>b [Å]</b>	11.025(10)
<b>c [Å]</b>	15.523(17)
<b><math>\alpha</math> [°]</b>	90.00
<b><math>\beta</math> [°]</b>	107.76(8)
<b><math>\gamma</math> [°]</b>	90.00
<b>Cell volume [Å<sup>3</sup>]</b>	2041(3)
<b>Z</b>	4
<b>Density [g/cm<sup>3</sup>]</b>	1.658
<b>Absorption coefficient <math>\mu</math> [mm<sup>-1</sup>]</b>	2.636
<b><i>F</i> (000)</b>	1024
<b><math>\Theta</math> range for data collection [°]</b>	1.84-26.98
<b>Index range (<i>h</i>/<i>k</i>/<i>l</i>)</b>	-15/-13/-18
<b>Collected reflections</b>	15077
<b>Unique reflections</b>	3965
<b>Observed reflections [<i>F</i><sub>0</sub>&gt;4<math>\sigma</math><i>F</i><sub>0</sub>]</b>	3531
<b>Absorption correction</b>	0.4954-0.6778
<b>Goodness-of-fit on <i>F</i><sup>2</sup>(<i>GOF</i>)</b>	1.028
<b>Final <i>R</i> indices [<i>F</i><sub>0</sub>&gt;4<math>\sigma</math><i>F</i><sub>0</sub>]</b>	<i>R</i> <sub>1</sub> = 0.0279, <i>wR</i> <sub>1</sub> = 0.0739
<b><i>R</i> indices (all data)</b>	<i>R</i> <sub>2</sub> = 0.0323, <i>wR</i> <sub>2</sub> = 0.0772
<b>Largest difference peak an hole [e·Å<sup>-3</sup>]</b>	0.713 and -0.589
<b>internal identification number</b>	TSK062
<b>CCDC number</b>	CCDC-941933



Table 7.2: Crystallographic data for **3-8**

<i>[Mn(CO)<sub>3</sub>(tmqa)]Br</i>	<b>3-8</b>
Empirical formula	C <sub>33</sub> H <sub>24</sub> BrMnN <sub>4</sub> O <sub>3</sub>
Molecular weight [g/mol]	659.41
Temperature [K]	100.00
Wavelength Mo-K $\alpha$ [Å]	0.71073
Crystal size [mm]	0.78 x 0.32 x 0.32
Crystal system, space group	monoclinic, <i>P</i> 2 <sub>1</sub> / <i>c</i>
<i>a</i> [Å]	16.4923(9)
<i>b</i> [Å]	13.8229(7)
<i>c</i> [Å]	14.3262(8)
$\alpha$ [°]	90.00
$\beta$ [°]	110.227(2)
$\gamma$ [°]	90.00
Cell volume [Å <sup>3</sup> ]	3064.6(3)
<i>Z</i>	4
Density [g/cm <sup>3</sup> ]	1.5463
Absorption coefficient $\mu$ [mm <sup>-1</sup> ]	1.787
<i>F</i> (000)	1456.8902
$\Theta$ range for data collection [°]	1.32-26.00
Index range ( <i>h</i> / <i>k</i> / <i>l</i> )	-21/-18/-19
Collected reflections	45659
Unique reflections	6030
Observed reflections [ <i>F</i> <sub>0</sub> >4 $\sigma$ <i>F</i> <sub>0</sub> ]	5031
Absorption correction	0.6242-0.7457
Goodness-of-fit on <i>F</i> <sup>2</sup> ( <i>GOF</i> )	1.0451
Final <i>R</i> indices [ <i>F</i> <sub>0</sub> >4 $\sigma$ <i>F</i> <sub>0</sub> ]	<i>R</i> <sub>1</sub> = 0.0290, <i>wR</i> <sub>1</sub> = 0.0633
<i>R</i> indices (all data)	<i>R</i> <sub>2</sub> = 0.0414, <i>wR</i> <sub>2</sub> = 0.0685
Largest difference peak an hole [e·Å <sup>-3</sup> ]	0.4280 and -0.5734
internal identification number	CN13013
CCDC number	not yet assigned

Table 7.3: Crystallographic data for **3-15**

$[Mn(CO)_3(py_3tacn-\kappa^3N)]PF_6$	<b>3-15</b>
Empirical formula	C <sub>27</sub> H <sub>30</sub> F <sub>6</sub> MnN <sub>6</sub> O <sub>3</sub> P
Molecular weight [g/mol]	686.46
Temperature [K]	100.00
Wavelength Mo-K $\alpha$ [Å]	0.71073
Crystal size [mm]	0.56 x 0.27 x 0.25
Crystal system, space group	triclinic, <i>P</i> -1
a [Å]	9.5672(10)
b [Å]	9.619(1)
c [Å]	16.5465(16)
$\alpha$ [°]	105.687(3)
$\beta$ [°]	93.487(3)
$\gamma$ [°]	104.461(3)
Cell volume [Å <sup>3</sup> ]	1406.0(3)
Z	2
Density [g/cm <sup>3</sup> ]	1.6213
Absorption coefficient $\mu$ [mm <sup>-1</sup> ]	0.609
<i>F</i> (000)	705.3175
$\Theta$ range for data collection [°]	1.29-26.00
Index range ( <i>h</i> / <i>k</i> / <i>l</i> )	-11/-12/-20
Collected reflections	16951
Unique reflections	5531
Observed reflections [ $F_0 > 4\sigma F_0$ ]	4462
Absorption correction	0.6504-0.7454
Goodness-of-fit on $F^2$ (GOF)	1.0394
Final <i>R</i> indices [ $F_0 > 4\sigma F_0$ ]	$R_1 = 0.0392$ , $wR_1 = 0.1015$
<i>R</i> indices (all data)	$R_2 = 0.0534$ , $wR_2 = 0.1170$
Largest difference peak an hole [e·Å <sup>-3</sup> ]	0.6859 and -0.4634
internal identification number	CN13008
CCDC number	not yet assigned

Table 7.4: Crystallographic data for **3-30**

<i>[MnBr(CO)<sub>3</sub>(dpx)]</i>	<b>3-30</b>
Empirical formula	C <sub>21</sub> H <sub>12</sub> BrMnN <sub>4</sub> O <sub>3</sub>
Molecular weight [g/mol]	503.20
Temperature [K]	102.20
Wavelength Mo-K $\alpha$ [Å]	0.71073
Crystal size [mm]	0.40 x 0.37 x 0.20
Crystal system, space group	triclinic, <i>P</i> -1
a [Å]	7.3786(11)
b [Å]	10.6925(19)
c [Å]	13.2497(19)
$\alpha$ [°]	98.572(7)
$\beta$ [°]	102.544(5)
$\gamma$ [°]	106.787(5)
Cell volume [Å <sup>3</sup> ]	951.5(3)
Z	2
Density [g/cm <sup>3</sup> ]	1.7562
Absorption coefficient $\mu$ [mm <sup>-1</sup> ]	0.7254
<i>F</i> (000)	500.3303
$\Theta$ range for data collection [°]	1.62-25.99
Index range ( <i>h/k/l</i> )	-9/-13/-16
Collected reflections	14391
Unique reflections	6292
Observed reflections [ $F_0 > 4\sigma F_0$ ]	3637
Absorption correction	0.4776-0.6584
Goodness-of-fit on $F^2$ ( <i>GOF</i> )	0.9806
Final <i>R</i> indices [ $F_0 > 4\sigma F_0$ ]	$R_1 = 0.0291$ , $wR_1 = 0.0719$
<i>R</i> indices (all data)	$R_2 = 0.0413$ , $wR_2 = 0.0859$
Largest difference peak an hole [e·Å <sup>-3</sup> ]	0.5045 and -0.6921
internal identification number	CN14032a
CCDC number	not yet assigned

Table 7.5: Crystallographic data for **3-34**

<i>[Mo(NO)(CO)<sub>2</sub>(iPr<sub>3</sub>tacn)]PF<sub>6</sub></i>	<b>3-34</b>
Empirical formula	C <sub>17</sub> H <sub>33</sub> F <sub>6</sub> MoN <sub>4</sub> O <sub>3</sub> P
Molecular weight [g/mol]	582.39
Temperature [K]	100.00
Wavelength Mo-K $\alpha$ [Å]	0.71073
Crystal size [mm]	0.46 x 0.38 x 0.25
Crystal system, space group	orthorhombic, <i>Pbca</i>
a [Å]	17.1434(16)
b [Å]	14.9459(14)
c [Å]	18.1606(17)
$\alpha$ [°]	90.00
$\beta$ [°]	90.00
$\gamma$ [°]	90.00
Cell volume [Å <sup>3</sup> ]	4653.2(8)
Z	8
Density [g/cm <sup>3</sup> ]	1.6625
Absorption coefficient $\mu$ [mm <sup>-1</sup> ]	0.707
<i>F</i> (000)	2372.4946
$\Theta$ range for data collection [°]	2.13-26.00
Index range ( <i>h/k/l</i> )	-22/-19/-24
Collected reflections	68440
Unique reflections	4562
Observed reflections [ <i>F</i> <sub>0</sub> >4 $\sigma$ <i>F</i> <sub>0</sub> ]	3891
Absorption correction	0.6825-0.7457
Goodness-of-fit on <i>F</i> <sup>2</sup> ( <i>GOF</i> )	1.0102
Final <i>R</i> indices [ <i>F</i> <sub>0</sub> >4 $\sigma$ <i>F</i> <sub>0</sub> ]	<i>R</i> <sub>1</sub> = 0.0223, <i>wR</i> <sub>2</sub> = 0.0469
<i>R</i> indices (all data)	<i>R</i> <sub>1</sub> = 0.0304, <i>wR</i> <sub>2</sub> = 0.0536
Largest difference peak an hole [e·Å <sup>-3</sup> ]	0.4816 and -0.3588
internal identification number	CN14015
CCDC number	not yet assigned

## Selbständigkeitserklärung

Hiermit erkläre ich an Eides statt, dass ich die Dissertation

*“Novel manganese- and molybdenum-based photoactivatable CO releasing molecules: Synthesis and biological activity”*

selbständig angefertigt und keine anderen als die von mir angegebenen Quellen und Hilfsmittel benutzt habe.

Ich erkläre außerdem, dass diese Arbeit weder in gleicher oder in anderer Form bereits in einem anderen Prüfungsverfahren vorgelegen hat.

Ich habe früher außer den mit dem Zulassungsgesuch urkundlich vorgelegten Graden keine weiteren akademischen Grade erworben oder zu erwerben versucht.

Würzburg, den \_\_\_\_\_

\_\_\_\_\_  
(Christoph Nagel)